STRENGTHENING OF UNREINFORCED MASONRY BUILDINGS USING SURFACE-MOUNTED STEEL BANDS

by

Thainswemong Choudhury

DEPARTMENT OF CIVIL ENGINEERING
INDIAN INSTITUTE OF TECHNOLOGY GUWAHATI
GUWAHATI-781039, INDIA

October 2019

STRENGTHENING OF UNREINFORCED MASONRY BUILDINGS USING SURFACE-MOUNTED STEEL BANDS

A Thesis Submitted
in Partial Fulfillment of the Requirements
for the Degree of

DOCTOR OF PHILOSOPHY

by

Thainswemong Choudhury

DEPARTMENT OF CIVIL ENGINEERING
INDIAN INSTITUTE OF TECHNOLOGY GUWAHATI
GUWAHATI-781039, INDIA

October 2019

CERTIFICATE

It is certified that the work contained in this thesis titled "*Strengthening of Unreinforced Masonry Buildings using Surface-Mounted Steel Bands*" by **Mr. Thainswemong Choudhury** (126104024), has been carried out under my supervision and submitted to Indian Institute of Technology Guwahati for the award of the degree of **Doctor of Philosophy**. This work has not been submitted elsewhere for a degree to the best of my knowledge and belief.

Date: 15 October 2019
Place: IIT Guwahati

Dr. Hemant B. Kaushik
Professor
Department of Civil Engineering
Indian Institute of Technology Guwahati
Guwahati-781039, Assam, India

ABSTRACT

Numerous earthquakes in different parts of the world have shown that unreinforced masonry (URM) buildings perform quite poorly when subjected to strong ground motions. Despite their high seismic vulnerability, URM buildings are still widely constructed due to inexpensive construction materials, and construction procedure perceived easier by many. Therefore, it is of utmost importance to develop a suitable evaluation procedure for the URM buildings that not only assists in structural assessment of these buildings, but also can be used in their preliminary design. In addition, based on the seismic assessment, development of simple strengthening solutions for such vulnerable building typology has become an important issue to improve their seismic behavior.

The assessment of URM buildings can be carried out using experimental, numerical, and analytical methods. Each of these approaches has various challenges. As for instance, conducting experimental studies on full-scale building specimens is expensive and need sophisticated equipment with complex laboratory setup. The numerical simulation requires huge computational effort and input data, which is not available easily. Therefore, the availability of test results and data is scarce in many developing countries that have a huge concentration of URM buildings. Moreover, the quality of masonry found in these countries are inferior to those found in some developed countries where ample data is available. This results in under-developed design codes, and thus, improper design and construction of URM buildings in seismically active regions of many developing countries. Moreover, the analytical approaches in the updated codes of various countries may not be suitable to be used elsewhere due to the significant variation in material properties and construction practices. Therefore, this study consists of experimental, numerical, and analytical evaluation of URM walls and buildings with and without strengthening. Initially, a preliminary numerical study was carried out over a tested URM building using three popular FE software considering three different material constitutive models under continuum modeling approach (Equivalent Frame Method, Mohr-Coulomb failure criteria, and Concrete Damage Plasticity model). Despite predicting the lateral strength of the URM building with reasonable accuracy, the numerical approaches could not predict the progressive damage and failure modes satisfactorily. To get more insight into the lateral

load behaviour of URM walls and building and to generate the input data required for numerical simulations, pseudo-static in-plane cyclic tests were carried out on three full-scale URM walls with different opening configurations and three single room URM buildings, constituting the walls, which were already tested. The tests were carried out over unstrengthened (1 specimen) as well as strengthened URM buildings (2 specimens) in order to evaluate the effectiveness and suitability of using the surface-mounted steel bands as a strengthening scheme. One specimen was strengthened using surface-mounted steel bands on both faces (external as well as internal) of all the walls horizontally at lintel level (Model 1), and the other was strengthened using similar horizontal steel bands at sill and lintel levels and vertical bands around the openings (Model 2). Model 2 showed significant improvement in the lateral strength, deformability, and energy dissipation capacity of the URM building. The proposed strengthening scheme is really simple to implement on site due to requirement of simple equipment, and locally available material and workforce. Moreover, the proposed scheme does not change the natural characteristics and aesthetics of the URM buildings.

The URM walls and buildings were then simulated in Abaqus and Strand7 to estimate the lateral strength and study the numerical damage output. The shortcomings of the existing numerical methods were addressed by introducing a new homogenized discretization method for numerical simulation of URM buildings. The suggested discretization method was found to be predicting the lateral strength and crack pattern evolution of the URM buildings with better accuracy. The lateral strength of individual walls was also estimated analytically using several existing methods suggested in various codes and literature. Finally, a systematic combination of in-plane and out-of-plane strengths of individual walls, estimated using available analytical methods, was suggested to estimate the lateral strength of URM buildings.

Further, parametric numerical studies were carried out on unstrengthened as well as strengthened URM building models by varying some of the important parameters like wall thickness, aspect ratio (l/h) of walls, tensile strength of masonry, width and thickness of the steel bands, and cross-sectional area of the steel bands. Based on regression analysis of the obtianed data, empirical equations were developed for estimation of the lateral strength of the unstrengthened URM building as well as of the strengthened URM building.

ACKNOWLEDGEMENT

I would like to express my deep and sincere gratitude to Professor Hemant B. Kaushik, for his warm encouragement and thoughtful guidance. It has been a great and memorable experience working under him. I appreciate all his contributions of time, suggestions and ideas to make my Ph.D. experience productive and stimulating. I want to thank him for the immense patience, coordination, understanding and encouraging interactions, which had been a significant driving force for me to carry out my research work. I also thank the members of my doctoral committee: Professor Anjan Dutta, Professor Santosha K. Dwivedy, and Professor Kaustubh Dasgupta for their time, interest, suggestions and helpful comments.

I am especially grateful to my Erasmus Mundus Heritage Doctoral program advisor Professor Gabriele Milani, for inspirational discussions, encouragement, and insightful support during and after my program period. I am also thankful to Dr. Elisa Bertolesi for providing wholehearted insightful assistance on addressing various numerical issues I faced during my stay. I want to express my gratitude to my friends Niro Akbary, Johanna Scholz, and Viktoria Scheff for the beautiful and memorable moments in Italy and Germany. I would also like to thank my friends Dr. Hitesh Shrimali, Dr Ranvir Singh, Dr. Darshana Joshi, Dr. Pandi Pitchai and Dr. Vijay Venugopalan for the great time in Italy. Special thanks to Mrs. Emanuela Zonca, Ms. Barbara Del Sole and staffs at ABC and DICA of Politecnico di Milano, Italy, for the effective, hasselfree and friendly assistance in sorting out the official requirement and making my work experience at POLIMI most comfortable and memorable one.

I want to thank scientific officer Dr. Arun Borsaikia and the laboratory technical assistants Mr. Biswajit Debnath, Mr. Pranab Hazarika and Mr. Sourab Mudoi for their assistance and support in carrying out my experiments smoothly. I owe to my colleagues cum friend, Biswajit Chand and Nishant Sharma for their whole-hearted help in carrying out my experiments and various other assistance during my entire stay at IIT Guwahati. I am thankful to Dr. Syed Humayun Basha for his support in introducing the laboratory test setup and during the testing procedure. Above all, I would like to thank my wonderful and

most amazing friends Dr. Debayan Dhar, Nzanthung Ngullie, Niro Akbary, Aurelia Sangma, Sivapradeep Poreddy, Liyingbeni Odyuo, Dr. Anamika Mog, Sandeep Kalyanpur, Tanmoy Deb for their support. My sincere gratitude to Brother Thaiu Mog for his regular encouragement and moral support. My thanks are due to staff, faculty, and students at Department of Civil Engineering who helped me and provided support for the studies. I thank the Erasmus Mundus Heritage team for providing timely support for conducting the studies in Italy. The funding for the research work provided by the Department of Science and Technology, Government of India, under Research Grant No. SB/S3/CEE/0018/2014 is acknowledged.

My beloved Guruji Late. Panyawansa Mahathero and wonderful friend Late. Zuboni Humtsoe will always be remembered.

Last but not the least, I would like to thank Guruji U Wannadaza, my Mom (Mrs. Krairi Mog Choudhury), my Dad (Mr. Thaikhai Choudhury), sister (Chanda Choudhury), my most super lovely wife (Mrs. Parul Mog) and my elder brother (Mr. Sushil Mog) for holding my hand during tough times and supporting me during my doctoral studies.

THAINSWEMONG CHOUDHURY

TABLE OF CONTENTS

Abstract *i*

Acknowledgement *iii*

List of Tables *ix*

List of Figures *xi*

List of Symbols *xix*

Chapter 1 Introduction **1**

1.1. Overview 1

1.2. Types of Masonry Buildings in India 3

1.2.1. Unreinforced Brick Masonry with Reinforced Concrete Slab 4

1.2.2. Unreinforced Brick Masonry with Pitched Clay Tile Roof 4

1.2.3. Unreinforced Brick Masonry with Timber Roof 5

1.2.4. Unreinforced Brick Masonry with GI Sheet Roof 5

1.2.5. Seismic Vulnerability of Unreinforced Brick Masonry Buildings 6

1.3. Behavior of URM Buildings During Past Earthquakes 6

1.3.1. Bhuj, Gujarat Earthquake, 2001 7

1.3.2. North Kashmir Earthquake, 2005 7

1.3.3. Sikkim Earthquakes, 2006, 2011 8

1.3.4. Varzaghan-Ahar twin Iran Earthquakes, 2012 10

1.3.5. Christchurch Earthquakes, 2010, 2011 11

1.3.6. Nepal Earthquake, 2015 11

1.3.7. Common Observations 12

1.4. Strengthening of URM Buildings 13

1.5. Scope and Objectives of the Present Study 14

1.6. Organization of the Thesis 15

Chapter 2 Literature Review **17**

2.1. Overview 17

2.2. Behavior of URM Walls Subjected to Lateral Loading 18

2.2.1. In-Plane Behavior of Masonry Walls 18

2.2.1.1. Gap Areas 24

2.2.2. Out-of-plane Behavior of Masonry Walls 25

2.2.2.1. Gap Areas 28
2.3. Behavior of URM Buildings Subjected to Lateral Loading 29
2.3.1. Gap Areas 33
2.4. Strengthening of URM Buildings 33
2.4.1. Indian Code Provisions: Design and Strengthening of Masonry Buildings 36
2.4.2. Gap Areas 37
2.5. Summary and Identified Gap Areas 38

Chapter 3 Preliminary Numerical Investigation 41
3.1. Overview 41
3.2. Numerical Modelling 43
3.2.1. Strand7 FE Code 43
3.2.2. Abaqus FE Code 45
3.2.3. SAP2000 Equivalent Frame Approach 48
3.3. Building Geometry and FE Discretization 50
3.4. Non-linear Analysis and Results 53
3.4.1. Numerical analysis of URM building 55
3.4.2. Strengthening Scheme #1: Steel Bands at the Lintel Level 58
3.4.3. Strengthening Scheme #2: Steel Bands at Lintel and Sill Level 60
3.4.4. Strengthening Scheme #3: Horizontal Steel Bands at Lintel and Sill Level and Vertical Steel Bands around the Openings 61
3.5. Sensitivity Analysis Varying Thickness and Width of the Steel Flats 63
3.6. Design Equations for Estimation of Capacity 65
3.7. Influence of Openings in Masonry Building 67
3.7.1. Influence of only External Bands and Combination of External and Internal Bands 68
3.8. Summary 71

Chapter 4 Experimental Study on URM Walls 73
4.1. Overview 73
4.2. Tests on Masonry Constituents 74
4.2.1. Compressive Test on Bricks 74
4.2.2. Compressive Test on Mortar 75
4.2.3. Triplet Shear Test 75
4.2.4. Tensile Bond Test 76
4.2.5. Compressive Test on Masonry Prism 78

4.3. Experimental Evaluation of URM walls 79
4.3.1. Experimental Results 81
4.3.1.1. Wall 1 (Model 1) 81
4.3.1.2. Wall 2 (Model 2) 82
4.3.1.3. Wall 3 (Model 3) 84
4.3.1.4. Comparison of Response of URM Walls 86
4.4. Summary 87

Chapter 5 Experimental Study on Strengthening of URM Buildings 89
5.1. Overview 89
5.2. Experimental Setup 91
5.3. Testing of URM Building (Unstrengthened) 96
5.4. Testing of Strengthened Building 1 (Model 1) 99
5.5. Testing of Strengthened Building 2 (Model 2) 102
5.6. Summary 108

Chapter 6 Estimation of Lateral Strength of URM Building 111
6.1. Overview 111
6.2. Numerical Study of URM walls 112
6.2.1. Numerical Results 114
6.2.1.1. Wall 1 114
6.2.1.2. Wall 2 115
6.2.1.3. Wall 3 116
6.3. Numerical Study of URM Buildings 117
6.4. Analytical Evaluation 119
6.4.1. Lateral Strength of URM Walls 119
6.4.1.1. In-Plane Resistance of Walls 119
6.4.1.2. Out-of-Plane Resistance of Walls 122
6.4.1.3. Comparison of Wall Responses 126
6.4.2. Lateral Strength of URM Building 128
6.5. Summary 129

Chapter 7 Homogenized Discretization Method for Numerical Simulation of URM Building 131
7.1. General 131
7.2. Numerical Simulation of URM Building 134
7.2.1. Numerical FE Modelling 134

7.2.2. Results 141
7.2.2.1. Wall 1 141
7.2.2.2. Wall 2 142
7.2.2.3. Wall 3 144
7.2.2.4. URM Building 145
7.2.2.5. Parametric Numerical Study of URM Buildings 148
7.3. Numerical Simulation of Strengthened URM Building 149
7.4. Summary 152

Chapter 8 Summary and Conclusion 155

8.1. Overview 155
8.2. Summary 156
8.2.1. Preliminary Numerical Investigation of URM buildings 156
8.2.2. Material Characterization and Experimental Evaluation of URM Walls 157
8.2.3. Experimental Evaluation of a Strengthening Scheme for URM Buildings 158
8.2.4. Numerical and Analytical Study for Estimation of Lateral Strength of URM Buildings 159
8.2.5. Development of Homogenized Discretization Method for Numerical Simulation of URM Building 160
8.3. Conclusions 161
8.4. Recommendation for Future Work 163

References ***165***

List of Publications ***179***

LIST OF TABLES

Table No.	Caption	Page No.
Table 3.1.	Concrete damage plasticity properties	48
Table 3.2.	Flexure and Shear capacities generated for masonry elements (Piers)	49
Table 3.3.	Shear capacities generated for masonry elements (Spandrels)	50
Table 3.4.	Geometry of walls, windows and doors	52
Table 3.5.	Mechanical properties of the material used in brick masonry building	53
Table 3.6.	Damage Contours of URM buildings with four different opening configurations (Model A, Model B, Model C, Model D)	68
Table 3.7.	Moment and Shear capacity curves for individual masonry walls strengthened using only external and using both external and internal steel bands	69
Table 4.1.	Mechanical properties of masonry materials	79
Table 6.1.	Analytical estimation of the in-plane strength of URM walls	126
Table 6.2.	Analytical estimation of the out-of-plane strength of URM walls in kN	127
Table 6.3.	Combined in-plane and out-of-plane strength of URM walls estimated using different methods and normalized with respect to the experimental capacity of 88.4 kN	129

LIST OF FIGURES

Figure No.	Caption	Page No.
Figure 1.1.	Brick masonry structures since ancient times to existing construction practices.	2
Figure 1.2.	Map of India showing concentration of URM buildings in region with large populations (Seismic zones from BIS 2016, Population from Census 2011).	3
Figure 1.3.	Type of URM buildings: (a) Unreinforced brick masonry with reinforced concrete slab, and (b) Unreinforced brick masonry with pitched clay tile roof (Kumar, 2002).	4
Figure 1.4.	Type of URM buildings: (a) Overview of unreinforced brick masonry with timber roof, (b) Structural details of roof (Jain, 1993).	5
Figure 1.5.	An unreinforced brick masonry house with GI sheet on roof.	6
Figure 1.6.	Collapse of the upper storey of a URM building under construction at Bhachau in Gujarat (Jain et al., 2001).	7
Figure 1.7.	Failure in URM Buildings: (a) Out-of-Plane collapse of URM walls, and (b) Diagonal cracks in window openings and tilting of walls during North Kashmir Earthquake (National Disaster Management Division 2006).	8
Figure 1.8.	Traditional masonry for proven earthquake resistance: (a) *Dhajji-dewari* system of timber-laced masonry for confining masonry in small panels, (b) *Taq* system of embedding timber logs in thick walls (Rai and Murty, 2005).	8
Figure 1.9.	Excellent performance shown by retrofitted Archive building during 2006 Sikkim earthquake (arrows indicate locations of steel flats used to retrofit the building after 1988 Bihar-Nepal earthquake) (Kaushik et al., 2006).	9
Figure 1.10.	Performance of the retrofitted Archive building during 2011 Sikkim Earthquake: (a) out-of-plane movement of the walls bending the steel flats, (b) missing steel bars that should connect the steel flats on both faces of the walls, and (c) failure of the welded connection in the steel flats due to out-of-plane movement of the walls.	9
Figure 1.11.	Performance of URM buildings during 2012 Iran earthquakes: (a) Failure of heavy steel jack-arch, concrete roofs and walls of URM buildings, (b) out-of-plane collapse of walls in URM buildings, and (c) buildings compliant with minimum code requirements survived the earthquake with minor damages (Razzaghi and Ashtiany, 2012).	10
Figure 1.12.	Severe Damage to several types of URM structures during the Canterbury earthquakes (Hare 2013).	11

Figure 1.13. Buildings strengthened with steel frames survived the Canterbury earthquakes with repairable damage (EERI 2013). 11

Figure 1.14. Performance of URM buildings during Nepal Earthquake: (a) in-plane wall damage, and (b) out-of-plane collapse of masonry walls (Lizundia et al. 2016). 12

Figure 2.1. In-plane Failure pattern of masonry walls: (a) shear failure, (b) rocking/flexural failure, (c) diagonal shear failure, and (d) toe crushing failure. 19

Figure 2.2. In-plane test setup for URM wall (Russel and Ingham 2010). 20

Figure 2.3. Inclined diagonal cracks due to in-plane loads (Javed et al., 2015). 22

Figure 2.4. Out of plane collapse mechanism of URM walls. 25

Figure 2.5. Out-of-plane test set up of URM wall (Vaculik and Griffith 2018). 26

Figure 2.6. Two face crack patterns of OOP test on URM walls with vertical pre-compression value of (a) 0.10 MPa, (b) 0 MPa, (c) 0.10 MPa, (d) 0.05 MPa, and (e) 0 MPa (Vaculik and Griffith 2018). 27

Figure 2.7. Lateral load testing of URM building (a) tested structure, (b) observed crack pattern in different walls (Moon et al., 2006; Yi et al., 2006a). 31

Figure 2.8. Effectiveness of polypropylene-band used as strengthening of URM building. Lateral load performance of (a) the unstrengthened model, and (b) the strengthened model (Sathiparan et al., 2012). 35

Figure 2.9. (a) Details of the 'Splint and Bandage' strengthening technique, and (b) shock-table test showing the effectiveness of using ferro-cement bands (welded wire mesh in concrete/mortar) applied on the URM walls as strengthening scheme. The building on the left was not strengthened, while the building on the right was strengthened using the 'Splints and Bandage' technique (Kadam et al., 2015, 2018). 36

Figure 3.1. Abaqus material non-linear behavior in uniaxial (a) tension, and (b) compression, Stress-strain curve of masonry prism in (c) tension, and (d) compression. 46

Figure 3.2. Abaqus: (a) modified Drucker-Prager strength domain, and (b) yield surface in the deviatoric plane corresponding to different values of K_c ($-\sigma'_1$, $-\sigma'_2$, $-\sigma'_3$ are principal stresses in three axis and $-S_1, -S_2, -S_3$ are yield/flow surfaces in the deviatoric plane). 47

Figure 3.3. Smooth Druker-Prager failure criterion adopted in the simulations, *p*-*q* plane. 47

Figure 3.4. Unreinforced brick masonry prototype analyzed: (a) Plan view (All units are in m), (b) 3D FE model (2903 eight-noded solid element and 5676 nodes), and (c) Equivalent frame model of the masonry. 51

Figure 3.5. Capacity curves for the unreinforced prototype and Strand7 model at two different values of masonry cohesion. 54

Figure 3.6. Capacity curves with and without RC ring beam at lintel level. 55

Figure 3.7. Capacity curve comparison among computational approaches and Experimental evidences. 55

Figure 3.8. Comparison between numerical inelastic deformation and experimental crack pattern exhibiting a mixed failure combining rocking and diagonal shear cracking: (a) Plastic strain, and (b) Damage pattern of the tested structure by Shahzada et al. (2012). 56

Figure 3.9. Stress contours figures developed using (a) Abaqus, and (b) Strand7. 57

Figure 3.10. SAP2000 results: (a) Non-linear pushover results for Equivalent frame, (b) Non-linear Moment - Rotation curve for Moment Hinges, and (c) Non-linear Force - Displacement curve for shear hinges. 57

Figure 3.11. Capacity curves obtained for URM buildings with steel flats and with RC ring beam. 58

Figure 3.12. Steel flats used as surface-mounted bands at the lintel level. 59

Figure 3.13. Stress contour on 4 faces of the building due to application of steel bands at lintel level. 59

Figure 3.14. Plastic strain in masonry after providing steel bands at lintel level. 59

Figure 3.15. Capacity curve comparison for Strengthening Scheme #1 using three numerical approaches with the unstrengthened specimen tested by Shahzada et al. (2012). 59

Figure 3.16. Steel bands mounted at the lintel and sill level (Double steel band). 60

Figure 3.17. Stress contour due to application of steel bands at lintel and sill level. 60

Figure 3.18. Plastic strain region due application steel bands at lintel and sill level. 61

Figure 3.19. Capacity curves after the application of double level steel band and comparison with the originally tested unstrengthened specimen by Shahzada et al. (2012). 61

Figure 3.20. FE discretization of URM building strengthened using surface-mounted horizontal double steel bands at lintel and sill level and vertical steel bands around the openings. 62

Figure 3.21. Strengthening Scheme #3: (a) Stress Contour, and (b) Equivalent plastic strain patch. 62

Figure 3.22. Strengthening Scheme #3 Capacity curves obtained with the three numerical models and their comparison with experimental results (unreinforced case) reported by Shahzada et al. (2012). 62

Figure 3.23. Capacity curve comparison between strengthened and un-strengthened building obtained using Abaqus. Shahzada et al. (2012) represents the un-strengthened prototype. 63

Figure 3.24. Masonry building with Strengthening Scheme #1. Capacity curves obtained considering bands having different cross-sectional area: (a) width increase, and (b) thickness increase. 64

Figure 3.25. Masonry building with Strengthening Scheme #2. Capacity curves obtained considering bands having different cross-sectional area: (a) width increase, and (b) thickness increase. 64

Figure 3.26. Masonry building with Strengthening Scheme #3. Capacity curves obtained considering bands having different cross-sectional area: (a) width increase, and (b) thickness increase. 65

Figure 3.27. Masonry building with Strengthening Scheme #1. Factor α_L for different cross-sectional areas of the steel bands and corresponding best fitting interpolation: (a) width increase, and (b) thickness increase. 66

Figure 3.28. Masonry building with Strengthening Scheme #2. Factor α_L for different cross-sectional areas of the steel bands and corresponding best fitting interpolation: (a) width increase, and (b) thickness increase. 66

Figure 3.29. Masonry building with Strengthening Scheme #3. Factor α_L for different cross-sectional areas of the steel bands and corresponding best fitting interpolation: (a) width increase, and (b) thickness increase. 67

Figure 3.30. Capacity curve comparison of URM building with 4 opening configurations. 69

Figure 3.31. URM building strengthened using Strengthening Scheme #3 with: (a) only external steel bands, and (b) both external and internal steel bands. 70

Figure 3.32. Capacity comparison of the strengthening schemes for Model D obtained using Abaqus. 70

Figure 4.1. Compression test of bricks. 74

Figure 4.2. Compression test of cement mortar cubes. 75

Figure 4.3. Triplet Shear Test: (a) Setup 1, (b) Setup 2, and (c) Failure mechanism observed. 76

Figure 4.4. Tensile bond test: (a)Experimental setup of Z Specimen, (b) Free body diagram of Z-shaped specimen, and (c) Free body diagram of top brick displaying loads and stress distribution. 77

Figure 4.5. Tensile bond test: (a) tension bond failure of Z-shaped specimen (b) idealized tensile stress-strain curve. 78

Figure 4.6. Masonry displaying: (a) compression test, and (a) average compressive stress-strain curve. 79

Figure 4.7. Experimental setup for testing of URM walls. 80

Figure 4.8. Slow cyclic testing of: (a) solid wall (Wall 1), (b) wall with a door opening (Wall 2), (c) wall with a window opening (Wall 3), and (d) applied displacement history. 80

Figure 4.9. Lateral load testing of Wall 1: (a) load arrangement and crack formation and (b)(c) closer view of the crack propagation at the bottom of the wall. 81

Figure 4.10. Hysteresis response and capacity envelop curve obtained for Wall 1. 82

Figure 4.11. Cumulative energy dissipation curve obtained for Wall 1. 82

Figure 4.12. Lateral load testing of Model 2: (a) crack formation at 6 mm, (b) (c) closer view of crack at the base, and (c) closer view of crack near the top of the door opening. 83

Figure 4.13. Hysteresis and capacity curve obtained for Wall 2. 83

Figure 4.14. Cumulative energy dissipation curve obtained for Wall 2. 84

Figure 4.15. Lateral load testing of Wall 3: (a) crack along the whole length of the wall at the bottom at 12 mm displacement level, and (b) closer view of the crack formed at the wall bottom. 84

Figure 4.16. Hysteresis curve and strength envelop curve obtained for Wall 3. 85

Figure 4.17. Cumulative energy dissipation curve of Wall 3. 85

Figure 4.18. Comparison of hysteresis curves of three walls. 86

Figure 4.19. Comparison of capacity envelop curves of three walls. 87

Figure 4.20. Comparison of cumulative energy dissipation curves. 87

Figure 5.1. Overview of the URM building specimens: (a) unstrengthened URM Building (denoted as URM), (b) building strengthened using horizontal steel bands at lintel level (denoted as Model 1), and (c) building strengthened using horizontal steel bands at sill and lintel levels and vertical bands adjacent to openings (denoted as Model 2). 92

Figure 5.2. Experimental setup: (a) Plan, and (b) Elevation of the building showing loading arrangement, sensors, and openings in the walls. 93

Figure 5.3. Stage wise construction of URM building up to: (a) base, (b) window, (c) lintel level, (d) roof level, (e) parapet wall, and (f) completion. 94

Figure 5.4. Details of surface-mounted steel flats: (a) wall section in plan (b) wall section in elevation. 95

Figure 5.5. Displacement history applied on URM building specimens. 95

Figure 5.6. Experimental setup of URM building. 96

Figure 5.7. Damage pattern observed during the slow cyclic lateral load testing of full-scale URM building: (a) Damage observed in Wall 2 and Wall 3*, and (b) Damage observed in Wall 3 and Wall 1*. 97

Figure 5.8. Damage observed in different walls inside the unstrengthened URM building during the lateral load testing. 98

Figure 5.9. Lateral load response of un-strengthened URM specimen: (a) hysteresis curves and capacity envelope, and (b) cumulative energy dissipation capacity. 98

Figure 5.10. Experimental setup of strengthened URM building specimen 1 (Model 1). 99

Figure 5.11. Damage observed in different walls during testing of the strengthened building 1 (Model 1): (a) Wall 2 and Wall 3*, and (b) Walls 3 and 1*. 100

Figure 5.12. Damage observed in different walls inside Model 1 during the lateral load testing. 101

Figure 5.13.	Steel band failure at the junction of Walls 2 and 3*.	101
Figure 5.14.	Lateral load response of strengthened specimen (Model 1): (a) hysteresis curves and capacity envelope, and (b) cumulative energy dissipation capacity.	102
Figure 5.15.	Experimental setup of strengthened URM building specimen (Model 2).	103
Figure 5.16.	Damage observed in different walls during lateral load testing of the strengthened building 2 (Model 2): (a) Walls 2 and 3*, and (b) Wall 3 and 1*.	104
Figure 5.17.	Damage observed in different walls inside the Model 2 during the lateral load testing.	105
Figure 5.18.	Hysteresis curves of strengthened building 2 (Model 2).	105
Figure 5.19.	Comparison of lateral load response of all the specimens: (a) capacity envelope, and (b) cumulative energy dissipation.	106
Figure 5.20.	Rotation observed in plan in due to twisting action at 15 mm displacement level in: (a) URM Building, (b) Model 1, and (c) Model 2.	106
Figure 5.21.	Location of strain gauge in Model 2: (a) External wall surface, and (b) Internal wall surface.	107
Figure 5.22.	Strains measured on steel flats at 30 mm displacement level.	108
Figure 6.1.	FE models of wall specimens tested in the present study: (a) Wall 1, (b) Wall 2, and (c) Wall 3.	113
Figure 6.2.	Finite element models of URM Building: (a) View 1, and (b) View 2.	113
Figure 6.3.	Comparison of experimental and numerical results for Wall 1: (a) load displacement curves, (b) damage observed experimentally, (c) damage pattern in Abaqus, and (d) damage pattern in Strand7.	115
Figure 6.4.	Comparison of experimental and numerical results for Wall 2: (a) load displacement curves, (b) damage observed experimentally, (c) damage pattern in Abaqus, and (d) damage pattern in Strand7.	116
Figure 6.5.	Comparison of experimental and numerical results for Wall 3: (a) load displacement curves, (b) damage observed experimentally, (c) damage pattern in Abaqus, and (d) damage pattern in Strand7.	117
Figure 6.6.	Comparison of the numerically obtained capacity curve with the experimental capacity curve for URM building.	118
Figure 6.7.	Strain contour of the URM building shown along the four walls obtained using Strand7.	118
Figure 6.8.	Damaget contour of the URM building shown along the four walls obtained using Abaqus.	119
Figure 7.1	Numerical models adopted for the analysis of the tested specimens: (a) isotropic FE model with damage and softening (b) non standard two-step homogenization model	135

Figure 7.2 Two-step homogenization approach for the analysis of masonry walls. Step 1: homogenization at the meso scale and determination of elastic properties of continuum elements (blue) and elastic and inelastic properties of vertical (yellow) and horizontal (red) interfaces. 137

Figure 7.3 Homogenized masonry behavior deduced from Step 1 in the homogenization model. –a: mortar interfaces input behavior. –b: homogenized horizontal and vertical stretching. 138

Figure 7.4 *Detail of Step 2 disc*retization (macro-scale) in the homogenization approach. Discretization of parallelepiped 8 noded elements for elastic parts (blue), horizontal interfaces (red) and vertical interfaces (yellow). Red and yellow solid elements obey a CDP model in Abaqus. 139

Figure 7.5 Detail of the discretization of elastic cells and interfaces (left) and state of stress of interface in the plane t-r between two adjacent solid elements (right). 140

Figure 7.6. Lateral load behavior for Wall 1: (a) Experimentally observed response, (b) Capacity curve comparison of the numerical models with experimental specimen, (c) Damaged model of commonly used homogenized model, and (d) Damaged model of the proposed homogenized model. 142

Figure 7.7. Lateral load behavior of Wall 2: (a) Experimentally observed response, (b) Capacity curve comparison of the numerical models with experimental specimen, (c) Damaged model of commonly used homogenized model, and (d) Damaged model of the proposed homogenized model. 143

Figure 7.8. Lateral load behavior of Wall 3: (a) Experimentally observed response, (b) Capacity curve comparison of the numerical models with experimental specimen, (c) Damaged model of commonly used homogenized model, and (d) Damaged model of the proposed homogenized model. 144

Figure 7.9. Damage pattern observed during the slow cyclic lateral load testing of full-scale URM building: (a) damage observed in Wall 2 and Wall 3*, and (b) damage observed in Wall 1* and Wall 3. 146

Figure 7.10. Comparison of the capacity curves for the URM building obtained from experimental study with those obtained using numerical simulation. 146

Figure 7.11. Damage pattern predicted by numerical simulation of full-scale URM building model: (a) using commonly used homogenized model, and (b) using proposed homogenized model. 147

Figure 7.12. 3D plot of variation of α_L with respect to tensile strength of masonry and aspect ratio for: (a) half brick wall, (b) full brick wall, (c) one and a half brick wall, and (d) double brick wall. 149

Figure 7.13. Reduced nodal connectivity between steel bands and masonry elements: (a) strengthened URM building, (b) simulation of Wall 3*,

(c) simulation type 1, (d) simulation type 2, (e) simulation type 3, and (f) simulation type 4. 150

Figure 7.14. Capacity curve comparison of various reduced nodal connectivity schemes. 151

Figure 7.15. Capacity curves obtained for different cross-sectional areas of steel band. 152

LIST OF SYMBOLS

Symbol		Description
ε_c^{pl}	:	Equivalent plastic strain compression
- S_i	:	Yield/flow surfaces in the deviatoric plane (i = 1, 2, 3)
ν	:	Poison's ratio
θ	:	Slope of the diagonal crack line
k_f	:	Constant equal to 0.85
f_{dt}	:	Diagonal tensile strength
ε_t^{pl}	:	Equivalent plastic strain in tension
$f_{ut}^{'}$	:	Lateral modulus of rupture
A	:	Area of net mortared section of wall
A_d	:	Design cross-sectional area of the shear-resisting portion of the wall member
a_f	:	Aspect factor based on the wall geometry
A_p	:	Cross-sectional area of the specimen parallel to the bed joint
A_s	:	Cross-sectional area of steel bands
B	:	Height factor
c	:	Coulomb friction
d_c	:	Compressive damage variables
d_t	:	Tensile damage variables
e	:	Eccentricity of n
E_0	:	Initial elastic modulus
f_a	:	Maximum axial stress
f_b	:	Maximum bending stress
fb_o	:	Bi-axial compression strength
fc_o	:	Uniaxial compression strength
f_m	:	Compressive strength of masonry prism
f_{ms}	:	Characteristic shear strength
f_t	:	Flexural tensile strength of masonry
f_{vd}	:	Shear strength of masonry
f_{vko}	:	Initial shear strength
f_{vlt}	:	Flexural tensile strength of brick unit
f_{vlt}	:	Flexural tensile strength of brick unit
f_{xd}	:	Design flexural strength appropriate to the plane of bending
G	:	Slope of assumed crack line
h	:	Height of the pier
H	:	Height of the wall
h_1	:	Height of diagonal crack

List of Symbols

h_d : Design height of wall and is taken as $h/2$
h_{eff} : Height to resultant of seismic force (effective height of wall)
h_u : Height of brick unit
k : Factor
k_1, k_2 : Coefficients based on boundary conditions
k_b : Numerical factor used to calculate the shear stress due to torque acting on a rectangular cross-section
K_c : Parameter representing the ratio between the distance from the hydrostatic axis of the maximum compression and tension
k_p : Perpend spacing factor
l : Length of the pier
L : Length of the wall
l_b : Length of the brick specimen
l_d : Design length of the wall
l_{mj} : Length of the mortar joint
l_o : Length of opening
l_u : Length of brick unit
m : Moment
M_{cd} : Diagonal bending moment capacities of the masonry
M_{ch} : Horizontal bending moment capacities of the masonry
M_e : Moment at mid height of the wall
M_e : Moment demand
M_r : Moment of resistance
N : Vertical load on pier
p : Hydrostatic pressure stress
P : Axial compression stress due to gravity loads
p_a : Evolution parameter
P_D : Superimposed dead load at the top of the wall
P_v : Failure load
P_W : Self-weight of the pier
q : Mises equivalent stress
Q_{CE} : Bed-joint sliding/rocking strength
Q_{CL} : Toe crushing/ diagonal tension strength
R_1, R_2 : Restraint factors for the supported vertical edges of the wall
R_{f1}, R_{f2} : Restrain condition
t : Thickness of the pier
t_{bar} : Thickness of the bar
t_j : Mortar joint thickness
t_u : Thickness of brick unit
t_w : Thickness of wall
V_0 : Shear bond strength of the wall section
V_1 : Shear friction strength
V_b : Base shear

V_{dt} : Diagonal tension failure
V_{tu} : Crushing failure
$V_{u,flex}$: Flexure failure
V_{us} : Shear sliding failure
W : Weight of the brick unit
w_b : Width of the brick specimen
w_d : Lateral surface pressure
w_d : Maximum lateral surface pressure
w_{d1} : Uniformly distributed load in the plane of failure acting on the wall panel per m length of the wall
Z : Section modulus of the pier section
Z_1 : Elastic section modulus of unit height or length of the wall
Z_d : Section modulus
Z_u : Section modulus of brick units
α_1, α_2 : Bending moment coefficients based on fixity at the edges of the wall
α_i : Factor equal to 0.5 for fixed-free cantilever wall, 1.0 for fixed-fixed wall pier
α_L : Ratio between peak horizontal load and total weight of the structure
α_v : H/l
β : 0.67 for l/h_{eff}<0.67; l/h_{eff} when 0.67≥ l/h_{eff} ≤1.0 and 1.0 when l/h_{eff}>1.0.
β_s : Support conditions
β_o : Material angle of friction
γ_{me} : Sliding shear strength of masonry
$\Delta\varepsilon^{\alpha}$: Equivalent creep strain rate
ε_c : Total strain in compression
ε_t : Total strain in tension
μ : Ratio of strength parallel to bed joint to strength normal to bed joint as per Eurocode 6
μ_c : Sliding coefficient of the masonry joints
$-\sigma'_i$: Principal stresses in three axis (i = 1, 2, 3)
σ_c : Uniaxial compressive stress
σ_t : Uniaxial tensile stress
τ_u : Ultimate shear bond stress
ϕ : The capacity reduction factor
ψ : Boundary condition factor

Chapter 1
INTRODUCTION

Contents

1.1. Overview 1
1.2. Types of Masonry Buildings in India 3
1.3. Behavior of URM Buildings During Past Earthquakes 6
1.4. Strengthening of URM Buildings 13
1.5. Scope and Objectives of the Present Study 14
1.6. Organization of the Thesis 15

1.1. OVERVIEW

Masonry has been one of the most commonly used construction materials since ancient times all over the world. A significant number of well-preserved masonry structures, like the great wall of China, pyramids in Cairo, Taj Mahal in India, Colosseum in Italy and many more, still exist proving that masonry structures are not only capable of resisting the earthquake loads satisfactorily, but also can successfully withstand various environmental impacts. India is one of the oldest users of masonry as a construction material and a large number of unreinforced masonry (URM) buildings, which include government offices, residences, schools, markets, and monumental structures, are commonly found throughout India.

The construction practice of using masonry in India dates back to the time of *Harappa* and *Mohenjo-Daro* (Figure 1.1), and even today, the use of brick masonry has been a common construction practice in the country, especially in rural areas. Primary reasons for continuation of such construction practice in India are inexpensive and readily available construction materials and labour, and high durability of masonry.

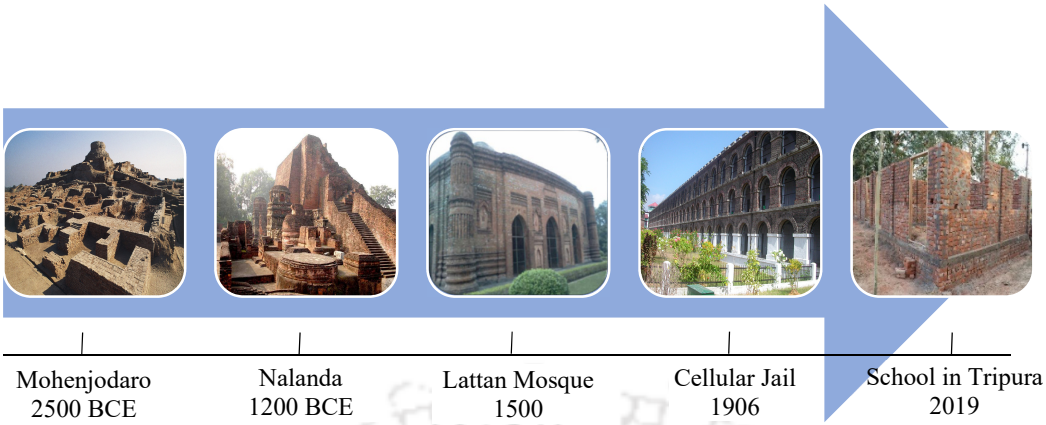

Figure 1.1. Brick masonry structures since ancient times to existing construction practices.

One of the primary advantages of masonry construction is that the same element can be used to perform a variety of functions. Masonry walls are used in a structure for division of space, thermal and acoustic insulation, as well as for protection from fire and weather. Masonry walls are known to carry the vertical loads in a very safe and stable way because of their high compressive strength. However, due to their huge mass and high stiffness, URM buildings also attract large seismic forces during strong earthquake shakings. It is a well-known fact that masonry is very weak in tension; therefore, seismic vulnerability of URM building is quite high unless they are adequately strengthened (Hendry et al., 1997; Tomaževič, 2011). The high seismic vulnerability of URM buildings is due both to the particular configuration (often characterized by open space, slender walls, lack of active connections among the structural elements) and to the mechanical properties of the masonry material (highly non-linear behavior and very small tensile strength) (Shariq et al., 2008). In addition, the following reasons have long been identified for the seismic vulnerability and risk associated with URM buildings (Cardoso et al., 2005):

a) Age and consequent degradation of structural materials leading to a decrease of local and global stiffness and strength
b) Large number and variety of structural changes that these structures undergo during service time without considering their effect on the seismic performance
c) Non-compliance to the design codes, especially the seismic design codes.

Due to these issues and the characteristic behavior of masonry, many URM structures have performed poorly during past earthquakes.

1.2. Types of Masonry Buildings in India

A recent census showed that a large number of buildings in India, especially in rural areas, are still constructed using URM. There is a huge concentration of URM buildings in high seismic zones, for example, the regions near the Himalayan foothills (see Figure 1.2). Interestingly, most of the regions having high density of URM buildings are also the regions with large population density.

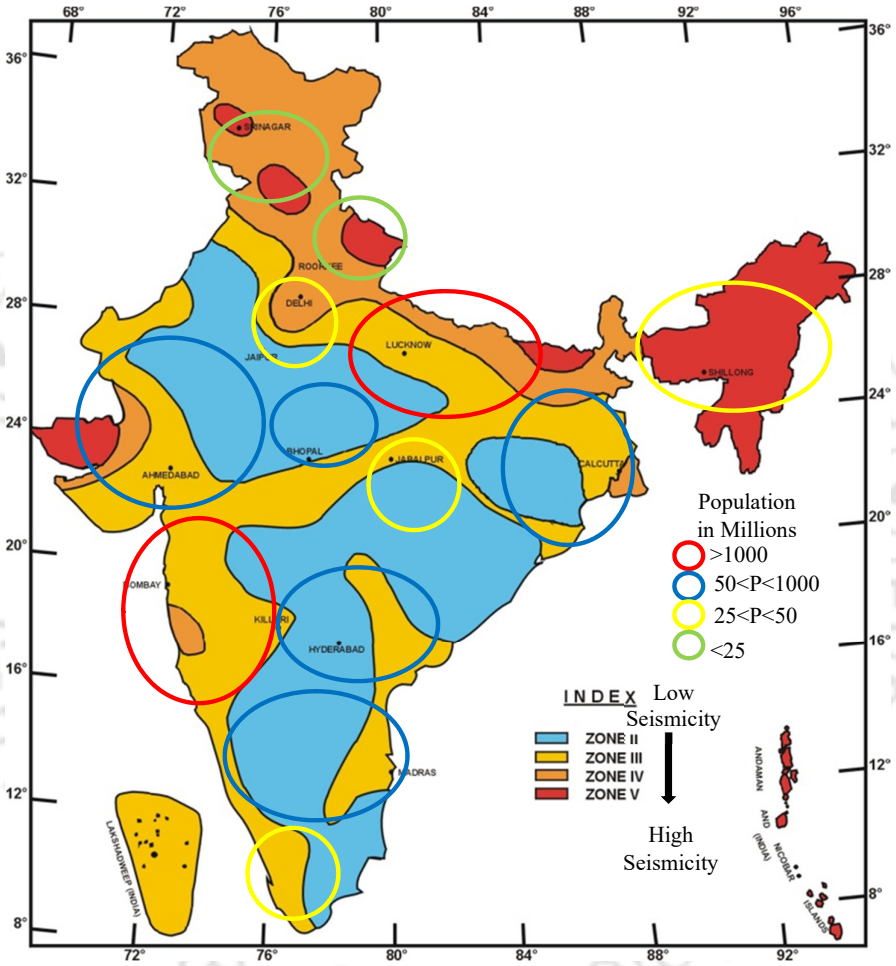

Figure 1.2. Map of India showing concentration of URM buildings in region with large populations (Seismic zones from BIS 2016, Population from Census 2011).

Broadly, four categories of unreinforced brick masonry buildings are commonly found in India. Each of these are discussed below in brief.

1. Unreinforced brick masonry with reinforced concrete slab
2. Unreinforced brick masonry with pitched clay tile roof
3. Unreinforced brick masonry walls in mud mortar with timber roof
4. Unreinforced brick masonry with GI sheet roof

1.2.1. Unreinforced Brick Masonry with Reinforced Concrete Slab

URM buildings with reinforced concrete (RC) slab can be found in all parts of the country. People in both rural and urban areas have adopted to construct this type of buildings. The buildings in rural areas are mostly of single-storey; however, in urban areas, the URM building of two to three storeys are commonly constructed (Figure 1.3a). Although, the RC slab holds the walls together more efficiently due to rigid diaphragm action, construction of such buildings without seismic features can be vulnerable to earthquake effects. These type of buildings exhibited rather poor performance during the Koyna (1967), Killari (1993), Jabalpur (1997), and Bhuj (2001) earthquakes in India (Sinha and Brzev, 2002).

1.2.2. Unreinforced Brick Masonry with Pitched Clay Tile Roof

Using pitched clay tile roof over URM buildings is a traditional construction practice followed in India for centuries. Buildings of this construction type are commonly used for residential, commercial, and public purposes throughout India, especially in the northern and central parts, where good quality clay for brick production is widely available. These types of buildings are widely constructed both in rural and urban areas. (Figure 1.3b). The walls are constructed using clay bricks laid in mud, lime or cement/mortar. The peculiar roof of these buildings does not act like a rigid diaphragm. These buildings are mostly built without any seismic considerations and hence, they are considered to be moderately-to-highly vulnerable to earthquake effects (Kumar, 2002).

(a) (b)

Figure 1.3. Type of URM buildings: (a) Unreinforced brick masonry with reinforced concrete slab, and (b) Unreinforced brick masonry with pitched clay tile roof (Kumar, 2002).

1.2.3. Unreinforced Brick Masonry with Timber Roof

URM buildings with timber roofing have been a traditional construction practice prevalent both in the urban and rural areas of northern India (Figure 1.4). Typically, this is a single-story construction. In many cases, the unreinforced brick masonry walls are constructed using mud mortar without any seismic provisions. The roof structure consists of timber beams supported over the walls. Clay tiles or bricks are laid at the top of the timber beams; finally, mud overlay is used on the top of the tiles or bricks for thermal protection and to prevent leakage. Naturally, the roof does not behave like a rigid diaphragm. The primary seismic deficiencies of such buildings are heavy roofs and low-strength masonry walls, which render the building more vulnerable to seismic effects (Khan and Khalid, 2002).

(a) (b)

Figure 1.4. Type of URM buildings: (a) Overview of unreinforced brick masonry with timber roof, (b) Structural details of roof (Jain, 1993).

1.2.4. Unreinforced Brick Masonry with GI Sheet Roof

This type of construction practice is found in the eastern and northeastern part of India. Buildings of this construction type are used for residential and public purposes. This is a single-story construction used both in rural and urban areas (Figure 1.5). The walls are constructed using clay bricks laid in mud, lime or cement/mortar. The roof is made of GI sheet and does not behave as a rigid diaphragm. These buildings are generally built without any seismic provisions and are considered to be moderately-to-highly vulnerable to earthquake effects (Ansary 2003).

Figure 1.5. An unreinforced brick masonry house with GI sheet on roof.

1.2.5. Seismic Vulnerability of Unreinforced Brick Masonry Buildings

Seismic risk of unreinforced masonry buildings can be assessed by first assessing the seismic vulnerability of the buildings. Three approaches are generally used for the vulnerability assessment: (a) the empirical approach which is based on damage statistics from past earthquakes; (b) the analytical approach which is based on simulation of the seismic response of selected buildings; and (c) the hybrid approach which is based on a combination of analytical and empirical approaches (Singh et al., 2013). The hybrid approach is often useful due to the fact that sufficient empirical data for a range of building types subjected to different intensity levels can be generated and the analytical results are calibrated with the empirical data. The vulnerability analysis of the above mentioned four categories of unreinforced brick masonry buildings in India was done by Ansary (2003), Khan and Khalid (2002), Kumar (2002), Sinha and Brzev (2002), respectively, by considering the various building features like architectural aspects, building configuration, structural details, load resisting systems, floor and roofing system, foundation and site conditions, etc. These studies reported that the above category of buildings can be classified to have medium to high seismic vulnerability.

1.3. Behavior of URM Buildings During Past Earthquakes

The twenty-first century has already seen several damaging earthquakes worldwide. Some of these earthquakes resulted in severe damage to URM buildings demonstrating the high seismic vulnerability of these buildings. Performance of URM buildings during some of these earthquakes, which resulted in large-scale destruction of URM buildings, is discussed here.

1.3.1. Bhuj, Gujarat Earthquake, 2001

The powerful earthquake struck the Kutch area in Gujarat at 8:46 am on 26 January 2001. The M_w 7.9 quake caused a significant loss of life and property. Buildings in the affected area were mainly the older non-engineered buildings made with load-bearing masonry walls supporting the tiled roof or RC slab roof. Buildings constructed with brick masonry in mud/cement mortar were commonly constructed in the area. Some of the notable deficiencies of these buildings were: (a) walls were not sufficiently connected to each other and to the roof, (b) separation of the 40-60 cm thick masonry walls into two distinct wythes, and (c) failure of the rather heavy RC slab or "Mangalore" clay tile roofing system with thick wooden logs as purlins and rafters. Many such URM buildings collapsed during the earthquake as shown in Figure 1.6 (Jain et al., 2002).

Figure 1.6. Collapse of the upper storey of a URM building under construction at Bhachau in Gujarat (Jain et al., 2001).

1.3.2. North Kashmir Earthquake, 2005

On 8 October 2005, at 8:50 am local time, a major earthquake struck the northern Kashmir. The moment magnitude of the earthquake was about 7.6. Majority of buildings in this region were constructed using unreinforced masonry. These masonry constructions represent box-type structures in which the lateral load resistance against the earthquake forces was provided by the membrane action of the diaphragms (floors and roofs) and bearing walls. Both in-plane and out-of-plane damages was observed in the buildings located in the affected areas (Figure 1.7). However, typical timber-laced brick masonry constructions, commonly called *Dhajji-dewari* and *Taq* had displayed a remarkable performance during the earthquake. Presence of the closely spaced wooden members in the masonry walls reduced the crack propagation and prevented the out-of-plane collapse (Figure 1.8) (Rai and Murty, 2005).

(a) (b)

Figure 1.7. Failure in URM Buildings: (a) Out-of-Plane collapse of URM walls, and (b) Diagonal cracks in window openings and tilting of walls during North Kashmir Earthquake (National Disaster Management Division 2006).

(a) (b)

Figure 1.8. Traditional masonry for proven earthquake resistance: (a) *Dhajji-dewari* system of timber-laced masonry for confining masonry in small panels, (b) *Taq* system of embedding timber logs in thick walls (Rai and Murty, 2005).

1.3.3. Sikkim Earthquakes, 2006, 2011

On 14 February 2006, a moderate earthquake (M_w 5.3) hit Sikkim at 6:25 am (Kaushik et al., 2006). Among many building stocks which suffered a varied level of damages, stone and brick masonry buildings bore most of the brunt. It was reported that a two storey URM Archive building in Gangtok (the capital city of Sikkim), which was retrofitted using 50 mm × 8 mm steel flats on the surfaces of the walls after 1988 Bihar-Nepal Earthquake, had survived the earthquake with no damages (Figure 1.9). This indicates that timely and sensible retrofitting of vulnerable buildings can save such building from damages in future earthquakes. On 18 September 2011, an earthquake of M_w 6.9, followed by several aftershocks with magnitudes more than 4.0, struck Sikkim at 6:11 pm local time. Several casualties with significant damages to URM buildings were reported in the entire state of Sikkim and part of West Bengal and Bihar in India (Kaushik and Dasgupta, 2014). The

Archive building, which was strengthened with steel flats after 1988 Bihar-Nepal Earthquake and survived the 2006 Sikkim earthquake, suffered moderate level of damages in the 2011 earthquake (Figure 1.10).

Figure 1.9. Excellent performance shown by retrofitted Archive building during 2006 Sikkim earthquake (arrows indicate locations of steel flats used to retrofit the building after 1988 Bihar-Nepal earthquake) (Kaushik et al., 2006).

(a)

(b) (c)

Figure 1.10. Performance of the retrofitted Archive building during 2011 Sikkim Earthquake: (a) out-of-plane movement of the walls bending the steel flats, (b) missing steel bars that should connect the steel flats on both faces of the walls, and (c) failure of the welded connection in the steel flats due to out-of-plane movement of the walls.

Severe cracking at numerous locations of the walls and out-of-plane movement of walls were reported in this earthquake. It was reported that the poor maintenance of the retrofitting components was one of the primary reasons for such damages. The steel flats used for retrofitting were found to have rusted at various locations. Moreover, the steel bars used to connect the bands on the two faces of the walls were found to have broken over the years (Figure 1.10b). At some locations, the welded connection between steel flats at the corner of the building also failed due to out-of-plane movement of the walls (Figure 1.10c). Though the poor maintenance resulted in significant reduction in effectiveness of the retrofitting measures, the simple and cost-effective retrofitting scheme prevented the collapse of the building.

1.3.4. Varzaghan-Ahar twin Iran Earthquakes, 2012

On 11 August 2012, twin earthquakes with M_w 6.4 and M_w 6.3 hit the twin cities of Varzaghan and Ahar in Iran. Most of the buildings, which suffered damages, were the adobe and URM buildings. The main reasons of failure of these building were heavy roofs, in-plane and out-of-plane failure of walls and non-compliance of codes (Figure 1.11a, 1.11b). It was also observed that the URM building with seismic features, like ring beams and minimum code compliance suffered only minimal damages (Figure 1.11c). The report also emphasized the significance of the introduction of reinforced concrete ring beam in the masonry building construction for improved earthquake performance (Razzaghi and Ashtiany, 2012).

(a) (b) (c)

Figure 1.11. Performance of URM buildings during 2012 Iran earthquakes: (a) Failure of heavy steel jack-arch, concrete roofs and walls of URM buildings, (b) out-of-plane collapse of walls in URM buildings, and (c) buildings compliant with minimum code requirements survived the earthquake with minor damages (Razzaghi and Ashtiany, 2012).

1.3.5. Christchurch Earthquakes, 2010, 2011

A M_w 7.1 earthquake struck the Canterbury region of New Zealand on 4 September, 2010. This was followed by two strong earthquakes in the nearby regions on 22 February, 2011 (M_w 6.2) and 13 June 2011 (M_w 5.9). The damage was mostly observed in the central part and eastern suburb of Christchurch city. More than thousand buildings suffered extensive damage. A good number of these buildings were URM buildings (Figure 1.12) including important heritage structures and residential buildings, which were on the verge of collapse due to irreparable damage (Hare 2013). The damages consisted of both in-plane and out-of-plane collapse of URM walls. It was also reported that the suitably strengthened URM and heritage buildings performed very well and provided a model for such retrofitting in other cities (Figure 1.13).

Figure 1.12. Severe Damage to several types of URM structures during the Canterbury earthquakes (Hare 2013).

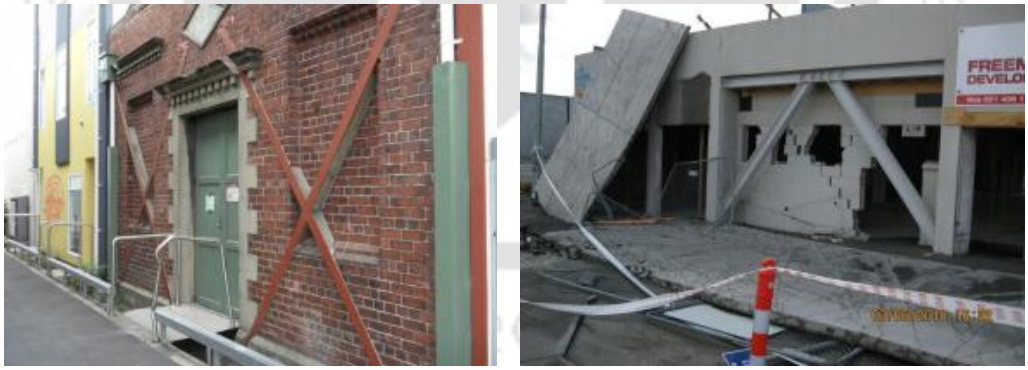

Figure 1.13. Buildings strengthened with steel frames survived the Canterbury earthquakes with repairable damage (EERI 2013).

1.3.6. Nepal Earthquake, 2015

On 25 April 2015 at 11:56 am local time, Gorkha earthquake of M_w 7.8 hit Nepal followed by a strong earthquake sequence. Over 672 aftershocks were recorded in the year following the main shock. The destruction was widespread covering various types of residential and government buildings. Hundreds of historical and cultural URM monuments were severely

damaged (Figure 1.14). Walls in URM bearing wall buildings are typically made from brick masonry, stone masonry, or adobe using mud, lime, or cement mortar.

(a) (b)

Figure 1.14. Performance of URM buildings during Nepal Earthquake: (a) in-plane wall damage, and (b) out-of-plane collapse of masonry walls (Lizundia et al. 2016).

The URM walls rest on either a brick or stone foundation. Roofing in these buildings primarily consisted of corrugated GI sheets or clay tiles on wooden joists. In several cases, masonry wythes were reported to be poorly connected and the seismic features recommended for URM walls in seismic-prone areas were found to be missing. Therefore, wythe delamination was commonly observed in many URM buildings. Besides, in-plane wall damage was generally observed in the form of cracks in wall piers near openings and out-of-plane damage was observed in large number of URM buildings primarily due to poor diaphragm to wall ties (Lizundia et al., 2016; Varum et al., 2018).

1.3.7. Common Observations

Based on the behavior of URM buildings from several recent earthquakes in India and other countries, the following points can be noted:

- The corners of walls near openings are most vulnerable.
- Out-of-plane collapse of walls was commonly observed if connectivity between walls, slabs, and other structural elements was not proper.
- In-plane shear failure was commonly observed in walls with larger and more number of openings.

- Buildings with reinforced ring beam or lintel bands and those strengthened with some strengthening schemes performed satisfactorily with minor damages.
- Strengthening of URM buildings was not common due to the absence of design and construction guidelines.
- It is extremely important to strengthen the vulnerable URM buildings to improve the lateral load behavior of such buildings.

1.4. STRENGTHENING OF URM BUILDINGS

Post-earthquake reconnaissance reports by various authors cite that buildings constructed following the code provisions and those strengthened in a timely manner have survived even major earthquakes with repairable damages (Kaushik and Dasgupta, 2014; Kaushik et al., 2006; Murty et al., 2006; National Disaster Management Division, 2006). Strengthening of URM buildings is significant not only for saving a large number of humans residing in such buildings, but also for saving the monumental, heritage, and religious structures from severe damage during earthquakes. Such strengthening schemes should be simple, easily implementable, and cost-effective.

The existing codes like IS 13935 (BIS, 2009) recommend grout or epoxy injection in existing weak walls and use of split and bandage technique using wire mesh as a strengthening solution. The codes also recommend tying the walls by pre-stressing techniques. Besides, the recent strengthening interventions suggest the use of fiber-reinforced polymer; such materials bear the substantial cost and need skilled supervision. Moreover, the given strengthening solutions by codes require sophisticated equipment and skilled labour, which one way or other does not seem to be sustainable. It has also been observed that various strengthening schemes were adopted in the past to strengthen such buildings, and steel has been a popular choice of material for strengthening. For example, El-Borgi et al. (2005) proposed a retrofit scheme to strengthen a historical building at Tunisia that consisted of a steel frame attached directly to the portrait room structure with added fluid viscous dampers. Recent studies indicate that tying wall with steel ties prevents separation and disintegration of walls, and improves seismic behavior of the structure (Borri et al., 2009; Vincente et al., 2011). Besides Branco and Guerreiro (2011) showed that the use of steel ties can be less expensive and does not contribute to an excessive increase in the structure's weight, and it minimizes the interruption of the normal functioning of the building. According to Tassios (2010), addition of steel elements as shear

connectors, along transversal wall intersections, in case of cracks for stitching or in case of passing through connectors of three-leaf masonry, can be adopted to strengthen masonry wall. Therefore, due to various advantages of steel, use of steel members to strengthen the vulnerable unreinforced masonry buildings can be a sustainable solution to reduce the seismic risk associated with such buildings.

1.5. SCOPE AND OBJECTIVES OF THE PRESENT STUDY

The motivation of the present study comes from the fact that the lateral load performance of large number of URM buildings constructed in seismically-prone regions of developing countries require immediate strengthening intervention. A simple, easily implementable using locally available materials, and cost-effective strengthening scheme is required to be developed for its wide adoptability and acceptability. One such strengthening scheme using surface-mounted steel bands was developed and tested in the present study. To scientifically investigate the suitability and effectiveness of using surface-mounted steel bands as a strengthening scheme for URM buildings, the following objectives and work plans were formulated for the present study.

i. **Experimental evaluation of URM walls with various opening configurations**
   Masonry walls are the most important structural component of the URM buildings. Understanding the influence of various openings configurations (door, window) on the lateral load carrying capacity of the walls are relevant for the initial study. Full-scale individual URM walls were tested under slow-cyclic lateral loading and their lateral load behavior was evaluated.

ii. **Experimental evaluation of the strengthening scheme**
   Single storey full-scale URM building specimens were tested under cyclic lateral loads to understand the lateral load response and failure modes of un-strengthened URM building. Two new specimens of the full-scale URM building were then strengthened using surface-mounted steel bands in different configurations and subjected to slow-cyclic lateral loading. The building specimens were composed of the individual wall specimens already tested. Enhancement in the lateral load behavior of the strengthened buildings was evaluated based on the experimental study.

iii. **Analytical evaluation of the lateral strength of URM buildings**

Based on the experimental results, simple analytical models were developed to estimate the lateral load carrying capacity of URM buildings using the lateral capacity of individual URM walls. Several relations available in the past literature for estimation of lateral strength of URM walls were utilized in development of the analytical models, and most effective model for lateral strength estimation was suggested based on a comparative study.

iv. **Numerical evaluation of the lateral load behavior of URM walls and buildings**

The experimentally obtained data was utilized in the development of nonlinear numerical simulation models using various existing modeling methods. The calibrated numerical models were used in a parametric study to understand the influence of several important parameters, like aspect ratio, tensile strength of masonry, wall thickness, etc., on the improvement of lateral load behavior due to strengthening. A novel homogenized discretization method was also proposed for numerical simulation of URM buildings for improving the accuracy of damage prediction.

v. **Empirical estimation of lateral strength of URM buildings**

Based on regression analysis of the experimental and numerical results, simple empirical relations were developed to estimate the lateral load carrying capacity of the strengthened URM buildings using some of the important building and material parameters.

The present study is an effort to evaluate the suitability and effectiveness of a simple strengthening scheme for URM buildings using surface-mounted steel bands. For achieving this primary objective, full-scale walls and buildings (un-strengthened and strengthened) were tested under quasi-static lateral loading, and analytical, numerical, and empirical models were developed for the assessment of their lateral load carrying capacity.

1.6. ORGANIZATION OF THE THESIS

The present study broadly addresses five main aspects related to unreinforced masonry discussed in five main chapters of the thesis. After providing introduction and reviewing the literature in Chapter 1 and 2, respectively, Chapter 3 covers the preliminary numerical investigation to study the effectiveness and suitability of the existing numerical evaluation

methods for URM buildings. This is followed by characterization of the material properties of masonry and experimental evaluation of the individual walls with various opening configurations as discussed in Chapter 4. The next chapter provides details on experimental evaluation of the strengthening scheme for the URM building by testing three URM buildings. Chapter 6 presents the numerical evaluation of the walls and buildings that were previously tested. The chapter also discusses the applicability and effectiveness of various analytical methods in estimating the in-plane and out-of-plane capacity of the URM walls constituting the building. Chapter 7 provides details on development of a new simulation technique of URM walls and buildings. The empirical equations developed to evaluate the overall lateral load carrying capacity of the building are also discussed along with the effectiveness of adopting the suggested strengthening intervention. The thesis is concluded with the final observations and recommendations in Chapter 8.

Chapter 2
LITERATURE REVIEW

Contents

2.1. Overview 17
2.2. Behavior of URM Walls Subjected to Lateral Loading 18
2.3. Behavior of URM Buildings Subjected to Lateral Loading 29
2.4. Strengthening of URM Buildings 33
2.5. Summary and Identified Gap Areas 38

2.1. OVERVIEW

Numerous past earthquakes worldwide have demonstrated the poor performance of unreinforced masonry (URM) buildings due to several reasons. The high seismic vulnerability of URM buildings is primarily due to low tensile and shear strength of masonry, high seismic weight, and low ductility. Besides, factors like building geometry, wall-to-wall connectivity, lateral stiffness, imposed loads, and presence of nonstructural members highly influence the seismic behavior of URM buildings. Despite this, URM buildings are widely adopted in many countries even today due to inexpensive construction and readily available material. About 70% of India's population lives in rural areas, where a good number of people still live in various forms of masonry houses. Besides, sizeable building stocks in various cities located in earthquake-prone areas are also masonry buildings. In a large number of cases in several developing countries, URM buildings were built considering mostly the vertical loads and reference to seismic codes were generally not accounted for. Since URM buildings represent a good number of building stock in seismic areas of these countries, seismic assessment and strengthening of URM buildings have become a crucial issue for study.

A typical URM building consists of foundation, structural walls, and either rigid or flexible diaphragm based on the type of roofing system. During an earthquake, the buildings are subjected to a series of cyclic horizontal shakings, which will cause bending and shear stress in the structural wall components since they are the primary load resisting elements of the building. In order to evaluate the performance of the building, it is essential to understand the mechanics of the structural walls that constitute the primary load bearing member of the building. This chapter reviews the literature on relevant works related to the behavior of the URM structural walls and URM buildings subjected to lateral loading. The provisions suggested by various existing codes of practice of different countries have also been discussed. Based on the structural performance of the walls and buildings, various strengthening interventions suggested by codes and developed by various authors have been elaborated in this chapter.

2.2. BEHAVIOR OF URM WALLS SUBJECTED TO LATERAL LOADING

URM buildings typically consist of foundations, URM walls oriented in orthogonal directions to each other, and rigid floor/roof that acts as a diaphragm and is connected to the walls. The URM walls are typically stiff structural elements, which are the main structural elements to resist the loads both vertically and laterally. These walls can be categorized into in-plane and out-of-plane walls depending on the direction of earthquake motion relative to the plane of the walls. The walls oriented parallel to the action of earthquakes are called in-plane walls, and the walls perpendicular to in-plane walls are defined as out-of-plane walls. The failure mechanism of these two wall categories are discussed in the following subsections.

2.2.1. In-Plane Behavior of Masonry Walls

Numerous past experimental studies have concluded that the URM walls subjected to in-plane horizontal loads may fail in one of the following four ways: (i) sliding shear failure, (ii) flexural/rocking failure, (iii) diagonal shear failure, and (iv) toe crushing failure (ASCE/SEI 41-13 2014; Magenes and Calvi 1997; Petry and Beyer 2015; Shahzada et al. 2012; Tomaževič 2011; Wilding and Beyer 2016). The mode of failure is influenced by many factors, such as the aspect ratio of the walls, level of axial compression stresses, boundary conditions, and the strength characteristics of the materials used for construction. The failure occurs when the principle tensile stress due to the combination of vertical and horizontal loads exceeds the tensile strength of the masonry material. However, the amount

of axial load acting over the wall primarily controls the type of failure in the URM walls. Low axial load and poor-quality mortar lead to sliding shear failure when the wall is subjected seismic action. Sliding shear is primarily the shearing of the wall in two parts resulting in sliding of the upper part of the wall over the horizontal mortar joints (Figure 2.1a). The rocking/flexural failure occurs at the base of the wall when the horizontal load or displacement demand increases, and shear is carried by compressed masonry. The final failure is achieved by overturning action of the wall, and cracks generate from one end of the wall progressing along the mortar line till failure (see Figure 2.1b). At high level of vertical axial load, diagonal shear and toe crushing failure are common. Diagonal shear failure, which is also termed as diagonal tension failure is characterized by diagonal cracks developed in the wall where the cracks follow either the mortar joints or pass through the brick units or both (Figure 2.1c). However, in the case of high shear resistance and vertical loads, crushing of compressed zones at the end of the wall takes place, leading to toe crushing failure (Figure 2.1d)

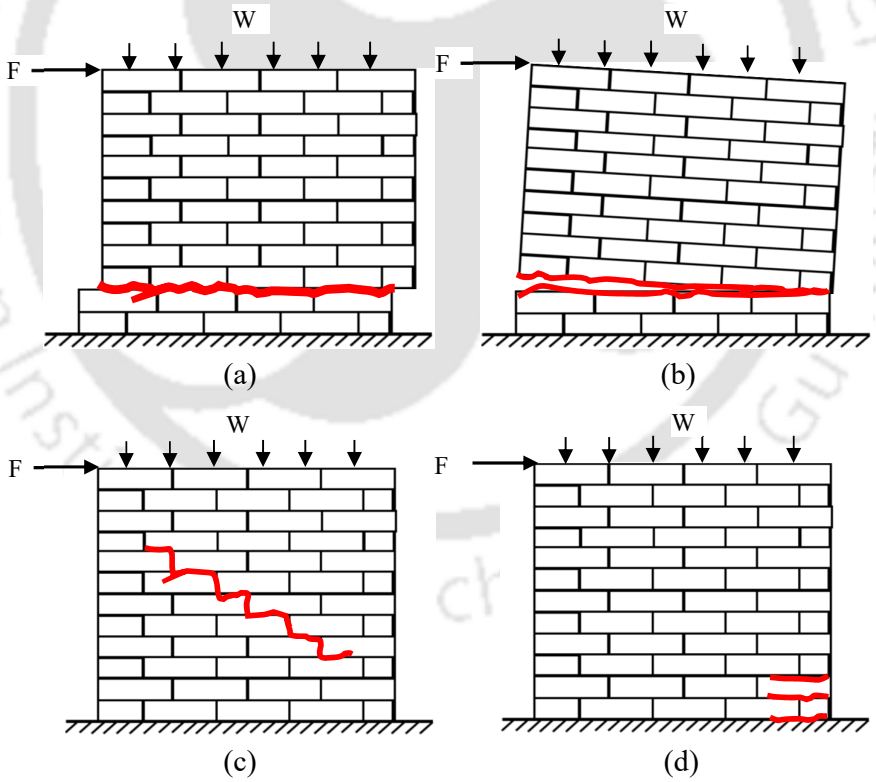

Figure 2.1. In-plane Failure pattern of masonry walls: (a) shear failure, (b) rocking/flexural failure, (c) diagonal shear failure, and (d) toe crushing failure.

The empirical equations to calculate the strengths associated with these failure modes were given by Magenes and Calvi (1997). The equations were developed based on the contributions by Turnšek and Čačovič (1970) and Mann and Müller (1980). The failure criterion suggested by Turnšek and Čačovič (1970) was based on the assumption that the masonry is a homogeneous and isotropic material. Whereas, the theory suggested by Mann and Müller (1980) considered masonry as anisotropic material, a behavior most coherent with the actual behavior of brick masonry. The equations were verified by Calderini et al. (2009) and stressed the necessity of defining suitable strength domain of masonry piers through a set of criteria, considering one approach for each failure mode (*rocking/crushing, bed joint sliding, diagonal cracking*). A different set of equations to estimate the lateral strength for various failure modes were also developed by Yi et al. (2008), and the equations were verified by Russel and Ingham (2010) by performing experimental study on six solid URM wall specimens (Figure 2.2). The equations were further improved and were introduced in ASCE/SEI 41-13 (2014).

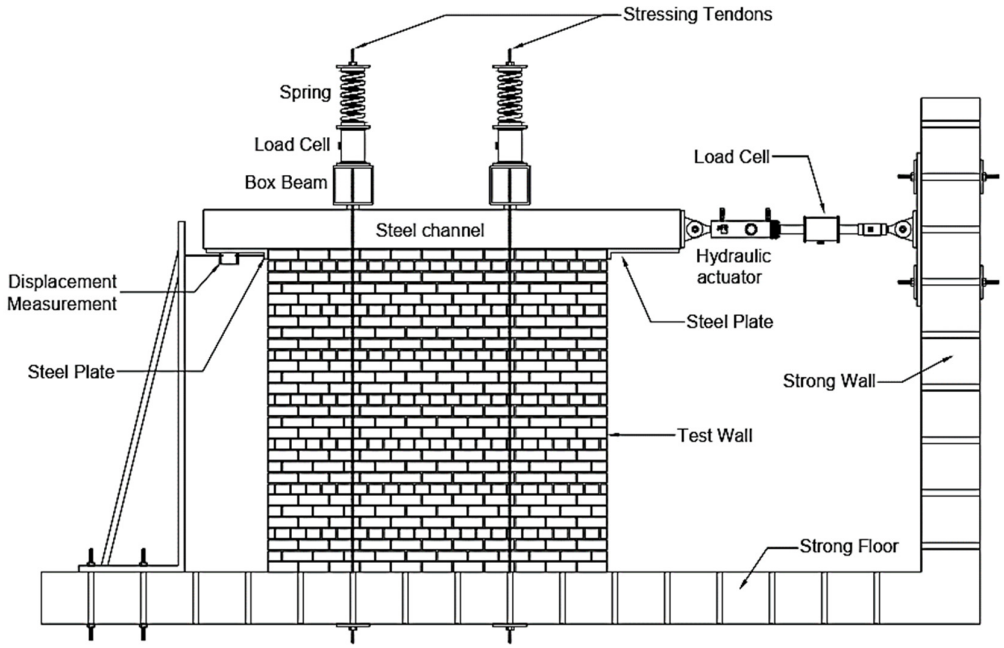

Figure 2.2. In-plane test setup for URM wall (Russel and Ingham 2010).

The approaches to evaluate the lateral strength suggested by Magenes and Calvi (1997) did not consider the effective height of the masonry piers, and the role of openings in the walls were neglected. However, Yi et al. (2008) included effective height in their proposed approaches based on location of openings in the URM walls. Moon et al. (2006) also affirmed the proposed approach and found the effective height of the wall with opening to

be either horizontally or at 45° or at the steepest possible angle. Mojsilović (2011) suggested a new system of in-plane failure regime, which considers slip failure along the head joints line, which could be observed in compression tests and which could compromise the safety of the design based on the existing criterion. Mojsilović (2011) also proposed the simplified variation of uniaxial masonry strength as a function of the angle of inclination of the principal compressive stress relative to the head joints direction; the simplified approach was developed for practical applications. However, the suggested novel approach still needs further research on predicting the various failure modes, and the discrepancies in the previous approaches were not addressed in this work.

The role of geometric irregularities, mostly related to the irregular walls and openings, in the lateral strength estimation was addressed by Parisi and Augenti (2013). The openings in walls were characterized by (i) openings of different sizes, (ii) openings misaligned in the horizontal and/or vertical direction, or (iii) a variable number of openings per storey. The proposed methodology suggests use of a global irregularity index (indicates whether a perforated wall is regular or not) and *a partial irregularity index,* which quantifies the distribution of irregularity throughout the masonry wall. Despite the improvement in the formulation, authors recommended further research to address issues like the seismic capacity sensitivity to offset irregularities, role of different number and size of openings, and investigation on the effects of complex irregular configurations on seismic capacity.

Javed et al. (2015) carried out an experimental investigation over 12 URM walls in the in-plane direction based on typical geometry and pre-compression levels. The influence of relative pre-compression level and aspect ratio on the damage pattern, ultimate drift ratio, and equivalent viscous damping of the walls were examined. It was observed that the magnitude of the relative pre-compression level influenced the extent of cracking in walls and cracking patterns of walls with the same aspect ratio (Figure 2.3). Most of the shear cracks in walls with higher pre-compression levels passed through the bed and head mortar joints, causing stair-stepped cracks. On the other hand, shear cracks in walls with lower pre-compression level passed through bed and head mortar joints as well as brick units. It was also seen that moderate increases in relative pre-compression levels caused increases in ultimate drift ratios. However, the walls tested were solid walls, and damage patterns on

walls with various opening configurations with different pre-compression levels could be an essential topic for study.

Figure 2.3. Inclined diagonal cracks due to in-plane loads (Javed et al., 2015).

To study the influence of wall geometry and vertical pre-compression on the in-plane walls with openings, Allen et al. (2015) carried out experimental study on 12 full-scaled wall specimens and established force-displacement relationships for walls with openings. Besides, it was observed from the experimental results that at low axial load, failure was likely to be confined to the piers. At higher axial loads, spandrel failure and mixed failure modes were likely to occur.

Wilding and Beyer (2016) introduced an analytical model to compute the monotonic force-displacement response of in-plane loaded unreinforced brick masonry walls accounting for walls failing in shear or flexure where the masonry wall was modeled as elastic in compression with zero tensile strength using a Timoshenko beam element. The diagonal cracking of shear critical walls was represented by one critical diagonal crack, and the ultimate drift capacity of the wall was determined based on an approach evaluating a plastic zone at the wall toe. The method was validated by performing cyclic full-scale tests on unreinforced masonry walls made with vertically perforated clay units. The study claimed that the proposed methodology outperforms the current empirical code equations concerning stiffness and ultimate drift capacity estimates and yields similar results concerning the strength prediction. However, as seen in most other cases, the method was

validated using solid wall. It's suitability over varying super-imposed load, wall geometry and presence of openings are yet to be ascertained. The authors in their work (Wilding and Beyer 2018a), also studied 79 shear-compression tests of modern URM walls of different masonry typologies from the literature. They showed that both the initial and the effective stiffness increase with increasing axial load ratio and that the effective-to-initial stiffness ratios are approximately 75% rather than the stipulated 50%. Therefore, they proposed an empirical relationship that estimates the elastic modulus as a function of the axial load and the masonry compressive strength. In addition, Wilding and Beyer (2018b) also developed an analytical model to predict the ultimate in-plane drift capacity for both shear and flexure controlled URM walls based on a series of tests on URM walls.

One of the significant challenges in analysis of the URM masonry walls is to take into account the uncertainty involved in defining the material properties of the masonry, which is mainly due to workmanship and various stages of construction (Rao et al., 1996). Tabbakhha and Deodatis (2016) studied the effect of random spatial variability of mortar joint properties on the lateral strength of masonry walls under in-plane loads. The tensile strength of mortar joints is considered a random variable whose variation represents different quality of workmanship. Their findings revealed that increasing the correlation of bed joint properties has a harmful effect on the lateral strength of unreinforced masonry walls with good and poor workmanship quality. Therefore, the authors recommended that quality control in the site during construction can help in reliable prediction of the wall strength and failure mechanism.

Despite the numerous upgrades in estimating the lateral in-plane strength of the URM walls, most of the existing codes still lag in implementing the latest recommendations. Codes like Eurocode 6 (EN 1996-1-1, 2005) and Australian Standard (AS-3700, 2018) suggest the in-plane lateral capacity of a URM wall to be equal to the shear resistance of the wall at the base calculated by multiplying the loaded area with the unit shear strength of the masonry. The Australian Standard also expresses the in-plane strength as the sum of the bond strength and the frictional strength. Whereas in the Indian code (BIS, 1987), the lateral design load is estimated by taking the minimum of flexural, compressive, tensile and shear strength. Codes like, ASCE/SEI 41-13 (2014) and New Zealand Seismic Assessment Guideline (NZSEE et al., 2017) adopted some of the advanced methods of structural assessment taking into account the various failure modes,

and practices that were suggested for estimation of the lateral load corresponding to each failure modes.

Additional details about the methods developed by past researchers and recommended by the design and assessment codes along with all the relevant equations are provided in chapter 6.

2.2.1.1. Gap Areas

Review of some of the recent relevant literature related to the in-plane behavior of URM walls shows that numerous experimental, numerical, and analytical studies have been conducted on to develop methods for estimation of lateral strength of URM walls. In addition, several design and assessment codes recommend some methods for the estimation of lateral strength of URM walls. Considering the huge variation in the material properties of masonry and the construction methodologies, a large difference in the recommendations of different studies and codes was observed. Influence of openings on the lateral strength of URM walls has been studied on limited configurations of window and door sizes and locations. Following gap areas are identified in the state-of-the-art with respect to the in-plane behavior of URM walls:

- Influence of different wall geometry and boundary conditions on the lateral load behavior of the low-strength masonry walls has not been studied.
- Not all studies have considered the influence of effective height of walls, especially when openings are present in the walls, on the capacity estimation. Further in-depth study on the influence of openings on the in-plane strength of the wall is required to be carried out.
- The contribution of the lateral strength of individual walls to the overall strength of the building has not been studied in detail. Such a study can enhance the effectiveness of seismic design of the wall components in the building.
- A feasibility study is required to be carried out on applicability of various analytical methods suggested by the codes of various countries as well as by the past researchers in estimation of lateral strength of URM walls, especially those constructed using low-strength masonry used commonly in developing countries.

2.2.2. Out-of-plane Behavior of Masonry Walls

Out-of-plane (OOP) mechanisms occur with out-of-plane kinematics of one or more walls of masonry buildings, causing the loss of its original configuration during large seismic excitations (Figure 2.4). The OOP failure mechanism mainly results due to the deficient connection between the walls of the URM buildings (Murty, 2002). The analytical methodologies to evaluate the out-of-plane failure mechanism was developed by Sinha (1978) by introducing the fracture line method and the approaches were further improved by Hendry et al. (1997). This method considered masonry as a homogenous material, and the internal actions like moments were assumed to be acting along the cracks in the walls simultaneously; such assumptions grossly overestimate the OOP strength of the wall. On the other hand, Priestley (1985) suggested a velocity-based approach to analyze the wall subjected to out-of-plane lateral loads considering the energy balance of the responding wall. The main disadvantage of this procedure is that the energy demand is very sensitive to the selection of elastic natural frequency and is only relevant for a narrow band of frequencies. Lawrence and Marshall (2000) introduced the virtual work method for analysis of URM walls under OOP loads, and developed a method to estimate the OOP strength. The method included the influence of both vertical and diagonal crack heights along with the moments along vertical and diagonal crack lines. Griffith et al. (2004) carried out static and dynamic tests on URM wall panels subjected to out-of-plane loading to develop an empirical force-displacement relationship that can be used for displacement-based method of analysis.

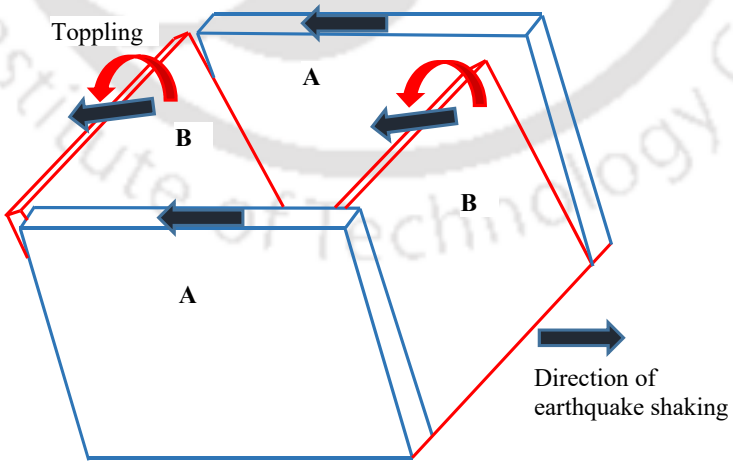

Figure 2.4. Out of plane collapse mechanism of URM walls.

Willis et al. (2006) and Griffith and Vaculik (2007) made a significant improvement to the Virtual work method. The improved method prescribed the ultimate OOP strength to be factored sum of the horizontal moment capacity and the diagonal moment capacity considering the aspect ratio and the design length of the wall. Prior to the addition, the moments were multiplied with coefficients k_1, k_2, which depend on the boundary conditions of vertical edges of the walls and presence of openings. The suggested method improved the accuracy since it covered a wide range of parameters like wall geometries, different wall configurations with and without openings, boundary conditions, etc. However, this approach assumed that the diagonal cracks form at a specific angle related to masonry unit geometry and joint thickness, and excludes the collapse load minimization procedure. The modified version was added in the Australian masonry standard AS 3700 (2018).

Derakhshan et al. (2018) conducted tests on a series of walls under out-of-plane loading to improve the virtual work method of strength estimation. The effectiveness of the virtual work method was further evaluated by Vaculik and Griffith (2018) by comparing the behavior of the half and full-scaled URM walls subjected to shake table and quasi-static cyclic loading (Figure 2.5 and Figure 2.6). They found both the test results to be in a good agreement with the standardized theoretical prediction method. The proposed method was also found effective in predicting the capacity of single leaf URM and cavity walls especially considering the two way bending (Graziotti et al., 2016, 2019).

Figure 2.5. Out-of-plane test set up of URM wall (Vaculik and Griffith 2018).

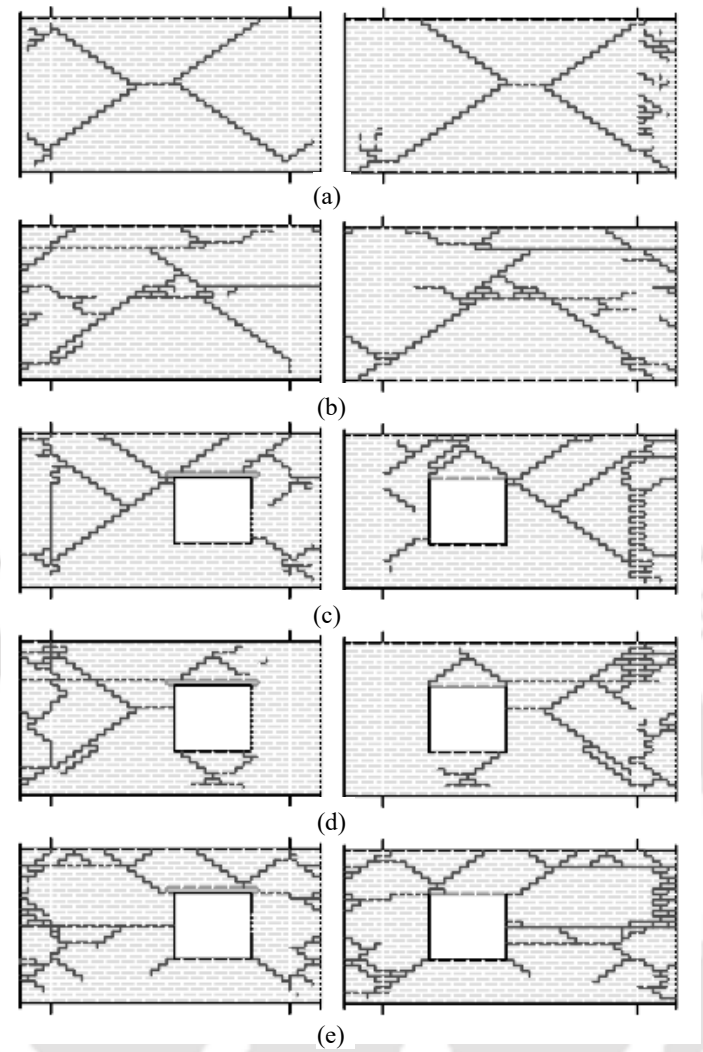

Figure 2.6. Two face crack patterns of OOP test on URM walls with vertical pre-compression value of (a) 0.10 MPa, (b) 0 MPa, (c) 0.10 MPa, (d) 0.05 MPa, and (e) 0 MPa (Vaculik and Griffith 2018).

Besides, the effect of plaster finish was included in the improved method through which a lower bound estimate of the wall strength can be estimated. Interestingly, it was observed that the existing analytical predictive models for out-of-plane force-displacement behavior results into an over-prediction in some cases (Penner and Elwood, 2016). This was attributed to the one-way spanning condition without rigid boundary restraints used in the previous methods, which were later improved by Walsh et al. (2018).

One of the major challenges for the numerical simulation of the walls subjected to combined in-plane and out-of-plane loading is the availability of adequate constitutive material models. Such assessment along both the in-plane and out-of-plane directions have

been tried using finite element method and macro-model approach, and techniques have been developed for estimation of the overall capacity of URM walls (D'Altri et al., 2018; Maccarini et al., 2018; Noor-E-Khuda and Dhanasekar, 2018). In the absence of accurate nonlinear properties required in detailed finite element simulation, a simplified way of assessing the masonry wall structures was also adopted in which the structural components were converted into equivalent frames (Roca et al. 2005). Such type of analyses provided an acceptable prediction of the overall response of the structure.

Codes like IS 1905 (BIS, 1987) suggest an analytical method based on elastic plate theory; the lateral capacity against the OOP loads is calculated by adding the direct stresses due to the total vertical load and stresses due to external bending moment and equating the sum to the tensile bond strength of the masonry. Such empirical equations and methods mostly provide highly conservatives values as there is no consideration of the possible failure modes. Whereas, Eurocode 6 (EN 1996-1-1, 2005) suggests calculation of moment demand (M_{ED}) concerning the lateral loading that creates horizontal bending resulting in failure parallel to bed joints, and vertical bending resulting in failure perpendicular to bed joints. These moments can be equated to the moment of resistance (M_{RD}) to check the safety of the wall subjected to lateral pressure. The OOP capacity can be calculated using Australian Standard AS-3700 (2018) by adding the horizontal moment capacity with the diagonal moment capacity and multiplying it by a set of factors like the aspect factor, capacity reduction factor, and perpend spacing factor, and coefficients k_1, k_2, which depend on the boundary conditions of vertical edges of the walls and presence of openings.

Additional details about the methods developed by past researchers and recommended by the design and assessment codes along with all the relevant equations are provided in chapter 6.

2.2.2.1. Gap Areas

The established codes of various countries and past studies have provided analytical methods to estimate the structural capacity of walls along the out-of-plane direction based on experimental observations in different countries. However, codes in many developing countries, including India, have not been revised for long due to limited resources and data. Despite the significant advances in predicting the failure pattern and lateral load carrying capacity of URM walls in the out-of-plane direction, more studies are required to be undertaken primarily on URM buildings constructed with low-strength masonry used

widely in many developing countries. Kaushik et al. (2007) and Sarangapani et al. (2002) reported that the compressive strength of masonry prisms constructed using Indian burnt clay bricks varies between 3 to 8 MPa depending upon the geographical location. The updated codes of various countries may not be suitable to be used elsewhere due to the significant variation in material properties and construction practices adopted in different parts of the world. Hence, a feasibility study on the suitability and effectiveness of the analytical methods, code provisions, and equations suggested in various past studies on estimation of lateral strength of URM buildings along the out-of-plane direction needs to be carried out. It is also crucial to ascertain if the lateral strength of individual URM walls, which are much easier to test or analyze, obtained using experimental, numerical, or analytical methods, can be systematically combined to realistically estimate the lateral strength of full URM buildings.

2.3. BEHAVIOR OF URM BUILDINGS SUBJECTED TO LATERAL LOADING

Although numerous experimental studies were carried out in the past on individual URM wall components, limited experimental studies were carried out on URM buildings to evaluate the performance of various building components and the buildings as a whole when subjected to seismic loads. This was primarily due to the requirement of sufficient space, sophisticated equipment, and complicated test setups to perform such tests. Such kind of tests, especially those carried out on full-scale specimens, are also incredibly cost-intensive. Some of the recent studies related to the experiments performed over URM building are reviewed here. Costley and Abrams (1996) performed an experimental investigation over two reduced scaled two-storey building system with flexible diaphragms, subjected to a series of simulated ground motions. Based on the experimental results, it was found that flexural tension is likely to be the primary mode of failure and the flexural tension cracking leads to the rocking behavior of the pier. The test also highlighted the beneficial effect of flanges on the response of in-plane loaded walls and is responsible for influencing the strength and failure modes of the pier. On the other hand, Magenes et al. (1996) tested a full scaled two storey building with rigid diaphragms subjected to seismic loads. The test indicated various modes of failure associated with the masonry components at structural level. The experimental results showed that shear failure modes seem to be the most dangerous and are difficult for assessment. On the other hand, the sliding failure depends on the friction coefficient of mortar joints, and the rocking failure modes of piers were not very sensitive to the masonry strength. One of the important findings in the

experiments performed in both tests is the significance of vertical stresses that play a key role in all of the failure modes.

Yi et al. (2006) carried out an experimental investigation over a full-scaled two story URM masonry building subjected to quasi-static loadings (Figure 2.7). As expected, it was observed that the tested structure has large initial stiffness. The damage in the structure was characterized by cracks that developed in the masonry walls. Based on the damages, global structural behavior such as global rocking of an entire wall, and local responses, such as, rocking and sliding of each individual pier were observed in the masonry walls with different configurations. Their study also stressed on the formation of flanges in perpendicular walls, and concluded that the overturning moments had significant effects on the behavior of the tested structure. The experimental results of URM buildings tested by Costley and Abrams (1996), Magenes et al. (1996) and Yi et al. (2006b) made a significant contribution in developing the equations to estimate the various modes of failures of URM walls. These equations are also used in ASCE/SEI 41-13 (2014) for the lateral strength assessment of URM walls.

The influence of openings on the seismic performance of URM buildings was studied by Shariq et al. (2008). In the study, finite element analysis was carried out for a single storey one-room masonry building with different aspect ratios and different positions of openings in walls subjected to the lateral loads in orthogonal directions. The authors showed that the critical direction of seismic force for the development of maximum stresses in the walls of a room with openings is along the short wall of the room. In addition, it was observed that the maximum principal tensile stress and maximum shear stress developed in the shear walls generally increase as the aspect ratio of the building increases, which is greatly influenced by the position of openings. It was also observed that the increase in number of openings in a wall results in increase in the stresses around the openings. However, the study lagged addressing key parameter like the influence of opening in defining the effective geometric details (for example, effective height, effective length) of the piers concerning the aspect ratios and location of openings in the building, which are prime information for structural assessment of the walls.

Shahzada et al. (2012) carried out pseudo-static test over a full-scaled single storey single room URM building. The measured response of the test structure was compared with the estimated response obtained using three capacity evaluation procedures, which were

mostly associated with the in-plane walls. Nevertheless, the authors did not include the contribution of the out-of-plane capacity of the orthogonal walls in the estimation of overall strength of the URM building. It was clear from the test results that there was a significant difference in the estimated response and the experimentally obtained results, though the in-plane mode of failure of the wall components obtained analytically were in good agreement with the experimentally obtained failure modes.

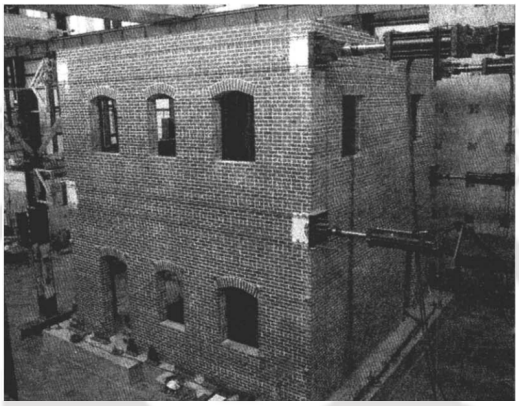

(a)

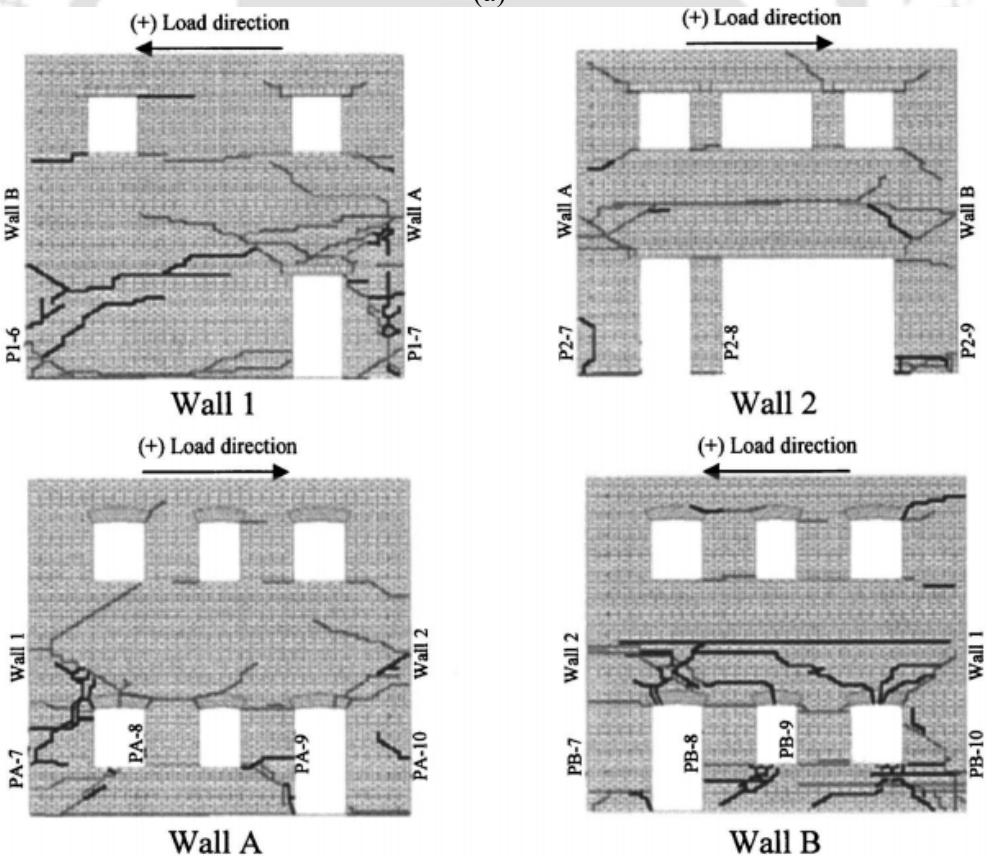

(b)

Figure 2.7. Lateral load testing of URM building (a) tested structure, (b) observed crack pattern in different walls (Moon et al., 2006; Yi et al., 2006a).

Aldemir et al. (2015), while testing a two storey URM building subjected to cyclic loading, found that the walls in the building mostly failed in a diagonal tension mode. The failures were concentrated mostly on the first storey and flange effect was visible in the test results in the form of cracks propagating in an inclined manner. Therefore, the authors recommended consideration of full height approach for the effective height calculation related to the piers in order to achieve the stiffness match with the numerical model. Kallioras et al. (2018) carried out a uni-directional shake-table test on a full-scale, single-storey unreinforced masonry building with flexible diaphragms, and showed significant out-of-plane damage in zones of high acceleration response, such as the roof gables. Damage due to the in-plane response of the walls was instead mostly associated with rocking of slender piers. It was also seen that slender piers developed flexural rocking in-plane mechanisms, and a lintel nearly collapsed during the final stages of the test. These tests provide a unique data set that captures at full scale the in-plane and out-of-plane behavior of URM walls, and the influence of flexible diaphragms on the global dynamic response of entire buildings.

There has been significant improvement in numerical assessment procedures for URM buildings. Most of these procedures includes the finite element analyses based on proper constitutive laws for the masonry components. The numerical assessment of masonry is performed mostly considering the macro-modelling approach. A commonly adopted one is the "Equivalent Frame Method" which was initially introduced by Magenes and Fontana (1998). The approach became quite popular and was later improved by various other researchers (Dolatshahi et al., 2018; Giovanni et al., 2016; Pasticier et al., 2008; Singh et al., 2013; Wilding and Beyer, 2016). However, this approach does not predict the damage area and progressive failure pattern accurately. The limitations were overcome by adopting the 3D solid elements to accurately model the structure and using suitable failure criteria to define the material model, e.g., *Mohr-Coulomb failure criteria* and *Concrete Damage Plasticity* model. (Gattesco et al., 2015; Mallarddo et al., 2008; Milani et al., 2007). Besides introduction of Discrete Element method for numerical evaluation of masonry structures has further improved the efficiency of the numerical approaches (Miglietta et al. 2017; Pantò et al. 2016). Additional details on some of the commonly used numerical assessment procedures are provided in later chapters while carrying out nonlinear analyses of URM walls and buildings.

2.3.1. Gap Areas

Based on the review of the available literature related to the experimental and numerical study on the unreinforced brick masonry buildings, it was observed that most of the individual studies were conducted on a single masonry building. A systematic experimental and numerical study on URM buildings with wide range of building geometry and opening configurations can be a potential gap area for research. Such studies can make an effective contribution in redefining the various parameter required for numerical simulation of URM buildings for lateral load analysis. Moreover, a detailed and systematic experimental study on individual walls of a URM building and the whole URM building comprising the tested walls is required to be carried out to understand and evaluate the contribution of the lateral strength of individual URM walls to the lateral strength of the whole URM building. Such a study may also provide an insight to the possible contribution of the box action in URM buildings with rigid floor diaphragms.

2.4. Strengthening of URM Buildings

A large number of studies have been conducted in the past to develop and suggest strengthening schemes for seismically vulnerable URM buildings with the primary objective to improve their seismic performance, thereby reducing the risk of collapse during strong ground shaking. Tomaževič et al. (1996) conducted an experimental study on four strengthening schemes for URM building specimens. The first specimen was constructed with wooden floors and freely supported timber joists without steel ties, and the second specimen was constructed with reinforced-concrete slab with bond-beams along the walls. The third and fourth specimens were identical to the first specimen with a modification that the walls were tied with pre-stressed steel ties and steel ties, respectively. The experimental results showed that the first specimen without wall ties did not prevent separation of the walls, resulting in the out-of-plane vibration and disintegration of the upper storey. Similar damage was also observed in the second specimen, but at a higher energy level. The third and fourth specimens with the walls tied with steel ties retained integrity up until their final collapse. Both the pre-stressed and simply placed ties efficiently prevented separation of the walls and excessive out-of-plane vibration. Owing to retained integrity of the structure, lateral load-resistance and deformability, as well as the energy dissipation capacity was significantly improved due to the strengthening. This showed the significance and effectiveness of the strengthening schemes for the URM structures. Benedetti et al. (1998), after performing shake table test over 24 URM building specimens with various retrofitting

schemes, showed that the use of horizontal ties, vertical steel beams, and curved steel blades improved the seismic performance of these building specimens significantly. However, the distribution of only the horizontal steel beams on the walls created a damage pattern showing a tendency of the walls to be cut by the horizontal beams. This fact points out the importance of an appropriate distribution of forces induced by the strengthening.

El-Borgi et al. (2005) introduced a scheme to strengthen a historical URM building at Tunisia that consists of a steel frame directly attached to the portrait room structure with added fluid viscous dampers. The strengthening scheme was suggested based on the vulnerability assessment of the historical building, wherein it was ascertained that the URM structure was deficient in transferring the lateral loads safely to the foundation. The main objectives of strengthening the URM building are mostly to prevent separation and disintegration of the walls to improvement of the seismic behavior of structure. The targets can be attained by tying walls of the structure with steel ties (Borri et al., 2009; Vincente et al., 2011; Kaushik et al., 2006; Kaushik and Jain, 2007). Over and above, Branco and Guerreiro (2011) showed that the use of steel ties can be less expensive, does not contribute to an excessive increase in the structures' weight, and minimizes the interruption of the normal functioning of the building. According to Tassios (2010), addition of steel elements as shear connectors along transversal wall intersections, in case of cracks for stitching or in case of passing through connectors of three-leaf masonry, can be suitably used to strengthen masonry walls.

Apart from the use of steel, various types of strengthening interventions have been found to be effective in improving the seismic performance of the URM building. Vintzileou (2008) proved that even the use of timber ties contributes to substantial enhancement of the ultimate strain of masonry subjected to compression, accompanied by reduction of the opening of vertical cracks. Sathiparan et al. (2012) showed that polypropylene (PP)-band retrofitting technique could enhance the safety of both existing and new masonry buildings, even during severe ground motions (Figure 2.8). Kadam et al. (2015, 2018) evaluated the performance of Ferro-cement (welded wire mesh in concrete/mortar) applied on the URM walls, also known as 'Splints and Bandage' technique, as a retrofitting scheme (Figure 2.9). It was observed that the retrofitted specimens exhibited minimal damages when compared with the un-retrofitted ones, and hence can be used as effective alternative strengthening techniques for URM buildings.

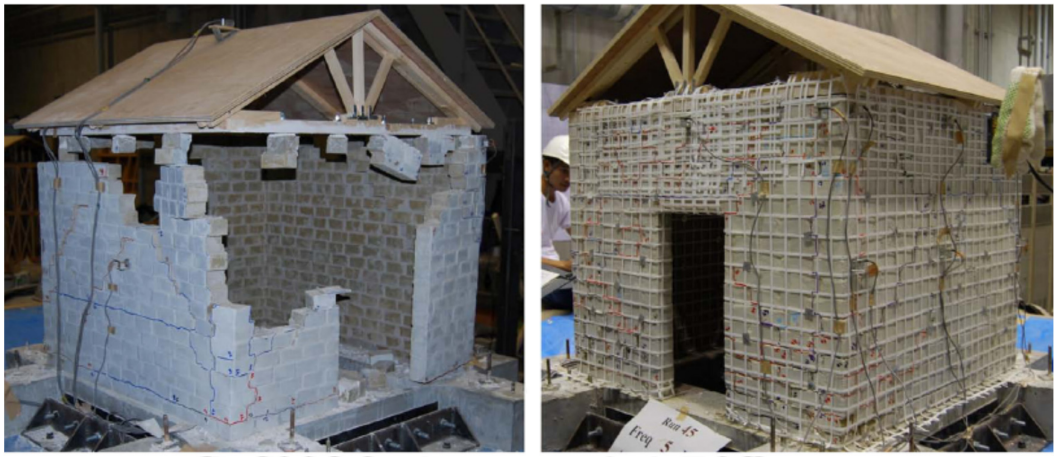

(a) (b)

Figure 2.8. Effectiveness of polypropylene-band used as strengthening of URM building. Lateral load performance of (a) the unstrengthened model, and (b) the strengthened model (Sathiparan et al., 2012).

The study of various other alternative strengthening schemes over the walls and buildings were also conducted by numerous authors in the past. For example, Shrestha et al. (2011) attempted retrofitting of historical masonry constructions using Cu-Al-Mn shape memory alloy bars. Another technique is the application of welded wire mesh and micro-concrete on the URM walls which improved both its in-plane and out-of-plane performance significantly (Kadam et al., 2014, 2015). On the other hand, Rahman and Ueda (2016) studied the performance of URM walls after strengthening using fiber-reinforced polymer (FRP) and carbon fiber-reinforced polymer (CFRP). The authors showed that the in-plane shear strength of the strengthened walls was considerably improved by using either of the FRPs, but the ductility was compromised when CFRP is used as a strengthening material. It was also seen that the strengthening of the URM buildings using FRP had marginal effect on the structural performance at the service load condition, but it contributed a lot at some accidental overloading, such as, earthquake, where the seismic demand was high. Similar improved performances of the URM walls strengthened with FRP strips was also shown by Konthesingha et al. (2015). However, the major drawback of using various FRPs or advanced materials like shape memory alloys, is that the material and the strengthening procedure is extremely cost intensive and require skilled manpower.

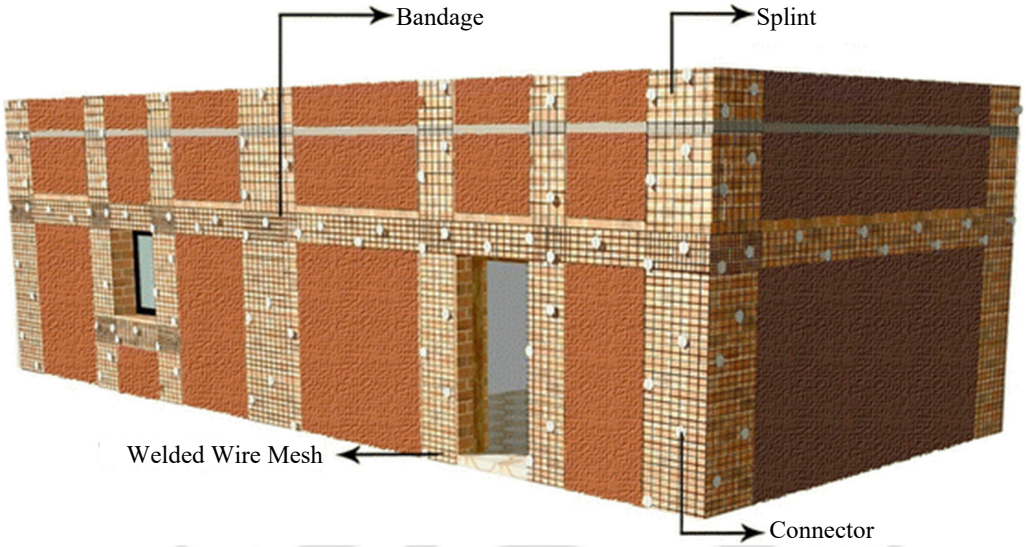

(a)

(b)

Figure 2.9. (a) Details of the 'Splint and Bandage' strengthening technique, and (b) shock-table test showing the effectiveness of using ferro-cement bands (welded wire mesh in concrete/mortar) applied on the URM walls as strengthening scheme. The building on the left was not strengthened, while the building on the right was strengthened using the 'Splints and Bandage' technique (Kadam et al., 2015, 2018).

2.4.1. Indian Code Provisions: Design and Strengthening of Masonry Buildings

In India, some design codes are available that provide guidelines to improve the seismic capacity of the buildings. IS 4326 (BIS, 1993) recommends the provision of lintel and roof

bands during the period of construction. Though the code provides some thumb rules on size and reinforcement detailing of the lintel and roof bands along with some guidelines on walls with openings, it is silent about the expected increase in capacity due to the provision of the bands. IS13828 (BIS, 1993b) suggests improvement of connectivity between walls, which are orthogonal to each other by alternating toothed joints in walls at corner and T-junction. However, due to complexity in the construction process, such recommendations are rarely adopted in the existing construction practice. The code also emphasizes strengthening the masonry near and around the openings by providing sufficient reinforced concrete rings, which will reduce the stress concentration in areas on the wall near the openings. Again, such recommendation is ad-hoc in nature without any quantification. IS13935 (BIS, 2009), which is mainly the code for repair and strengthening of buildings, recommends strengthening the existing walls by injecting epoxy into it. In order to improve the connectivity between the walls, the code also recommends use of pre-stressed wires to tie the opposite walls. Such processes need sophisticated instruments, skilled manpower and is cost-intensive. To make the retrofitting technique easier, the code has also suggested use of 'Splint and Bandage' technique using wire mesh as discussed earlier (Kadam et al., 2015, 2018).

2.4.2. Gap Areas

Though various authors have recognized the use of steel elements as a good and sustainable material for devising strengthening techniques for URM buildings, quantification of the increase in lateral load carrying capacity by adopting this technique has not been documented sufficiently. Numerous other alternative strengthening strategies using state-of-the-art material and techniques were developed for URM buildings exhibiting significant improvement in the seismic performance, but the methods involved use of sophisticated instruments and needed skilled manpower. Above all, the methods are highly cost-intensive as the strengthening material and manpower may not be available locally. It was also found that the suitability of various strengthening schemes with respect to the structural condition of the URM building was rarely suggested. Considering the case of strengthening using steel bands, a simple method of designing the strengthening scheme is still lacking. Some of the suggested strengthening schemes are ad-hoc in nature and fall short of addressing the important issue of the expected increase in the structural strength after strengthening.

2.5. SUMMARY AND IDENTIFIED GAP AREAS

Unreinforced masonry buildings still constitute a large part of the building stocks at various places in the world. A good number of these building are heritage structures, which are of national importance. Past studies have revealed that a large number of unreinforced masonry buildings that were not retrofitted, got damaged severely or collapsed during recent earthquakes. Therefore, strengthening with proper technique is essential to increase the service life of such buildings. The strengthening scheme should respect the heritage of the original structure, and therefore, be compatible with the original structural behavior. The priorities of the retrofit work can be recognized through systematic assessment of seismic vulnerability of existing masonry structure and recognize the most critical areas which need special attention. Considering the structural performance, conventional strengthening techniques can be adopted to strengthen the structure, irrespective of any artistic or architectural restraints.

Review of past literature has revealed that a significant amount of contributions was made by various researchers in improving the analytical methodology of assessment of URM walls. Methods were developed for assessment of in-plane as well as out-of-plane strength of URM walls considering various failure modes and covering a wide range of geometry and boundary conditions. Significant research work has also been carried out on developing strengthening schemes for URM walls and buildings using several conventional as well as state-of-the art techniques. Different materials like reinforced concrete bands, pre-stressed steel, wire mesh, various FRP types, shape memory alloys, etc., have been suggested to be used in the strengthening of URM buildings. The present review of the past studies has revealed various issues that were not adequately covered in the past research work, and therefore, the following points were identified as the potential gap areas that can be addressed in the present experimental, numerical, and analytical study:

- A suitable numerical method is required to be developed to study the performance of URM walls and buildings to predict their failure modes with acceptable accuracy. Such a study requires experimental validation to gain confidence on the developed numerical method.
- The applicability and suitability of the available analytical methods to analyze the URM walls with various opening configurations is required to be studied. This is especially important considering the large variation in the material properties of

masonry and the construction practice. Again, such a study requires experimental validation.

- Testing and analyzing individual URM walls have been found to be much simpler and faster than testing the full buildings. Therefore, suitability of scientifically combining the lateral strengths of the individual walls of a URM building to estimate the lateral strength of the whole URM building is required to be studied by testing the individual walls of a building as well as the whole building.
- A simple and cost-effective strengthening scheme for seismically vulnerable URM buildings is required to be developed using locally available materials and manpower. The number of seismically vulnerable URM buildings is so huge that developing inexpensive, but effective, strengthening scheme for URM buildings is very important for its adoptability by people living in such buildings.
- A numerical method is required to be developed for assessment and prediction of lateral load carrying capacity of the buildings strengthened using the developed scheme.
- An analytical method is required to be developed for design of such an inexpensive strengthening scheme for URM building. Development of simple empirical equations for design and evaluation of the inexpensive strengthening scheme will further improve the adoptability of the scheme, especially in the far-flung seismically active areas.

The applicability and significance of such a study will increase manifold if the study is carried out on full-scale specimens of URM walls and buildings. The outcome of the study will help in developing a scientific and engineered approach for structural assessment of URM walls and buildings. It will also assist in formally designing the strengthening scheme for the URM buildings, and can further be useful in the development of formal codes of practice on design of seismic strengthening techniques. These identified gap areas have been considered as the primary objectives of the present study.

Chapter 3
PRELIMINARY NUMERICAL INVESTIGATION

Contents

3.1. Overview 41
3.2. Numerical Modelling 43
3.3. Building Geometry and FE Discretization 50
3.4. Non-linear Analysis and Results 53
3.5. Sensitivity Analysis Varying Thickness and Width of the Steel Flats 63
3.6. Design Equations for Estimation of Capacity 65
3.7. Influence of Openings in Masonry Building 67
3.8. Summary 71

3.1. OVERVIEW

Masonry is a quite complex material that exhibits some peculiar features, such as, very low tensile strength due to weak mortar joints, orthotropy in both the elastic and inelastic range, non-associated friction, bricks crushing, etc. that can hardly be taken all into account with simplified material models (Milani et al., 2006; Page, 1981). The aim of the present work is to study the effectiveness of the existing numerical evaluation methods for URM buildings. For this, three different software are considered, namely, Strand7, Abaqus and SAP2000, which are quite popular and commonly used in structural engineering.

Within Strand7 (2013) and Abaqus (2010), a FE (finite element) modelling by means of 3D brick finite elements is used. A macroscopic approach is adopted for masonry, i.e., the heterogeneous character of the material due to assemblage of bricks and mortar is disregarded and average material properties are assumed. Strand7 gives only the possibility to perform non-linear analyses with an isotropic Mohr-Coulomb failure criterion, whereas

in Abaqus material softening can be accounted for by means of the adoption of a so-called Concrete Damage Model (CDP, also called Concrete Damage Plasticity Model).

CDP implemented in Abaqus was originally conceived for concrete (Lubliner et al., 1989), but an adaptation to masonry is still possible in presence of irregular textures (i.e. when masonry behaves as a quasi-isotropic material) or assuming equivalent material properties. On the other hand, the classic No Tension Material models (NTM) (Lucchesi et al., 1997) in Strand7, which are isotropic nature, are much simpler than CDP. The simplicity in the numerical method is by assuming materials with low tensile strength and the limited compressive strength. Such assumptions are widely recognized in the scientific community as quite effective to realistically represent the masonry behavior beyond the elastic limit.

When dealing with Strand7 software (Mallarddo et al., 2008; Pelà & Benedetti, 2009), the limitations introduced are even bigger. Both non-associativity of masonry under shear and softening are disregarded in the context of an isotropic modelling. However, the classic assumption of elastic-perfect plasticity has the advantage that (1) requires very few material properties (failure cohesion and friction angle) and (2) exhibits robustness and stability in the non-linear range, hence allowing performing analyses up to failure with relative easiness. On the other hand, for instance the Italian code (NTC 2008), allows the utilization of material following a Mohr-Coulomb failure criterion (and hence isotropic) for masonry structural elements (such as piers and spandrels). One disadvantage of this approach is that the displacement-based design cannot be managed due to the infinite ductile behavior of the material. However, various past literatures have shown that the failure mechanisms and load carrying capacity can be estimated with reasonable accuracy.

The last procedure, dealt within SAP2000, is more straightforward and is based on the so called “Equivalent Frame” approach. The equivalent frame schematization is recommended by many advanced codes for masonry, such as the Italian one (NTC 2008), and relies into a schematization of a masonry building by means of a frame constituted by beams with elasto-plastic bending/shear concentrated hinges with limited deformation capacity and rigid links in the overlapping regions. The ultimate strengths of unreinforced and reinforced masonry elements (piers and spandrels) are hereafter deduced from a well-established mesoscopic modelling strategy (Cundari & Milani, 2013; Milani et al., 2009).

In the current comprehensive numerical study, a single bay URM building, which was experimentally tested by Shahzada et al., (2012), was treated as benchmark. Since all material properties are not provided in the literature, the basic analytical model is calibrated to match the lateral force-displacement data reported in the experimental study. The calibrated analytical model is then used to study the influence of three different strengthening schemes (using steel bands) on the behavior of URM buildings. A very good agreement is observed in the behavior of the masonry building when modelled using different software, considering the three different modelling complexities.

3.2. NUMERICAL MODELLING

Several 3D pushover analyses on a small masonry building, described in detail in the following Section are performed to characterize numerically its global behavior under horizontal loads in absence and presence of strengthening interventions (Steel bands). In particular, following three commercial codes are used: Strand7, Abaqus and SAP2000. A brief overview of the features of the material models implemented in the aforementioned software are provided below.

3.2.1. Strand7 FE Code

In Strand7 (2013), within the elasto-plasticity theory, only isotropic material models with associated flow rule are available. In the present simulations, a Mohr-Coulomb failure criterion with associated flow rule is assumed, which is the main feature exhibited by the masonry, i.e., frictional behavior and limited tensile strength. With such assumptions, there is no possibility to deal with compression crushing when 3D elements are used. An elastic-perfectly plastic behavior is adopted, which obviously does not allow reproducing the well know masonry finite ductility. Since, out-of-plane failures are possible in a 3D model, nonlinear geometry effects are also considered. In absence of specific indications provided by the Indian codes of practice, values of cohesion and friction angle are assumed in agreement with the Italian code requirements for existing buildings (NTC 2008). Such values were taken considering the fact that the Italian code allows the utilization of material following a Mohr-Coulomb failure criterion for masonry structural elements (such as piers and spandrels). Under out-of-plane action, the friction angle does not affect the behavior of masonry buildings irrespective of the type and quality of the masonry; however, there is a significant influence of cohesion in masonry on the lateral load response of URM buildings (Milani et al. 2006, Mallarddo et al. 2008, Pela and Benedetti 2009). In general, when the

quality of masonry is very poor, cohesion decreases considerably, whereas it has been observed that friction angle exhibits quite constant values. For historic masonry where the chemo-physical deterioration of the mortar joint does not allow having confidence on a minimum tensile carrying capacity, no tension material models (NTM) are usually adopted (Lucchesi et al. 1997). In NTMs, it is assumed that masonry behaves elastically in compression, whereas the maximum principal stress allowed cannot be beyond zero. Such mathematical condition translates practically into an implementation inside standard elasto-plastic commercial FE codes of materials with quasi zero or vanishing tensile strength, and therefore a Mohr-Coulomb material model is adopted, also with vanishing cohesion. Such constraint may cause difficulties in convergence, especially near the formation of a failure mechanism of the structure and even in presence of vertical loads only.

In order to circumvent such intrinsic drawbacks and in absence of adequate experimentation (such as indirect tensile tests on triplets, shear tests at different levels of pre-compression, etc.), two different values of cohesion are assumed in the simulations, one correspondent to an average-good quality of the masonry material, the other to a weaker one. Usually, softening material models with arc length solvers are not available, and therefore, code allows to conventionally perform elastic-perfectly plastic analyses, which are simple, and in any case are capable of providing good prediction of failure loads and the active collapse mechanisms.

Steel bands, where present, are modelled by means of elastic plate (shell) elements. The shell elements are connected to the masonry material using node-to-node connection (no interface elements are used). In real buildings, such node to node connections cannot be provided; the connections between the bands and the masonry walls are achieved with the help of steel bolts and nuts provided at fixed spacing (typically ranging from 20 to 40 centimeters) as discussed in later chapters. Here it is worth noting that an efficient strengthening is obtained when the steel bands remain in the elastic range, therefore an elastic material model is adequate. The same procedure is adopted in Abaqus, whereas, in the equivalent frame model, steel bands effect is considered at a meso-mechanical level for the evaluation of the moment-rotation and shear-displacement curves of spandrels and piers. As a matter of fact, meso-mechanical FE models of piers and spandrels are constituted by 3D (masonry) and 2D (steel bands) elements identical to those used at a structural level.

3.2.2. Abaqus FE Code

Pushover analyses are also carried out using Abaqus (2010) assuming a Concrete Damage Plasticity (CDP) material model for masonry, which is available within the software and within many other FE codes. Although a CDP approach is conceived for isotropic fragile materials like concrete, it has been widely shown that its basic constitutive law can be also adapted to masonry (Acito et al., 2014; Barbieri et al., 2013; Bayraktar et al., 2010; Brandonisio et al., 2013; Clementi et al., 2018). It is worth noting, indeed, that experimental results reported by Page, (1981) on regular masonry wallets and successive numerical models (Milani et al. 2006) show that such material exhibits a moderate orthotropy ratio (around 1.2) under biaxial stress states in the compression-compression region. Obviously, such feature cannot be considered when an isotropic model, like the present one, is utilized. However, the utilization of isotropic models is commonly accepted in the literature (like concrete smeared crack approach available in both Ansys and Adina) after an adaptation of the parameters to fit an average behavior between vertical and horizontal compression. A suitable model should also consider the ratio between the ultimate compression strength in biaxial stress states and in uniaxial conditions. Such ratio, which exhibits some similarities between concrete and masonry, is reasonably set equal to 1.16. The CDP model allows analyzing materials with different strength in tension and compression, assuming distinct damage parameters. Compressive crushing is also described by means of the introduction of plastic deformation with a parabolic softening law.

In tension, see Figure 3.1a, the stress-strain response follows a linear-elastic relationship, until the peak stress σ_{t0} is reached. Then, micro-cracks start to propagate in the material, a phenomenon which is macroscopically represented by softening in the stress-strain relationship. Under axial compression, the response is linear up to the value of the yield stress σ_{c0} (Figure 3.1b). After the yield stress, the response is typically characterized by hardening, which anticipates compression crushing, represented by a softening branch beyond the peak stress σ_{cu}. Damage variables in tension and compression are defined by means of the following standard relationships given in Eq. 3.1a and Eq. 3.1b:

$$\sigma_t = (1-d_c) E_0 \left(\varepsilon_c - \varepsilon_c^{pl}\right) \tag{3.1a}$$

$$\sigma_t = (1-d_t) E_0 \left(\varepsilon_t - \varepsilon_t^{pl}\right) \tag{3.1b}$$

where σ_t and σ_c are the uniaxial tensile and compressive stress, respectively, E_0 is the initial elastic modulus, ε_t and ε_c are the total strain in tension and compression, respectively; ε_t^{pl} and ε_c^{pl} are the equivalent plastic strain in tension and compression, respectively. The terms d_t and d_c are the tensile and compressive damage variables.

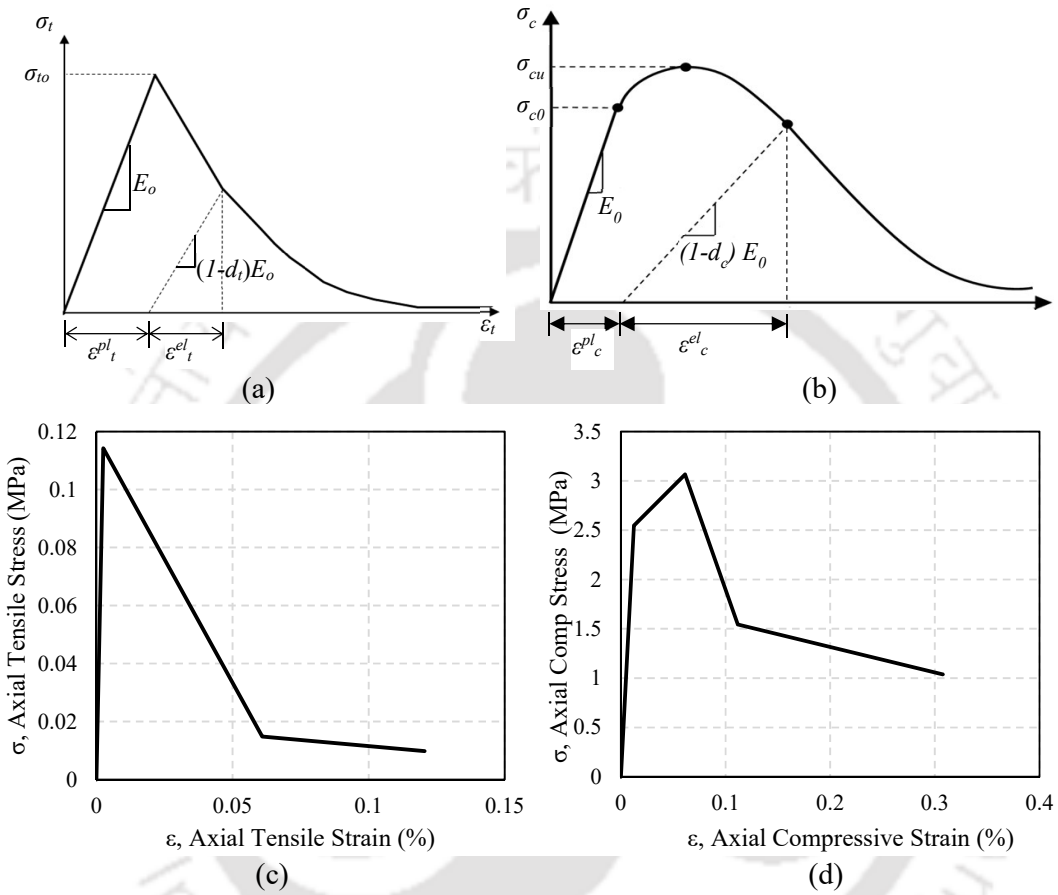

Figure 3.1. Abaqus material non-linear behavior in uniaxial (a) tension, and (b) compression, Stress-strain curve of masonry prism in (c) tension, and (d) compression.

In the present study, damage is assumed active in tension only, since the tensile strength of the masonry material is very low, especially in comparison with the compressive one. When strain reaches a critical value, the material elastic modulus degrades in the unloading phase to $E < E_0$. In particular, within the simulations, a reduction equal to 5% of the Young's modulus with respect to the initial value is assumed for a plastic deformation equal to 0.003 (Valente and Milani, 2016).

The strength domain is a standard Drucker Prager DP surface modified with a so-called K_c parameter (Figure 3.2) representing the ratio between the distance from the

hydrostatic axis of the maximum compression and tension, respectively. As per user's guide it is kept equal to 0.667 in all computations (López-Patiño et al.,2017; Bertolesi et al.,2016). The tension corner is regularized with a correction parameter referring to eccentricity, see Figure 3.3. The user guidelines suggest a default value of 0.1 for eccentricity. A value of 10° was adopted for the dilatation angle for the inelastic deformation in the nonlinear range, which is in agreement with the data suggested by Pluijim and Van Der (1993). The ratio between the bi-axial (fb_o) and uniaxial (fc_o) compression strength has been kept equal to 1.16 as suggested by Page (1981) for concrete (masonry behavior found to be similar). The values of the various inelastic parameters adopted for the analyses are defined in Table 3.1. Details on building geometry and mechanical properties of the materials are given in the next section.

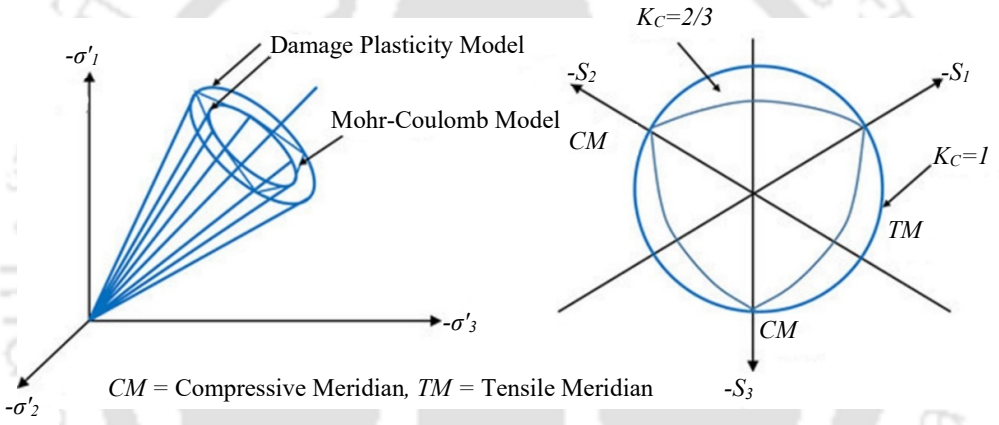

Figure 3.2. Abaqus: (a) modified Drucker-Prager strength domain, and (b) yield surface in the deviatoric plane corresponding to different values of K_c ($-\sigma'_1$, $-\sigma'_2$, $-\sigma'_3$ are principal stresses in three axis and $-S_1$, $-S_2$, $-S_3$ are yield/flow surfaces in the deviatoric plane).

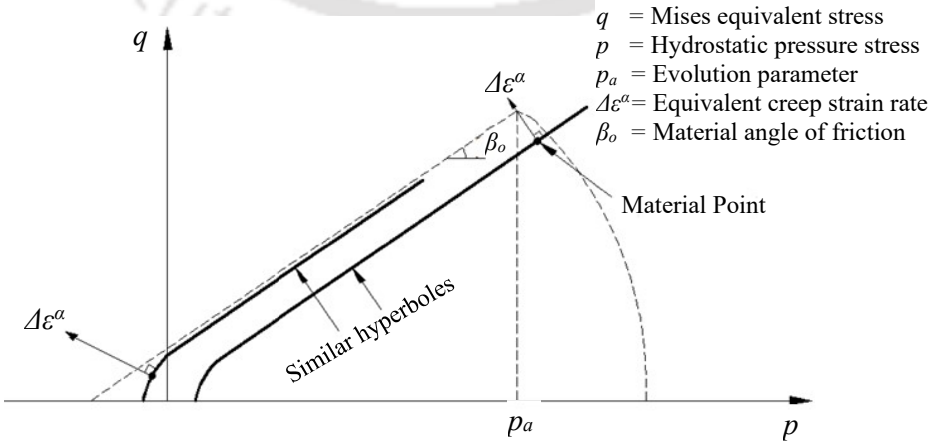

Figure 3.3. Smooth Druker-Prager failure criterion adopted in the simulations, *p*-*q* plane.

Table 3.1. Concrete damage plasticity properties

Dilatation Angle	Eccentricity	f_{bo}/f_{co}	K_c	Viscosity Parameter
10	0.1	1.16	0.667	0.0001

Whilst the utilization of the CDP model is probably more in agreement with the actual behavior of masonry, its utilization requires experienced users and huge computational time, especially when 3D FE models with many elements are used. Steel bands are modelled in Abaqus exactly in the same way as done within Strand 7.

3.2.3. SAP2000 Equivalent Frame Approach

SAP2000 (2011) is used to perform pushover analyses of URM building using "Equivalent Frame approach". The estimation of the load carrying capacity of the structure is done by means of introduction of concentrated plasticization hinges by mimicking the failure of different masonry elements like spandrels and piers, under shear and flexure (Cundari and Milani, 2013; Milani et al., 2009;Singh et al., 2013). In this method, a masonry building is modelled by means of an equivalent frame where columns are represented as piers and beams as spandrels. Rigid links (i.e., linear elastic beams with large stiffness) are used to model the connection between piers and spandrels. Deformable beams are assumed elasto-plastic with concentrated plasticization due to shear and flexure. The approximation works reasonably well for regular buildings, even if it has been shown that the reduction to an equivalent frame is not unique, but is inapplicable for structures with many irregularities or in all those cases where the identification of piers and spandrels is not possible (e.g., masonry churches) (Quagliarini et al., 2017).

For the case under study, the masonry prototype of Figure 3.4a-b is converted into the equivalent frame depicted in Figure 3.4c.The non-linear behavior of the hinges can be determined by various possibilities. The most straightforward approach is the use of code of practice like ASCE/SEI 41-13 (2014) and Italian code (NTC, 2008). However, the evaluation of the load carrying capacity of the single structural elements does not link well to the existing 3D URM building models. For this reason, in order to determine the ultimate shear and moment capacity of each structural element, a homogenized finite element approach is utilized, as suggested Milani et al. (2009) and Cundari and Milani (2013). Such approach simplifies the numerical evaluation to a great extent. It is to be noted that each pier and spandrel is extracted from the URM building, and after the imposition of suitable

boundary conditions, is loaded up to failure with a distribution of actions mimicking shear and bending separately. For each load case, either a shear-displacement or moment-rotation pushover curve is obtained for each pier and spandrel element. For simplistic modelling of masonry walls, Salokinos et al. (2003) and Pastier et al. (2008) suggested the use the moment-rotation (M-θ) plastic hinges at both end of the pier and a shear-displacement (V-δ) plastic hinge at the mid span of the spandrel. The interaction between axial force and shear/bending moment in the piers was not accounted for as the vertical loading in the single storey building was low. Therefore, either a shear-displacement or moment-rotation relationship is defined for plastic hinges in the equivalent frame elements representing piers and spandrels in SAP2000 (Table 3.2 and Table 3.3).

Table 3.2. Flexure and Shear capacities generated for masonry elements (Piers)

Element	Deformation due to Moment	Plastic Strain due to Moment	Deformation due to Shear	Plastic strain due to Shear
Pier 1 Pier 2	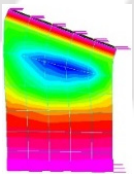	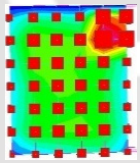	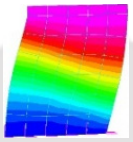	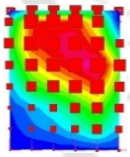
	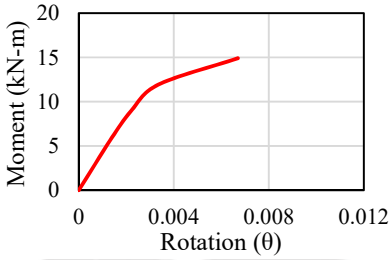		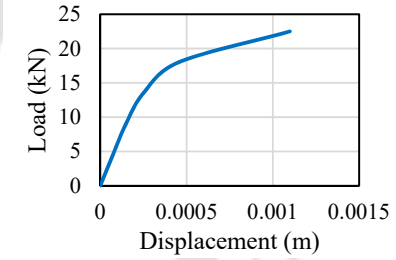	
Pier 5 Pier 6 Pier 7	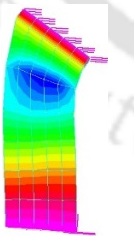	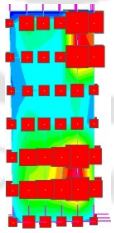	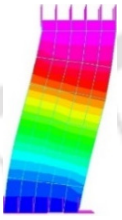	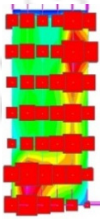
	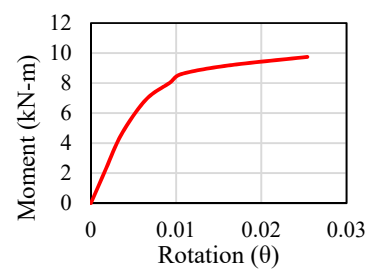		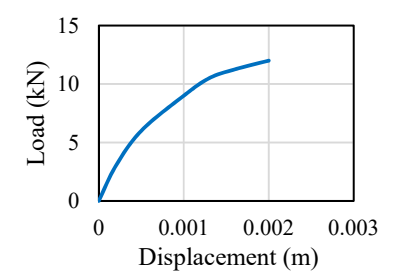	

The values are implemented to define the hinges in the equivalent frames in SAP2000. For spandrels, it is reasonably assumed that only shear failure is possible due to its geometry (deep members). In Table 3.3, Spandrel 1 corresponds to the spandrel above the door and Spandrel 2 corresponds to the spandrel above window 1. Similar input properties for each pier and spandrel are generated for the strengthened cases also. Once input properties are generated for all elements, pushover analyses on the whole equivalent frame are carried out.

Table 3.3. Shear capacities generated for masonry elements (Spandrels)

Element	Deformation due to Shear	Plastic strain due to Shear
Spandrel 1	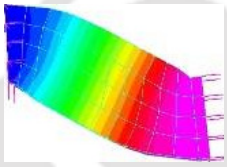	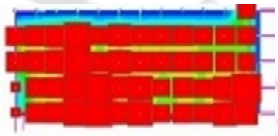
	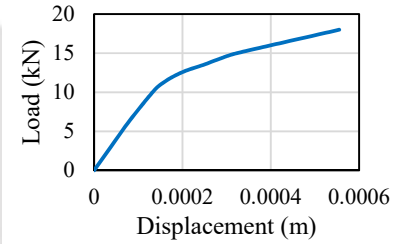	
Spandrel 2	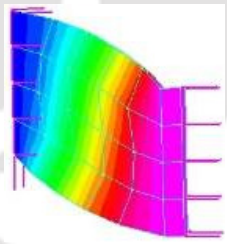	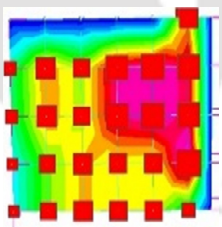
	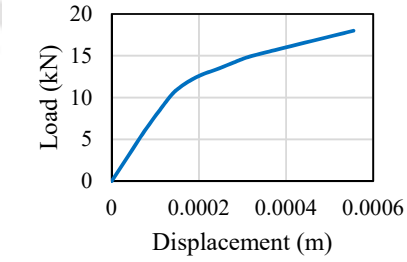	

3.3. BUILDING GEOMETRY AND FE DISCRETIZATION

With the aim of evaluating the numerical analyses to study the performance of a typical masonry building subjected to quasi-static horizontal loads incremented up to failure, a

small one story masonry prototype experimentally tested by Shahzada et al. (2012), is considered. The prediction of the lateral load carrying capacity of the building by means of three numerical approaches previously discussed represents a good benchmark for the systematic evaluation of their applicability in design practice (Figure 3.4). Three different strengthening interventions with steel bands, discussed in the sequel, are finally numerically analyzed to estimate (1) the increase in the load bearing capacity due to strengthening and (2) the agreement of the results obtained using three different numerical approaches.

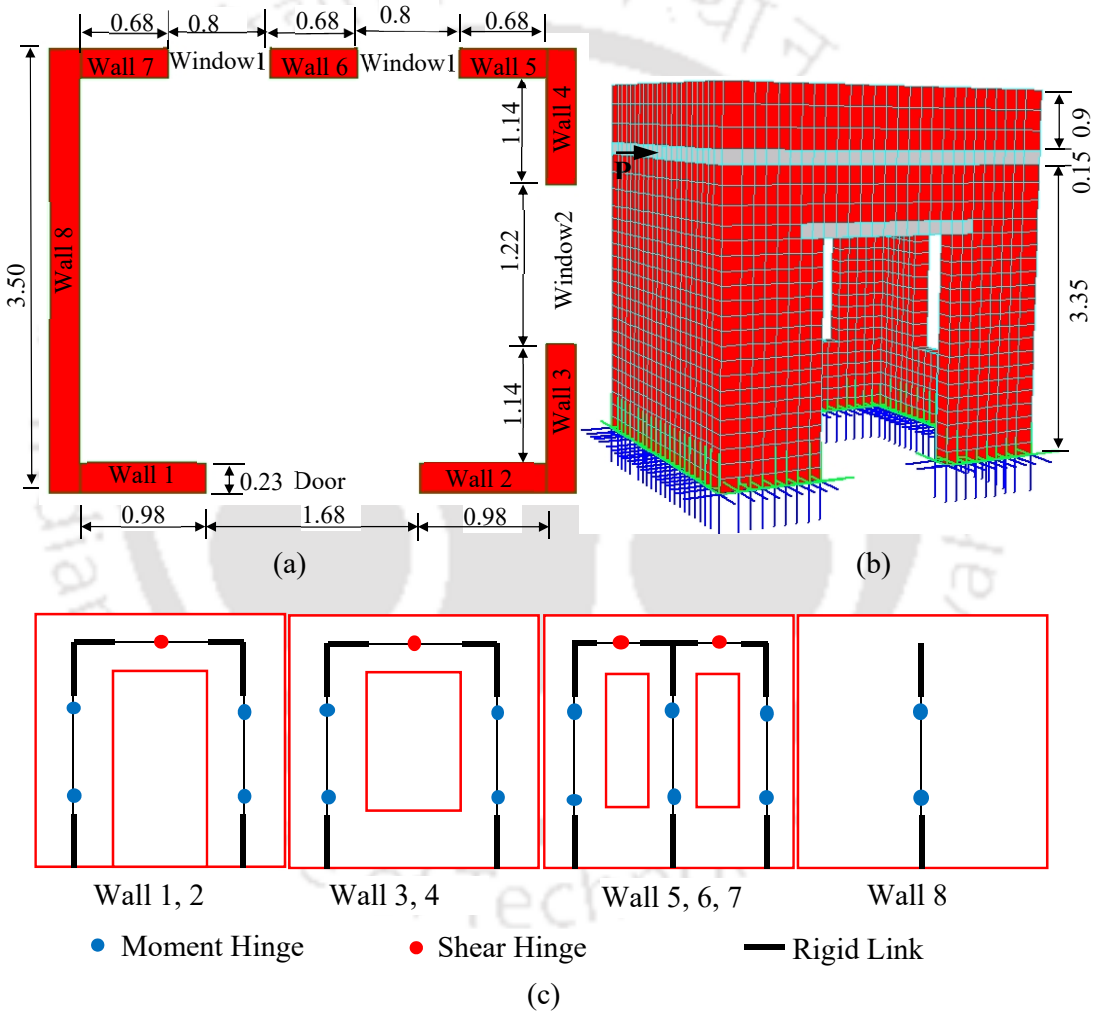

Figure 3.4. Unreinforced brick masonry prototype analyzed: (a) Plan view (All units are in m), (b) 3D FE model (2903 eight-noded solid element and 5676 nodes), and (c) Equivalent frame model of the masonry.

Shahzada et al. (2012) performed an experimental study on a full-scale one-story unreinforced brick masonry building subjected to quasi-static horizontal loads incremented

up to failure of the structure. The experimental results in terms of force-displacement (capacity) curves are used in the present study to benchmark previously discussed numerical models and to calibrate the unknown mechanical parameters to adopt a suitable modelling of masonry elements. When some parameters are missing from experimentation, they are kept in agreement with consolidated literature in the field. The building geometry and dimensions of the walls (spandrels, lintels and piers), as well as the dimensions of the openings (windows and doors) are fully defined in Figure 3.4 and Table 3.4. The unreinforced small building is a one storeyed structure with dimensions in plan equal to 3.50m × 3.64m (Figure 3.4). The structure is built with walls constituted by 0.23m thick brick masonry with English bond pattern. Reinforced concrete lintel beams, 0.15m high and 0.23m wide, are provided above all openings to improve stability against vertical loads near openings. To further improve stability against gravity loads a reinforced concrete slab, 0.15m inches thick, constitutes the plan roof. Small brick masonry parapets, 0.34m thick are disposed all around the slab. A horizontal concentrated load is applied to the wall without openings by means of a single load cell, at the level of R.C slab as illustrated in Figure 3.4. Displacements are measured at the mid-point on the R.C slab on the opposite wall.

Table 3.4. Geometry of walls, windows and doors

Element	Dimensions	Element	Dimensions
Wall 1,2	0.99 m × 3.35 m	Door	1.68 m × 2.59 m
Wall 3,4	1.14 m × 3.35 m	Window 1	0.8 m ×1.68 m
Wall 5,6,7	0.686 m × 3.35 m	Window 2	1.22 m × 1.68 m
Wall 8	3.51 m × 3.35 m	-	-

A few preliminary mechanical properties of masonry as given in Table 3.5 are provided in Shahzada et al. (2012). Remaining material properties required in three approaches have been taken from established literature. Pushover analyses within Strand7 and Abaqus are conducted utilizing the discretization shown in Figure 3.4b and constituted by 2903 eight-noded solid element and 5676 nodes. The sizes were finalized after carrying out the convergence test over the models. The solid elements used in strand7 were the simple 8-noded solid elements, whereas in Abaqus C3D8 elements, which are also 8-noded solid elements, were used. During the mesh finalization process, it was found that the simulation results provided nearly similar results without discretizing along the thickness of the wall, therefore the same has been maintained throughout the remaining analysis and this has significantly reduced the simulation time. All nodes located at the base of the

structure are fully restrained. The vertical dead load is directly applied to walls head and a concentrated load incremented up to failure of the structure is applied at the point where the quasi-static load was applied as per the experimental model.

The analyses performed using Strand7 are carried out considering a Mohr-Coulomb failure criterion for masonry with a friction angle of 30^{o} and cohesion value of 0.15 MPa (NTC 2008). The non-linear analyses performed using Abaqus assumed for the Concrete Damage Plasticity model for which the non-linear parameters are reported in Table 3.1. The maximum strength in tension and compression are calculated using the Mohr-Coulomb yield criterion under plane stress conditions. Material non-linearity is defined exclusively for masonry elements, whereas concrete lintels/slabs and steel bands are assumed to behave elastically. Such assumption is quite reasonable considering that concrete and steel strength are much larger than that of masonry.

Table 3.5. Mechanical properties of the material used in brick masonry building

Property	Value
Masonry Unit Compressive Strength	12.4 MPa
Compressive Strength of Mortar	5.05 MPa
Compressive Strength of Masonry Prism	3.02 MPa
Masonry Diagonal Tensile Strength	0.05 MPa
Elastic Modulus of Masonry	1227 MPa
Specific Weight of masonry material	1495 kg/m^3
Elastic Modulus of Steel	2x10^5 MPa
Density of Steel	7865 kg/m^3

3.4. NON-LINEAR ANALYSIS AND RESULTS

Pushover analyses in absence and presence of retrofitting (three strengthening configurations) are carried out using the aforementioned FE software in the longitudinal positive X direction, in agreement with experimentation. From experimental results, the maximum lateral load carrying capacity of the structure is around 106.76 kN. Using the above mechanical parameters, it is found that all the models fail at a horizontal load of about 133.45 kN, which is about 25% higher than the experimental value.

In order to rationally investigate the reasons of such differences in the load carrying capacity, and to improve the accuracy of the Finite Element models, further analyses are carried out by varying the following mechanical properties:

i. The introduction of non-linearity for reinforced concrete elements, as expected, has negligible influence on the overall load carrying capacity of the structure. The use of different concrete strengths results into a minimal change in the load carrying capacity, since concrete behaves in a linear elastic way.

ii. A variation of the elastic modulus, in agreement with classic theorems of limit analysis, does not have any effect on a variation of the overall load bearing capacity, whereas it is important to calibrate the initial elastic global stiffness. Conversely, masonry tensile strength (and hence cohesion in a Mohr-Coulomb or Drucker-Prager model, as those adopted in the present simulations) is a key parameter for correct evaluation of the load carrying capacity of such typology of buildings, where the reduced number of stories and the slenderness of the walls make the role played by self-weight less important. Masonry tensile strength is not provided in the paper by Shahzada et al. (2012), therefore it can be varied to fit the experimental data. It is found that a reduction of masonry tensile strength from 0.17 MPa to 0.1155 MPa (due to cohesion reduction from 0.15 MPa to 0.1 MPa in a pure Mohr-Coulomb failure criterion) results into a corresponding reduction of the ultimate load, as depicted in Figure 3.5, where quite a satisfactory agreement with the experimental pushover curve may be noted. Therefore, in further studies, a cohesion value of 0.1 MPa is used. Only numerical results obtained with the first numerical approach (Strand 7) are represented for the sake of clearness.

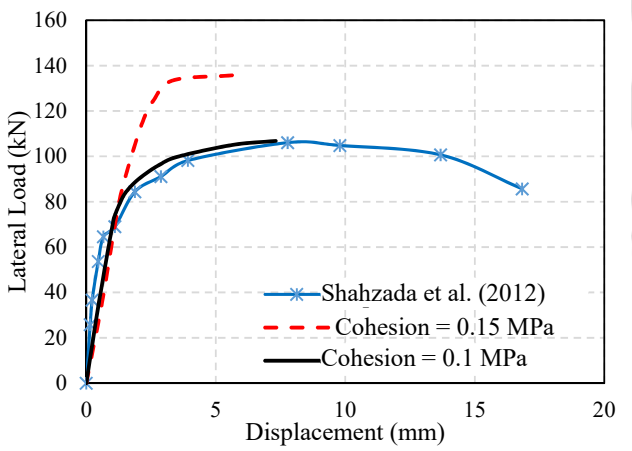

Figure 3.5. Capacity curves for the unreinforced prototype and Strand7 model at two different values of masonry cohesion.

Additional analyses are carried out in presence of a continuous ring beam at lintel level, and the results in terms of pushover curves are compared with the model with

discontinuous RC lintels in Figure 3.6. As can be observed, with the introduction of a continuous ring beam, the capacity of the unreinforced brick masonry building increases approximately by 25%.

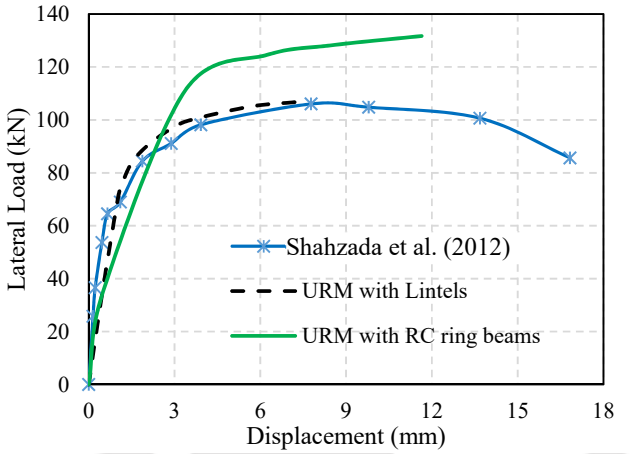

Figure 3.6. Capacity curves with and without RC ring beam at lintel level.

In Figure 3.7, a comparison between experimental pushover curve and those obtained using the three aforementioned numerical approaches is reported. From the results obtained, it is noticeable that the numerical results, especially the lateral strength, generated by all the commercial codes, match quite well with the experimental results.

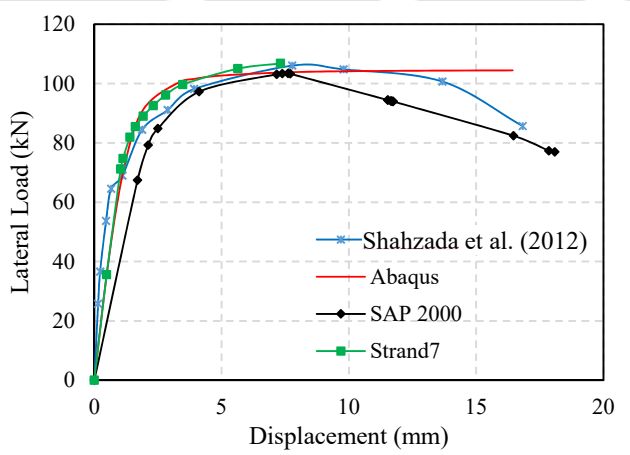

Figure 3.7. Capacity curve comparison among computational approaches and Experimental evidences.

3.4.1. Numerical analysis of URM building

The equivalent plastic strain patch, which is one of the outcomes of the numerical simulations both in Strand 7 and Abaqus, gives interesting information on the modes of failure of the different elements and the active failure mechanism, to compare with

experimental crack pattern. As can be noted from Figure 3.8a, where the equivalent plastic strain is represented at the end of the simulations (failure point), a concentration of inelastic deformation occurs near the openings. Wall 6 exhibits an equivalent plastic strain patch that suggests failure due to rocking, and Walls 1, 2, 5 and 7 exhibit a mixed failure combining rocking and diagonal shear cracking. The numerical results are considered to be in satisfactory agreement with experimental crack patterns, see Figure 3.8b.

Distribution of equivalent stresses (Mises equivalent measure) is found to exhibit peaks near the corners of the openings, with concentrations mostly related to the stiffness of the reinforced concrete lintel. The stress contour resulting from the numerical analyses conducted using Strand7 and Abaqus shows nearly the same values and similar critical regions, Figure 3.9.

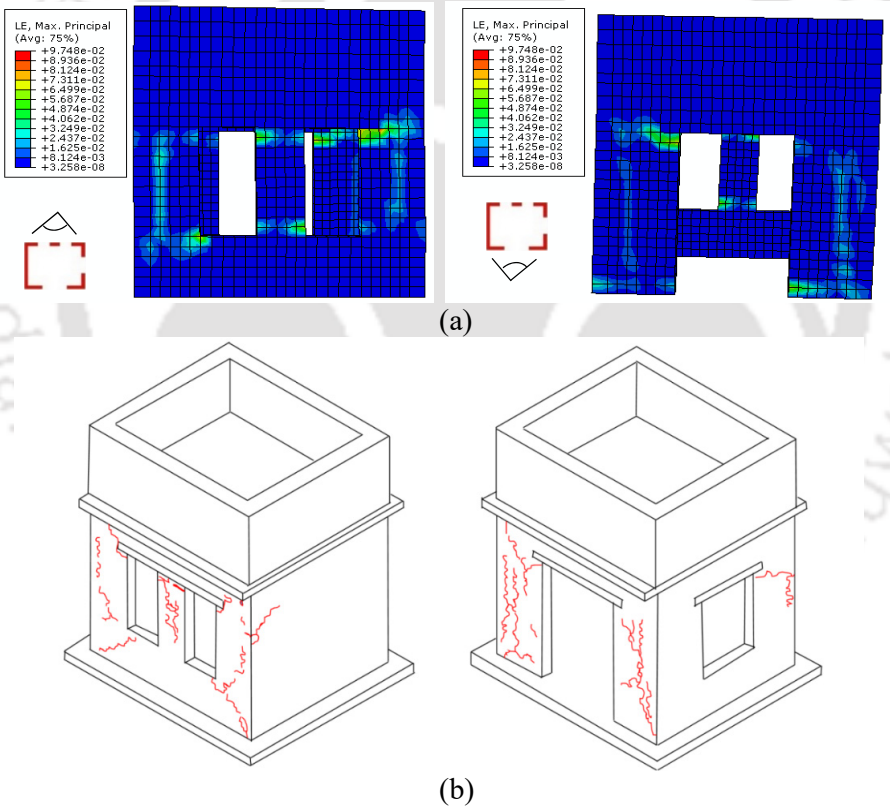

(a)

(b)

Figure 3.8. Comparison between numerical inelastic deformation and experimental crack pattern exhibiting a mixed failure combining rocking and diagonal shear cracking: (a) Plastic strain, and (b) Damage pattern of the tested structure by Shahzada et al. (2012).

The resulting active plastic hinges at the end of the simulations found in the equivalent frame approach and represented schematically in Figure 3.10, again appear in good agreement with 3D results of Strand7 and Abaqus. Since the current construction practice

in India is to adopt RC ring beams at lintel level (also known as lintel bands), it is interesting to compare the pushover curve obtained for URM building reinforced on the surface with steel flats at lintel level with that obtained for URM building with RC lintel band (Figure 3.11). It is found that the lateral capacity of the masonry structure strengthened with a 50 mm × 1 mm steel flat is nearly the same as that obtained with the ring beam. In the preliminary study, the steel bands are mounted on the external face of the walls only.

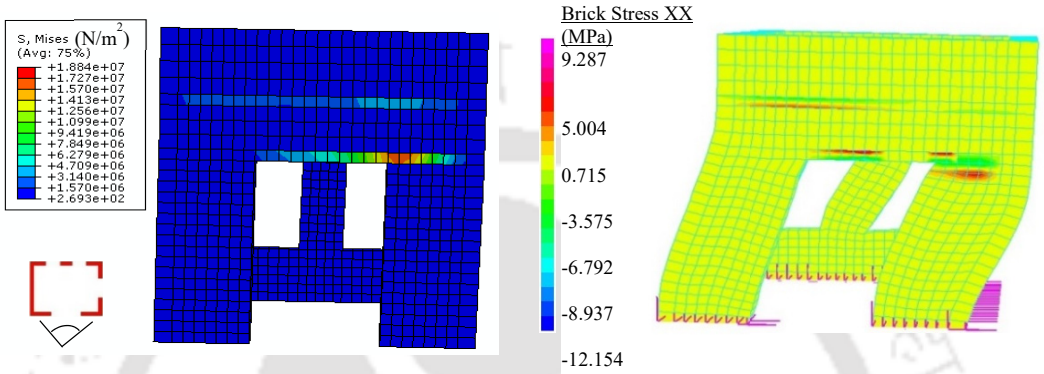

Figure 3.9. Stress contours figures developed using (a) Abaqus, and (b) Strand7.

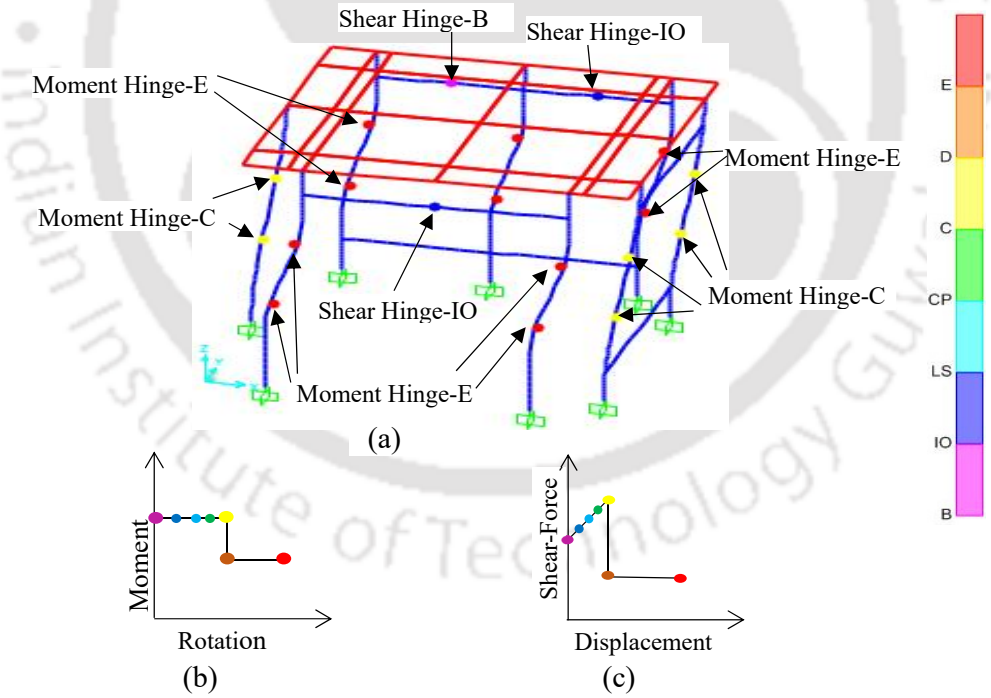

Figure 3.10. SAP2000 results: (a) Non-linear pushover results for Equivalent frame, (b) Non-linear Moment - Rotation curve for Moment Hinges, and (c) Non-linear Force - Displacement curve for shear hinges.

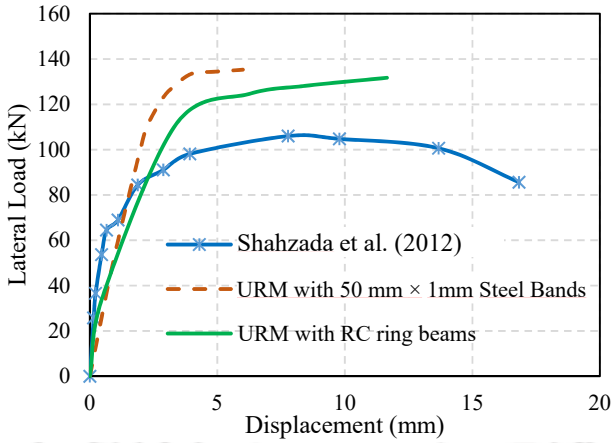

Figure 3.11. Capacity curves obtained for URM buildings with steel flats and with RC ring beam.

Considering the overall performance of the URM prototype, three strengthening schemes using steel flats are critically compared. The retrofitting schemes are the following:

i) Single steel bands mounted on wall surface at lintel level, Figure 3.12
ii) Double steel band at lintel and sill levels, Figure 3.16
iii) Horizontal double steel bands at lintel and sill levels and vertical continuous steel bands mounted near the openings, Figure 3.20

Initially the effectiveness of the three different strengthening schemes in improving the lateral load behavior of URM buildings is studied numerically and then further parametric analyses are carried out by varying the width and thickness of steel bands in each strengthening scheme.

3.4.2. Strengthening Scheme #1: Steel Bands at the Lintel Level

The numerical analyses conducted disposing steel bands at the lintel level show a sharp increase in the capacity, which is nearly 45% greater than the unreinforced case. Initially, the model is strengthened with a 15 cm wide and a 1 mm thick steel continuous band due to ease of connectivity to the discretized solid brick elements. The maximum stresses are concentrated on steel flats, see Figure 3.13, whereas the absolute value of the equivalent plastic strain reduced by 80% on masonry elements, see Figure 3.14. The failure mode remains essentially unchanged but a more visible “box action” may be observed. The capacity curves generated using the three different modelling strategies are nearly the same, as clearly shown in Figure 3.15.

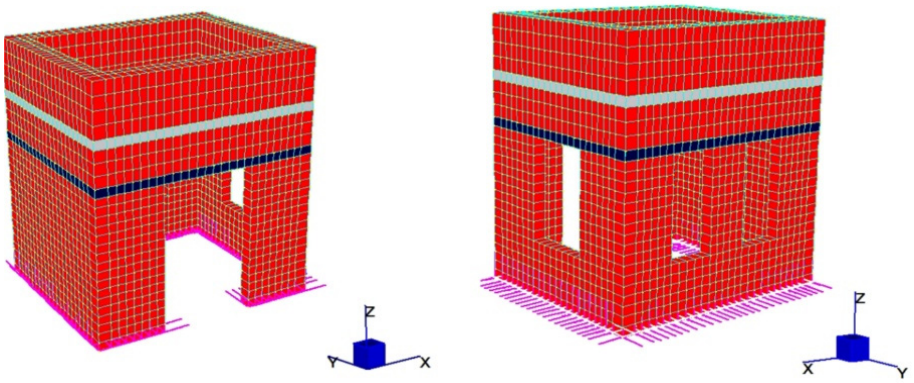

Figure 3.12. Steel flats used as surface-mounted bands at the lintel level.

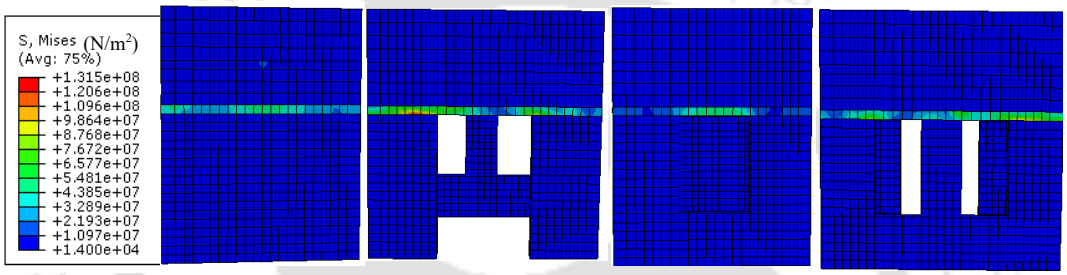

Figure 3.13. Stress contour on 4 faces of the building due to application of steel bands at lintel level.

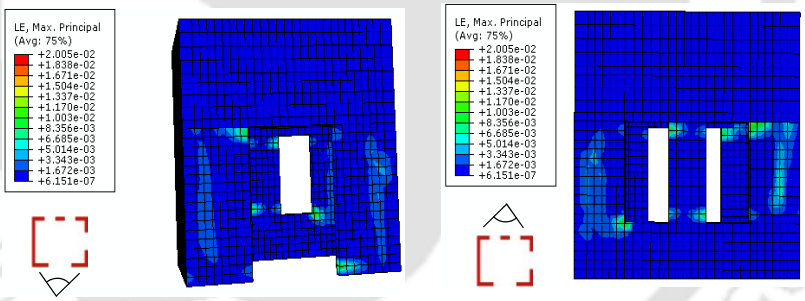

Figure 3.14. Plastic strain in masonry after providing steel bands at lintel level.

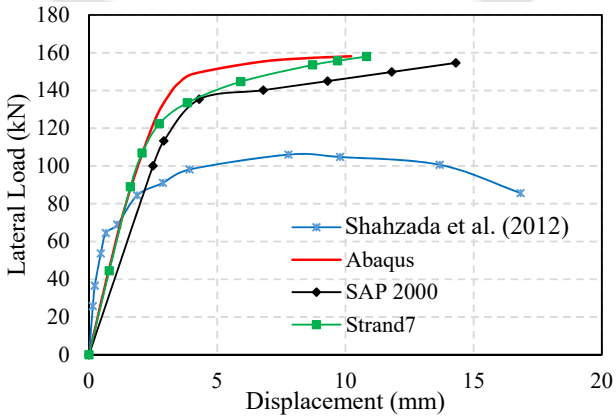

Figure 3.15. Capacity curve comparison for Strengthening Scheme #1 using three numerical approaches with the unstrengthened specimen tested by Shahzada et al. (2012).

3.4.3. Strengthening Scheme #2: Steel Bands at Lintel and Sill Level

A strengthening scheme with steel bands 15 cm wide and 1 mm thick positioned at lintel and sill levels (Figure 3.16) shows a considerable increase in the overall capacity of the structures, with an increase of about 70% with respect to the unreinforced case. Steel bands absorb a large amount of tensile stresses, as shown in Figure 3.17, a peculiar behavior which can justify the strong reduction of the diffusion of plastic regions in masonry elements, see Figure 3.18. Capacity curves obtained for these strengthening schemes are shown in Figure 3.19.

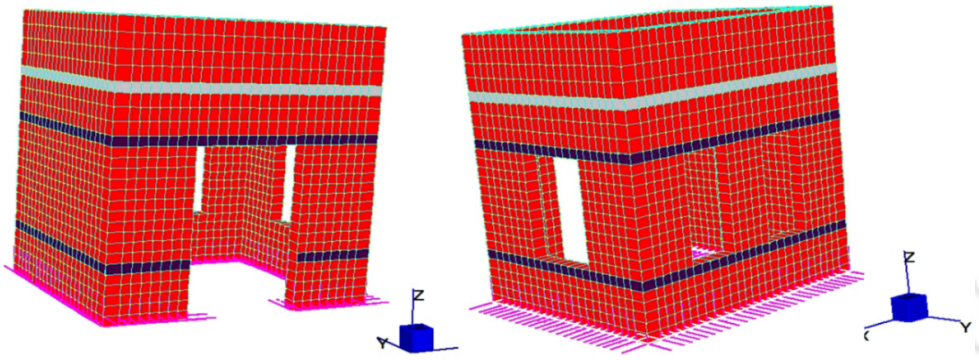

Figure 3.16. Steel bands mounted at the lintel and sill level (Double steel band).

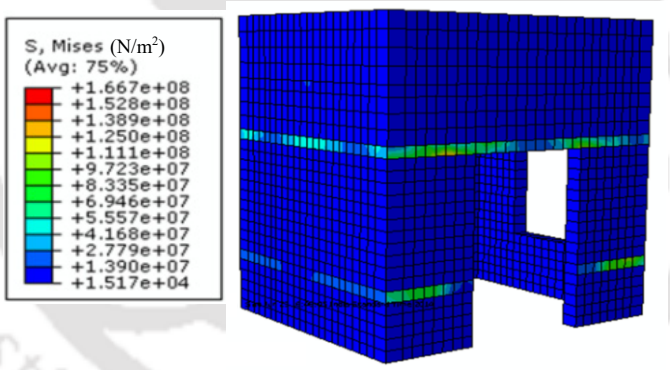

Figure 3.17. Stress contour due to application of steel bands at lintel and sill level.

The capacity curves generated by Straus7 and SAP2000 are almost superimposable, whereas Abaqus provides almost the same value of collapse load, but a lower ductility. The discrepancy may be justified remembering that Abaqus material model exhibits limited ductility both in tension and compression, whereas the other two models are essentially elastic-perfectly plastic.

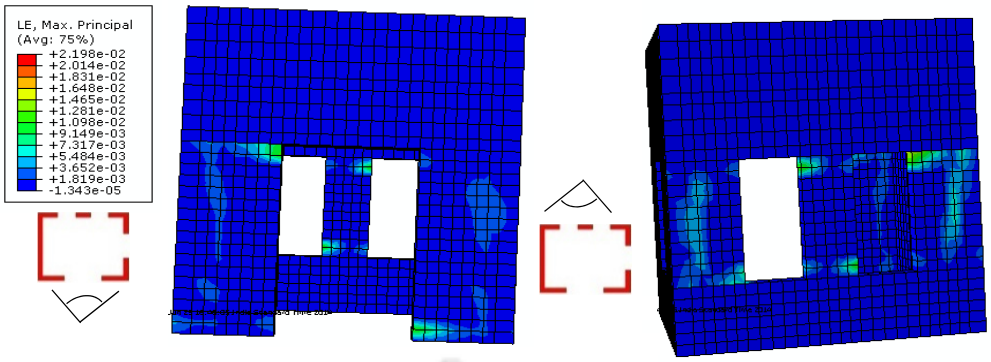

Figure 3.18. Plastic strain region due application steel bands at lintel and sill level.

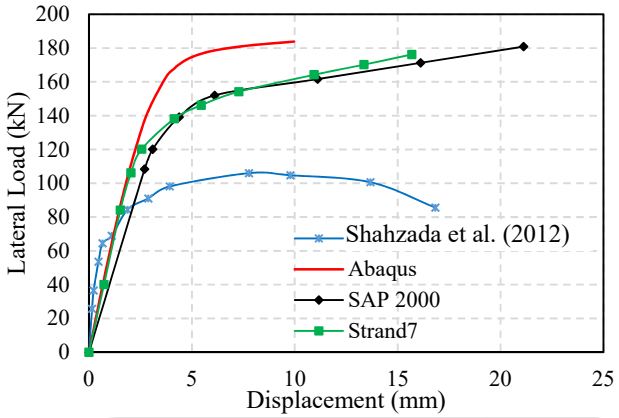

Figure 3.19. Capacity curves after the application of double level steel band and comparison with the originally tested unstrengthened specimen by Shahzada et al. (2012).

3.4.4. Strengthening Scheme #3: Horizontal Steel Bands at Lintel and Sill Level and Vertical Steel Bands around the Openings

With the introduction of vertical steel flats to the strengthening scheme #2 (Figure 3.20), the plastic strain regions as well as the plasticization intensity in masonry elements reduce considerably, see Figure 3.21. It is pretty clear from the results that steel bands play the structural role of absorbing almost all tensile stress concentrations, see Figure 3.21a, especially near critical regions, i.e., opening corners. As expected, the lateral load carrying capacity of URM building strengthened using scheme#3 further increases (about 85% more than URM building) as shown in Figure 3.22. Comparing the pushover curves associated to the three strengthening schemes, see Figure 3.23, where Abaqus curves are represented and compared with experimental data in the unreinforced case, it can be observed that all the strengthened buildings perform rather well, showing a considerable increase in the lateral load carrying capacity. As intuitively obvious, the last strengthening scheme with horizontal and vertical steel flats is associated to the highest collapse load for the structure along with a significant reduction of inelastic deformation on masonry elements.

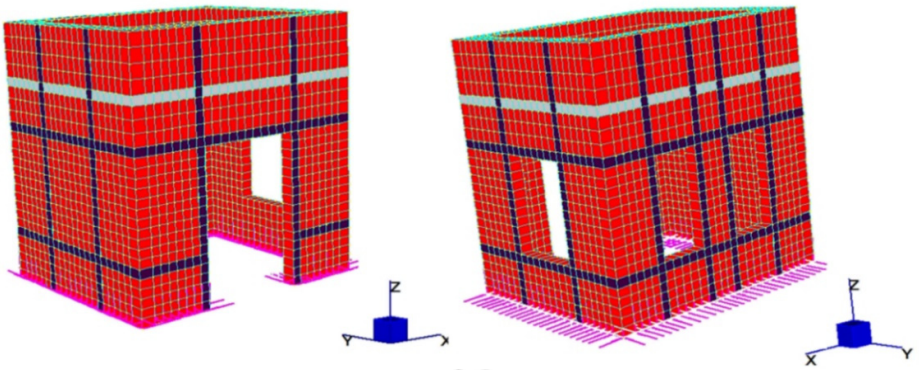

Figure 3.20. FE discretization of URM building strengthened using surface-mounted horizontal double steel bands at lintel and sill level and vertical steel bands around the openings.

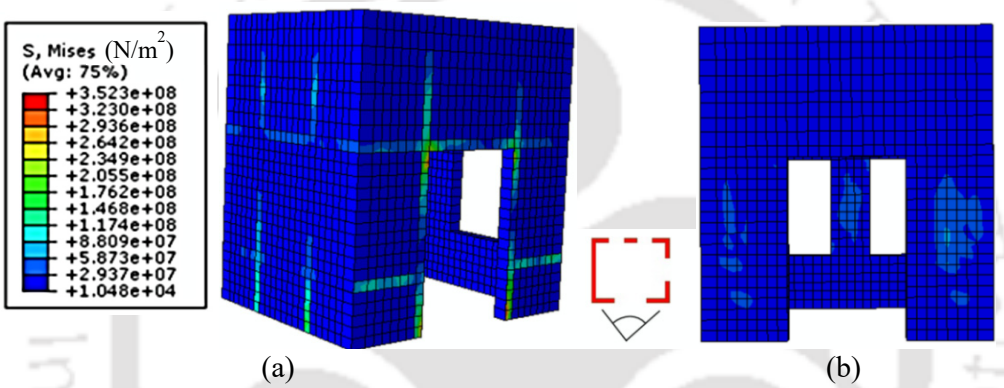

Figure 3.21. Strengthening Scheme #3: (a) Stress Contour, and (b) Equivalent plastic strain patch.

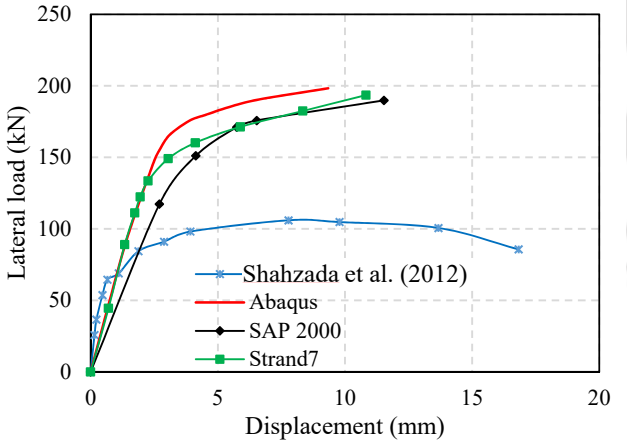

Figure 3.22. Strengthening Scheme #3 Capacity curves obtained with the three numerical models and their comparison with experimental results (unreinforced case) reported by Shahzada et al. (2012).

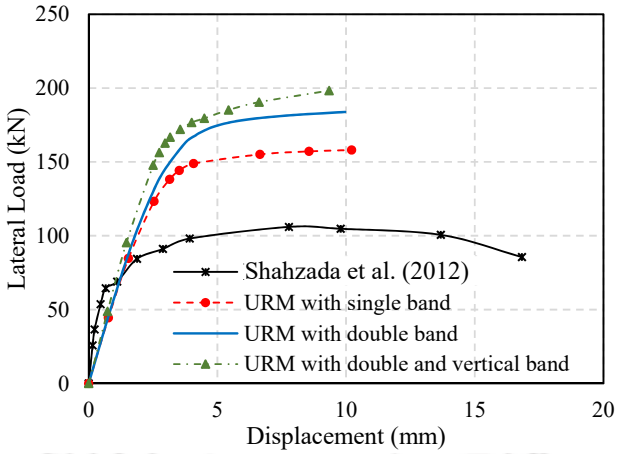

Figure 3.23. Capacity curve comparison between strengthened and un-strengthened building obtained using Abaqus. Shahzada et al. (2012) represents the un-strengthened prototype.

3.5. Sensitivity Analysis Varying Thickness and Width of the Steel Flats

It will be interesting to make some observations on the numerical behavior of the URM building in terms of load carrying capacity when the area of the steel bands used as strengthening measure is varied. Sensitivity analyses are conducted for all the three strengthening schemes considering steel bands with width equal to 10, 15 and 20 cm and maintaining the thickness equal to 1 mm. In parallel, another study is carried out by increasing the thickness and keeping the width equal to 5 cm. Thickness is increased in such a way that the reinforcement transversal area is kept equal to that considered in the previous set of simulations (100 mm^2, 150 mm^2 and 200 mm^2), so thicknesses equal to 2, 3 and 4 mm are taken into consideration. The aim is to have an insight into the effect (in terms of load bearing capacity) of increasing either the width or thickness of the bands. Since second order geometric effects are taken into consideration in the model, it is expected that the response is slightly different in the two cases. The pushover curves obtained numerically using strand7 are shown in Figure 3.24 to Figure 3.26. Figure 3.24 refers to the first strengthening scheme, Figure 3.25 to the second and Figure 3.25 to the third. As can be noted, an increase in the transversal area has in general, a negligible advantage in terms of load carrying capacity. Such response demonstrates that the steel bands with the smallest transversal area remain mainly in the elastic range even when failure of the building is reached, highlighting at the same time that the design of the cross section was adequate.

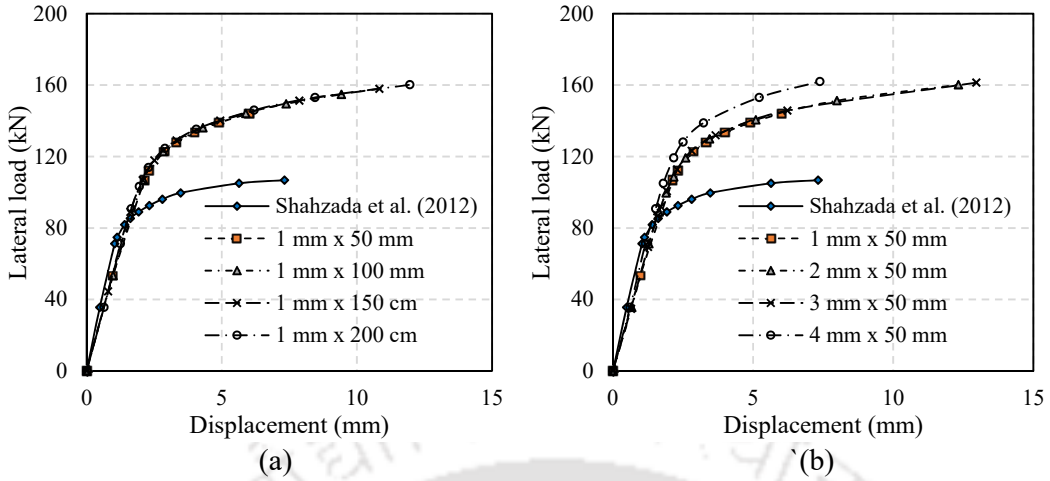

Figure 3.24. Masonry building with Strengthening Scheme #1. Capacity curves obtained considering bands having different cross-sectional area: (a) width increase, and (b) thickness increase.

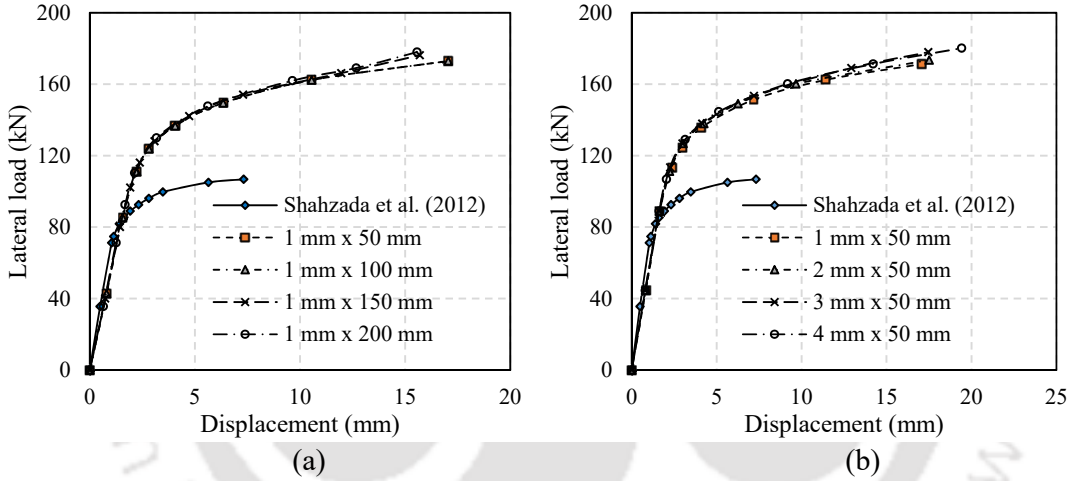

Figure 3.25. Masonry building with Strengthening Scheme #2. Capacity curves obtained considering bands having different cross-sectional area: (a) width increase, and (b) thickness increase.

Conversely, it can be stated that the present check can be useful to select the most suitable cross-sectional area to adopt for the steel bands. A small but perceivable advantage of the use of thick steel bands may be however noticed from the resultant pushover curves, probably linked to the capability of the numerical model to consider local buckling of the bands within the hypothesis of geometrical non-linearity.

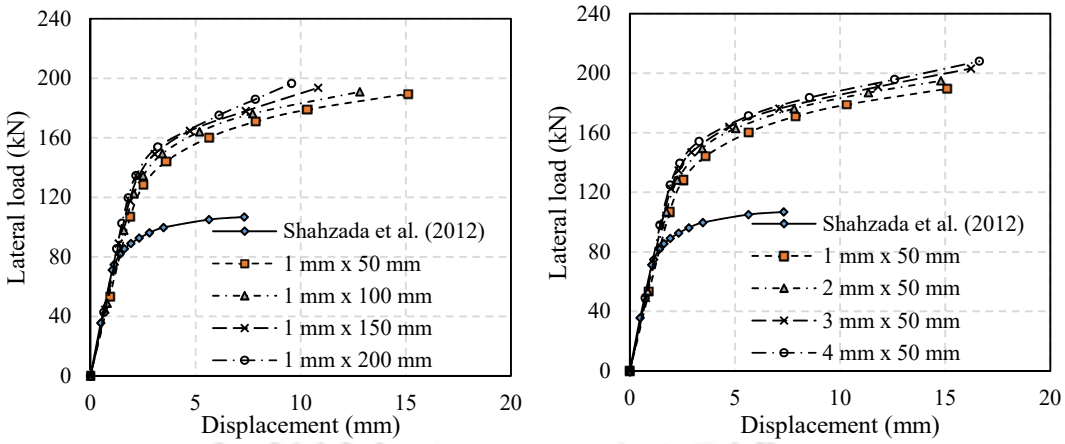

Figure 3.26. Masonry building with Strengthening Scheme #3. Capacity curves obtained considering bands having different cross-sectional area: (a) width increase, and (b) thickness increase.

3.6. Design Equations for Estimation of Capacity

From a detailed analysis of the pushover curves provided by all the numerical models in the cases of strengthening schemes investigated, it may be interesting to develop design equations capable of providing a direct estimate of the increase in the load bearing capacity as a function of the cross-sectional area of the bands used for strengthening. Such equations are derived directly from the numerical pushover curves through standard best fitting. In Figure 3.27- Figure 3.19, the α_L factor, representing the ratio between peak horizontal load and total weight of the structure is represented as a function of the steel bands cross-sectional area.

Figure 3.27 refers to the first strengthening configuration analyzed, Figure 3.28 to the second and Figure 3.29 to the third. Continuous thick lines refer to data extracted and post-processed from the numerical pushover curves, whereas dotted lines are interpolating functions. In the interpolating equation y represents α_L and x represents "A_s" the cross-sectional area of steel bands in mm^2. From the results of the simulations, it is interesting to notice that the interpolating functions are linear for Strengthening Schemes #2 and #3. Such property is particularly suitable for a very simplistic design of a possible seismic retrofitting. Strengthening Scheme #1 behavior exhibits, on the contrary, a quasi-hyperbolic behavior. Considering the increase in the load bearing capacity obtained in the three cases, the third strengthening configuration with increase in the bands' thickness, appears to be the most suitable scheme to be utilized in common design.

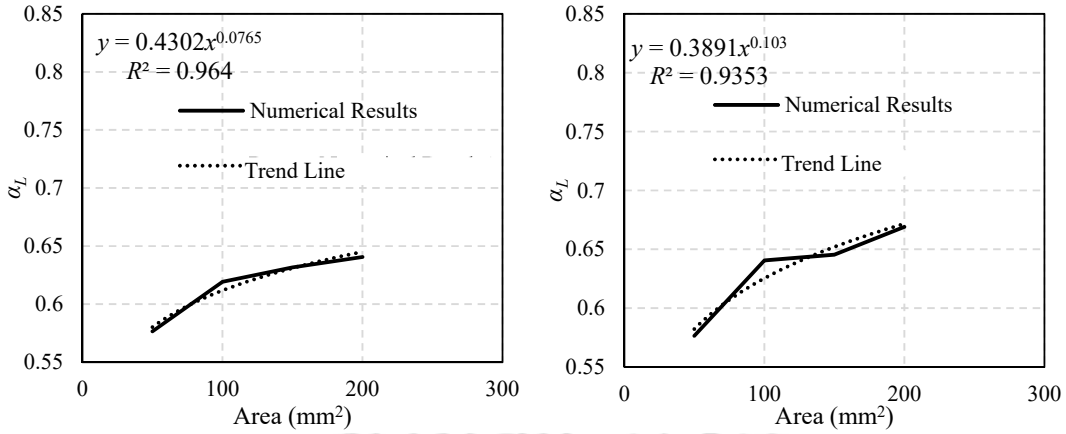

(a) (b)

Figure 3.27. Masonry building with Strengthening Scheme #1. Factor α_L for different cross-sectional areas of the steel bands and corresponding best fitting interpolation: (a) width increase, and (b) thickness increase.

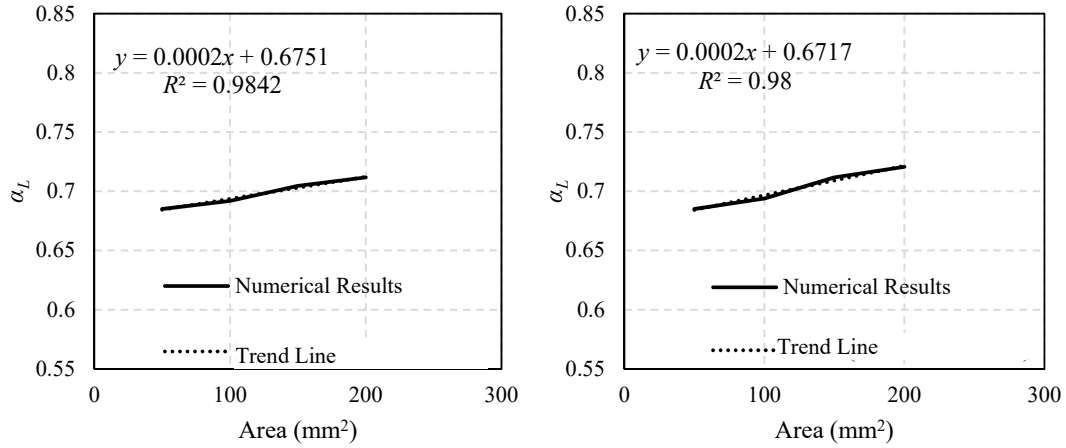

(a) (b)

Figure 3.28. Masonry building with Strengthening Scheme #2. Factor α_L for different cross-sectional areas of the steel bands and corresponding best fitting interpolation: (a) width increase, and (b) thickness increase.

Maximum increase in the lateral load carrying capacity of the URM building is observed (ranging from 75% to 83%) when strengthened using the scheme #3. The empirical equation developed for α_L considering double horizontal bands and vertical steel bands with thickness increase is given in Eq. 3.2:

$$\alpha_L = 0.0005A_s + 0.7318 \tag{3.2}$$

In any case, when restrictive money constraints are present, it can also be concluded that even a single band 1 mm thick and 50 mm wide is capable of increasing the lateral strength sufficiently. It has to be stressed that the above equations are generated based on the benchmark model analyzed in the previous section for comparison purposes. More

general equations can be deduced by carrying out a systematic parametric study where the building geometry, number of storeys, wall thickness, size and position of openings, etc., are varied.

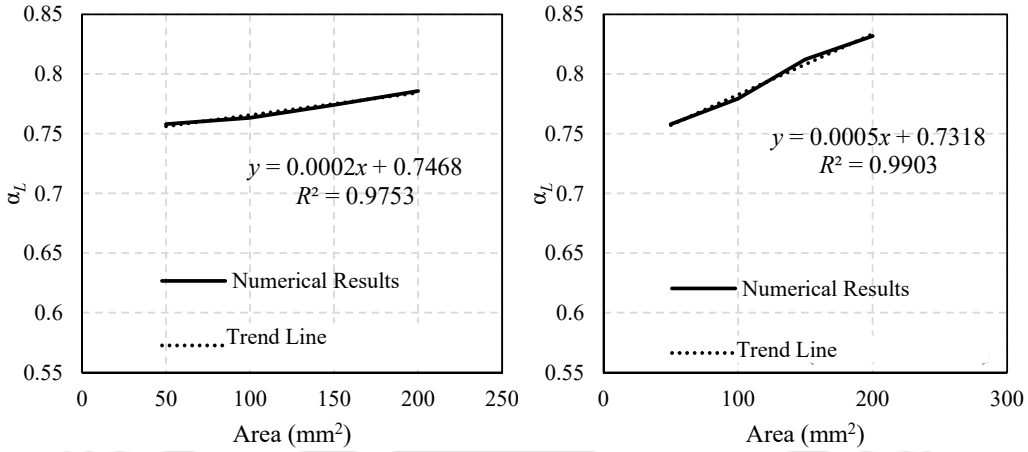

Figure 3.29. Masonry building with Strengthening Scheme #3. Factor α_L for different cross-sectional areas of the steel bands and corresponding best fitting interpolation: (a) width increase, and (b) thickness increase.

3.7. Influence of Openings in Masonry Building

Four commonly seen opening configurations are considered in the single storey URM building and numerical models are developed as shown in Table 3.6 to study the influence of openings on lateral load behavior of unstrengthened as well as strengthened URM building. The numerical simulations of the four models with various opening configurations have shown that the buildings with greater number of openings drastically alters the lateral load behavior of URM buildings. Besides the greater number of openings along the direction of the loads influences more in reducing the load carrying capacity of the structure (see Table 3.6 and Figure 3.30). This is apparent since the lateral load carrying capacity of Model C and Model D have delivered nearly the same results. Besides, building with greater number of openings have shown greater degree of damages with reduced lateral load carrying capacity.

3.7.1. Influence of only External Bands and Combination of External and Internal Bands

Since Model D with higher degree of damages generated lowest strength value, this model is considered in the further study in which the building is strengthened using surface-mounted external steel bands and both internal and external bands of 1mm thick and 10 mm wide. Before strengthening the whole building, the influence of strengthening individual URM walls (elements) using surface-mounted steel bands on the lateral strength of these walls is studied. The elemental strengthening of URM elements shows that the strengthening scheme in which both double horizontal as well as vertical steel bands are provided (Strengthening Scheme #3) increases both moment and shear capacity of the individual walls significantly (See Table 3.7).

Table 3.6. Damage Contours of URM buildings with four different opening configurations (Model A, Model B, Model C, Model D)

Plan of Models		Tension Damage Contours	
		View 1	View 2
A	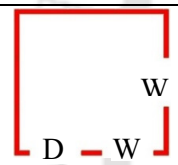	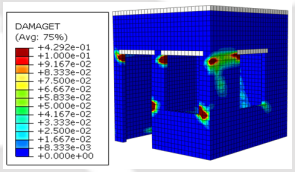	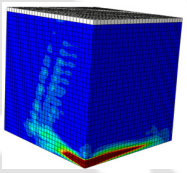
B	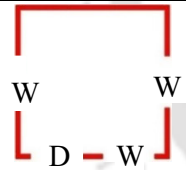	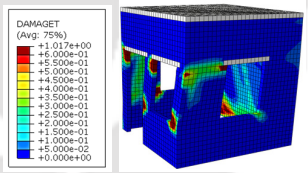	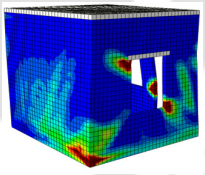
C	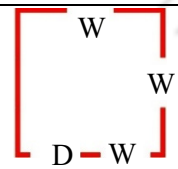	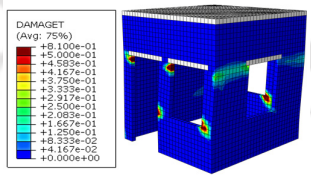	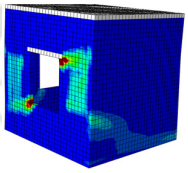
D	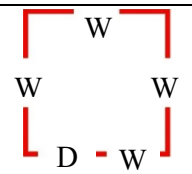	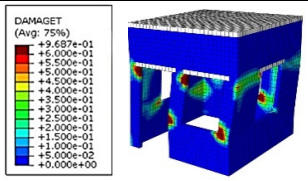	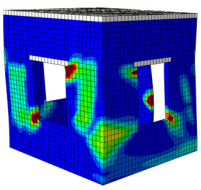

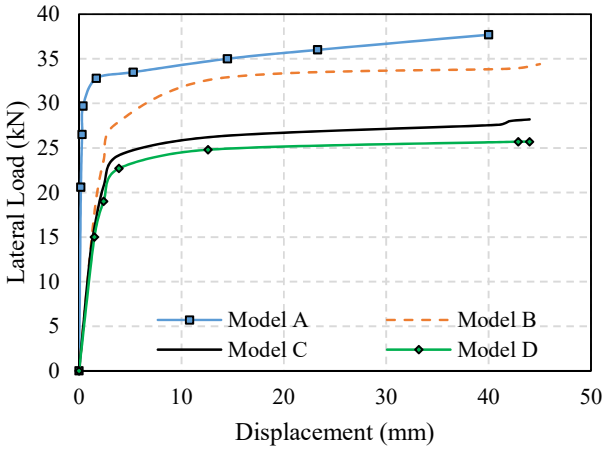

Figure 3.30. Capacity curve comparison of URM building with 4 opening configurations.

Table 3.7. Moment and Shear capacity curves for individual masonry walls strengthened using only external and using both external and internal steel bands

Wall	Moment-Rotation (θ) curve	Force-Displacement curve
Single Horizontal band 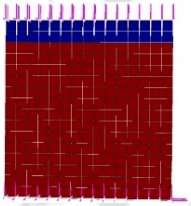	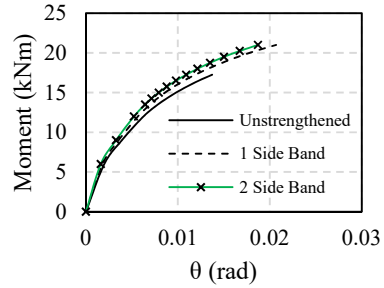	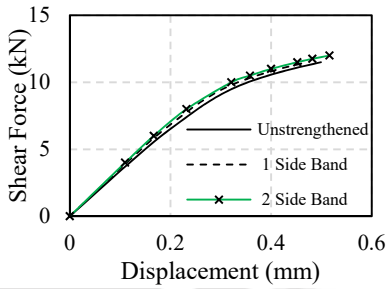
Double Horizontal band 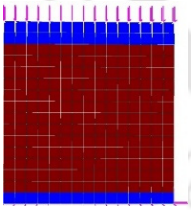	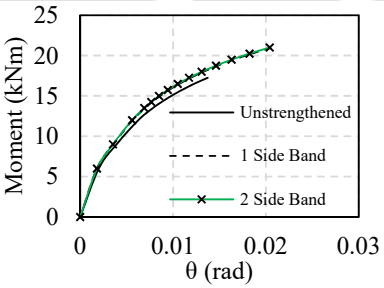	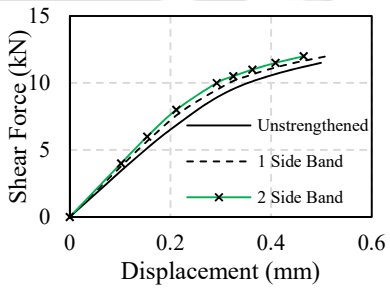
Double Horizontal and Vertical band 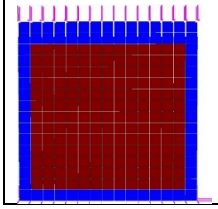	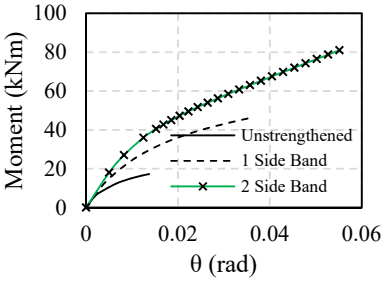	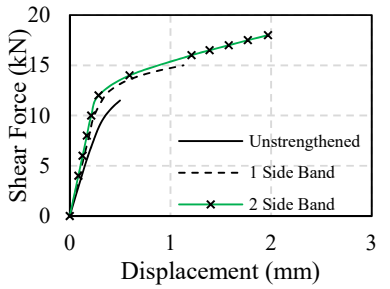

This is followed by the strengthening of the whole building Model D using Strengthening Scheme #3 on (i) only the external face of all the walls, and (ii) both external as well as the internal face of the all the walls as shown in Figure 3.31. Numerical results show that providing only the external bands or both external and internal bands improved the load carrying capacity of the URM building significantly (see Figure 3.32).

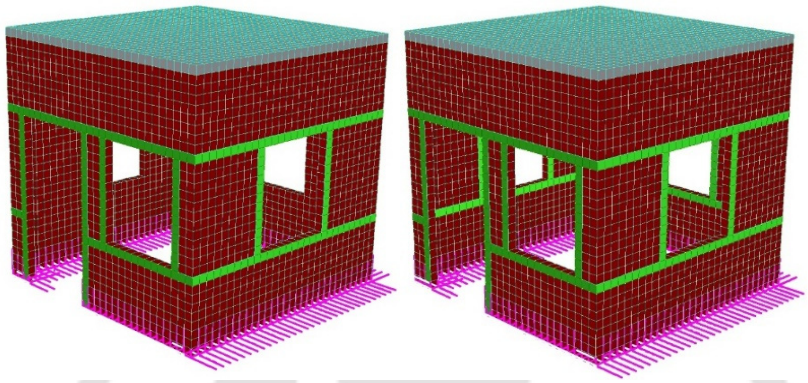

(a) (b)

Figure 3.31. URM building strengthened using Strengthening Scheme #3 with: (a) only external steel bands, and (b) both external and internal steel bands.

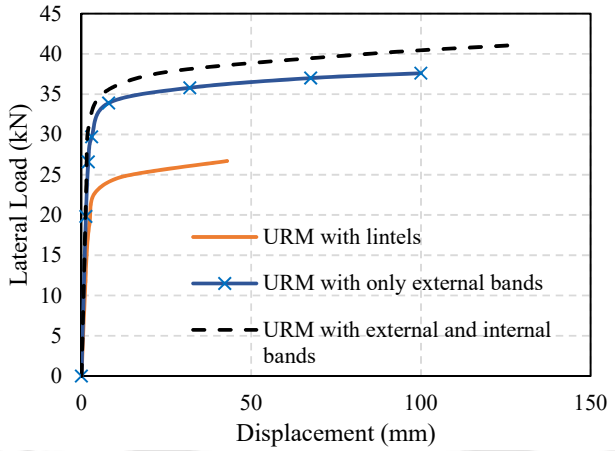

Figure 3.32. Capacity comparison of the strengthening schemes for Model D obtained using Abaqus.

Application of only the external steel bands increases the lateral load carrying capacity by about 30% approximately, and using both external and internal bands increases the load carrying capacity of the URM buildings by about 40%. By applying the earlier established empirical formula (Eq. 3.2) developed for URM building strengthened with double horizontal and vertical steel bands on the revised plan of the URM building, an error of 17% is found. Here weight of the structure (in terms of force) is considered as 61.61 kN and bands are provided with cross-sectional area of 10 mm^2. Hence the influence of the

openings in estimating the lateral load carrying capacity of the structure is a crucial issue and opens scope for more detailed analysis with different building plans and openings configurations with varying aspect ratios.

3.8. SUMMARY

Capacity assessment of URM buildings has been carried out numerically by performing non-linear static analyses using three FE commercial codes, namely, Strand7, Abaqus and SAP2000. A single storey unreinforced masonry building, experimentally tested in without any strengthening measure and loaded by means of a concentrated horizontal load up to failure, has been considered to initially validate the numerical models and calibrate mechanical parameters to adopt a suitable modelling strategy for masonry elements. Then, it has been hypothesized to strengthen the same masonry prototype by means of three different strengthening schemes using continuous steel bands mounted on wall surfaces. Following observations can be made from the simulation results:

- A single steel band mounted on wall surface at lintels level with moderate cross-section (1 mm x 50 mm) provides a reasonably high increase in the lateral load carrying capacity.
- Steel flats with increased thickness generally result in a slightly higher capacity than those with increased width (keeping cross-sectional area of the bands same).
- Higher values of the cross-sectional area of the bands do not contribute much to a further increase in capacity. In any case, all the three strengthening interventions are rather effective, being all associated to a considerable increase in the overall strength of the structure.
- Number of openings have a large influence over the capacity of the building but application of double horizontal bands along with vertical steel bands mounted on the wall surfaces both externally and internally increase the capacity of the structure significantly.

Empirical equations have been developed from the ultimate loads numerically estimated in all the cases analyzed. The developed empirical equations are based on a series of analyses on a single storey building with a single room. Though majority of brick masonry buildings in the South-East Asian countries are single storey with a few rooms, the applicability of the proposed equations will be limited to the strengthening of individual rooms.

Despite predicting lateral strength of URM buildings with reasonable accuracy, the numerical results of three different strengthening approaches exhibited certain limitations. As for instance, the equivalent frame method cannot predict the damage area and progressive failure pattern. However, the numerical approaches by Strand7 and Abaqus showed good similarity with the damage observed experimentally. But the damages predicted by the numerical approaches are in the form of contours, whereas the damages occurred in reality are in the form of cracks mostly between the mortar interface of the masonry units. Hence, an improved method of numerical simulation in the form of simulation process or improved discretization is required to be developed for predicting the failure with better accuracy. A systematic parametric study is required to be carried out on several possible building configurations by varying the aspect ratio, wall thickness, size and location of openings, etc., in order to develop generalized design equations.

Chapter 4
EXPERIMENTAL STUDY ON URM WALLS

Contents

4.1. Overview 73
4.2. Tests on Masonry Constituents 74
4.3. Experimental Evaluation of URM walls 79
4.4. Summary 87

4.1. OVERVIEW

Unreinforced masonry buildings have been in use since several centuries and continue to be the most widely used building typology in various countries, including India. The masonry walls are the most important structural elements in such buildings since they are the only elements to resist the vertical gravity loads as well as the lateral seismic loads. Experience during past earthquakes and experimental studies on masonry buildings have revealed that the in-plane resistance of the URM walls is the main lateral load resisting mechanism when out-of-plane failure is prevented (Kaushik and Dasgupta, 2014; Murty et al., 2006). The URM walls are brittle in nature and possess low tensile strength that make the structure seismically vulnerable. The structural vulnerability can be determined by evaluating the lateral load-carrying capacity of the walls constituting the building. An effective and the simplest way of determining the lateral strength of URM walls is to perform quasi-static cyclic experimental tests on the walls.

Therefore, in the present study, quasi-static, in-plane cyclic tests were conducted on three full-scale URM walls with different opening configurations (door, window). The tests of the walls are essentially required for numerical and analytical validations. Besides, the role of openings in the in-plane capacities of walls is also quite significant and important

to study. However, due to laboratory constraints, out-of-plane testing of the masonry walls was not carried out. The experimental results of different wall specimens displayed a fascinating failure pattern and lateral load-carrying capacity. These values can be conveniently used for estimation of the overall capacity of the building constituting the walls.

4.2. TESTS ON MASONRY CONSTITUENTS

The analytical and numerical evaluation of masonry walls and buildings are largely dependent on the various material parameters under the action of different loading conditions like tensile, compressive, shear, etc. Therefore, necessary tests were conducted to determine the various material properties of masonry, and the non-linear stress-strain curve was determined wherever necessary. At least seven sets of specimens were used to conduct each test so that the average values could be obtained with acceptable confidence.

4.2.1. Compressive Test on Bricks

Bricks are the major constituent materials of masonry walls and buildings. The solid fired clay bricks tested were the first-class bricks and had an average size of 220 mm × 110 mm × 70 mm. The WA (Water Absorption) and IRA (Initial Rate of Absorption) was measured following the code IS 3495 (BIS, 1992) and ASTM C67-13 (ASTM, 2013b). The average water absorption capacity of the bricks was measured to be about 13%, and the average IRA was measured to be 2.35 kg/m^2/min. The compressive strength was determined by placing the brick under direct uniaxial compressive loading (Figure 4.1) with a displacement rate of 0.16 mm/s which is as per the guidelines provided in ASTM C67-13 (ASTM, 2013b) and IS 3945 (BIS, 1992).

Figure 4.1. Compression test of bricks.

The frog of the brick was initially filled with mortar and the brick specimen was encased between soft plywood plates. The setup was then placed in the compressive testing machine between rigid steel plates with fog facing upwards. The average compressive strength achieved was about 21.20 MPa.

4.2.2. Compressive Test on Mortar

It is a common practice in India to use cement: sand mix mortar grade of ratio 1:6. As per ASTM C109/C109M-13 (ASTM. 2013b) and IS 2250 (BIS, 1995) the size of the mortar cube was fixed as 50 mm × 50 mm × 50 mm (Figure 4.2). The tests were carried out after 28 days of curing the mortar cubes. Before testing, the surfaces of the mortar cube and the bearing plates of the actuator were wiped clean to remove any unwanted loose particles. The test was conducted with a slow loading rate of 0.11 mm/s under compression testing machine, and the average compressive strength of the mortar cube was found to be 6.56 MPa.

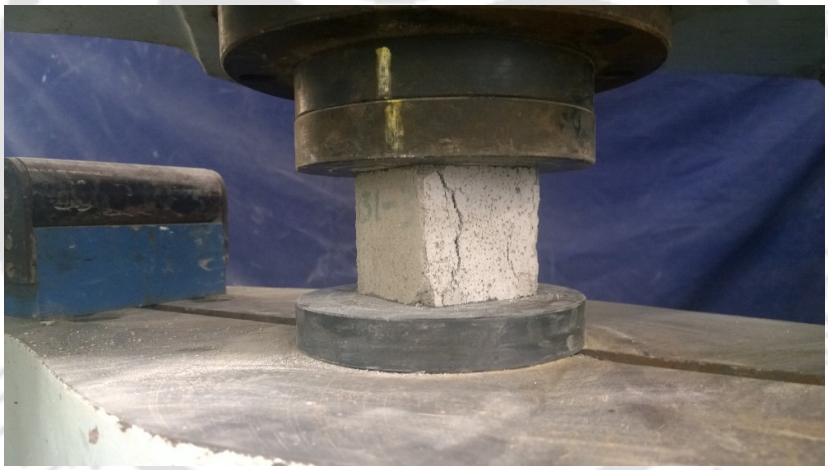

Figure 4.2. Compression test of cement mortar cubes.

4.2.3. Triplet Shear Test

Triplet shear test was conducted to determine the initial shear capacity of the mortar bond in zero compressive stress. The test was conducted as per the guidelines in BS-EN-1052 (2002). Before testing, the triplets constructed using 1:6 mortar grade were cured for 28 days. Two different sets of Triplets were constructed: one set was constructed in accordance with BS-EN-1052 (2002) represented as Triplet Shear Setup 1 (Figure 4.3a), and the other set constructed by shifting the central brick by about 10 mm represented as Triplet Shear Setup 2 (Figure 4.3b). The second set of arrangement was made because it requires much

less experimental setup, and therefore, it is easier to perform the test. The specimens were loaded up to failure under hydraulic pressure (Figure 4.3c).

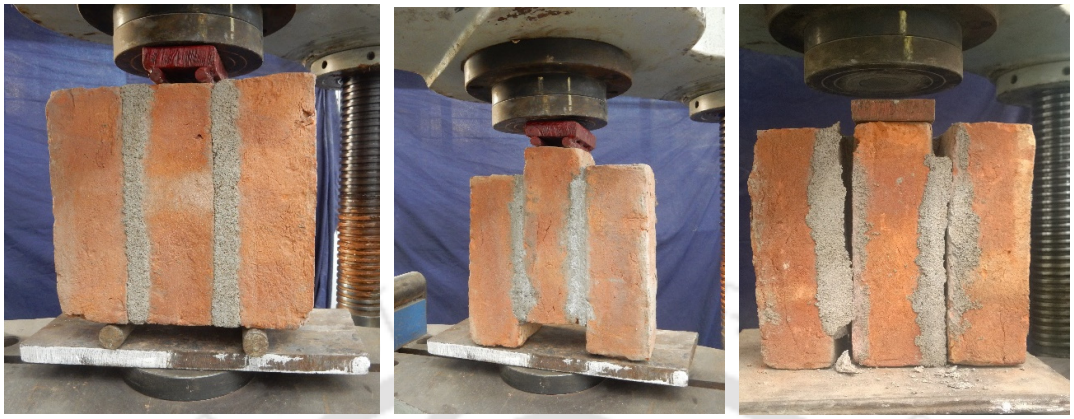

(a) (b) (c)

Figure 4.3. Triplet Shear Test: (a) Setup 1, (b) Setup 2, and (c) Failure mechanism observed.

The initial shear strength (f_{vko}) was calculated using the Eq. 4.1 as recommended in BS-EN-1052 (2002).

$$f_{vko} = \frac{F}{2A_p} \tag{4.1}$$

Where F is the peak shear strength obtained from the test, and A_p is the cross-sectional area of the specimen parallel to the bed joint. The first setup resulted in initial shear strength of 0.176 MPa, whereas the second setup resulted in a value of 0.164 MPa. The average value of the initial shear strength was considered as 0.17 MPa.

4.2.4. Tensile Bond Test

It has been observed from the past URM buildings that the failure occurs mainly at the joints between the mortar and the bricks. Hence, Khalaf (2005) suggested a procedure to determine the tensile bond strength between the mortar and the bricks (Figure 4.4). Khalaf assumed two types of stress distribution, one being linear and other being parabolic. For the present study, the linear stress distribution was considered since there was not much difference in the tensile stress using the two stress distributions. The flexural bond strength (f_t) was determined by using the Eq. 4.2 recommended by Khalaf (2005).

$$f_t = \frac{\left(0.5l_b^2 - l_b t_{bar} + 0.5t_{bar}^2\right)P_v + \left(0.75l_b^2 - 1.25l_b t_{bar} + 0.5t_{bar}^2\right)W}{\left(0.33l_{mj}^2 w_b\right)\left(1.5l_b - t_{bar}\right)} \tag{4.2}$$

Where, l_b, w_b, and l_{mj} are the length and width of the brick specimen and length of the mortar joint, respectively; P_v is the failure load; W is the weight of the brick unit, and t_{bar} represents the thickness of the bar. 1:6 mortar grade was used in the specimen, and the test was conducted after 28 days of curing. The average tensile bond stress was calculated to be 0.076 MPa.

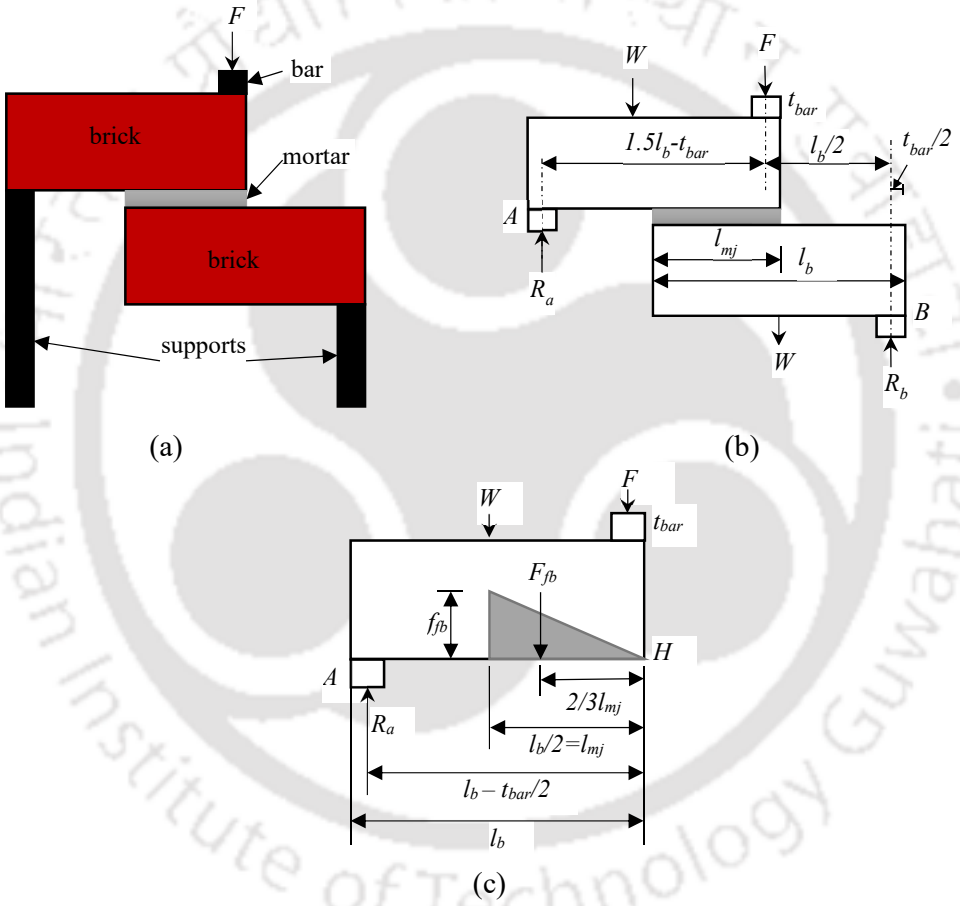

Figure 4.4. Tensile bond test: (a)Experimental setup of Z Specimen, (b) Free body diagram of Z-shaped specimen, and (c) Free body diagram of top brick displaying loads and stress distribution.

It is to be noted that during the tensile bond test, the material exhibited sudden brittle failure (Figure 4.5a), leaving no scope of capturing the post-peak softening behavior, which was required to define the tensile damage behavior of masonry material for the numerical analysis. Using the past results of Dhanasekar and Haider (2008) and Rai et al. (2014), a

tensile strain value of 0.0001 was therefore considered in the study corresponding to the peak tensile stress of 0.076 MPa. The post-peak behavior was assumed to be linearly falling till tensile stress of 0.015 MPa and corresponding strain value of 0.001, as shown in Figure 4.5b. The residual tensile stress of 0.015 MPa was further considered till strain value of 0.0015. These values in the tensile stress-strain curve were selected based on past literature to assist in smoother strength degradation required for convergence of numerical solution procedure during non-linear analyses.

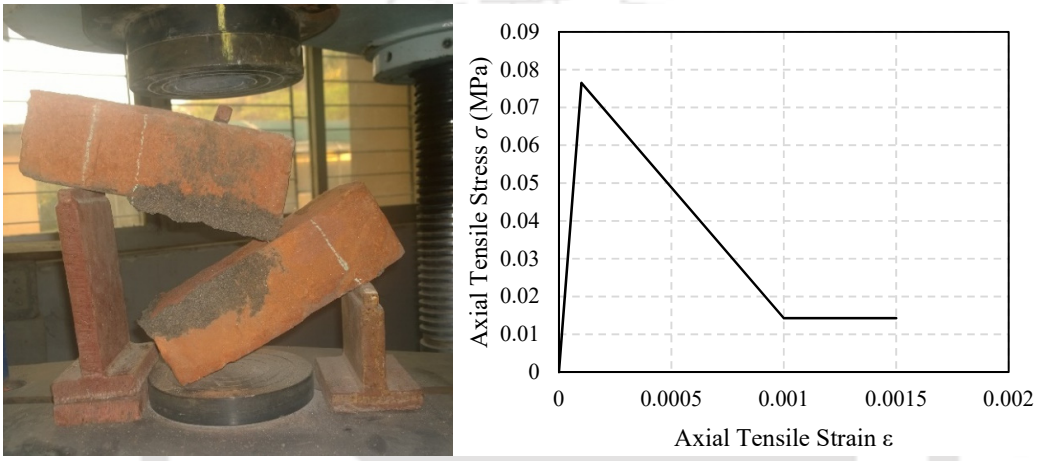

(a) (b)

Figure 4.5. Tensile bond test: (a) tension bond failure of Z-shaped specimen (b) idealized tensile stress-strain curve.

4.2.5. Compressive Test on Masonry Prism

Compression tests of masonry prisms were carried out following ASTM C1314-12 specifications (ASTM, 2012) and IS 1905 (BIS, 1987b). The prisms were constructed using first-class bricks and 1:6 cement: sand mortar grade. The specimens had an average height of about 425 mm, length of about 233mm, and thickness of about 115 mm. All the prisms were cured for minimum of 28 days before testing. The specimens were centrally placed between the loading plates of the compression testing machine (Figure 4.6a). A monotonic uniaxial compressive loading was applied to the specimen with a displacement rate of 0.16 mm/s. The average value of the compressive strength of the masonry prism (f_m) was 3.40 MPa. The average modulus of elasticity was calculated using the equation suggested by Kaushik et al., (2007) and it comes out to be 1732 MPa. The average stress-strain curve obtained for the masonry prisms is shown in Figure 4.6b. Various mechanical properties obtained from the tests are summarized in Table 4.1.

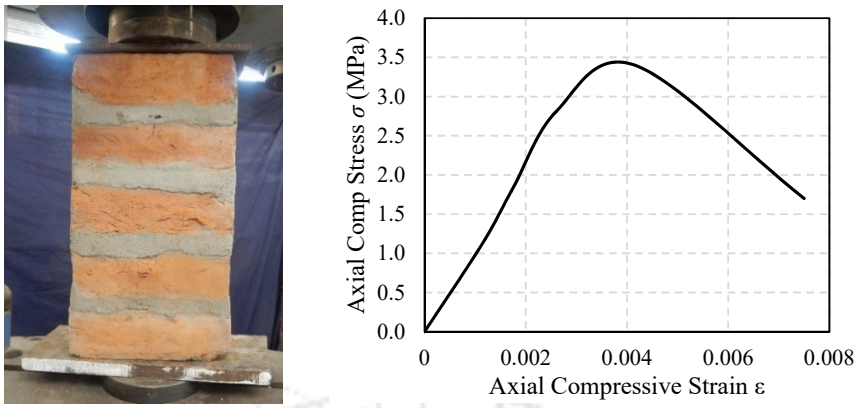

(a) (b)

Figure 4.6. Masonry displaying: (a) compression test, and (a) average compressive stress-strain curve.

Table 4.1. Mechanical properties of masonry materials

Property	Value	Remarks
Compressive Strength of Brick Unit	21.2 MPa	Experimentally obtained
Compressive Strength of Mortar (1:6)	6.56 MPa	Experimentally obtained
Compressive Strength of Masonry Prism	3.40 MPa	Experimentally obtained
Tensile Bond Strength (Z test)	0.076 MPa	Experimentally obtained
Elastic Modulus of Masonry	1732 MPa	Experimentally obtained
Shear Strength (Triplet Shear Test)	0.17 MPa	Experimentally obtained
Specific Weight of Masonry	1870 kg/m^3	BIS (1987a)
Elastic Modulus of Concrete	24768 MPa	BIS (2000)
Density of Concrete	2400 kg/m^3	BIS (1987b)

4.3. EXPERIMENTAL EVALUATION OF URM WALLS

Three full-scale URM walls with different opening configurations were subjected to the cyclic tests (Figure 4.7 and Figure 4.8a-c). All the walls were constructed in English bond and had height, length, and thickness as 3 m, 3 m, and 0.24 m, respectively. Reinforced concrete lintel beam, 1.3 m long with 0.24 m × 0.24 m section, was provided above all the openings. The lintel beams were reinforced with 8 mm diameter longitudinal bars and 6 mm diameter stirrups spaced at 0.1 m spacing. The pre-compression vertical load applied over the wall specimens was calculated considering a single storey building with the dimension 3 m × 3 m × 3 m bearing a reinforced concrete slab of 0.1 m thickness and 1 m parapet wall above it. The load was applied over a reinforced concrete slab of 1 m width and 0.1 m thickness constructed over the walls. The displacement history used in the cyclic tests was simulated by stepwise linearly increasing lateral displacement, as shown in Figure 4.8d. Three cycles of each displacement amplitude were applied on the specimens using a

servo-controlled hydraulic actuator of 250 kN force and 250 mm displacement capacity. A Linear Variable Displacement Transducers (LVDT) was used to record the displacement at the top of the wall. All the specimens were constructed on a reinforced concrete slab, which was rigidly anchored to the strong floor to prevent sliding during the cyclic loading.

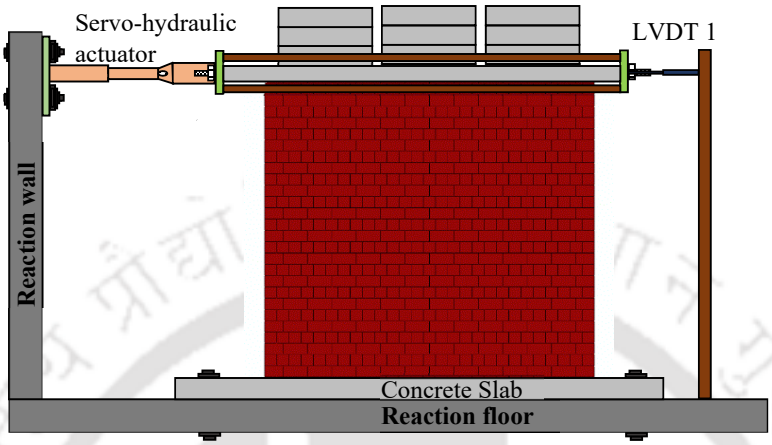

Figure 4.7. Experimental setup for testing of URM walls.

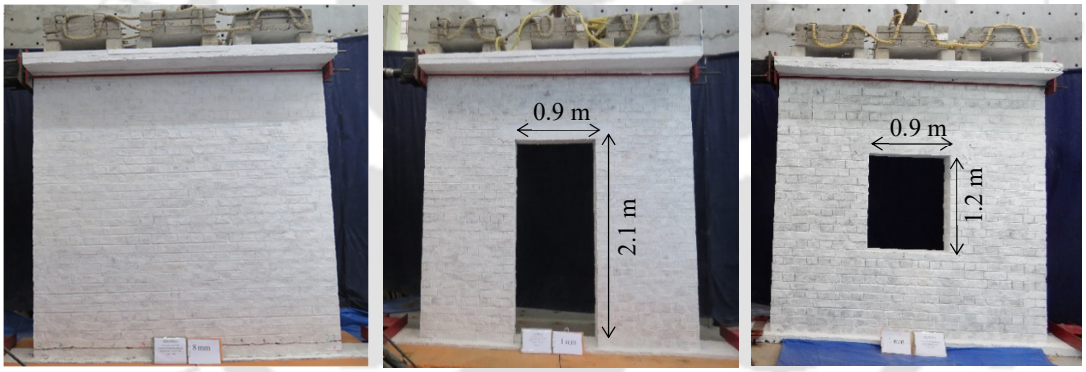

(a) (b) (c)

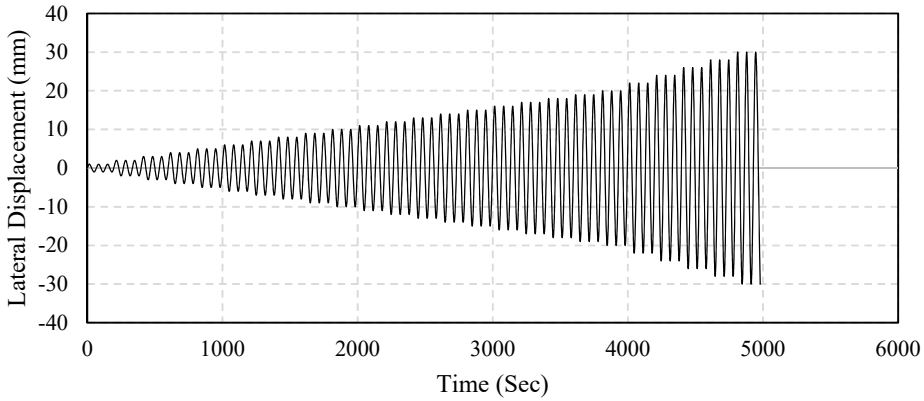

(d)

Figure 4.8. Slow cyclic testing of: (a) solid wall (Wall 1), (b) wall with a door opening (Wall 2), (c) wall with a window opening (Wall 3), and (d) applied displacement history.

4.3.1. Experimental Results

Lateral load response of all the three specimens was studied in terms of crack formation, lateral strength, energy dissipation, etc. All the models displayed different failure patterns and lateral load-carrying capacities, and the tests were continued until significant damage was observed. Although all the models finally failed in a brittle manner, each model started rocking motion after reaching a particular displacement level while sustaining the load till failure.

4.3.1.1. Wall 1 (Model 1)

Model 1 was the URM wall specimen without any opening. Under lateral loading, the first flexural crack occurred at the base of the model at 2 mm displacement level (Figure 4.9). The crack propagated further with an increase in displacement level initiating the sliding shear failure at 8 mm displacement level. The test was terminated at 9 mm displacement level due to the out-of-plane movement of the wall. The lateral load-carrying capacity of Model 1 was found to be 27.5 kN. A small bed joint crack was also observed at the top of the wall specimen at 6 mm displacement (Figure 4.9a). The hysteresis response, capacity envelop curve, and cumulative energy dissipation obtained for Model 1 are shown in Figure 4.10 and Figure 4.11, respectively. The hysteresis response of Model 1 resembles more or less a bi-linear elasto-plastic behavior with limited ductility. The cumulative energy dissipation curve shows a steady increase in the energy dissipation capacity till failure.

(a) (b)

(c)

Figure 4.9. Lateral load testing of Wall 1: (a) load arrangement and crack formation and (b)(c) closer view of the crack propagation at the bottom of the wall.

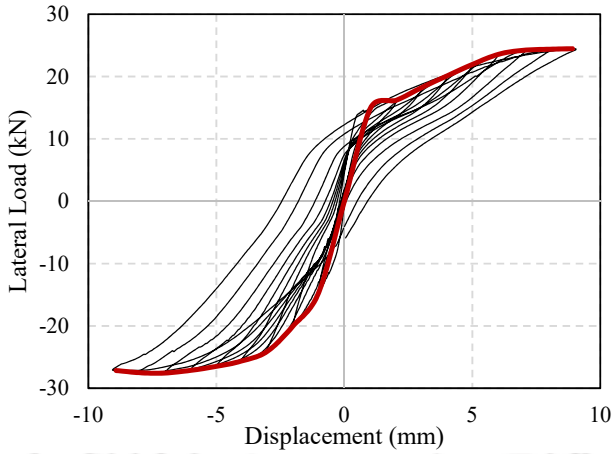

Figure 4.10. Hysteresis response and capacity envelop curve obtained for Wall 1.

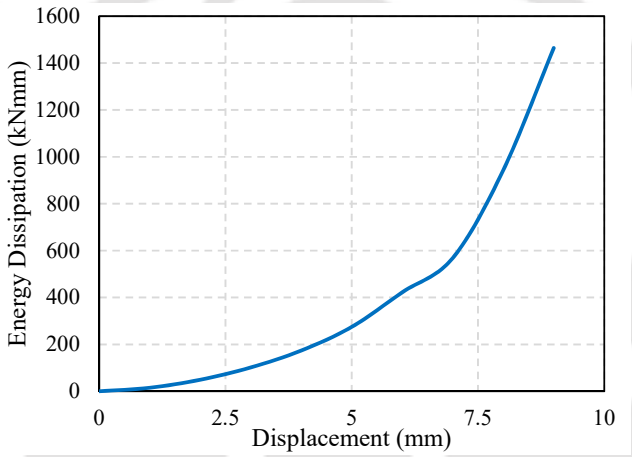

Figure 4.11. Cumulative energy dissipation curve obtained for Wall 1.

4.3.1.2. Wall 2 (Model 2)

Model 2 was the URM wall specimen consisting of a central door of size 0.9 m × 2 m. The cyclic test on the specimen resulted in a mixed failure mode of flexure and sliding shear-type (Figure 4.12). Small cracks appeared in the bottom of the specimen during the loading at 2 mm deformation level. At 4 mm deformation level, these cracks at the first bricklayer from the bottom started widening and extending. At 5 mm displacement level, cracks originated at the upper corners of the door opening, and these cracks subsequently extended towards wall edges till failure of the specimen at only 6 mm lateral displacement. The lateral load capacity of Model 2 is 19 kN, as shown in the hysteresis response in Figure 4.13. The strength envelops curve and cumulative energy dissipation curve also depict the sudden failure of the specimen at a low level of lateral deformability resulting in very low energy dissipation (Figure 4.14). The test was stopped at the first cycle of 6 mm displacement level to prevent complete disintegration of the wall. During the initial

displacement cycle up to 2 mm, the lateral load resistance of the model displayed a stiff rise, whereas during the later displacement cycles the capacity curve flattened until sudden failure. Clearly, there is a considerable influence of the presence of a door opening on the lateral load behavior of URM wall.

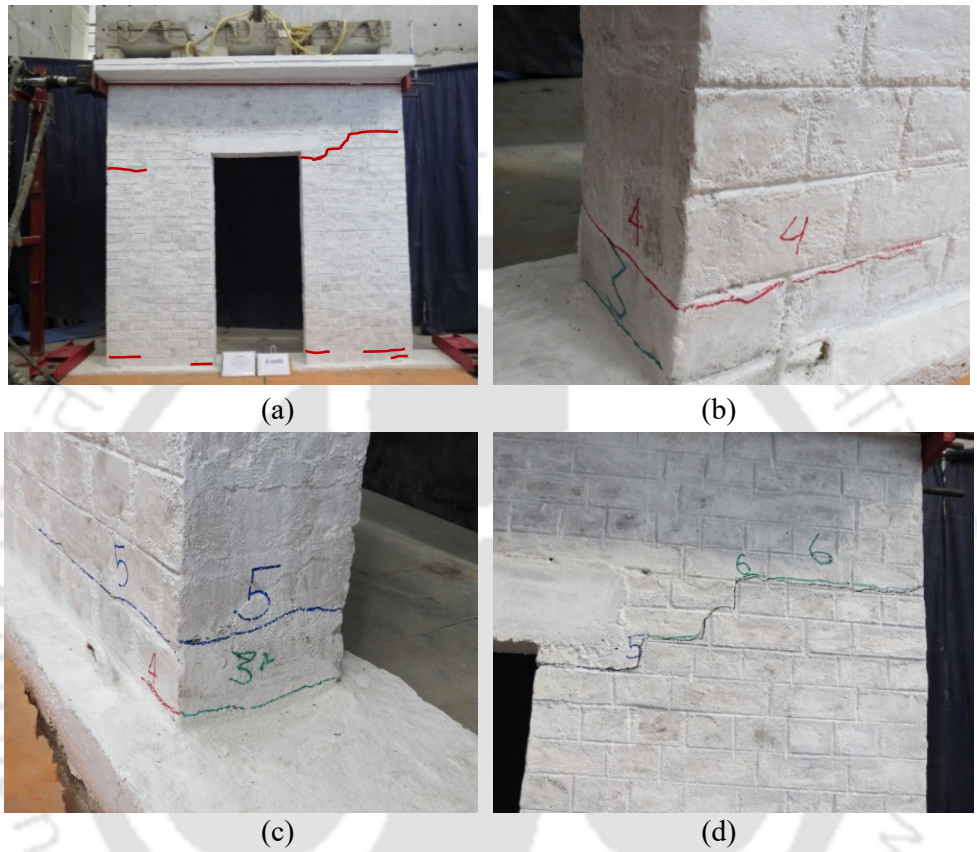

Figure 4.12. Lateral load testing of Model 2: (a) crack formation at 6 mm, (b) (c) closer view of crack at the base, and (c) closer view of crack near the top of the door opening.

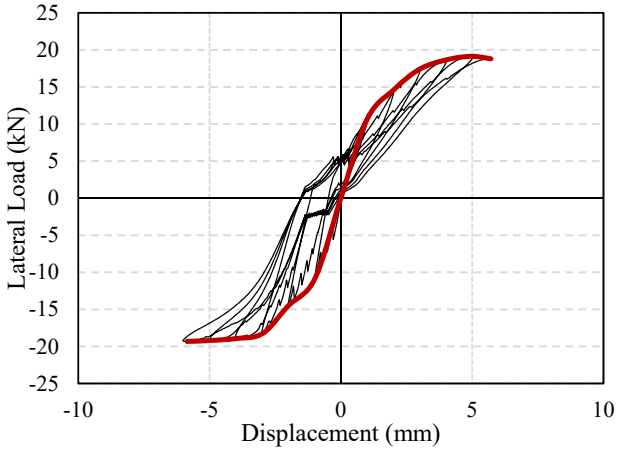

Figure 4.13. Hysteresis and capacity curve obtained for Wall 2.

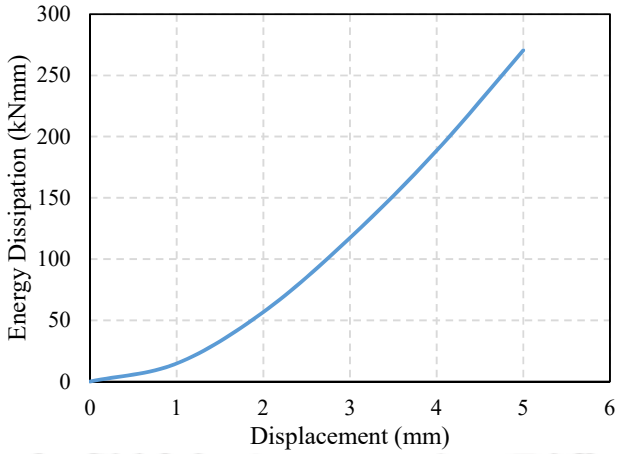

Figure 4.14. Cumulative energy dissipation curve obtained for Wall 2.

4.3.1.3. Wall 3 (Model 3)

Model 3 was the URM wall specimen consisting of a central window opening of size 0.9 m × 1.2 m. The cyclic test on Model 3 also resulted in a mixed failure of flexure and sliding shear type (Figure 4.15). Unlike other walls, small cracks started appearing quite early in Model 3 at 1 mm displacement level in the bottom brick course. At 3 mm displacement level, the cracks at the bottom layer widened further extending towards the middle portion of the wall, and by 12 mm displacement level, the cracks passed throughout the length of the model. However, no visible cracks were observed in any other locations. Generally, cracks were expected to form at the corners of the opening due to stress concentration as observed in Wall 2. Therefore, it appears to be a failure due to flexure at the bottom, followed by sliding due to the presence of a weaker course of masonry at the base of the specimen. The hysteresis curve, strength envelop curve, and energy dissipation curve generated from the test results are shown in Figure 4.16 and Figure 4.17, respectively.

(a) (b)

Figure 4.15. Lateral load testing of Wall 3: (a) crack along the whole length of the wall at the bottom at 12 mm displacement level, and (b) closer view of the crack formed at the wall bottom.

Similar to Wall 2, severe pinching was also observed in the hysteresis loops of Wall 3, resulting in lower energy dissipation capacity of Wall 3 compared to Wall 1. But, higher deformability of Wall 3 kept its energy dissipation capacity higher (more than two times) than that of Wall 2. In the case of Wall 1, Fig. 4.9 shows the formation of bed joint shear crack at the top of the wall for a partial length of the wall. The RC slab above the wall did not slide during the test. The crack formed much later than the flexural crack at the base of the wall. Whereas, in the case of Wall 3 (Fig. 4.15), the flexural cracks formed at the bottom of the specimen rather than near the corners of the window openings because of low axial load acting on the wall. It has been observed in several past studies (e.g., Javed et al. 2015, ASCE/SEI 41-13 2014; Magenes and Calvi 1997) that axial loads acting on the walls significantly influences the damage pattern of masonry walls under in-plane loading.

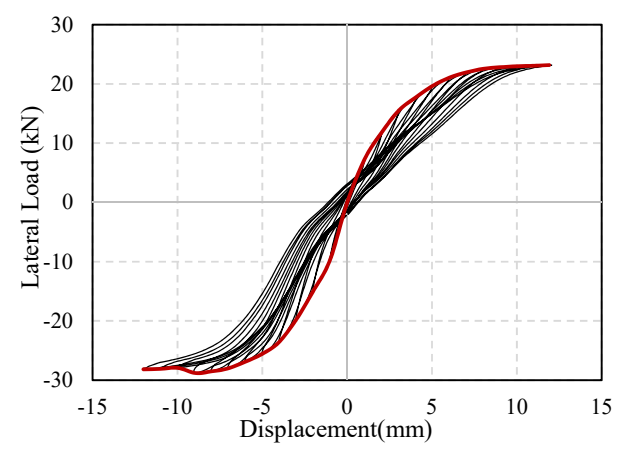

Figure 4.16. Hysteresis curve and strength envelop curve obtained for Wall 3.

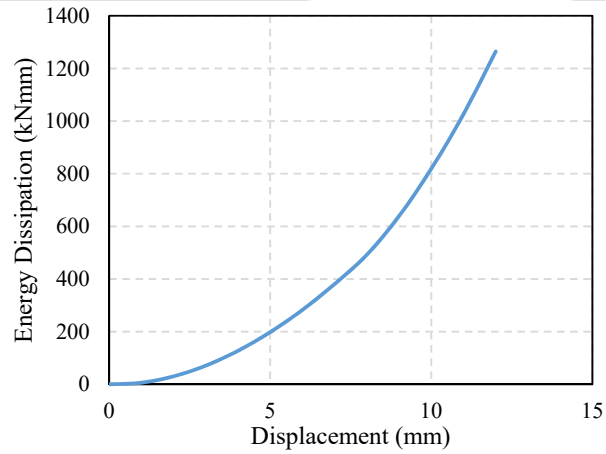

Figure 4.17. Cumulative energy dissipation curve of Wall 3.

4.3.1.4. Comparison of Response of URM Walls

Figure 4.18 compares the experimental lateral load responses of all the three walls. It can be noted from Figure 4.18 and Figure 4.19 that the lateral load capacity of the wall without any opening and wall with window opening does not differ much, though a significant reduction in energy dissipation capacity is visible due to the presence of opening (Figure 4.20). As shown in the comparison (Fig. 4.19), the lateral strength of the solid wall and the wall with window opening was more of less identical, though the wall with a window opening (Wall 3) had a marginally higher lateral strength in the Push direction. The minor difference may occur in such large-scale testing due to variety of reasons, for example, variation in masonry tensile strength, presence of RC lintel above window opening, etc. It is evident from the figure that the presence of openings reduces the energy dissipation capacity of the walls drastically. The energy dissipation capacity of Wall 1 specimen was higher than that of the Wall 3 specimen because the hysteresis curves obtained for Wall 1 specimen were more stable with significantly lesser pinching compared to Wall 3 (Fig. 4.18). The higher pinching in Wall 3 was obviously a result of presence of the window opening that in turn resulted in discontinuity and change in the load/stress path in the masonry wall. Therefore, the window size can be optimized to reduce the negative influence of openings on energy dissipation capacity. IS 4326 (BIS 1993) suggests providing a smaller opening size for improved lateral load capacity. The location of the opening also significantly affects the lateral strength of the structure. But if located centrally, the present results show that a standard window size of 0.9 m × 1.2 m, will not result in a significant reduction in the strength of the wall.

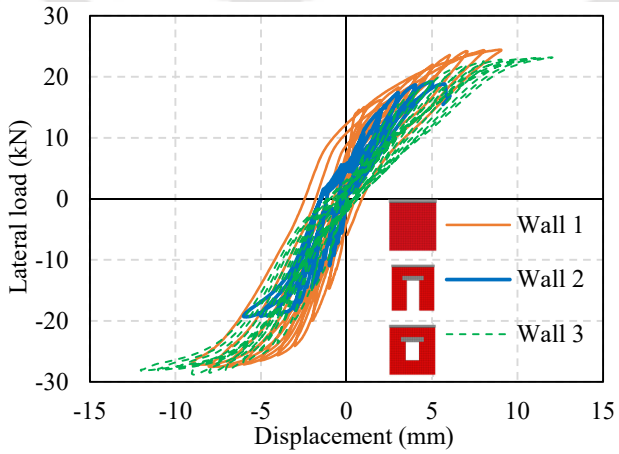

Figure 4.18. Comparison of hysteresis curves of three walls.

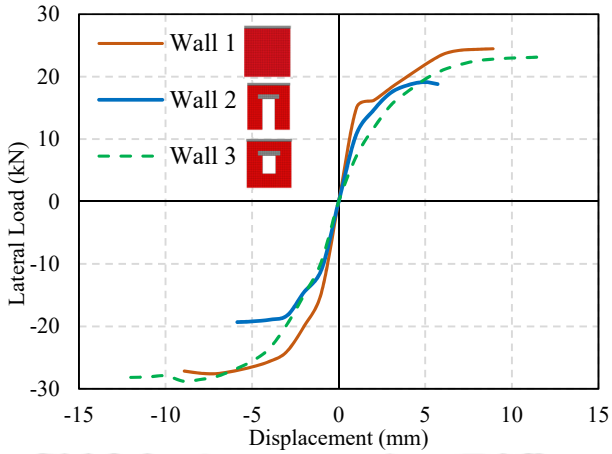

Figure 4.19. Comparison of capacity envelop curves of three walls.

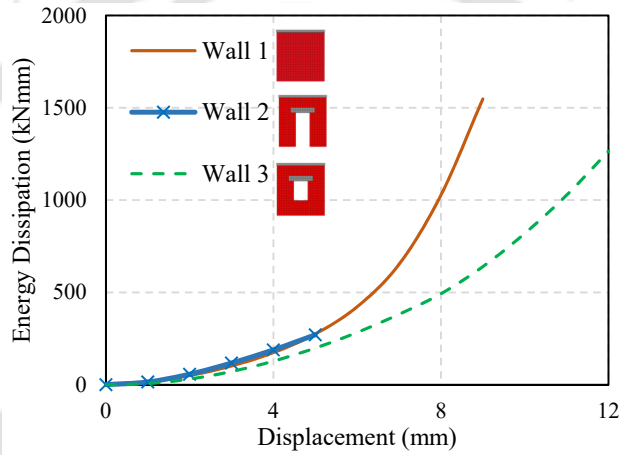

Figure 4.20. Comparison of cumulative energy dissipation curves.

4.4. SUMMARY

In this chapter, test results obtained by masonry constituents testing and in-plane quasi-static cyclic testing on URM walls were discussed. Out if the three walls, one wall was solid, the second consisted of a door in the center and the third consisted of a central window. The test of the walls displayed a varied level of lateral load-carrying capacity. The URM wall with central door displayed the least lateral load resisting capacity. The wall with a central window resulted in nearly similar lateral load values in comparison to a solid wall but with significantly lower energy dissipation capacity. The sliding shear failure seems to be the major governing failure criteria in the case of Wall 1 and Wall 3 since the failure occurred at the base of the wall by formation of longitudinal cracks. Whereas, flexural failure was the governing failure criteria in the case of Wall 2. These walls will be further numerically and analytically evaluated in the later chapters. The present test results

will be useful in understanding the influence and contribution of individual wall on the global strength of the building as a whole.

Chapter 5
EXPERIMENTAL STUDY ON STRENGTHENING OF URM BUILDINGS

Contents

5.1. Overview 89
5.2. Experimental Setup 91
5.3. Testing of URM Building (Unstrengthened) 96
5.4. Testing of Strengthened Building 1 (Model 1) 99
5.5. Testing of Strengthened Building 2 (Model 2) 102
5.6. Summary 108

5.1. OVERVIEW

A large number of unreinforced masonry (URM) buildings are presently in use fulfilling various needs like residential, industrial, monumental, worshipping, etc. Some of these buildings have both cultural as well as heritage values, and therefore, it is important that these buildings are made resistant to several hazards encountered during their service life. As observed during numerous past occasions, earthquakes pose a great hazard to such buildings primarily due to their large mass and intrinsic brittle nature. Nevertheless, unreinforced brick masonry buildings are still a popular choice of construction in various parts of the world, including developing countries like India, due to economically and easily available construction materials and construction tools. Performance during past earthquakes indicates that URM buildings are susceptible to a combination of in-plane and out-of-plane damage to individual walls, resulting in corner damage, roof damage, damage to the connection between walls and floor diaphragms, and partial or complete collapse (Lizundia et al., 2016). In a large number of cases, rebuilding and rehabilitation of URM

buildings damaged during earthquakes are carried out using the materials recovered from the debris, and a similar building is again constructed, while waiting for another disaster (Joshi and Kaushik, 2017). It is therefore important to develop simple and cost-effective strengthening schemes for URM buildings that can be easily implemented by the engineer on site, especially for developing countries, where millions of such buildings are seismically vulnerable.

Several strengthening measures have been suggested in the literature for URM buildings. Some of them include use of fiber-reinforced polymer wraps over walls, wall jacketing, grouting, splint and bandage technique using wire mesh, prestressing techniques, carbon and glass fibre-reinforced polymer grids, polypropylene bands, fiber-reinforced polymer composite overlays, shotcreting, etc. (BIS, 1993; Drysdale et al., 1999; Elgawady et al., 2004; EN 1998-3, 2005; FEMA 547, 2006; Hamid et al., 2005; Kadam et al., 2014; Marshall et al., 2000; Tomaževič 1999). Most of such schemes bear a heavy cost as they need specialized materials and skilled supervision, and limit further structural modifications once applied over the structural surface. Therefore, people living in earthquake-prone areas of several developing countries have adopted different cost-effective strengthening techniques suitable in that region depending upon availability of materials.

A two storey URM archive building at Gangtok in Sikkim (India) suffered damage during the 1988 Bihar-Nepal earthquake. Subsequently, it was retrofitted using steel bands all along the length of the building at various levels. A moderate earthquake of magnitude 5.3 hit the city in 2006, during which the retrofitted building performed really well and sustained no damage as observed by Kaushik et al. (2006). On 18 September 2011, another earthquake of magnitude 6.9 struck the region, during which several buildings suffered major damage, but the retrofitted archive building survived with some minor damages only (Kaushik and Dasgupta, 2014). Hence, such simple and cost-effective strengthening techniques make a sensible approach to strengthen URM buildings. Excellent seismic performance of URM buildings strengthened using such simple approaches shows that the strengthening scheme, if to be used in a large-scale intervention, need not be technically advanced but it should be sustainable in nature, acceptable to the society, and should assist in keeping the structural members together.

Besides, various studies carried out in different parts of the world indicate that tying URM walls with steel ties prevents separation and disintegration of the walls, and improves seismic behavior of the building (Borri et al., 2009; Vincente et al., 2011). Branco and Guerreiro (2011) observed that the use of steel ties could be less expensive, does not contribute to an excessive increase in the building's weight, and minimizes the interruption of the normal functioning of the building. According to Tassios (2010), the addition of steel elements as shear connectors along transverse wall intersections is quite beneficial for stitching the cracks in URM buildings. Due to these advantages, use of steel bands appears to be a sustainable methodology for strengthening the seismically vulnerable URM buildings, especially in those areas where it is difficult to transport other specialized construction equipment and materials.

Therefore, in order evaluate the effectiveness of the strengthening scheme, in which surface-mounted steel bands are used to tie the URM walls at various levels, three full-scale specimens of a single storey, single bay URM building were tested in the present study under pseudo-static slow cyclic lateral loading (Figure 5.1). The first building model was unstrengthened (Figure 5.1a), while the other two building models were strengthened using steel bands in different configurations. The second building was strengthened using horizontal steel bands only at lintel level along the whole perimeter of the building (Figure 5.1b). Whereas, the third building was strengthened using horizontal steel bands at the lintel as well as the sill level along the whole perimeter of the building. In addition, vertical steel bands were also used adjacent to the openings in the third building as shown Figure 5.1c. The steel bands were mounted both externally and internally on the surface of the walls and connected with the help of steel bolts. As shown in Figure 5.2a, one wall of the building (Wall 2) had a door opening (size: 0.9 m × 2.1 m), while the two adjacent walls (Wall 3* and Wall 3) had a central window opening (size: 0.9 m × 1.2 m). The fourth wall (Wall 1) was constructed without any opening. Such a configuration was used to test the suitability of the strengthening scheme for walls with different opening configurations.

5.2. EXPERIMENTAL SETUP

Dimensions of all the URM building models considered in the study for carrying out pseudo-static lateral load testing were the same, but as already discussed there were differences in opening configurations and strengthening schemes used. The base

dimensions of the buildings were kept as 3 m × 3 m and the height was also 3 m (Figure 5.2). These dimensions were chosen to reflect the size of a typical single room in a building.

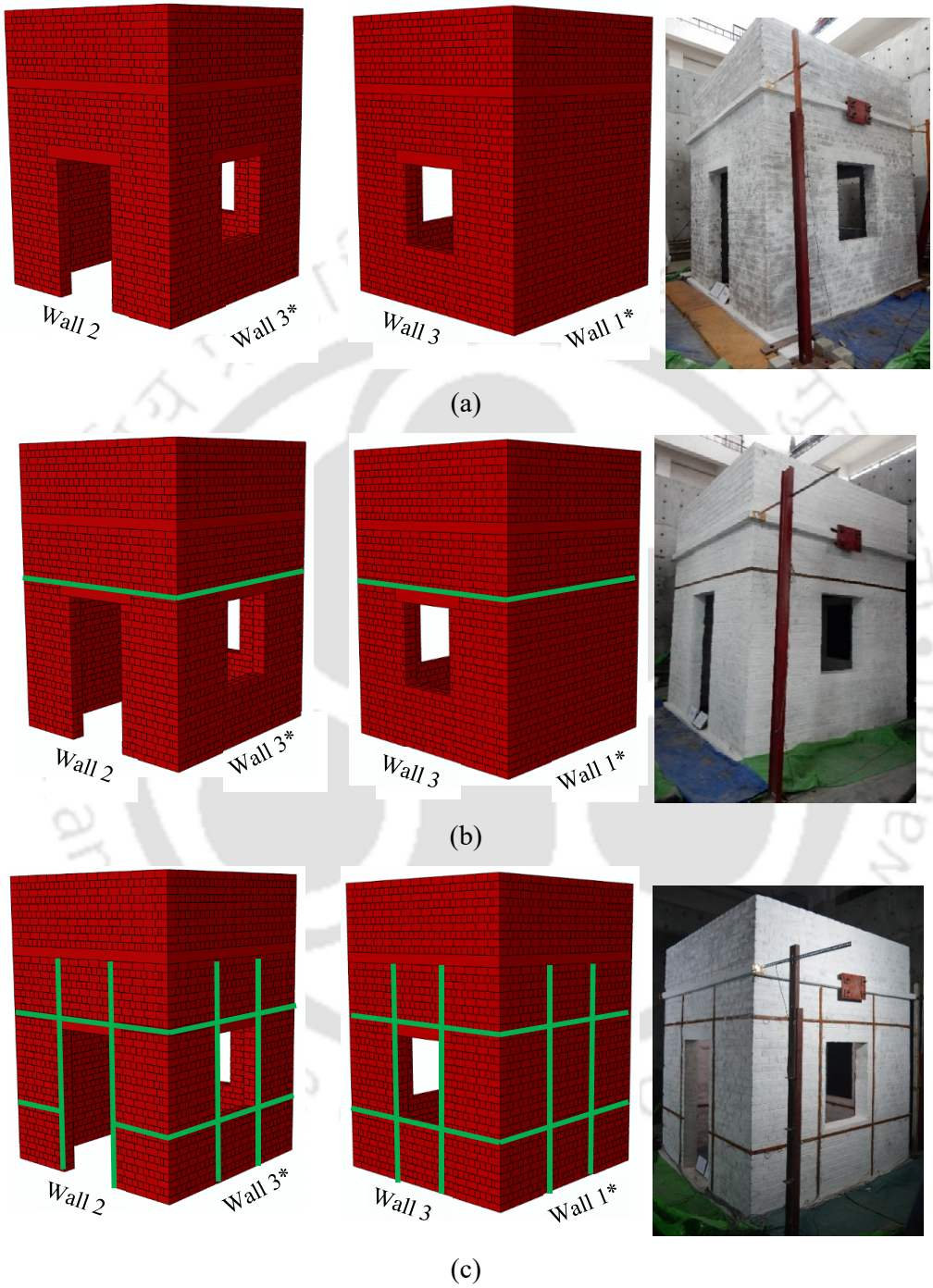

Figure 5.1. Overview of the URM building specimens: (a) unstrengthened URM Building (denoted as URM), (b) building strengthened using horizontal steel bands at lintel level (denoted as Model 1), and (c) building strengthened using horizontal steel bands at sill and lintel levels and vertical bands adjacent to openings (denoted as Model 2).

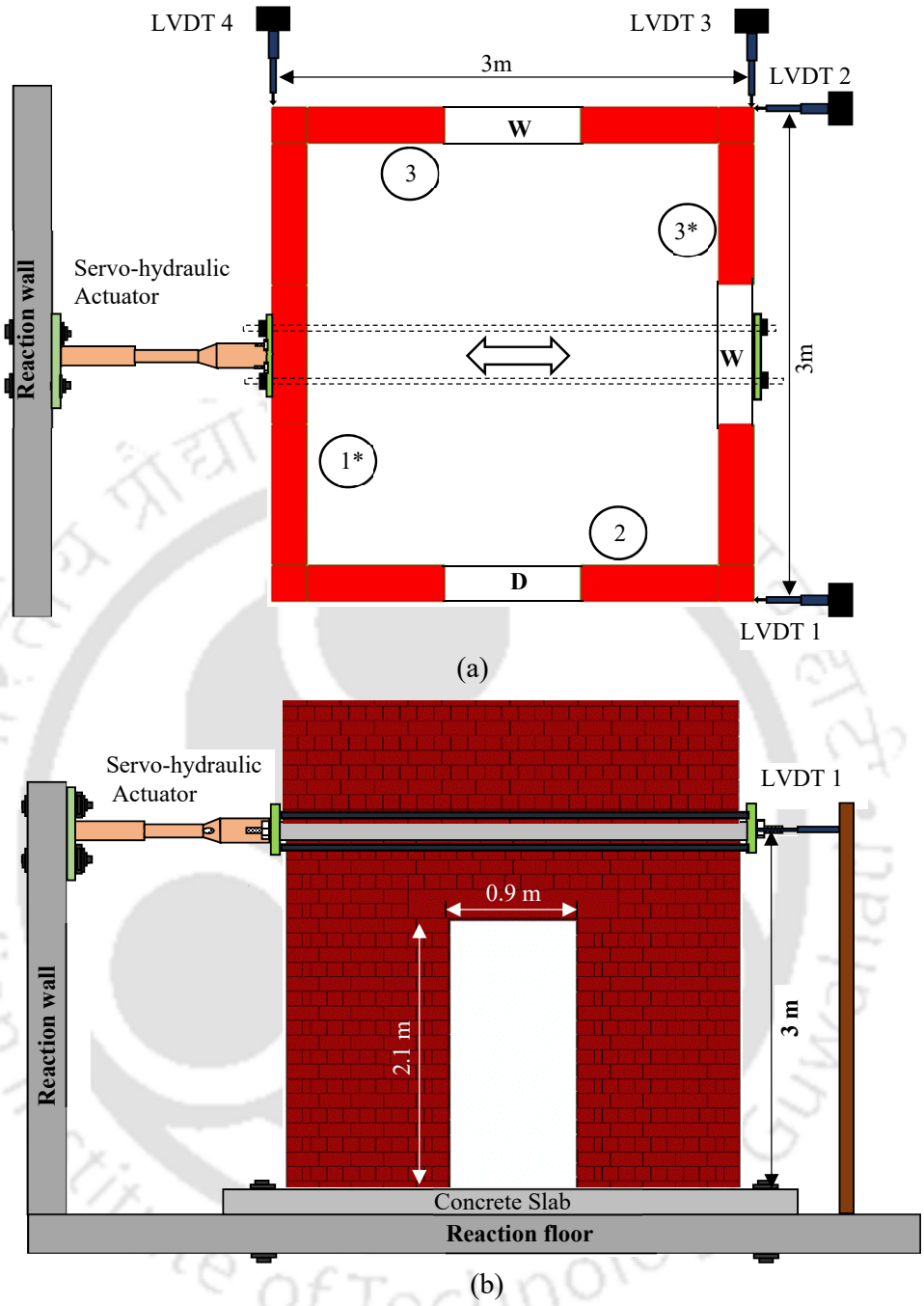

Figure 5.2. Experimental setup: (a) Plan, and (b) Elevation of the building showing loading arrangement, sensors, and openings in the walls.

Reinforced concrete lintel beams, 1.3 m long, 0.24 m wide and 0.24 m high were provided above all openings. The lintel beams were reinforced with 8 mm diameter longitudinal bars and 6 mm diameter stirrups spaced at 0.1 m spacing. A reinforced concrete slab of 0.1 m thickness was supported on top of the full brick thick walls of 0.24 m thickness and was reinforced with 8 mm diameter bars spaced at 0.1 m center-to-center in both directions. The

stage-wise construction of the URM building is shown in Figure 5.3. A full brick thick parapet wall of 0.9 m height was also constructed on the top of the slab over the walls. Additional weight of 10 kN was placed on the slab to simulate the load due to floor finish.

(a) (b) (c) (d) (e) (f)

Figure 5.3. Stage wise construction of URM building up to: (a) base, (b) window, (c) lintel level, (d) roof level, (e) parapet wall, and (f) completion.

All the steel flats used in the study were of the size 40 mm × 5 mm, and they were provided on both faces of the walls to provide a confinement effect. The external steel flats (bands) were connected to the internal bands by drilling 0.3 m long bolts of 10 mm diameter through the walls at an interval of about 0.5-0.7 m and fastening with nuts (Figure 5.4). The buildings were constructed on reinforced concrete slabs, which were fastened to the rigid strong floor to prevent sliding during the cyclic loading applied using a displacement-controlled servo-hydraulic actuator of 250 kN load and 250 mm displacement capacity. The cyclic loading was applied at the slab level of all the specimens with the help of rigid steel plates connected at both ends of the specimens using steel bolts. Three cycles of lateral loading were applied incrementally with increasing displacement levels on all the specimens. The displacement increment was kept at 1 mm till 20 mm displacement cycle after which the displacement was increased by 2 mm in loading cycles till failure (Figure 5.5). Four LVDTs were connected at four slab corners to record the rotation of the building in the plan due to unsymmetrical wall configurations (Figure 5.2a).

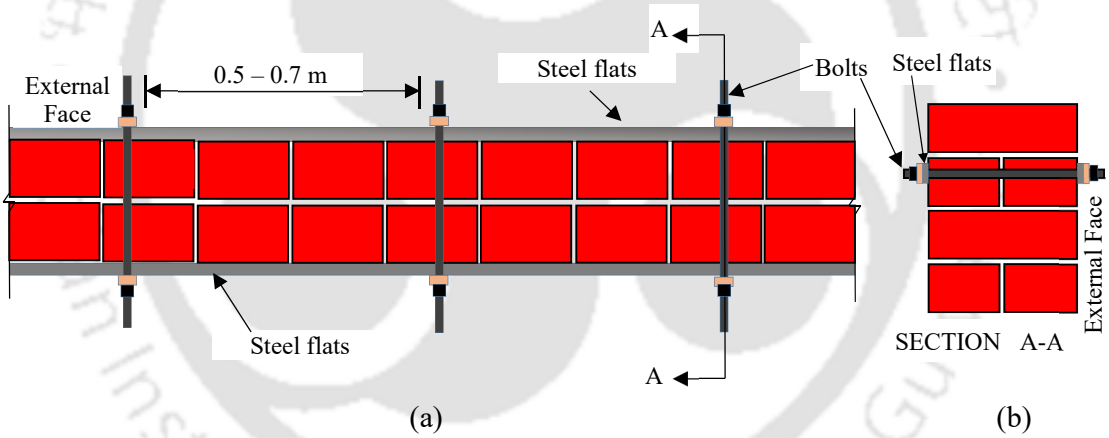

Figure 5.4. Details of surface-mounted steel flats: (a) wall section in plan (b) wall section in elevation.

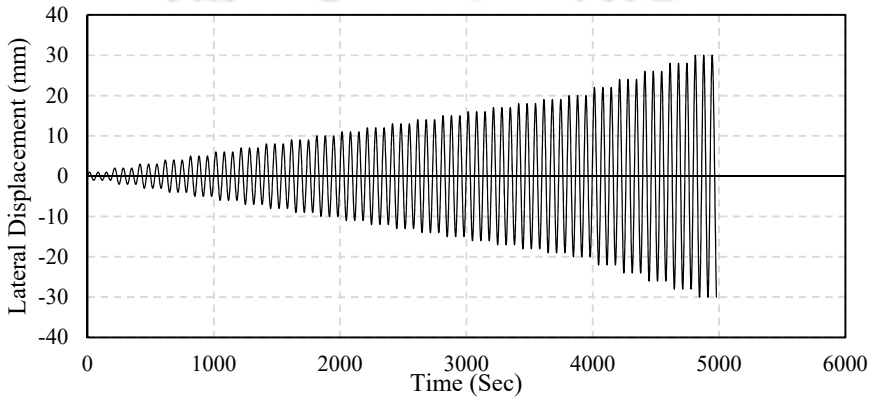

Figure 5.5. Displacement history applied on URM building specimens.

5.3. TESTING OF URM BUILDING (UNSTRENGTHENED)

The first specimen tested was a URM building without using any strengthening measures as shown in Figure 5.6. The first noteworthy observation was the damage in the form of cracks that occurred at the interface between the mortars and the bricks. Secondly, the cracks in the lower part of the pier propagated horizontally and the cracks in the upper part of the pier propagated diagonally near the openings in the Walls 2 and 3. On the other hand, both these cracks propagated both diagonally and horizontally in Wall 3*, and only horizontally in Wall 1*. Damages observed in the specimen at various levels of lateral displacement are discussed here and shown in Figure 5.7 and Figure 5.8. The initial response of the structure up to displacement of 1 mm, was essentially elastic and no visible crack was observed. With the increasing lateral displacements, cracks started forming gradually in various location of the piers.

Beyond 1 mm lateral displacement level, flexural cracks were initiated at the bottom layer of the wall near corners along the loading direction (i.e., in Walls 2 and 3). Diagonal shear cracks started appearing near the door and window openings at 5 mm displacement level, beyond which the cracks started progressing along the length of the wall. Shear cracks were also observed to develop at lintel level in the walls perpendicular to the loading direction (i.e., in Walls 1* and 3*) at 7 mm displacement level. By 12 mm displacement level, major cracks were visible throughout the walls at lintel level, and sill level around the openings and these cracks started connecting to other cracks. These cracks also joined the lintel level cracks formed in Wall 3 (Figure 5.7 and Figure 5.8).

Figure 5.6. Experimental setup of URM building.

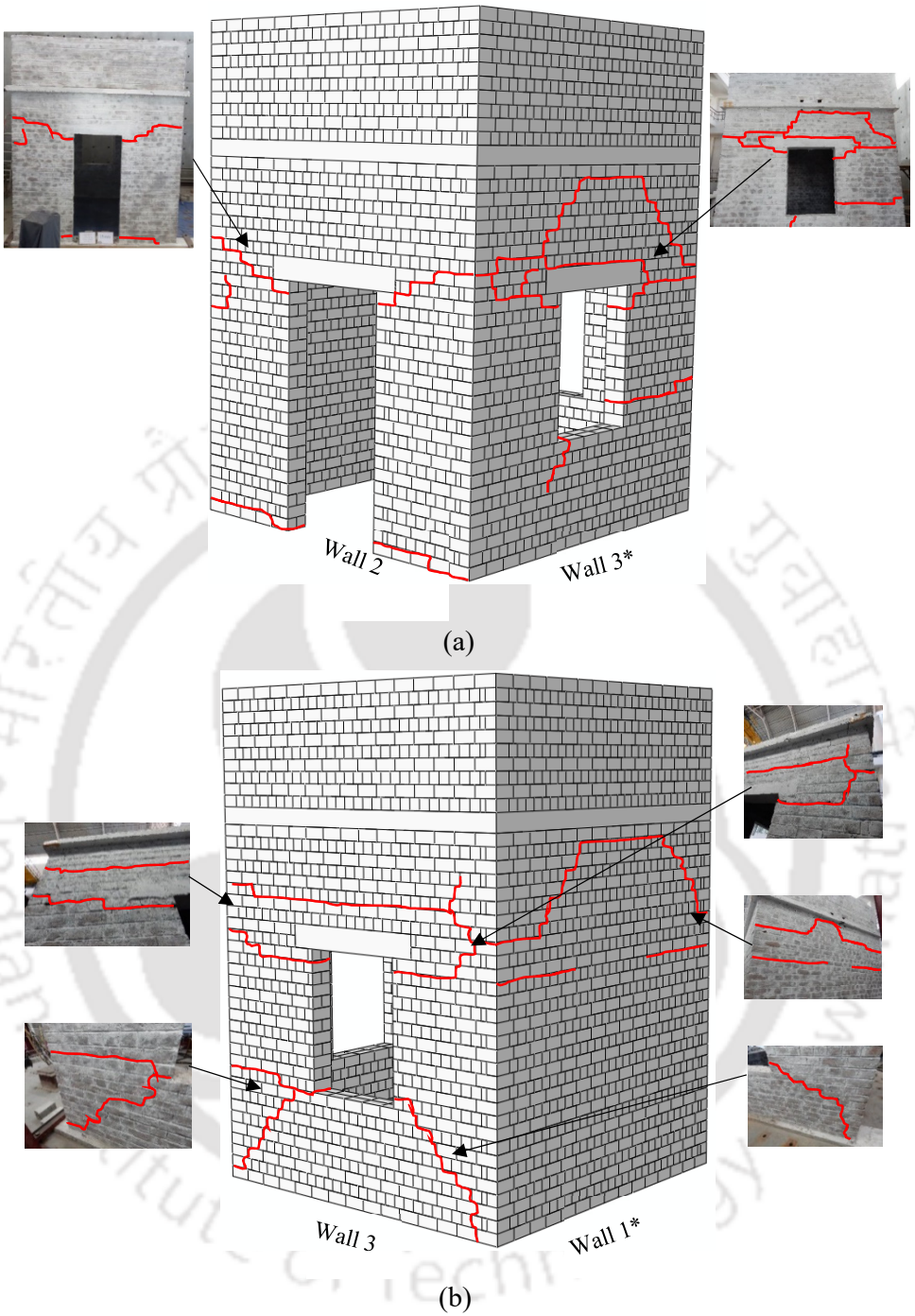

Figure 5.7. Damage pattern observed during the slow cyclic lateral load testing of full-scale URM building: (a) Damage observed in Wall 2 and Wall 3*, and (b) Damage observed in Wall 3 and Wall 1*.

The continuous cracks at the lintel level along the periphery of the building resulted in initiation of the rocking motion of the upper part of the building. At a displacement level of 17 mm, the cracks in Wall 3* and Wall 1* (out-of-plane action) widened prominently, resulting in an imminent out-of-plane failure. No further damage was observed in the

building specimen with further increase in the lateral displacement due to rocking motion of the upper part of the building. Therefore, the test was terminated at 20 mm displacement level. During the test, a mixed failure mechanism consisting of both shear and tensile failure in masonry was observed along with a torsional response of the specimen at higher displacement levels as shown in Figures 5.7 and Figure 5.8. The hysteresis curves and cumulative energy dissipation capacity of the specimen obtained during the test are shown in Figure 5.9a and Figure 5.9b, respectively. The capacity envelope curve obtained for the specimen is also superimposed over the hysteresis curves as shown in Figure 5.9a. The hysteresis curves show that the lateral load carrying capacity of the URM specimen is about 88 kN. The capacity was achieved at a lateral displacement level of 4 mm after which the specimen suddenly started losing the capacity due to the propagation of cracks through the walls. Finally, the test was stopped at 20 mm displacement cycle when the failure was imminent.

Figure 5.8. Damage observed in different walls inside the unstrengthened URM building during the lateral load testing.

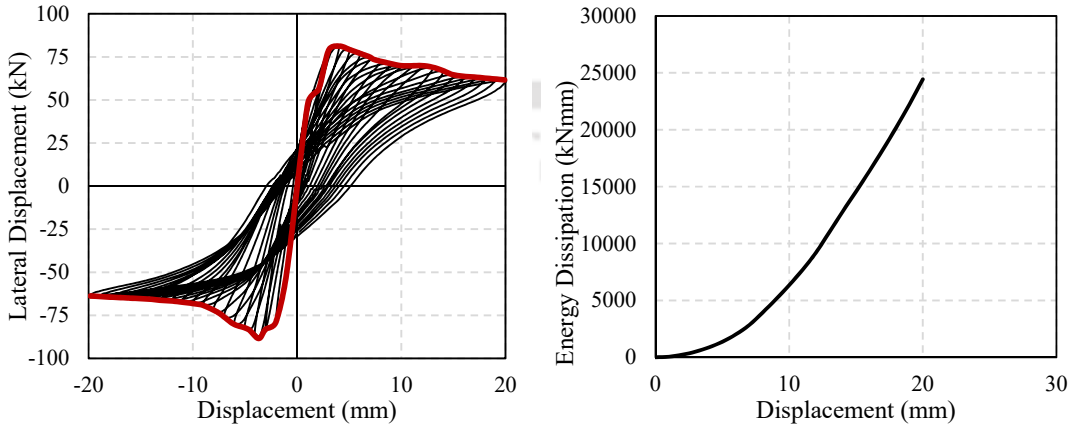

Figure 5.9. Lateral load response of un-strengthened URM specimen: (a) hysteresis curves and capacity envelope, and (b) cumulative energy dissipation capacity.

5.4. TESTING OF STRENGTHENED BUILDING 1 (MODEL 1)

In the first strengthening scheme, the URM building specimen was strengthened using surface-mounted steel bands (40 mm × 5 mm steel flat) at lintel level on both faces of all the walls along the whole length of the building as shown in Figure 5.10. The steel bands provided on the opposite faces of the walls were connected using steel bolts of 10 mm diameter through the thickness of the walls at a spacing varying from 0.5 m to 0.7 m (Figure 5.4). It was observed during the lateral load testing, that cracks started appearing near the openings in the masonry walls 2 and 3, at about 4 mm displacement level. The corner diagonal cracks near the openings were further extended into the walls at 5 mm displacement level, and at the same displacement level, flexural cracks started appearing in the walls perpendicular to the direction of loading (Wall 1* and Wall 3*). These cracks became more prominent at 8 mm displacement cycle and started propagating further along the length of different walls.

Figure 5.10. Experimental setup of strengthened URM building specimen 1 (Model 1).

At 16 mm displacement level, major cracks were formed in all the walls on both exterior as well as interior faces (Figure 5.11 and Figure 5.12). Beyond 16 mm displacement cycle, the part of the structure above the lintel level started rocking over the lower part because of continuous cracking in walls at lintel level along the entire length of the building. The steel bands failed at the junction of Walls 2 and 3* at 26 mm lateral displacement level (Figure 5.13), and subsequently, the test was stopped at 28 mm displacement to prevent complete disintegration of the walls.

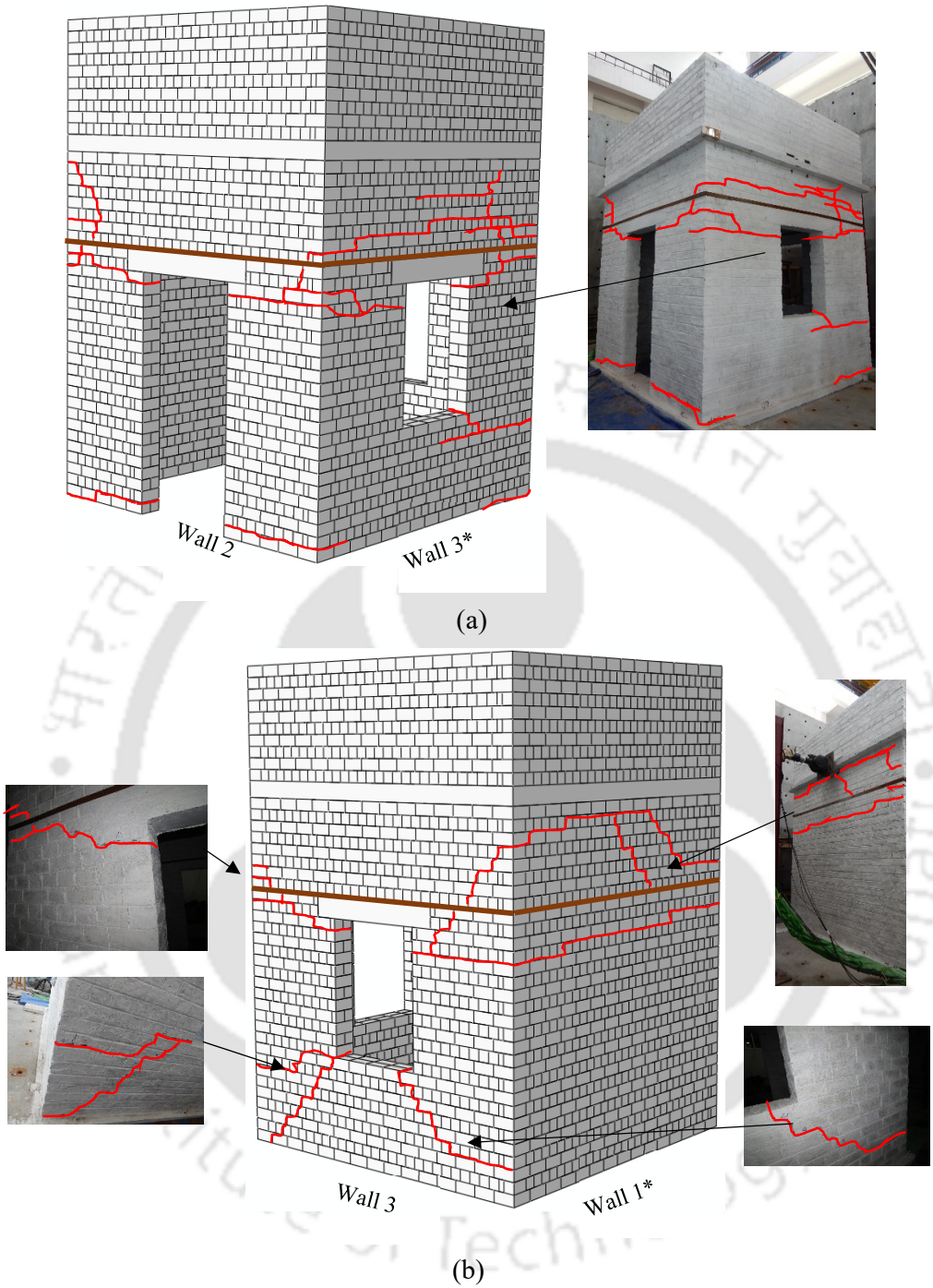

Figure 5.11. Damage observed in different walls during testing of the strengthened building 1 (Model 1): (a) Wall 2 and Wall 3*, and (b) Walls 3 and 1*.

During the lateral load testing, shear and tensile failure in the masonry was found to be the primary reason for the failure of the strengthened building 1. In addition, the building started twisting at higher displacement levels due to unsymmetrical damage in different walls. The hysteresis curves and the capacity envelope curve obtained from the

test are shown in Figure 5.14a. It can be seen that using a layer of steel band at the lintel level did not make any significant improvement in the lateral load carrying capacity of the URM building. The increased lateral load is found to be 90 kN (occurring at 4 mm lateral displacement) for Model 1 compared to 88 kN for the URM model. However, a remarkable improvement of about 40% was observed in the deformation capacity of the URM building when strengthened using a single band. The cumulative energy dissipation curve for Model 1 is plotted in Figure 5.14b, which shows that the energy dissipation was significantly higher by about 25% for the strengthened model. Similar to the URM building, the lateral load carrying capacity of the Model 1 also started deteriorating suddenly after reaching the maximum value as shown in the envelope curve of Figure 5.14a.

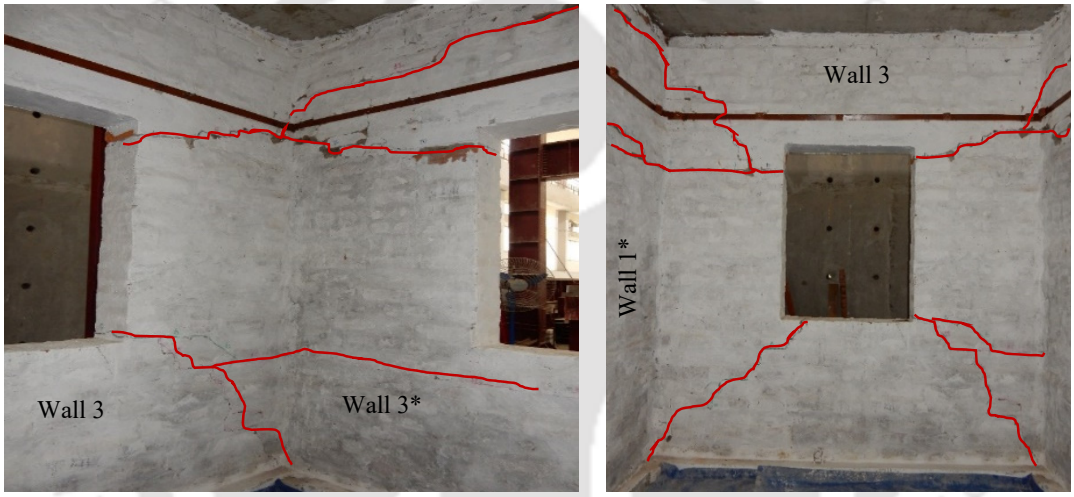

Figure 5.12. Damage observed in different walls inside Model 1 during the lateral load testing.

Figure 5.13. Steel band failure at the junction of Walls 2 and 3*.

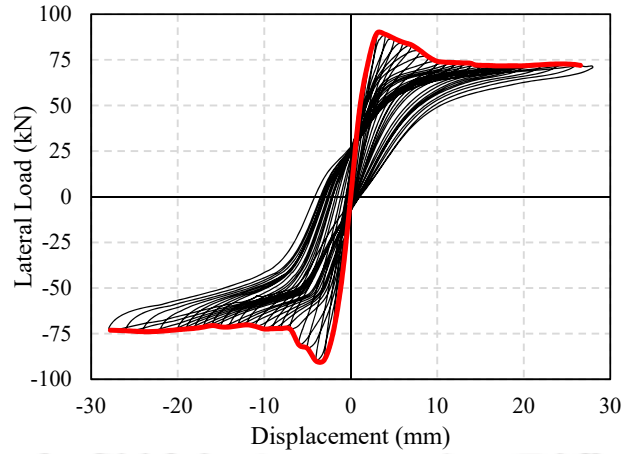

(a)

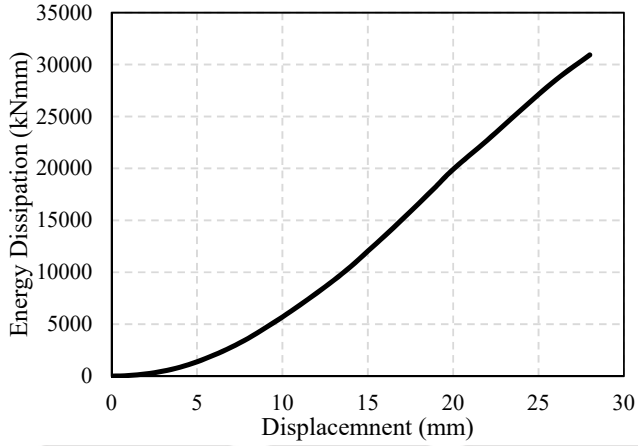

(b)

Figure 5.14. Lateral load response of strengthened specimen (Model 1): (a) hysteresis curves and capacity envelope, and (b) cumulative energy dissipation capacity.

5.5. TESTING OF STRENGTHENED BUILDING 2 (MODEL 2)

In the second strengthened specimen, horizontal steel bands were mounted on the surface of the walls at lintel as well as sill level in all the walls on both the faces throughout the length of the building, and additionally, vertical steel bands were provided adjacent to the openings as shown in Figure 5.1c and Figure 5.15. During the lateral load testing, flexural cracks at the base of the wall and shear cracks near the corners of the openings started appearing in all the walls along the loading direction at 4 mm displacement level, and these cracks started extending with increasing displacement levels. At 6 mm displacement level, visible cracks were formed at various levels in the walls perpendicular to the direction of loading (Wall 1* and 3*). As shown in Figure 5.16 and Figure 5.17, major cracks were visible on both the exterior and interior faces of all the walls at 15 mm displacement level.

As also observed in the response of Model 1, the part of the building above lintel level was seen to have separated from the lower part at 18 mm displacement level due to the formation of continuous cracks along the whole perimeter of the building resulting in rocking of the upper portion of the building. At 28 mm displacement level, the steel flats snapped at the junction of Walls 2 and 3*, Walls 3* and 3, and Walls 3 and 1*. The test was terminated at 30 mm displacement level to avoid complete failure of the walls.

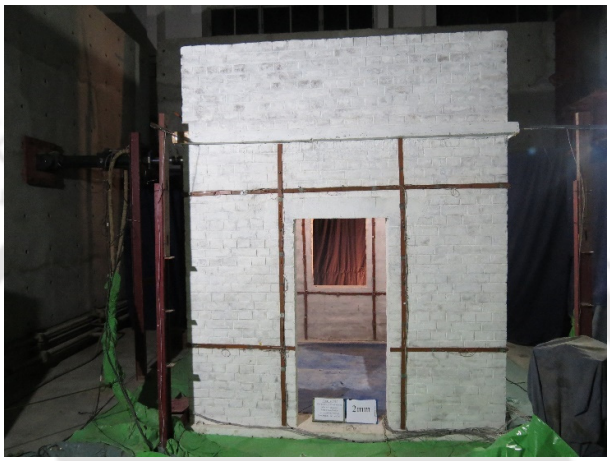

Figure 5.15. Experimental setup of strengthened URM building specimen (Model 2).

A similar failure mode, as observed in the other two specimens, consisting of shear and tensile failure along with a twisting mechanism at higher displacement levels was observed in Model 2. The twisting mechanism observed in the three specimens will be described later. The hysteresis curves along with the capacity envelope curves were generated for Model 2 using the test results as shown in Figure 5.18. It can be observed that the lateral load carrying capacity of Model 2 was highest at about 108 kN, occurring at a lateral displacement of 10 mm.

The capacity curves for all the specimens are also compared in Figure 5.19a. It is clear from the comparative curves that the lateral load response of Model 2 was significantly better than the other specimens both in terms of lateral load carrying capacity as well as the lateral deformability and ductility. Comparison of the cumulative energy dissipation curves for all the specimens (Figure 5.19b) also shows that Model 2 exhibited significantly higher energy dissipation (about 4-5 times higher) compared to the other specimens. Clearly, the URM building strengthened with steel bands along both vertical and horizontal directions displayed a promising performance with an increase of about 38%, 50%, and 450% in lateral load, deformability, and cumulative energy dissipation

capacity, respectively, compared to the un-strengthened specimen. Figure 20 shows the rotation observed in the three specimens in plan due to the twisting action. LVDTs were used to record this rotational motion of the RC slab of all the specimens as shown in Figure 5.2a.

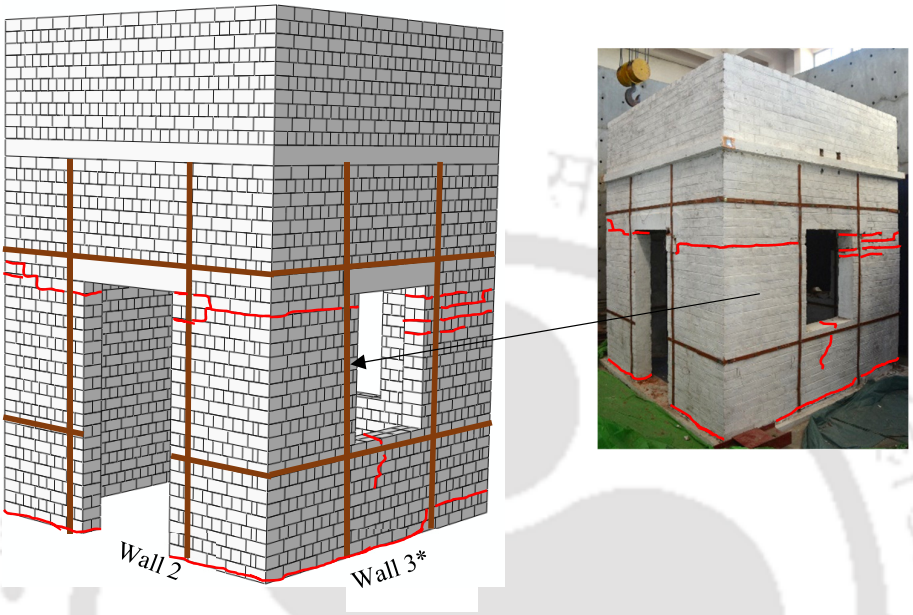

(a)

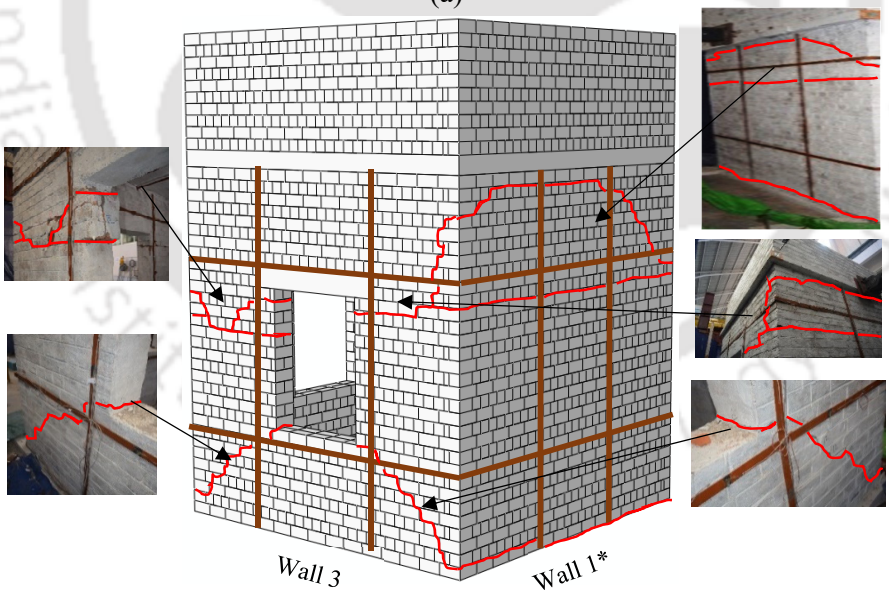

(b)

Figure 5.16. Damage observed in different walls during lateral load testing of the strengthened building 2 (Model 2): (a) Walls 2 and 3*, and (b) Wall 3 and 1*.

It is clear from the figure that strengthening of the buildings using surface-mounted steel bands also reduced the twisting behavior significantly. The out-of-plane displacement recorded at the top of the specimens reduced from 3.2 mm to about 50% after strengthening.

Figure 5.17. Damage observed in different walls inside the Model 2 during the lateral load testing.

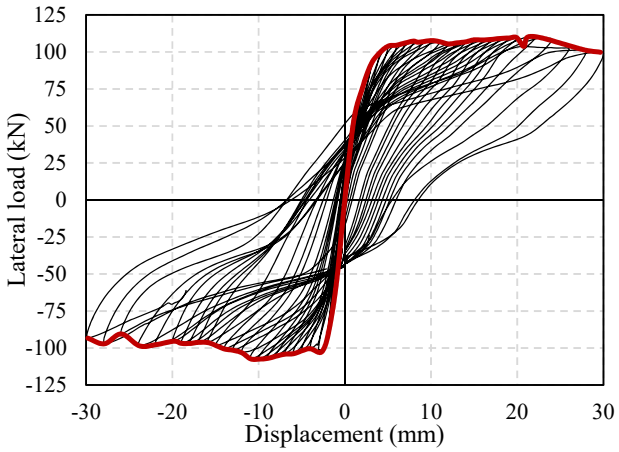

Figure 5.18. Hysteresis curves of strengthened building 2 (Model 2).

The lateral stiffness of all the specimens was found to be more or less same, but most importantly, Model 2 exhibited a much more stable post-peak response without losing the lateral strength significantly with increasing lateral displacement.

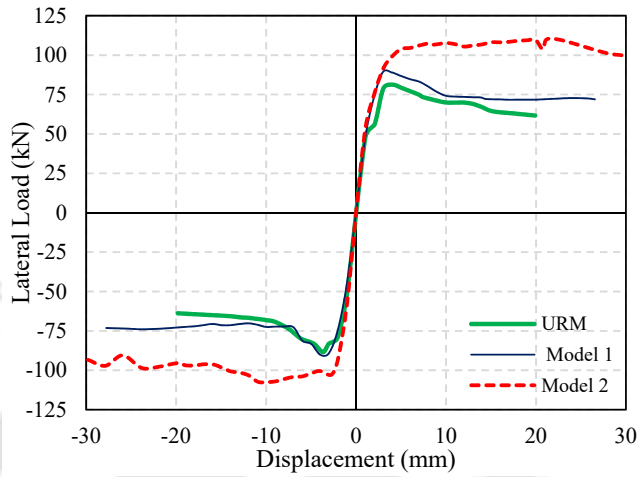

(a)

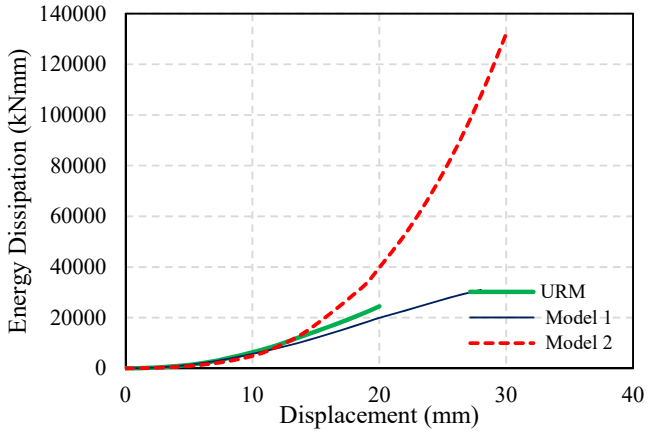

(b)

Figure 5.19. Comparison of lateral load response of all the specimens: (a) capacity envelope, and (b) cumulative energy dissipation.

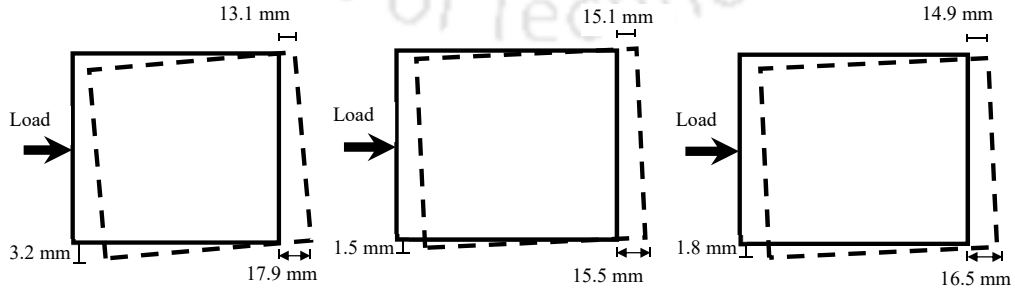

(a) (b) (c)

Figure 5.20. Rotation observed in plan in due to twisting action at 15 mm displacement level in: (a) URM Building, (b) Model 1, and (c) Model 2.

Sixty-one strain gauges were connected to the steel flats at various locations in Model 2 in order to measure the axial strain in the bands, and to find if any of the steel bands were subjected to nonlinear strains during the tests as shown in Figure 5.21. The recorded strains are shown in Figure 5.22. The points where comparatively large strain readings were recorded correspond to those where significant damage was observed, and these points are marked red. This signifies that the steel bands significantly contribute to the lateral load resistance and delay the formation of cracks and failure in the walls of the building. The strain gauges attached on the steel flats near the openings recorded high strain values confirming that these are the regions of high-stress concentration.

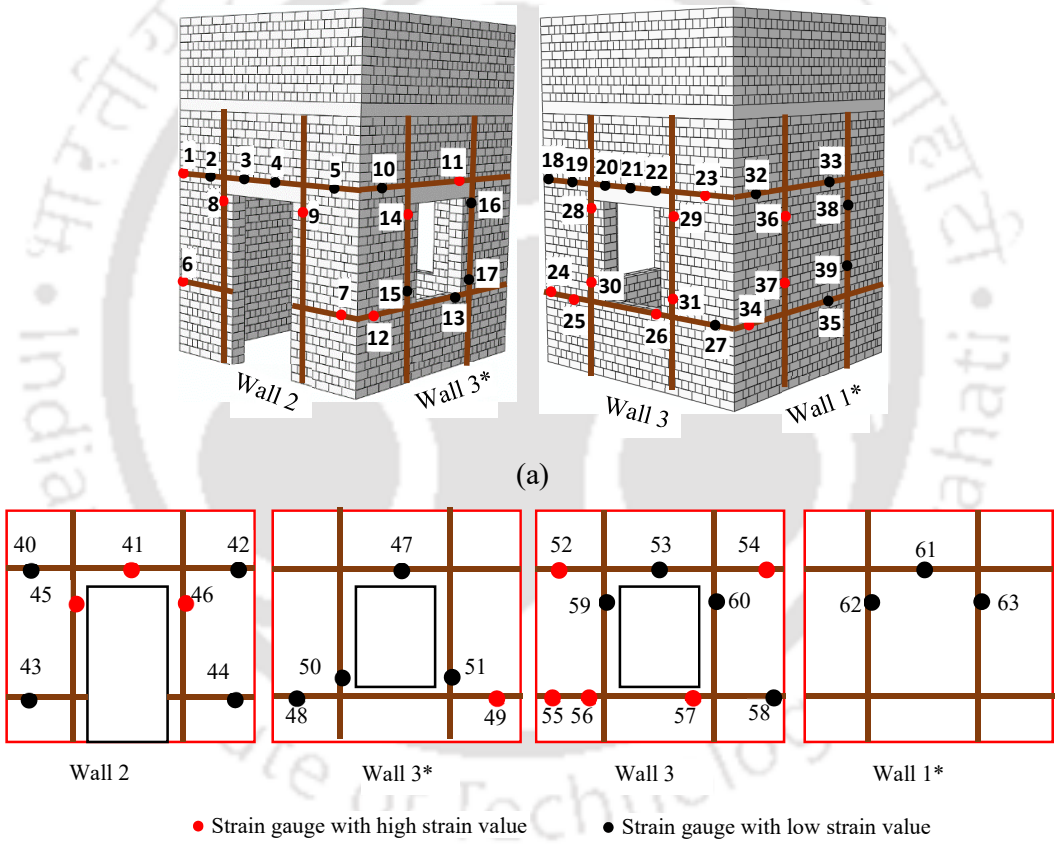

Figure 5.21. Location of strain gauge in Model 2: (a) External wall surface, and (b) Internal wall surface.

The final strain values recorded at 30 mm displacement level is shown in Figure 5.22. Even at the final displacement level, failure was not observed in the steel flats except at three junctions as already discussed. However, at this level, point 29 recorded the highest strain value of 0.0027, which is slightly higher than the yield strain of 0.0023, marking the

location of the highest damage area in masonry walls near the wall junction, where two walls meet (Wall 3* and Wall 3). This is the same location where failure was observed in the steel flats near the wall junctions during the experiment. Though, none of the other strain gauges were found to have exceeded the yield strain value, the high linear strain values recorded in some of the steel flats in critical locations show that the steel flats were contributing to the lateral resistance of the building.

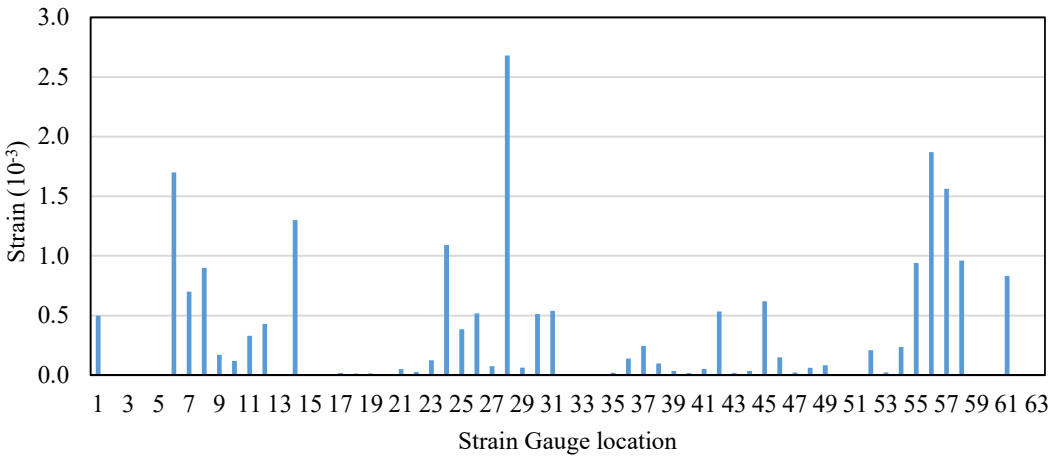

Figure 5.22. Strains measured on steel flats at 30 mm displacement level.

It is to be noted that Model 2 resembles the Strengthening Scheme #3 discussed in chapter 3, where the numerical simulation observed two times increase in the lateral strength of URM building. On the other hand, the experimentally obtained results showed about 38% increase in lateral strength value when compared with the URM building. This inconsistency in the numerical simulation results might have resulted due to perfect nodal connectivity assumed between the steel band elements and the masonry wall elements in the FE Model. Therefore, a more refined numerical simulation of the strengthened URM buildings will be carried out in the next chapter.

5.6. SUMMARY

A simple seismic strengthening strategy for unreinforced masonry buildings using surface-mounted steel bands is suggested in the present experimental study. The scheme is cost-effective, can be easily and quickly implemented on site, and does not require heavy equipment or manpower. Therefore, it can be used for strengthening a huge number of existing vulnerable URM buildings in earthquake-prone areas of developing countries. Pseudo-static, slow cyclic, lateral load testing of three full-scale URM buildings was

carried out to evaluate the effectiveness of the developed strengthening scheme in improving the lateral load behavior. Door and window openings were also considered in the walls of the building, in order to understand if there is an advantage of providing the steel bands in reducing the commonly observed damage around the openings. It was observed that providing a single steel band at lintel level on both faces of all the walls of the URM building (Model 1) did not result in any significant increase in its lateral load carrying capacity. However, a remarkable improvement was observed in the deformation capacity of the strengthened specimen. Therefore, another strengthening scheme (Model 2) was adopted in which the steel bands were provided both at lintel as well as sill level on both the faces of all the walls of the building. In addition, vertical steel bands were also provided around openings on both the faces of the walls. The test results showed that the lateral load carrying capacity of the strengthened specimen increased by about 38% to 110 kN, which corresponds to about 55% of the seismic weight of the building. In addition, the hysteresis response of Model 2 was observed to be significantly better and more stable than the un-strengthened specimen as well as Model 1. The lateral deformability and ductility displayed by Model 2 were far superior to the other specimens. Therefore, a simple strengthening scheme in which horizontal and vertical steel bands are provided at various levels on both faces of the walls can be recommended to strengthen the ordinary as well as heritage URM buildings that are seismically vulnerable.

Chapter 6
ESTIMATION OF LATERAL STRENGTH OF URM BUILDING

Contents

6.1. Overview 111
6.2. Numerical Study of URM walls 112
6.3. Numerical study of URM Buildings 117
6.4. Analytical Evaluation 119
6.5. Summary 129

6.1. OVERVIEW

Seismic assessment of buildings can be carried out using analytical, numerical or experimental methods. The most appropriate methodology to determine the structural behavior subjected to lateral load is by conducting experiments. However, conducting tests on full-scale buildings is highly expensive, time consuming, and may be feasible for a limited number of samples only. Numerical simulation techniques are usually adopted in lieu of experimental techniques, but the simulation requires exhaustive computational efforts and material data, which is not available easily. But despite a reduction in computational efforts in new FE programs due to use of better and efficient algorithms, the modeling process in numerical approach is time-consuming and may be challenging while modeling large structures. Established codes of various countries have provided analytical methods to estimate the structural capacity of walls, based on past experimental observations in those countries. Codes in many developing countries, including India, have not been revised for long due to limited resources and data. The updated codes of various countries may not be suitable to be used elsewhere due to the large variation in material

properties and construction practices. Hence, a feasibility study needs to be carried out on the suitability and effectiveness of the analytical methods, code provisions, and equations suggested in various past studies on estimation of lateral strength of URM buildings. It is important to ascertain if the lateral strength of individual URM walls, which are much easier to test or analyze, obtained using experimental, numerical, or analytical methods can be systematically combined to realistically estimate the lateral strength of full URM buildings.

Review of literature shows that numerous studies have been carried out on evaluation of lateral load behavior of URM walls under both in-plane as well as out-of-plane action. However, limited information was available on the lateral load behavior of the whole URM buildings, especially those constructed using low-strength masonry. The primary objective of the present study was to assess the lateral load carrying capacity of URM walls and building constructed using low-strength masonry. Experimental, numerical, and analytical approaches will be used on full-scale specimens of URM walls and building to relate the lateral strength of the URM building with that of the URM walls.

The quasi-static, in-plane cyclic test results obtained from tests conducted on three full-scale URM walls with different opening configurations (discussed in chapter 4) and one full-scale URM building (discussed in chapter 5) were used in this chapter for the numerical and analytical study. The URM walls and building were numerically modeled and nonlinear pushover analyses along in-plane direction were carried out using Strand7 (2013) and Abaqus (2010). Due to laboratory constraints, out-of-plane testing of the masonry walls was not carried out. However, both in-plane as well as out-of-plane strengths of the walls were estimated using the analytical relations available in recent literature. The experimental, numerical, and analytical results of different wall specimens and building displayed an interesting pattern. The results were finally used for the estimation of the overall capacity of the building.

6.2. NUMERICAL STUDY OF URM WALLS

One of the primary objectives of the present study was to numerically evaluate the lateral load behavior of the structural components (walls) of the URM building as well as the building as a whole. This was achieved by carrying out the nonlinear pushover analyses of the walls and the building using two numerical approaches - Strand7 (Strand 7.2 User's

Manual 2013)(Strand 7.2 User's Manual, 2013)(2013) and Abaqus (2010). The failure mechanism and the lateral capacity of all the models were tuned to reflect the experimentally observed behavior. The analyses were carried out by discretizing the walls into 1040 eight-noded solid elements and 1703 nodes in Model 1, 872 eight-noded solid elements and 1493 nodes in Model 2, and 944 eight-noded solid element and 1598 nodes in Model 3 as shown in Figure 6.1. The FE model of URM building consisted of 10160 eight-noded solid elements (Figure 6.2). All the nodes located at the base of the models were fully restrained to simulate the fixed base conditions for simplicity. The vertical dead load was applied over the slab and an incremental lateral load was applied at the slab level up to failure as done during the experimental study.

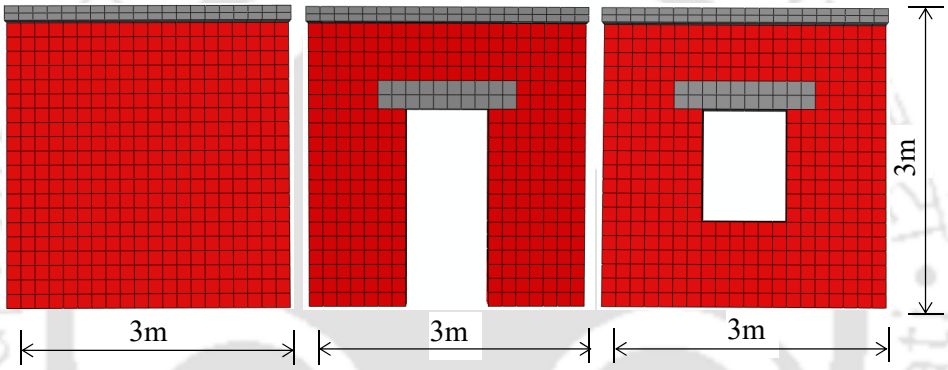

Figure 6.1. FE models of wall specimens tested in the present study: (a) Wall 1, (b) Wall 2, and (c) Wall 3.

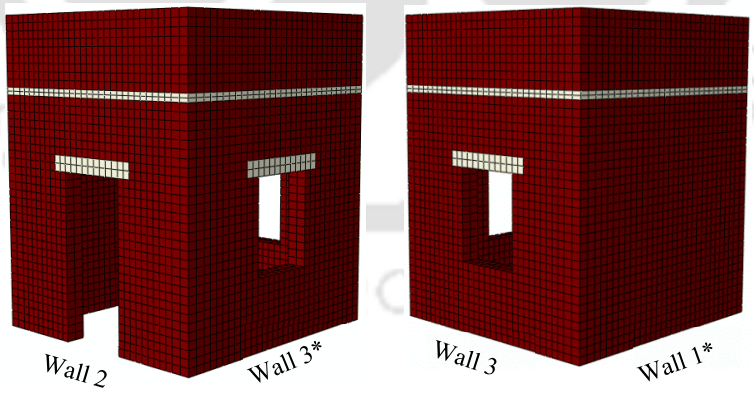

Figure 6.2. Finite element models of URM Building: (a) View 1, and (b) View 2.

The material characteristics used in the analysis were taken from Table 4.1. However, the numerical simulation carried out using Strand7 required a minor calibration to fix the value of φ (angle of internal friction), which was varied between 30° to 45° as

suggested in the past studies (NTC 2008). Finally, the Mohr-Coulomb failure criterion was considered for masonry with a friction angle of 35° and cohesion value of 0.145 MPa in order to calibrate the results with the experimental study. The maximum strength in tension and compression were calculated using the Mohr-Coulomb yield criterion under plane stress condition. As already discussed, the non-linear analyses in Abaqus was carried out considering the Concrete Damage Plasticity model for which the non-linear parameters were taken as: dilatation angle = 10°, eccentricity = 0.1, the ratio of initial equibiaxial and uniaxial compressive yield stress (fb_o/fc_o) = 1.16, parameter K_c = 0.667 and viscosity parameter = 0.0001, based on established literature (Lubliner et al., 1989; Page 1981). Material non-linearity was defined exclusively for masonry elements, whereas reinforced concrete lintels and slabs were assumed to behave elastically. Such assumption was made considering the fact that concrete possesses strength that was much larger than that of masonry, and therefore, no damage was observed in these elements during the tests. Tensile damage property was used for masonry elements for the non-linear analysis. During the tensile bond test, the material exhibited sudden brittle failure, leaving no scope of capturing the post peak softening behavior, which was required for simulating the tensile behavior of masonry in Abaqus. Hence, the experimentally obtained stress-strain curve (Figure 4.5b) in the post-peak region was modified according to the curve suggested in the Abaqus reference Manual (Abaqus,2010), which defines the damage criteria required to perform the analysis (Figure 3.1a).

6.2.1. Numerical Results

6.2.1.1. Wall 1

Pushover analysis was carried out using the aforementioned finite element programs along the in-plane direction, in accordance with the experimental study. In order to rationally use the results of the numerical study, calibration of the numerical model was carried out with the experimental results, and the same calibrated properties were used throughout the numerical study. After calibration, the force-displacement response predicted by Abaqus matched quite well with the experimental response (Figure 6.3a). As already discussed, Strand7 ignores the shear failure and material softening behavior. Therefore, though the drop in lateral capacity was not observed in the numerical simulation carried out using Strand7, the predicted lateral strength was quite close to that of the experimentally obtained values. The damage patch (DAMAGET or d_t defined as the tensile damage variable), which was one of the outcomes of the numerical simulation in Abaqus, gives interesting

information on the modes of failure of different elements and the active failure mechanisms. It can be observed from Figure 6.3b-c that the experimentally observed damage pattern (i.e., failure at the bottom of the wall) can be simulated in the numerical analysis using Abaqus. Strand7 can also indirectly provide an approximate damage pattern given by total strain values in masonry. As shown in Figure 6.3d, the maximum strain values occur at both the ends of the wall near the base. This observation also matches well with the experimentally observed damage pattern.

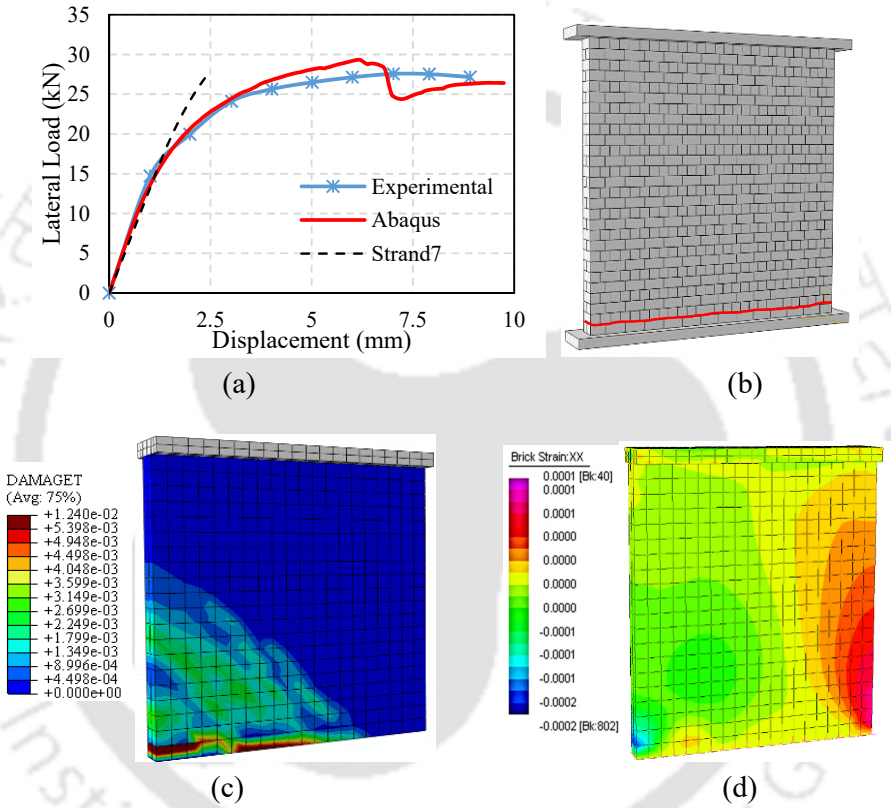

Figure 6.3. Comparison of experimental and numerical results for Wall 1: (a) load displacement curves, (b) damage observed experimentally, (c) damage pattern in Abaqus, and (d) damage pattern in Strand7.

6.2.1.2. Wall 2

Numerical analysis of Wall 2 was carried out by following the similar calibration techniques adopted earlier, and the analysis results show similar trends as shown by Wall 1. The lateral load behavior obtained from numerical simulations was found to match well with the experimental results (Figure 6.4). It can be noted from the results of numerical simulation that the tensile damage variable in Abaqus and the total masonry strain in Strand7 show a concentration of inelastic deformation near the top of door opening and at the bottom of the wall at the end of the simulation (failure point) as shown in Figure 6.4c-

d. Such a behavior matches well with the experimental response of the wall that exhibited a mixed failure combining flexure and sliding shear cracking (Figure 6.4b).

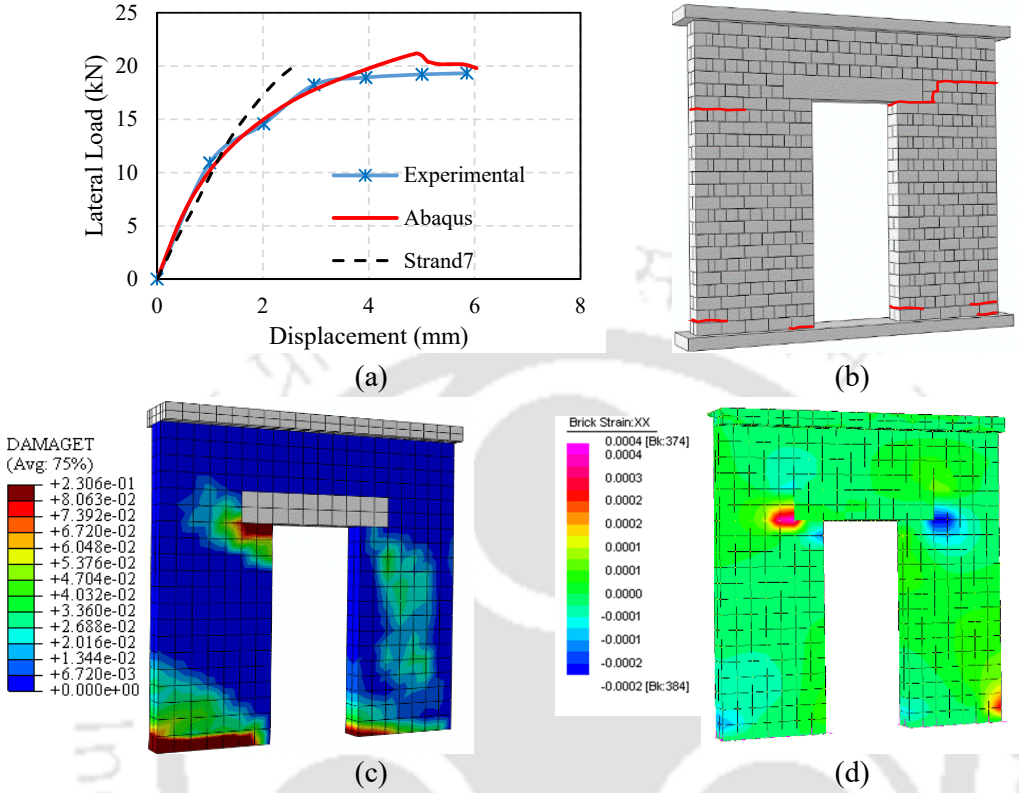

Figure 6.4. Comparison of experimental and numerical results for Wall 2: (a) load displacement curves, (b) damage observed experimentally, (c) damage pattern in Abaqus, and (d) damage pattern in Strand7.

6.2.1.3. Wall 3

Results of the numerical analyses conducted on the wall consisting of a central window opening show that the lateral force-deformation curve predicted by Abaqus closely matches with that of the experimental study (Figure 6.5a). As discussed already, Strand7 was also able to satisfactorily predict the lateral strength of Wall 3, though the complete non-linear response could not be predicted. However, the numerically simulated damage pattern of Wall 3, using both Strand7 and Abaqus, was significantly different when compared with the experimental results. The numerical analysis results correctly predicts the stress concentration near the corners of the opening (Figure 6.56.5c-d). Whereas, the experimental results showed flexural sliding failure at the base of the structure as shown in Figure 6.5b. This may be due to presence of a weaker course of masonry at the base of the test specimen. It was clear from the results that the tensile stress concentration occurs at the critical zones near the corners of the openings, which needs special attention.

After comparing the pushover curves obtained numerically for the three wall models, it was observed that the introduction of a door opening has a considerable negative influence on the lateral load carrying capacity of the URM wall. Model 1 having no openings, was associated with the highest collapse load, and Model 2 with a door opening, exhibited the least load carrying capacity. Model 3 with a central window opening fared better than Model 2 because of smaller opening size and its ideal location as discussed in the experimental results.

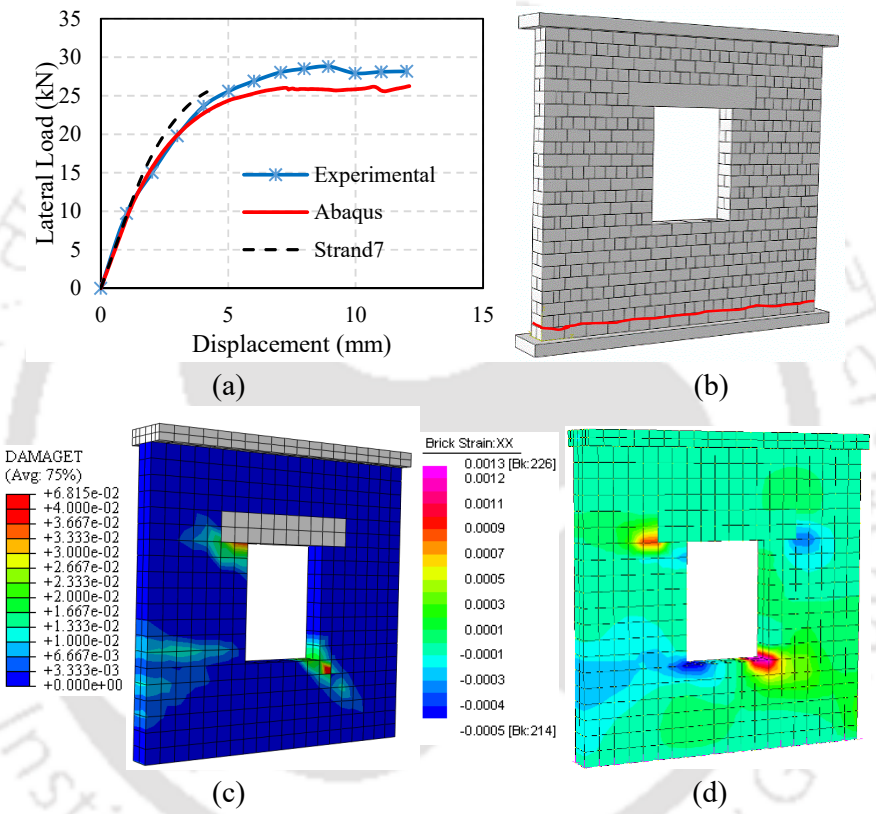

Figure 6.5. Comparison of experimental and numerical results for Wall 3: (a) load displacement curves, (b) damage observed experimentally, (c) damage pattern in Abaqus, and (d) damage pattern in Strand7.

6.3. Numerical Study of URM Buildings

The URM building model was also analyzed numerically using Strand7 and Abaqus. Using the material data obtained during material characterization, the numerical capacity of the building obtained using Abaqus matched well with the experimentally obtained capacity. Figure 6.6 shows that the force-deformation curve obtained using Abaqus matches closely with that obtained experimentally up to the peak load. In the post-peak regime, a decrease in capacity of the building was not observed in the numerically obtained Abaqus results; instead, the capacity curve exhibited elasto-plastic behavior. However, the damage contour

observed numerically matched well with the experimental results. Similarly, the lateral strength predicted by Strand7 also matches well with the experimental observation. The strain contours resulting from the numerical analyses conducted using Strand7 and the damaget variable observed in Abaqus show peaks near the corners of the openings indicating that the damage was prominently located near the openings in all the walls (Figure 6.8). Similar critical regions were also observed in the experimental response (Figure 5.5). Clearly, both Strand7 and Abaqus were able to successfully predict the lateral load response of the URM walls and building.

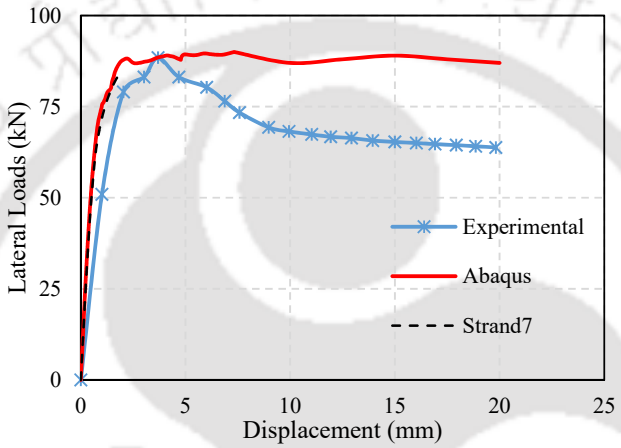

Figure 6.6. Comparison of the numerically obtained capacity curve with the experimental capacity curve for URM building.

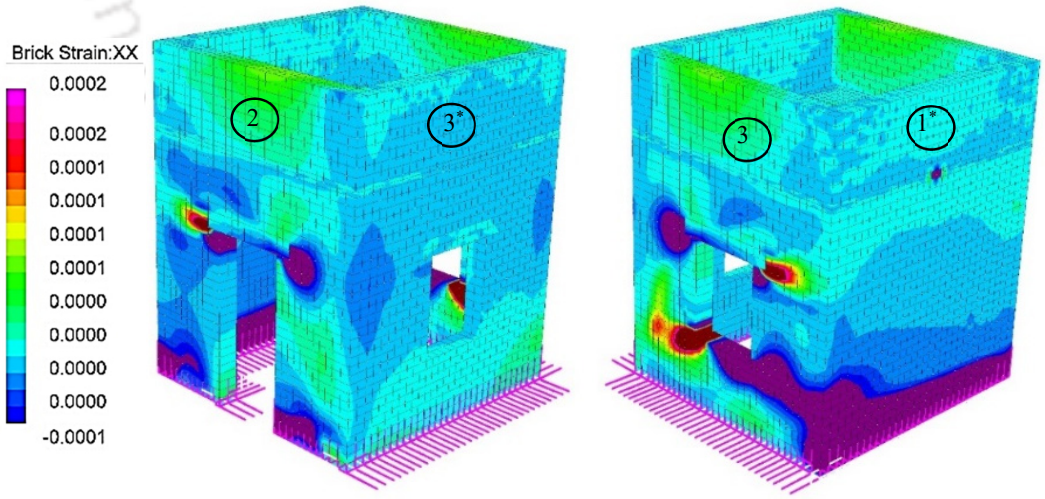

Figure 6.7. Strain contour of the URM building shown along the four walls obtained using Strand7.

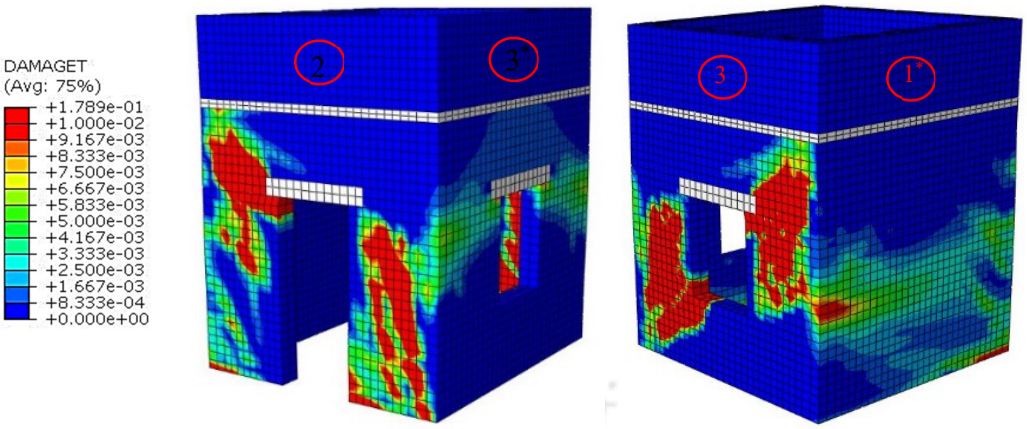

Figure 6.8. Damaget contour of the URM building shown along the four walls obtained using Abaqus.

6.4. Analytical Evaluation

The combined in-plane resistance of Walls 2 and 3 tested individually as discussed in chapter 4 comes out to be about 55% of the lateral load resistance of the full building. The remaining resistance was provided by (i) the out-of-plane resistance of Walls 1* and 3*, and (ii) the box action developed by the integrated action of the four walls depending upon the connectivity between the walls and the presence of RC slab on their top. Seismic codes of various countries provide analytical methods for estimation of in-plane as well as out-of-plane (OOP) capacity of individual URM walls. However, all the codes do not consider the modern assessment procedures in which the common failure modes of URM walls are properly considered in capacity estimation. In this section, the in-plane and out-of-plane capacity of individual URM walls were first estimated using the methods proposed in the past literatures and design codes. The capacities of the individual walls were then methodically combined to estimate the lateral strength of the URM building.

6.4.1. Lateral Strength of URM Walls

6.4.1.1. In-Plane Resistance of Walls

Magenes and Calvi (1997) defined three principal failure mechanisms for masonry piers subjected to in-plane loads: rocking, shear cracking and sliding failure/flexural failure, and provided empirical equations to estimate the horizontals loads corresponding to each failure criteria. The method to estimate the strength corresponding to the three failure modes, diagonal tension, shear sliding or flexure, and toe crushing, is given in Eq. 6.1-6.3. For low axial load, sliding stress or flexural failure governs. Sliding failure governs only if the given condition in Eq. 6.2 is valid, else flexural failure will be the governing criteria.

$$\text{Diagonal tension failure: } V_{dt} = \frac{f_{dt} lt}{\alpha_v}\sqrt{1+\frac{P}{f_{dt}}} \tag{6.1}$$

$$\text{Shear sliding failure: } V_{us} = lt\left(\frac{1.5c+\mu_c P}{1+3\frac{c\alpha_v}{P}}\right); \text{ if } \frac{N}{6\alpha_v} \le V_{us} < \frac{N}{2\alpha_v} \tag{6.2}$$

$$\text{Else, Flexure failure: } V_{u,flex} = \frac{M_u}{h_{eff}}; M_u = \frac{Pl^2 t}{2}.\left(1-\frac{P}{k_f f_m}\right) \tag{6.2a}$$

$$\text{Toe Crushing failure: } V_{tu} = \psi\frac{l^2 tP}{2h}\left(1-\frac{P}{0.85 f_m}\right) \tag{6.3}$$

where l, h and t are the length, height and thickness of the pier, respectively; c = coulomb friction taken as $1.25f_t$; f_t = flexural tensile strength of masonry; μ_c = 0.4, represents the sliding coefficient of the masonry joints; $\alpha_v = h/l$; P = axial compression stress due to gravity loads; N is the vertical load on pier which is $P_W + P_D$; P_D = superimposed dead load at the top of the wall; P_W = self-weight of the pier; k_f is a constant equal to 0.85; and ψ is the boundary condition factor, taken to be 2 when the masonry pier is fixed at both ends, and 1 when the pier is fixed on one end and free on the other.

The rocking failure is caused due to bed joint cracking, which leads to overturning of the wall along the loading direction. The shear cracking failure is caused by the inclined diagonal cracks along the bed and head joints in the wall. The sliding failure and flexural failure is caused due to the formation of horizontal cracks in the bed joints of walls carrying lower gravity loads. In the present study, the lowest of the horizontal loads corresponding to these three failure modes is considered as the critical failure load. ASCE/SEI 41-13 (2014) and New Zealand Seismic Assessment Guideline (NZSEE et al., 2017) adopted some of the advanced methods of structural assessment taking into account these three failure modes, and methods are suggested for estimation of the lateral load corresponding to each of the failure modes. The method to estimate the strength under sliding, rocking, toe crushing and diagonal tension failure modes are given in Eq. 6.4-6.7, out of which the minimum value is generally considered as the lateral resistance. Typically, for URM walls subjected to low axial loads, the rocking or sliding shear governs.

Bed-joint sliding strength: $Q_{CE} = \gamma_{me} A$ (6.4)

Rocking strength: $Q_{CE} = 0.9(\alpha_i P_D + 0.5 P_W)\frac{L}{h_{eff}}$ (6.5)

Toe crushing strength: $Q_{CL} = (\alpha_i P_D + 0.5 P_W)\left(\frac{L}{h_{eff}}\right)\left(1 - \frac{P}{0.7 f_m}\right)$ (6.6)

Diagonal tension strength: $Q_{CL} = f_{dt} A \beta \sqrt{1 + \frac{P}{f_{dt}}}$ (6.7)

where A = area of net mortared section of wall; γ_{me} = sliding shear strength of masonry; h_{eff} = height to resultant of seismic force (effective height of wall); L = length of the wall; α_i = factor equal to 0.5 for fixed-free cantilever wall and 1.0 for fixed-fixed wall pier; f_m = compressive strength of masonry prism; f_{dt} = diagonal tensile strength; β = 0.67 for L/h_{eff} <0.67; L/h_{eff} when 0.67≥ L/h_{eff} ≤1.0 and 1.0 when L/h_{eff}>1.0.

Based on the experimental observation on a two story URM building, Moon et al. (2006) defines the effective height of the wall with opening over which a compression strut develops. According to them, the compression strut can develop either horizontally or at 45º or at the steepest possible angle. These recommendations were adopted in ASCE 41-13, and therefore, this effect can be visible in walls with openings. However, there was no recommendations by Moon et al. (2006) or in ASCE 41-13 about the effective height to be considered for a solid wall. Magenes and Calvi (1997) also did not mention about the consideration of effective height in their proposed method. However, codes like, Eurocode 6 (2005), Indian Standards IS 1905 (1987a), recommend the use of effective height for the estimation of wall evaluation. In the present test, it was seen that in the case of Wall 1 (solid wall), the compression strut developed at nearly the full height of the wall. Whereas, in the case of the Wall 2 (URM wall with door opening), a horizontal crack parallel to the bed joint on one side and a diagonal crack on the other side was observed. The experimental test over Wall 3 (wall with window opening) have shown no sign of crack at the upper part of the openings. Only horizontal line cracks at the base of the specimen were observed, whereas the numerical simulation of the wall displayed diagonal failure areas near the openings (See Figure 4.15 and Figure 6.5).

Codes like Eurocode 6 (EN 1996-1-1, 2005) and Australian Standard (AS-3700, 2018) recommend the in-plane lateral capacity of a URM wall to be equal to the shear

resistance of the wall at the base calculated by multiplying the loaded area with the unit shear strength of the masonry. The shear resistance of wall in the in-plane direction (V_b) as per Eurocode 6 can be estimated using Eq. 6.8.

$$V_b = f_{vd}\, t_w L \tag{6.8}$$

where f_{vd} = shear strength of masonry given by $f_{vko} + 0.5P$, but not greater than $0.065f_b$ or f_{vlt}, where f_{vlt} = flexural tensile strength of brick unit; f_{vko} = initial shear strength; and t_w = thickness of wall.

The Australian Standard also expresses the in-plane strength as the sum of the bond strength and the frictional strength. The shear resistance of wall in the in-plane direction (V_b) can be estimated as the sum of shear bond strength (V_o) of the wall section and shear friction strength (V_1) as per Eq. 6.9-6.11.

$$V_b = V_o + V_1 \tag{6.9}$$

$$V_o = \phi\, f_{ms}\, A_d \tag{6.10}$$

$$V_1 = k_v\, P A_d \tag{6.11}$$

where ϕ = the capacity reduction factor and taken as 0.6; A_d = the design cross-sectional area of the shear-resisting portion of the wall member; f_{ms} is the characteristic shear strength which shall be taken as $1.25f_t$ but not greater than 0.35 MPa nor less than 0.15 MPa, and k_v is the shear factor to be taken as 0.3.

Whereas in the Indian code (BIS, 1987a), the lateral design load is estimated by taking the minimum of flexural, compressive, tensile and shear strength. Lateral strength is determined in terms of shear resistance (V_b) as the minimum of the value corresponding to flexural tensile stress (f_t) and flexural compressive stress (f_c) on the wall pier as given in Eq. 12-13.

$$f_t = f_b - f_a \text{ and } f_c = f_a + f_b \tag{6.12}$$

$$f_b = V_b\, h_{eff} / Z \tag{6.13}$$

where f_b = maximum bending stress; f_a = maximum axial stress; and Z = section modulus of the pier section. The code recommends h_{eff} as 0.75 times total height (H) of wall for solid wall, and $(0.75H+0.25)$ times the size of opening for wall with openings.

6.4.1.2. Out-of-Plane Resistance of Walls

The general methods for analysis of URM walls subjected to OOP loads are based on experimental observations and have been improving over time. The analysis as per IS 1905 (BIS,1987a) is based on elastic plate theory; the lateral capacity against the OOP loads is

calculated by adding the direct stresses due to the total vertical load and stresses due to external bending moment and equating their sum to the tensile bond strength of the masonry. Such empirical equations and methods mostly provide conservative values as there is no consideration of the possible failure modes. The uniformly distributed load in the plane of failure (w_{d1}) acting on the wall panel per m length of the wall as per IS 1905 can be calculated using Eq. 23-24.

$$f_t = \frac{M_e}{Z} - \frac{N}{A} \text{ (tension criteria)} \tag{6.14}$$

where f_t depends upon grade of mortar and the direction of bending. In the present study, f_t is determined from tests. N = total axial load; Z = section modulus of the pier section and e = eccentricity of N. M_e is the moment at mid height of the wall that can be calculated as:

$$M_e = \frac{Ne}{2} + \frac{w_{d1} h_{eff}^2}{8} \tag{6.15}$$

In most cases, the tension criteria governs the design, therefore, compression criteria is not discussed here.

The elastic plate theory and the conventional yield line method do not fit well for the analysis of URM walls. The analytical methodologies were improved by the introduction of the fracture line method by Sinha (1978) and Hendry et al. (1997). The fracture line method is used to calculate the ultimate lateral load resistance of the wall. A table is provided for moment (m) and β_s for various support conditions; a suitable relation between m and β_s for the present condition is given in Eq. 6.16. Equating the unknown lateral surface pressure w_d to the moment of resistance (M_r) obtained from Eurocode 6, the value of w can be calculated.

$$m = \frac{w_d L^2 \alpha_v^2}{12} \left(\frac{3\beta_s - \beta_s^2}{2\beta_s + \frac{\mu\alpha_v^2}{k}} \right) \text{ and } \beta_s = \frac{\mu\alpha_v^2}{2k} \left[\left(\frac{3k}{\mu\alpha_v^2} + 1 \right)^{\frac{1}{2}} - 1 \right] \tag{6.16}$$

where L = length of the wall; k is factor given by the authors; and μ is the ratio of strength parallel to bed joint to strength normal to bed joint as per Eurocode 6.

However, one of the major shortcomings of this method is that masonry is considered as a homogenous material and the internal actions like moments are assumed to be acting along the cracks in the walls simultaneously, which is not the case in reality. Hence, the adoption of this method may also overestimate the OOP strength of the wall. There is no direct method of estimating the OOP capacity of URM walls in Eurocode 6

(EN 1996-1-1, 2005), but it suggests calculation of moment demand (M_e) with respect to lateral loading that creates horizontal bending resulting in failure parallel to bed joints, and vertical bending resulting in failure perpendicular to bed joints. These moments can be equated to the moment of resistance (M_r) for safe design load (f_{xd}) estimation. The maximum lateral pressure (w_d) that can be resisted by the wall can be calculated by equating the applied moment M_e and the moment of resistance M_r given by Eq. 6.17-6.18.

$$M_e = \alpha_1 w_d L^2 \quad \text{per unit length of wall (plane of failure is parallel to bed joint)} \tag{6.17a}$$

$$M_e = \alpha_2 w_d L^2 \quad \text{per unit length of wall (plane of failure is perpendicular to bed joint)} \tag{6.17b}$$

In the present case, the plane of failure is considered to be parallel to the bed joint. α_1 and α_2 = bending moment coefficients based on fixity at the edges of the wall, and height to length ratio of the walls and can be obtained from the code.

$$M_r = f_{xd} Z_1 \tag{6.18}$$

where f_{xd} = design flexural strength appropriate to the plane of bending given in the code; Z_1 = elastic section modulus of unit height or length of the wall.

Lawrence and Marshall (2000) introduced the virtual work method; the uniformly distributed load in the plane of failure (w_{d1}) acting on the wall panel per m length of the wall is given by Eq. 6.19.

$$w_{d1} = \frac{2}{l_d^2}\left\{\frac{R_1 + R_2}{2} M_{ch} + \frac{h_v}{h_d} M_{ch} + \frac{h_1}{h_d}\left(1 + \frac{1}{G}\right) M_{cd}\right\} \frac{1}{\left(1 - \frac{1}{3}\frac{G l_d}{h_d}\right)} \tag{6.19}$$

where R_1 and R_2 = restraint factors for the supported vertical edges of the wall calculated according to AS-3700; h_v= height of vertical crack; h_1 = height of diagonal crack; h_d = design height of wall and is taken as $h/2$.

The virtual work method proposed by Lawrence and Marshall (2000) was later improved by Willis et al. (2006) and Griffith and Vaculik (2007). According to them, the maximum lateral surface pressure (w_d) that can be resisted by URM walls under two-way bending can be estimated using Eq. 6.20-6.23.

$$w_d = \frac{2a_f}{l_d^2}\left(k_1 M_{ch} + k_2 M_{cd}\right) \tag{6.20}$$

where a_f = aspect factor based on the wall geometry; l_d = design length of the wall and is taken as $L/2$, k_1 and k_2 are the coefficients based on boundary conditions; M_{ch} and M_{cd} are the horizontal and diagonal bending moment capacities of the masonry.

$$a_f = \frac{1}{\left(1-\frac{\alpha}{3}\right)};\ k_1 = \frac{R_{f1}-R_{f2}}{2}+1-\alpha;\ k_2 = \alpha\left(1+\frac{1}{G^2}\right) \text{ (without opening \& vertical edges supported)} \quad (6.21a)$$

$$a_f = \frac{1}{\left(1-\frac{\alpha}{3}\right)+\frac{l_o}{l_d}\left(1-\frac{\alpha}{2}\right)};\ k_1 = R_{f1};\ k_2 = \alpha\left(1+\frac{1}{G^2}\right) \text{ (with opening \& vertical edges supported)} \quad (6.21b)$$

where $R_{f1} = R_{f2} = 1$ (fully restrained against rotation); G is the slope of assumed crack line given by $G = \frac{2(h_u + t_j)}{l_u + t_j}$; $\alpha = \frac{Gl_{eff}}{h_{eff}}$; l_o=length of opening; l_u and h_u are length and height of brick unit; and t_j = mortar joint thickness.

$$M_{ch} = \text{minimum of} \left\{ \begin{array}{l} \frac{1}{2(h_u + t_j)}\left[(f_{vlt} - \nu P) h_u \frac{t_u^2}{6}\right] \\ \frac{1}{h_u + t_j}\left[\tau_u k_b 0.5(l_u + t_j) t_u^2\right] \end{array} \right\} \quad (6.22)$$

$$M_{cd} = \frac{\sin\theta}{h_u + t_j}\left[(\sin\theta)^3 \tau_u k_b 0.5(l_u + t_j) t_u^2 + (\cos\theta)^3 (f_t + P)\frac{0.5(l_u + t_j) t_u^2}{6}\right] \quad (6.23)$$

where t_u = thickness of brick unit; f_{vlt} = flexural tensile strength of brick unit; ν = Poison's ratio; τ_u = ultimate shear bond stress calculated as $1.6f_t + 0.9P$; θ = slope of the diagonal crack line; and k_b is a numerical factor used to calculate the shear stress due to torque acting on a rectangular cross-section.

This method provides greater accuracy over a wide range of wall geometries and caters to different wall configurations with and without openings. The method also reduces the emphasis on the lateral modulus of rupture and places more emphasis on the torsional resistance of bed joints. However, this approach assumes that the diagonal cracks form at a specific angle related to masonry unit geometry and joint thickness, and excludes the collapse load minimization procedure. In the later development, the above-mentioned approach was further improved by Lawrence and Page (2013), and this method is included in the Australian Masonry Standards (AS-3700, 2018). The OOP capacity is calculated using this standard by adding the horizontal moment capacity with the diagonal moment capacity and multiplying by a set of factors like the aspect factor, capacity reduction factor, and perpend spacing factor, and coefficients k_1, k_2, which depend on the boundary conditions of vertical edges of the walls and presence of openings. The lateral surface

pressure (w_d) in terms of two-way bending capacity of the wall can be calculated using the Eq. 6.24-6.26 following the procedure suggested by Walsh et al. (2018).

$$w_d = \frac{2a_f}{l_d^2}\left(k_1 M_{ch} + k_2 M_{cd}\right) \tag{6.24}$$

$$M_{ch} = \text{minimum of} \begin{Bmatrix} 2.0k_p\left(\sqrt{f_t}\right)\left(1+\frac{P}{f_t}\right)Z_d \\ 4.0k_p\left(\sqrt{f_t}\right)Z_d \\ \left(0.44 f_{ut}^{'} Z_u + 0.56 f_t Z_p\right) \end{Bmatrix} \tag{6.25}$$

$$M_{cd} = f_t^{'} Z_t \tag{6.26}$$

where $f_t^{'} = 2.25\sqrt{f_t} + 0.15P$; $Z_t = \dfrac{\frac{2B^2 t_u^2}{3B+1.8t_u}}{\left[\left(l_u + t_j\right)\sqrt{1+G^2}\right]}$; B = height factor $= \dfrac{h_u + t_j}{\sqrt{1+G^2}}$; k_p = perpend spacing factor; Z_d = section modulus; $f_{ut}^{'}$ =lateral modulus of rupture; Z_u = section modulus of brick units; Z_p = section modulus of perpend joints. Z_u and Z_p are taken equal to $Z_d = jt^2/6$ where j is the unit length of the wall.

6.4.1.3. Comparison of Wall Responses

In the present study carried out on URM buildings, Wall 2 and Wall 3 were subjected to in-plane loading, while Walls 1* and 3* were subjected to the OOP loading as shown in Figure 5.2 and Figure 6.2. Both the vertical edges of these walls were considered to be supported and opening was considered in Wall 3*.The lateral strength of the individual walls along both the in-plane as well as out-of-plane directions were evaluated analytically using the prescribed methods recommended by various codes and researchers and shown in Table 6.1 and Table 6.2. Among all the methods for in-plane strength estimation, the method recommended in the Indian code (BIS,1987a) was found to give very low values when compared with the experimental values (Table 6.1).

Table 6.1. Analytical estimation of the in-plane strength of URM walls

Wall	Experimental	Analytical strength normalised with respect to experimental strength				
	Strength (kN)	ASCE 41-13 (2014)	Magenes & Calvi (1997)	BIS (1987a)	AS-3700 (2018)	Eurocode 6 (2005)
Wall 1	28.6	1.13	0.86	0.80	3.10	1.76
Wall 2	19.3	0.70	0.50	0.50	3.30	1.83
Wall 3	28.8	0.50	0.60	0.40	2.26	1.75

Considering that several factors of safety are used in the code recommended capacity estimation procedure, it is obvious that the strengths estimated by the Indian code were significantly lesser than the experimentally obtained values. On the other hand, the lateral strength estimated using the Australian code (AS-3700, 2018) was very high for all the walls. The method recommended by Eurocode 6 (EN 1996-1-1, 2005) also provided significantly higher estimate of the in-plane strength of all the walls. Therefore, it appears that these codes may not be suitable for the masonry buildings constructed using low-strength masonry; however, more studies are required to be undertaken to validate these observations. Although the methods recommended by Magenes and Calvi (1997) and ASCE 41-13 (2014) estimated the in-plane strength for Wall 1 with higher accuracy, the estimation error was quite high for Walls 2 and 3; nevertheless the estimation by ASCE 41-13 was slightly better. The rocking mode of failure was found to be the governing criteria for all the walls when the in-plane lateral strength was evaluated using ASCE 41-13. On the other hand, Magenes and Calvi predicted shear sliding mode of failure in Walls 1 and 3 and flexural failure in Wall 2.

The out-of-plane capacity of URM walls estimated using various methods was found to vary from 8 kN to 40 kN in case of Wall 1* and from 3.7 kN to 35 kN in case of Wall 3* (Table 6.2). For both the walls, the maximum out-of-plane capacity was estimated by Eurocode 6 and the minimum by Griffith and Vaculik (2007). The procedure suggested by Walsh et al. (2017) was used to estimate the OOP strength using AS-3700 (2018). Both IS 1905 (BIS,1897a) and AS-3700 (2018) estimated similar OOP strength for both the walls, but the strengths were about three times higher than that estimated by Griffith and Vaculik (2007). The strength estimated by these codes for Wall 1* was higher than that estimated by Lawrence and Marshall (2000) as well as by Hendry et al. (1997).

Table 6.2. Analytical estimation of the out-of-plane strength of URM walls in kN

Wall	Griffith & Vaculik (2007)	Lawrence & Marshall (2000)	Hendry et al. (1997)	BIS (1987a)	AS-3700 (2018)	Eurocode 6 (2005)
Wall 1*	8.2	18.8	12.6	22.5	25.0	39.5
Wall 3*	3.7	15.0	11.1	7.7	6.6	35.0

On the other hand, the OOP strength estimated for Wall 3* by both BIS (1987a) and AS-3700 (2018) was found to be lower than that estimated by Lawrence and Marshall (2000) and Hendry et al. (1997). A minor difference in the OOP strength estimated for Wall 1*

(without opening) and Wall 3* (with opening) was observed when the methods recommended by Eurocode 6, Lawrence and Marshall (2000), and Hendry et al. (1997) were used. Clearly, no specific trend was observed in the estimation of OOP strength of URM walls using different methods signifying the underlying uncertainties in the OOP behavior of walls.

6.4.2. Lateral Strength of URM Building

As already discussed the combined experimental in-plane resistance of Walls 2 and 3 was only about 55% of the lateral load resistance of the full building. Therefore, the in-plane strengths of Walls 2 and 3 estimated using different methods are directly combined with the estimated OOP strengths of Walls 1* and 3*, and the combined strength values normalized with respect to the lateral strength of the building obtained experimentally (88.4 kN) are given in Table 6.3. As expected, a huge variation in the normalized lateral strength (from 0.44 to 2.30) was observed when different methods are combined for the estimation of lateral load resistance of the URM building. As already discussed, in addition to the combined resistance of the walls under in-plane and OOP action, there should be some contribution from the box action on the overall capacity of the URM building. However, the normalized strength predictions made by some of the combinations, especially those in which methods recommended in design codes were used, are already more than 1.0 signifying that the combined resistance of the four walls was even more than the experimentally obtained capacity. The comparison shown in Table 6.3 will be helpful in estimating the lateral strength of the URM building constructed with low-strength masonry by combining the in-plane and OOP strengths of individual URM walls and then adding the approximate contribution of the box action. Table 6.3 compares the analytically estimated lateral strength of URM building (normalized with respect to the experimental strength) obtained using different combinations. The analytically estimated OOP capacity of walls (1* and 3*) was also combined with the experimental in-plane capacity of the walls (2 and 3) for estimation of the overall lateral strength of the building. The lateral strength of the URM building constructed with low-strength masonry can therefore be conveniently predicted by combining the in-plane and OOP strengths of individual URM walls calculated using these analytical methods and then adding the contribution of the box action. Disregarding the normalized values greater than 1.0, the average contribution of the box action comes out to be about 35% of the lateral strength of the building (varies between 10-60%).

Table 6.3. Combined in-plane and out-of-plane strength of URM walls estimated using different methods and normalized with respect to the experimental capacity of 88.4 kN

		In-plane wall strength from					
		Present Tests	ASCE 41-13 (2014)	Magenes & Calvi (1997)	BIS (1987a)	AS-3700 (2018)	Eurocode 6 (2005)
OOP wall strength from	Griffith & Vaculik (2007)	0.68	0.45*	0.44	0.37	1.60	1.13
	Lawrence & Marshall (2000)	0.92	0.70	0.69	0.62	1.80	1.36
	Hendry et al. (1997)	0.81	0.58	0.57	0.51	1.70	1.25
	BIS (1987a)	0.88	0.75	0.64	0.58	1.80	1.32
	AS-3700 (2018)	0.90	0.77	0.66	0.60	1.80	1.30
	Eurocode 6 (2005)	1.40	1.20	1.15	1.10	2.30	1.80

* Explanation: Lateral load carrying capacity of URM building is estimated as 0.45 times 88.4 kN by combining the in-plane capacity of walls (2 and 3) from ASCE 41-13 (2014) and out-of-plane capacity of walls (1* and 3*) from Griffith & Vaculik (2007).

As already observed, the in-plane strength of the walls tested in the present study was realistically predicted by ASCE 41-13 (1997) and Magenes and Calvi (1997). Further, the method recommended by Griffith and Vaculik (2007) was found to be suitable for estimation of the OOP strength of URM walls (solid as well as with openings) constructed with weak masonry. The combined in-plane strengths of Walls 2 and 3 given by ASCE 41-13 (2014), Magenes and Calvi (1997), and present tests are added to the combined out-of-plane strengths of Walls 1* and 3* estimated using Griffith and Vaculik (2007) and shown in the dotted boxes in Table 6.3. It is clear that the combined actions of the four walls contribute about 45% of the lateral strength of the URM building if relevant analytical equations are used for strength estimation (inside dotted box). On the other hand, if the in-plane test result is combined with the OOP strength predicted by Griffith and Vaculik (2007), then the combined resistance of the four walls increased to about 68%. Rest of the lateral resistance is provided by the box action in the URM building.

6.5. SUMMARY

High seismic vulnerability of URM buildings is apparent from the huge loss of life and property observed during recent earthquakes worldwide (China, India, Indonesia, Italy, Iran, Nepal, New Zealand, etc.). It is utmost important to develop simple methods for seismic assessment of such buildings in order to quickly assess the seismic vulnerability of such building stock in a region for seismic risk reduction. A simple method of estimation of lateral load carrying capacity of URM buildings was demonstrated in the present study. The method was based on results obtained in an experimental study, a numerical study, and

an analytical study on URM walls and a URM building. Estimation of lateral load carrying capacity of URM buildings using experimental studies is feasible only for limited cases due to the requirement of large laboratory setup and associated costs. One of the major challenges while predicting the strength of the structure using numerical method was a requirement of a large number of input material characteristics, which were not available and, in most cases, require significant calibration. The calibrated lateral load response of the walls and the building obtained numerically was found to match with the experimentally observed behavior. Finally, methods recommended in various codes and literature were used to analytically estimate the lateral capacity of URM walls along in-plane as well as out-of-plane direction. It is demonstrated that some of the analytical methods recommended in codes and literature for determining lateral capacities of individual URM walls along the in-plane and out-of-plane direction can be methodically combined to obtain the lateral strength of URM building with acceptable accuracy. The method works equally well even when door and window openings are present in the walls of the building. The demonstrated method can be suitably used for quick assessment of lateral load carrying capacity of the URM buildings.

Chapter 7
HOMOGENIZED DISCRETIZATION METHOD FOR NUMERICAL SIMULATION OF URM BUILDING

Contents

7.1. General 131
7.2. Numerical Simulation of URM Building 134
7.3. Numerical Simulation of Strengthened URM Building 149
7.4. Summary 152

7.1. GENERAL

The seismic vulnerability of URM buildings can be determined by assessing the capacity of the structure, which can be achieved analytically or numerically. As already discussed in chapter 6, codes of various countries provide different empirical equations for calculating the in-plane and out-of-plane capacities of the individual URM walls constituting the building. Due to the uniqueness of the assumptions and calculation procedure, each approach can result in a different capacity value. Hence, a sufficiently advanced numerical method for comparison and calibration can be an added advantage to finalize a sound strengthening method, identify the most probable failure modes active, and provide a reliable capacity estimation. Due to material heterogeneity and anisotropic behavior of masonry, the numerical procedure for assessment of masonry structure are still under development. Unlike other construction materials like reinforced concrete and steel, common modeling approaches cannot be adopted for masonry, because of extreme complexity associated with its lateral load behavior and failure modes. Another key issue to consider is its extremely brittle behavior in tension. Despite the fact that various methodologies for a detailed seismic evaluation of URM buildings were suggested in the

recent past literature, a simplified numerical modeling able to keep in consideration all the essential features of masonry, was still required at a professional level. In the present chapter, a numerical simulation procedure that provides a fast and reliable tool for accurate predictions of the seismic response of URM structures is discussed.

Ip et al., (2018) categorized the different modeling strategies into five types, more or less depending upon the URM typologies to be studied: Equivalent Frame (EF), Finite element (FE), Finite-Discrete Element Method (FEM-DEM), Discrete Element (DEM), and approach with Macroblocks. The Discrete Element Method was relatively under-utilized in the numerical analysis of URMs, because it was suitable almost only when a micro-modeling, i.e., a distinct representation of bricks and mortar, can be adopted. It allows the separate discretization of the single blocks, usually assumed elastic or rigid, interacting typically with dry contact joints exhibiting friction. Compression crushing of the interface can be accounted as well. It usually requires a good amount of experience in modeling and the computational burden grows exponentially with the number of rigid blocks involved, meaning that for common buildings it was not easily applicable. The utilization of Macroblocks seems much more straightforward and accessible at a professional level; however, its accuracy strongly depends on engineer's experience and on the ability to identify in advance the shape of the macro-blocks involved in the activation of a failure mechanism.

The Equivalent Frame idealization, introduced probably the first time by Magenes and Fontana (1998) was characterized by an extreme simplification of the problem. A masonry wall was typically discretized with beam elements, and this requires a certain regularity of the wall, where masonry piers and spandrels may clearly be identified. Rigid joints were used as well to interconnect beams (spandrels) and columns (piers) in the crossing areas. The method was further modified by Brencich et al., (1998) and Lagomarsino et al., (2011) by introducing the use of macro-elements, replacing the beam elements and the introduction of orthotropic membrane element for the flexible diaphragms. Rinaldin et al. (2016) went a step ahead by describing each masonry component by means of non-linear multiple springs connected by rigid links. The piers and spandrels were modeled by placing non-linear springs at the two ends of the masonry elements to capture the flexural behavior and the shear in the middle. Though the approach delivers a good estimation of lateral load resistance and prediction of the failure

mechanism, the application remains limited to buildings with simple and regular geometry (Kappos et al., 2002; Pasticier et al., 2008). FE and FEM-DEM approaches do not exhibit such problems and they were suitable for both static non-linear pushover and non-linear time history analyses of URM structures with any kind of complexity and irregularity (Munjiza, 2005; Valente and Milani, 2016). However, non-linear FE modeling seems much easier to use, and has therefore, become more popular because it allows complex issues of analysis to be performed in a simpler way.

The early attempts to study entire masonry buildings with either plate and shell or full 3D elements probably date back to the end of 90's of the last century, because the approach was at that time still time consuming and theoretically difficult to govern. This might be due to the adoption of the Coulomb friction model to define the shear capacity of the contact surfaces between contiguous elements. The idea to deal with non-linear frictional interfaces and elastic elements was not abandoned, for instance, in the decade that followed, Yi et al., (2006) used contact interfaces with friction in the possible areas where the inelastic deformation was expected to concentrate and between elastic structural elements. In particular, they studied in the non-linear range an entire two-story building previously tested in laboratory and subjected to pseudo-dynamic loads. The analyses were improved rapidly by Milani et al., (2007) by introducing linearized homogenized surfaces for masonry and by making use of kinematic theorem of limit analysis. The utilization of robust 2D and 3D FE models with damage and plastic deformation inside the element volume represented a breakthrough in favor of the utilization of geometrically realistic 3D models and sophisticated non-linear materials. As a matter of fact, the so called concrete damage plasticity model (CDP) implemented in the commercial code Abaqus (2010), was originally conceived for concrete and immediately utilized in this field, starting from the end of the 80's. Its adaptation to masonry is relatively recent and has made the non-linear pushover analysis of masonry buildings an effective one. Such model follows an isotropic constitutive law and the uniaxial stress-strain behavior was characterized by different values of tension and compression strength, following in the post peak an elastoplastic softening behavior with damage. The multiaxial case was governed by a Drucker-Prager failure criterion (Acito et al., 2016; Choudhury et al., 2015), which can be suitably modified to approximate the Mohr-Coulomb law in a smooth way.

A strong simplification, which was however commonly accepted, was that masonry was characterized by an isotropic behavior, which was not obviously realistic for regular textures. As a consequence, the damage patterns sometimes mismatch when compared with the experimental ones. Hence, in this chapter, a new discretization method has been proposed and compared with the traditional homogenized model and the results were validated with an experimental study. In this case, the proposed model consists of multiple sets of the elementary unit, subdivided along its thickness in several layers and each unit consists of a set of discretized elastic cells, which were interfaced by a set of smaller units bearing the plastic damage properties. The validation of the proposed method was done by comparing the results with that obtained in an earlier experimental study in which both the full-scale masonry walls with various opening configurations and a single room building were tested.

7.2. NUMERICAL SIMULATION OF URM BUILDING

7.2.1. Numerical FE Modelling Strategies

Two different FE approaches were used to perform the numerical non-linear static analyses, namely a standard FE approach where masonry is modeled by means of (1) a homogeneous isotropic material with damage, plastic behavior and softening in both tension and compression and (2) an advanced homogenization approach where orthotropic behavior of the masonry material is accounted for at the meso scale by means of a suitable FE homogenization strategy and non-linearity is lumped on vertical and horizontal interfaces at the macro-scale (Figure 7). The following sub-sections briefly recall the main features of both models.

7.2.1.1. Standard Isotropic Damage-Plasticity Fe Approach

The first approach is a classic FE discretization where masonry is modeled by means of a homogeneous isotropic material (Figure 3.1a,b), exhibiting softening and distinct damage parameters in tension and compression. This is a commonly adopted and straightforward strategy available in the most widespread commercial codes, such as ABAQUS (the commercial code here used), where a so-called Concrete Damage Plasticity (CDP) model is available in the standard package.

As far as a multi-axial stress state is concerned, CDP exhibits a typical cohesive frictional behavior with a Drucker-Prager strength criterion. A non-associated plastic flow rule is adopted, with a dilation angle here assumed equal to 10°, in agreement with

consolidated literature in the field and in order to suitably simulate the non-dilatant behavior of masonry under shear actions and moderate compression. Drucker-Prager criterion is suitably modified by means of a K_c scalar parameter, representing the ratio between the second stress invariants on the tensile and the compressive meridians, which –if equal to 2/3- approximates in a smooth way the corresponding Mohr-Coulomb failure criterion. The ratio between biaxial and uniaxial compressive yield stress fb_o/fc_o is assumed equal to 1.16, thus properly simulating masonry behavior (Milani et al. 2006; Page 1981). A further smoothing of the tension corner is also adopted, which is obtained considering an additional parameter, called eccentricity, and set equal to 0.002, as per the Abaqus User's Guide (2010).

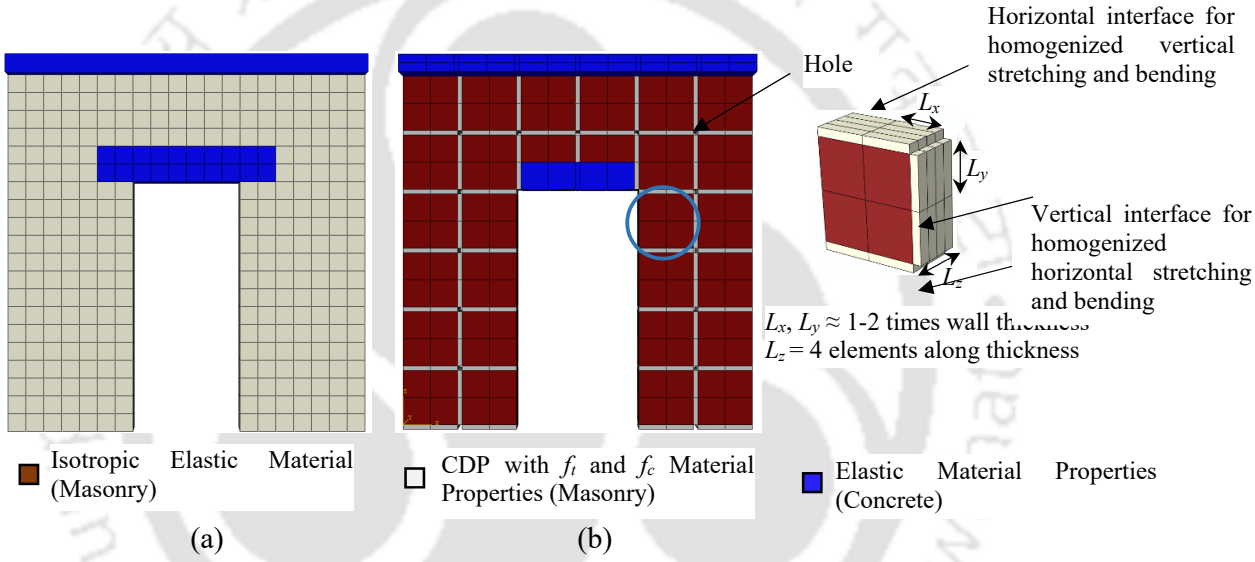

Figure 7.1 Numerical models adopted for the analysis of the tested specimens: (a) isotropic FE model with damage and softening (b) non standard two-step homogenization model

The base of all the models is assumed rigidly fixed to the ground, according to the experimental protocol. Pushover analyses of the URM building model are carried out in order to systematically evaluate the active failure modes and lateral load carrying capacity.

The adopted discretization, see also Figure 7.1a, is quite refined and consists of 872 solid elements and 1493 nodes for Wall model 1, 944 brick elements and 1598 nodes for Wall model 2, 1040 solid elements and 1703 nodes for Wall model 3, and 8455 solid elements and 13404 nodes for the whole URM building model.

Material non-linearity is defined exclusively for masonry elements, whereas, concrete lintels/slabs are assumed to behave elastically. Such an assumption appears fully

reasonable, considering the fact that concrete and steel possess a strength that is much larger than that of masonry.

Uniaxial stress strain relationships used in the first numerical model are shown in Figure 4.6b. As far as the homogeneous isotropic approach is concerned, experimental values, where available, are directly assumed in the formulation of the uniaxial stress-strain relationships of the isotropic material.

During the tensile bond test, the material exhibited sudden brittle failure, leaving no scope of capturing the post-peak softening behavior, which is required to define the tensile damage behavior of masonry material for the numerical analysis (Lubniner et al. 1989; Page 1981). Using the past results of Dhanasekar and Haider (2008) and Rai et al. (2014), a tensile strain value of 0.0001 was considered in the study corresponding to the peak tensile stress of 0.076 MPa. The post peak behavior was assumed to be linearly falling till tensile stress of 0.015 MPa and corresponding strain value of 0.001 as shown in Figure 4.5b. The residual tensile stress of 0.015 MPa was further considered till strain value of 0.0015. These values in the tensile stress-strain curve were selected based on past literature in order to assist in smoother strength degradation required for convergence of the Abaqus solution procedure during non-linear analyses.

Predictions are certainly acceptable from a practitioner standpoint, but if a more precise insight is needed, then an increase of sophistication is mandatory. This is the reason why in the present paper a second, much more refined model, is discussed. Such latter approach bases on homogenization and the discretization at a structural level is simply obtained as in Figure 7.1b, as it will be discussed in the following sub-section.

7.2.1.2. Two Step Discrete Homogenization Model

The two-step homogenization model proposed as second numerical approach relies into a preliminary homogenization of the masonry material to determine macroscopic elastic and inelastic properties to adopt at a structural level and a subsequent structural analysis carried out with elastic orthotropic elements linked by non-linear interfaces. The procedure is fully described in Figure 7.2. Step 1 occurs at the meso scale and allows to deduce, by means of a suitable homogenization approach, the elastic and inelastic masonry properties that will be used in Step 2 at the macro-scale.

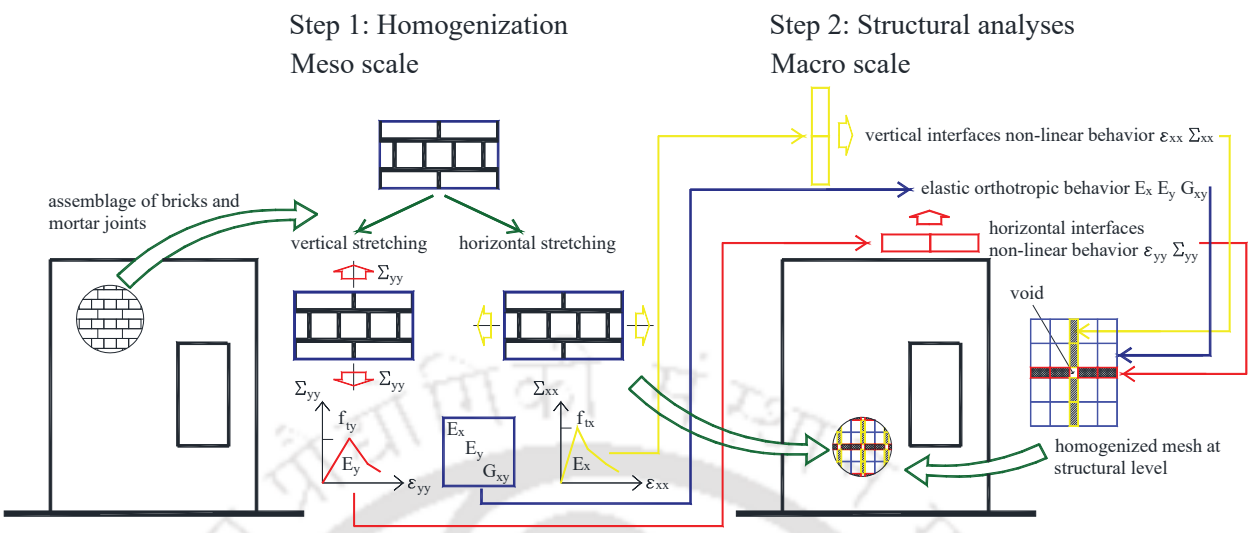

Figure 7.2 Two-step homogenization approach for the analysis of masonry walls. Step 1: homogenization at the meso scale and determination of elastic properties of continuum elements (blue) and elastic and inelastic properties of vertical (yellow) and horizontal (red) interfaces.

Step 1 can be roughly summarized as follows:

1) A Representative Element of Volume (REV, also known as unit cell) constituted by few bricks and mortar joints is found, which generates the entire structure by repetition.
2) Non linear stress-strain relationships to use at a structural level are derived solving a suitable incremental boundary value problem, provided that the unit cell is, for instance, discretized into FEs. Here, the procedure originally proposed by Milani (2011a) (see also Milani 2011b and Milani & Bertolesi 2017) for further developments and modifications) is considered as reference, modifying the approach to the English Bond pattern. The meso-scale level is fully handled within Matlab software. The approach relies into a rough FE discretization of the bricks by means of few elastic constant stress triangular elements and joints reduced to interfaces with a softening cohesive-frictional behavior. The procedure is particularly simple for running bond masonry, because it allows to solve the incremental homogenization problem in the inelastic phase in quasi-analytical form. The reader interested into the details of the model is referred to (Milani & Bertolesi 2017) Here it is worth only noting that for an English bond texture, a semi-analytical

approach is not possible and a standard FE approach with the rough discretization of Figure 7.2 is used. In addition, in order to reduce the number of material properties required by the two step model, it is assumed that bricks are rigid (in practice, a very large Young modulus is utilized) and all deformability is lumped on joints reduced to interfaces. Joints stress-jump of displacement mono-axial relationship adopted in the unit cell is depicted in Figure 7.3a.

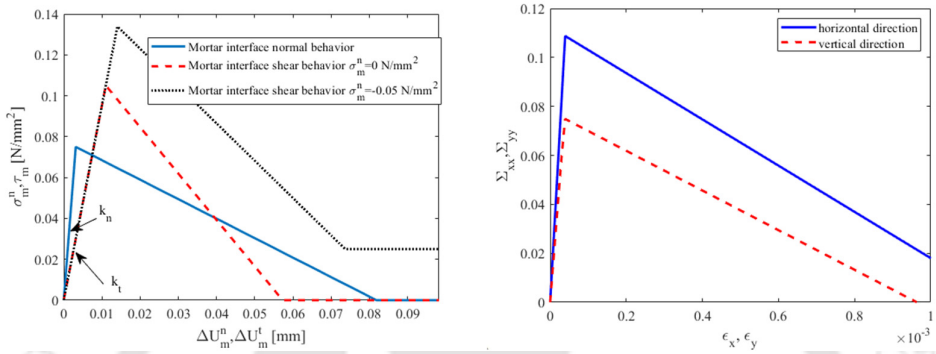

(a) (b)

Figure 7.3 Homogenized masonry behavior deduced from Step 1 in the homogenization model. –a: mortar interfaces input behavior. –b: homogenized horizontal and vertical stretching.

A linear softening behavior is assumed to simplify the approach to a great extent. Initial elastic stiffness k_n, tensile strength f_t and ultimate ductility Δ_m^u of mortar interfaces are tuned in order to obtain, under vertical stretching, see Figure 7.3b, a homogenized behavior very close to that used in the first approach, see Figure 4.5b. The resultant homogenized stress-strain relationship obtained for horizontal stretching is reported in Figure 7.3b. As can be observed, the response is –as expected- orthotropic, with a quite marked softening. The larger strength exhibited by masonry under horizontal stretching is classically linked to the shear contribution of the bed joints, as shown for instance in (Milani et al. 2006, Cecchi & Milani 2008). A frictional cohesive (Mohr-Coulomb) interaction between normal and shear stresses is assumed for joints. Mortar joints tangential behavior (in absence of normal stress) is depicted in Figure 7.3a; a friction angle equal to 30° is adopted, in agreement with consolidated literature. The present homogenization model (elastic or rigid bricks, joints reduced to interfaces and utilization of a 2D approach) does not allow to properly predict masonry compressive behavior. Consequently, the same stress-strain relationship adopted in the first model, **Error! Reference source not found.**b, is used here at the macro-scale (Step 2).

Step 2 relies in the macro-scale (structural) implementation of the homogenization model. At the macro-scale, Abaqus FE commercial code is used. The structural implementation is a discretization constituted by 8-noded "brick" elements with almost square shape (blue elements in Figure 7.4) exhibiting an elastic orthotropic behavior and thin solid parallelepiped damaging elements with non-linear behavior, approximating structural interfaces.

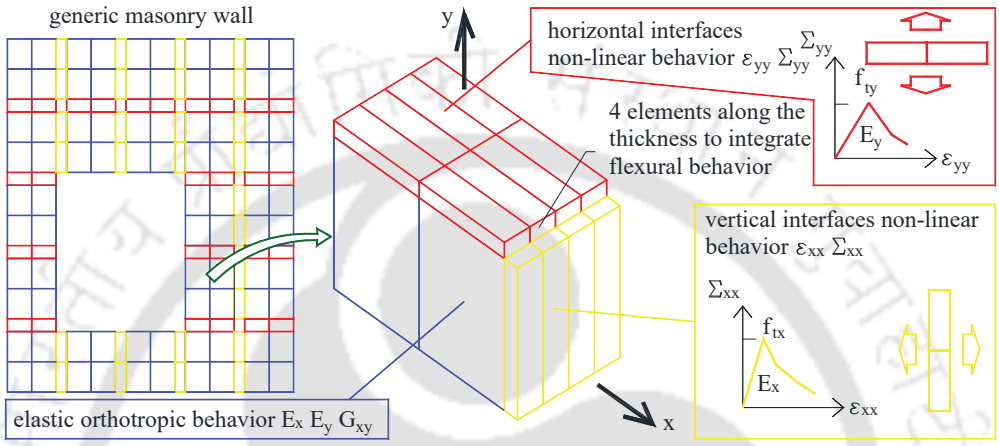

Figure 7.4 Detail of Step 2 discretization (macro-scale) in the homogenization approach. Discretization of parallelepiped 8 noded elements for elastic parts (blue), horizontal interfaces (red) and vertical interfaces (yellow). Red and yellow solid elements obey a CDP model in Abaqus.

Since such elements should approximate interfaces, their thickness is bounded by a limit distorsion ratio of the parallelepiped elements, which cannot exceed in any case 1:6 to avoid integration inaccuracies. In such approximation, these latter elements represent the homogenized interfaces. For them, distinct mechanical properties are adopted, depending if their orientation is horizontal (red elements) or vertical (yellow interfaces). In order to favor the mono-dimensional behavior, at the intersection between horizontal and vertical interfaces the space is left empty, i.e. square holes are present, see Figure 7.4. For such "interface" elements, the standard Concrete Damage Plasticity CDP model available in Abaqus is adopted, with a mono-axial stress-strain behavior identical to that provided by the homogenization model in the particular case studied in the present paper, see Figure 7.3.

The two-step homogenization approach proposed here for the first time has a twofold advantage: first of all, in this way an orthotropic behavior is obtained using a standard commercial code where sophisticated material models accounting for distinct properties

along material axes -as clearly required by masonry- are not available; second, the present implementation supersedes all the disadvantages exhibited by the Homogenized Rigid Body and Spring Models HRBSMs available in the literature, see for instance (Silva et al. 2017; Casolo & Milani 2010; Bertolesi et al. 2018), where a cumbersome identification of the springs representing the interfaces is needed and numerical instabilities are possible due to the large elastic modulus adopted to represent the (elastic) rigid elements. Furthermore, to couple in- and out-of-plane loads in RBSMs is not an easy task, whereas in the present improved implementation without rigid elements, a simple out-of-plane integration suffices, thanks to the utilization of 4 8-noded brick elements along the thickness (a fair compromise between accuracy and numerical stability).

For practical purposes, only vertical and horizontal non-linear interfaces are utilized, but there are no particular complications if diagonal interfaces are required, the only practical effort needed being to set up a geometrically more complex mesh.

It is finally worth mentioning that homogenized interfaces, realized at the macro-scale by means of solid elements, thanks to the particular topology of the mesh adopted (especially as a consequence of the holes present at the intersection between vertical and horizontal interfaces), exhibit a state of stress approximating quite accurately that of zero-thickness interfaces. As a matter of fact, with reference to Figure 7.5, authors experienced that the stress components acting on the *t-r* plane between two neighboring elements are negligible.

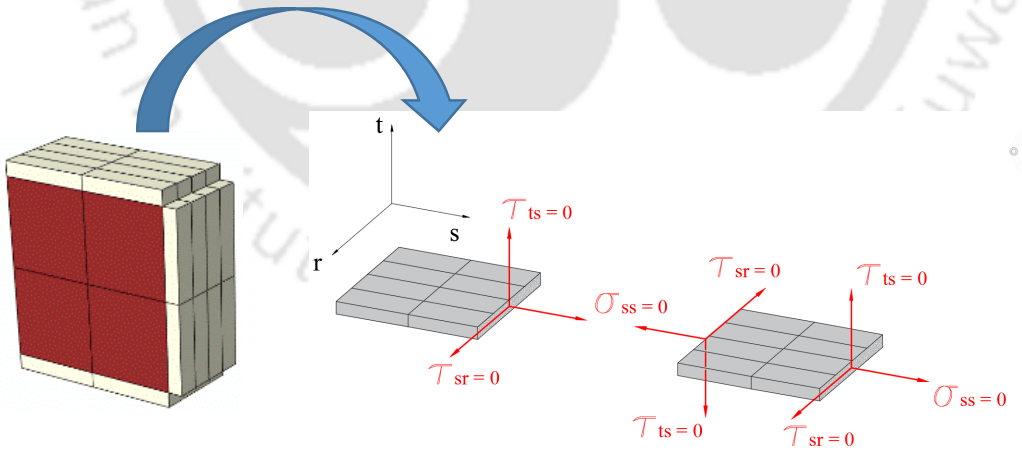

Figure 7.5 Detail of the discretization of elastic cells and interfaces (left) and state of stress of interface in the plane t-r between two adjacent solid elements (right).

On the other hand, it is worth noting that a user defined element has been recently implemented in a Fortran-subroutine in Abaqus by one of the authors (Scacco et al. 2020) where for parallelepiped elements stresses σ_{ss}, τ_{sv}, τ_{st} in Figure 7.5 are enforced to zero,

finding results in terms of stresses at a structural level very near to those obtained with the present, more straightforward, implementation.

A much less refined discretization –when compared with the previous numerical isotropic FE approach- is required for the two-step homogenization strategy: it consists of 1208 solid elements and 1932 nodes for Wall model 1, 1352 solid elements and 2142 nodes for Wall 2, 1512 solid elements and 2322 nodes for Wall model 3, and 6816 solid elements and 9718 nodes for URM building model.

7.2.2. Results

The responses of all the specimens experimentally tested (3 shear walls and 1 room building) were numerically reproduced with the help of both the commonly used homogenized and the proposed homogenized model. In particular, global pushover curves and crack pattern evolution obtained with both the models were compared with experimental evidences. All the tested specimens exhibited obviously different failure patterns and lateral load carrying capacities with a dominant brittle behavior at failure and activation of different failure mechanisms. Tests were terminated after a significant amount of damage was observed in the specimens, but immediately before the imminent collapse of the structure, in order to avoid the risk of damage to the testing equipment.

7.2.2.1. Wall 1

The first specimen (Wall 1) was a solid shear wall without any opening. As already discussed in Chapter 4, the flexural crack started forming at the bottom of the wall and propagated to the entire length of the specimen initiating sliding shear failure at a lateral displacement level of 8 mm (Figure 7.2a). The bed joint shear crack also formed at the top of the specimen, but it did not continue any further with the advancement of the displacement cycles. The FE model of Wall 1 was numerically analyzed using the two approaches discussed above. The terms CDM and PDM in Figure 7.2, refers to *Commonly used Discretization Model* and *Proposed Discretization Model*, respectively. It is noticeable that the numerical pushover curves obtained using both the discretization models matched quite well with the experimentally obtained curve. Moreover, the lateral load behaviour obtained using the pushover analyses carried out over the model of the solid wall using two discretization models delivered results which were in good agreement with the experimental results (Figure 7.2 c-d). Though the bed joint shear crack at the top of the

specimen could not be predicted in the numerical simulations, the damage at the bottom of the specimen, responsible for the final failure of the specimen, was appropriately predicted by both the commonly used discretization model as well as the proposed discretization model. Therefore, any of the two discretization models can be conveniently used for numerical simulation of solid masonry shear walls.

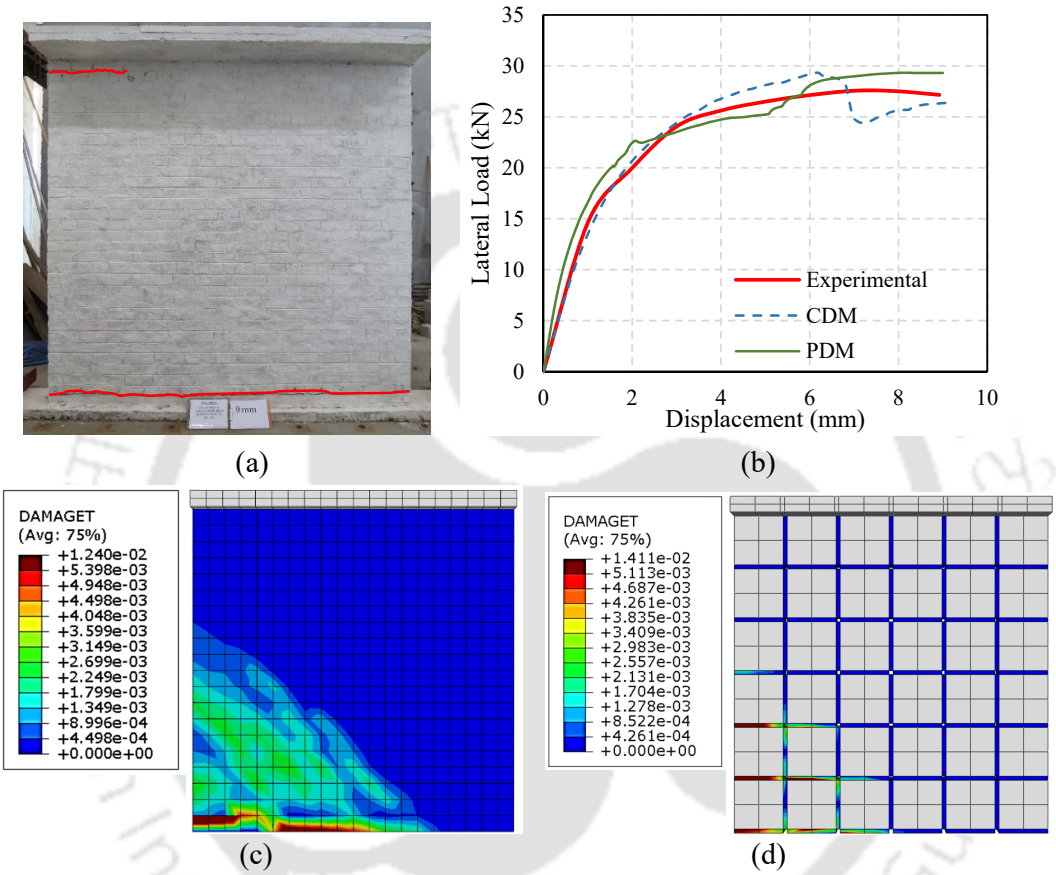

Figure 7.6. Lateral load behavior for Wall 1: (a) Experimentally observed response, (b) Capacity curve comparison of the numerical models with experimental specimen, (c) Damaged model of commonly used homogenized model, and (d) Damaged model of the proposed homogenized model.

7.2.2.2. Wall 2

The second tested specimen (Wall 2) was a URM wall with a central door of size 0.9 m × 2 m. The test resulted in a failure mode consisting of a combination of both sliding shear and flexural response. The test continued up to a displacement level of 6 mm when cracks at the upper corner of the door reached the wall edges and cracks at the bottom also extended along the entire length of the wall course exhibiting sliding mode of failure. This resulted in the failure of the specimen in shear sliding mode as well as flexural mode as

shown in the damaged state of Wall 2 in Figure 7.3a. The lateral load capacity achieved from the test was about 19 kN.

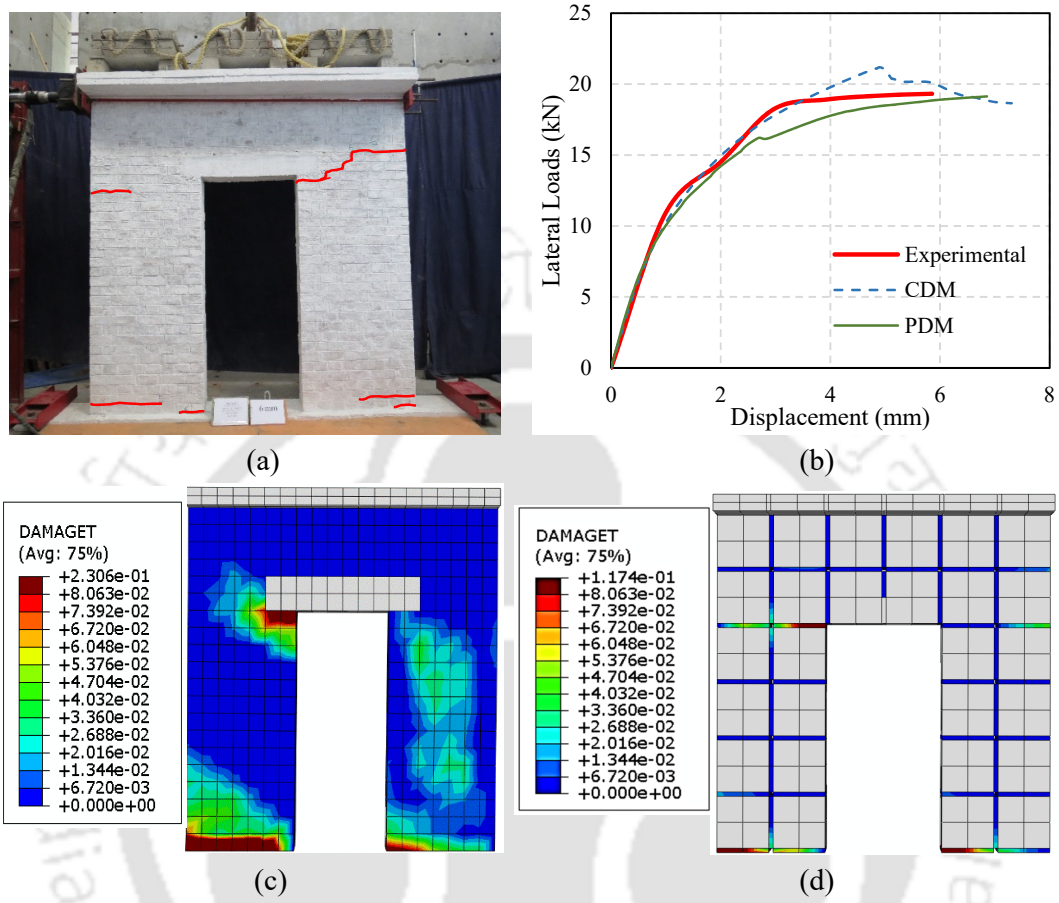

Figure 7.7. Lateral load behavior of Wall 2: (a) Experimentally observed response, (b) Capacity curve comparison of the numerical models with experimental specimen, (c) Damaged model of commonly used homogenized model, and (d) Damaged model of the proposed homogenized model.

It is noticeable from Figure 7.3b that the capacity curves obtained from the pushover analyses carried out using both the discretized models are in good agreement with the experimental results. However, the capacity curve generated using the proposed discretization model provided a smoother curve closely matching with the experimental curve in comparison to the curve obtained from commonly used discretized model. In addition, the *Damaged Model* obtained using the proposed discretization model matched quite closely with the damage states observed experimentally as shown in Figure 7.4c and Figure 7.3d. The damage contour obtained in the commonly used discretization model, as shown in Figure 7.3c, covers a larger area, which is not the case when compared to that obtained experimentally. Moreover, the damaged area projected by the CDM in the right

pier of Wall 1 (Figure 7.3c) was not observed in the experimental study. Hence, the unrealistic damage projected by the commonly adopted discretization model in some members can be avoided by adopting the proposed discretization model.

7.2.2.3. Wall 3

The third URM shear wall specimen (Wall 3) consisting of a central window opening of size 0.9 m × 1.2 m was tested under cyclic loads. The lateral load response of the specimen again exhibited a mixed failure mode of flexure and sliding shear type as shown in Figure 7.8a. The test continued till the cracks emanating from both ends of the wall met at about 12 mm displacement level. However, no cracks were observed at any other location of the specimen. The wall specimen with window opening displayed a load carrying capacity of about 28 kN (Figure 7.4b).

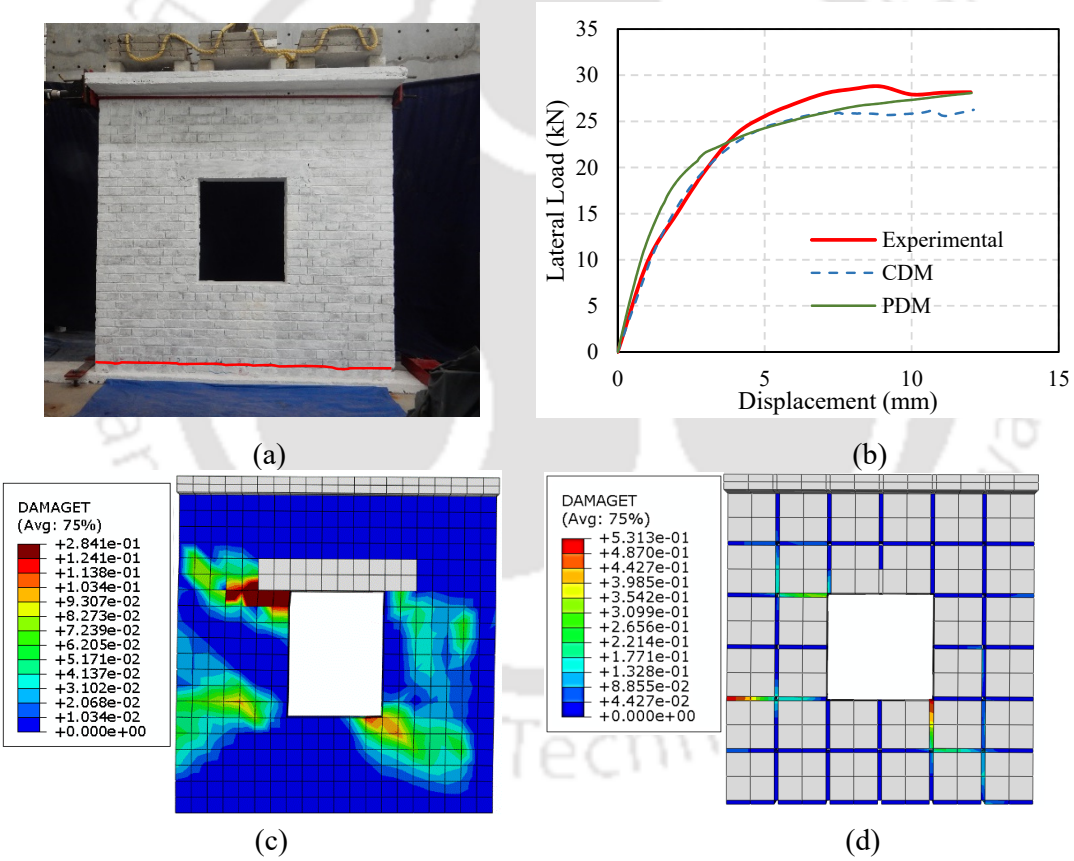

Figure 7.8. Lateral load behavior of Wall 3: (a) Experimentally observed response, (b) Capacity curve comparison of the numerical models with experimental specimen, (c) Damaged model of commonly used homogenized model, and (d) Damaged model of the proposed homogenized model.

The numerical analysis conducted by adopting two different discretization models exhibited a different response in comparison to the experimentally observed response. Stress concentration was observed in the numerical response near the window opening, and therefore, damage was prominently observed near the opening (Figure 7.4 c-d). However, such damage near window opening was not observed in the experimental response, which exhibited failure due to flexure cracking and subsequent sliding at the bottom of the shear wall. Such a contrasting difference in observed failure modes may be because of the presence of a possible weaker course of masonry in the test specimen. However, the lateral strength of the shear wall estimated by both the discretization models was found to be in good agreement with the experimental results. The commonly used discretization model (CDM) exhibited slightly lesser strength compared to the experimentally observed strength; whereas, the proposed discretization model (PDM) delivered a smoother capacity curve with closer lateral capacity value (Figure 7.4b).

7.2.2.4. URM Building

The URM building, shown in Figure 5.1a, was tested under slow cyclic lateral loading till failure. During the testing small cracks started appearing in the bottom brick layer at an early stage of lateral deformation of about 1mm. The cracks were observed in the walls, which were along the loading direction, particularly, Wall 2 as shown in Figure 7.6a. Subsequent cracks started forming near the door and window openings of Wall 2 and Wall 3* at 5 mm displacement level (Figures 7.5a-b). These cracks gradually widened and extended further with increasing displacement levels. At 7 mm displacement level, cracks started developing in the walls perpendicular to the loading direction, particularly in Wall 3*. The cracks developed in the perpendicular walls were located mostly near the upper corner of the window opening in Wall 3 and below the roof slab in Wall 1* (Figure 7.5b). The test exhibited a mixed failure mechanism consisting both of tensile and shear type. In addition, torsional response was also observed in the buiding at higher displacement levels due to plan asymmetry. The lateral load capacity made a gradual increase up to 4 mm displacement level, beyond which a sharp degradation in the capacity was observed as shown in Figure 7.6. At 12 mm displacement level, the cracks near the openings in Wall 2, Wall 3*, and Wall 3 propogated throughout the length of the walls and started joining each other. These cracks also joined the lintel level cracks formed in Wall 3 (Figure 7.5). These continous cracks at the lintel level along the periphery of the building resulted in initiation of the rocking motion of the upper part of the building. At a displacement level

of 17 mm, the cracks in Wall 3* and Wall 1* (walls under out-of-plane action) widened prominently resulting in an imminent out-of-plane failure. No further damage was observed in the building specimen with further increase in the lateral displacement as the upper part of the building was simply undergoing rocking motion. Therefore, the test was terminated at 20 mm displacement level. The lateral load capacity achieved from the test was about 88 kN at 4 mm displacement level, which correspond to about 44% of the seismic weight of the building and 0.67% lateral drift (Figure 7.6).

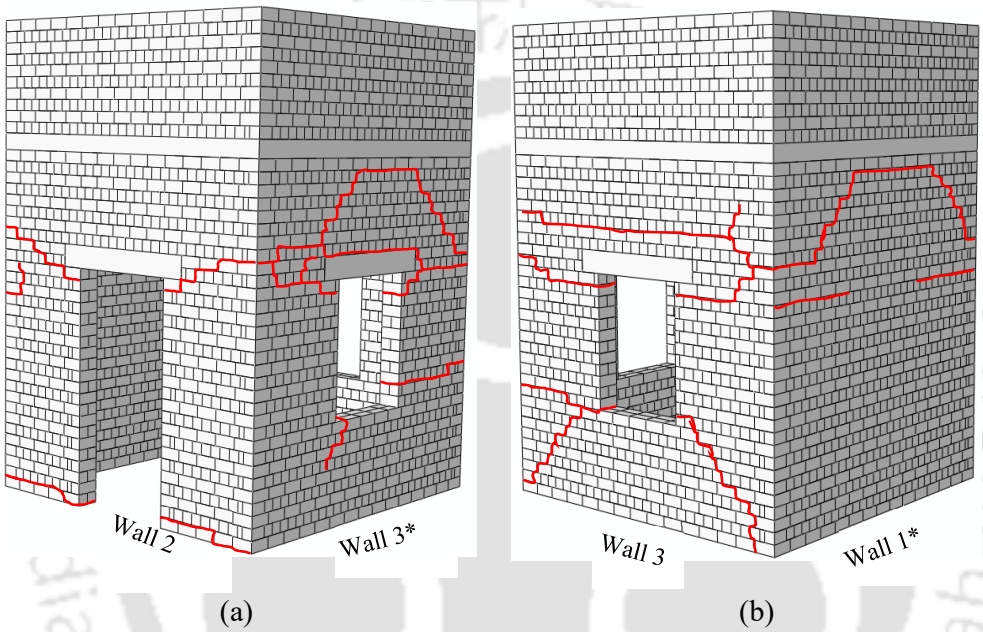

Figure 7.9. Damage pattern observed during the slow cyclic lateral load testing of full-scale URM building: (a) damage observed in Wall 2 and Wall 3*, and (b) damage observed in Wall 1* and Wall 3.

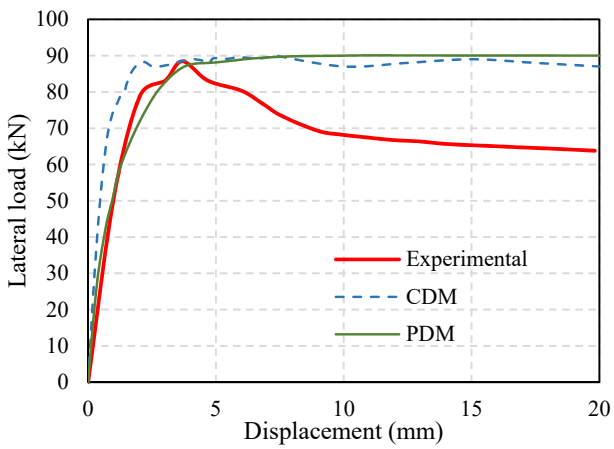

Figure 7.10. Comparison of the capacity curves for the URM building obtained from experimental study with those obtained using numerical simulation.

The building model was numerically analyzed using two methods of discretization. Pushover analyses of the building model simulated using both the discretization models delivered capacity curves, which were in good agreement with the capacity curve obtained experimentally (Figure 7.6). However, the damage predicted using the two approaches were significantly different. The damage contour of the commonly used discretization model was widely spread and did not match well with the experimentally obtained damaged pattern (Figure 7.7a).

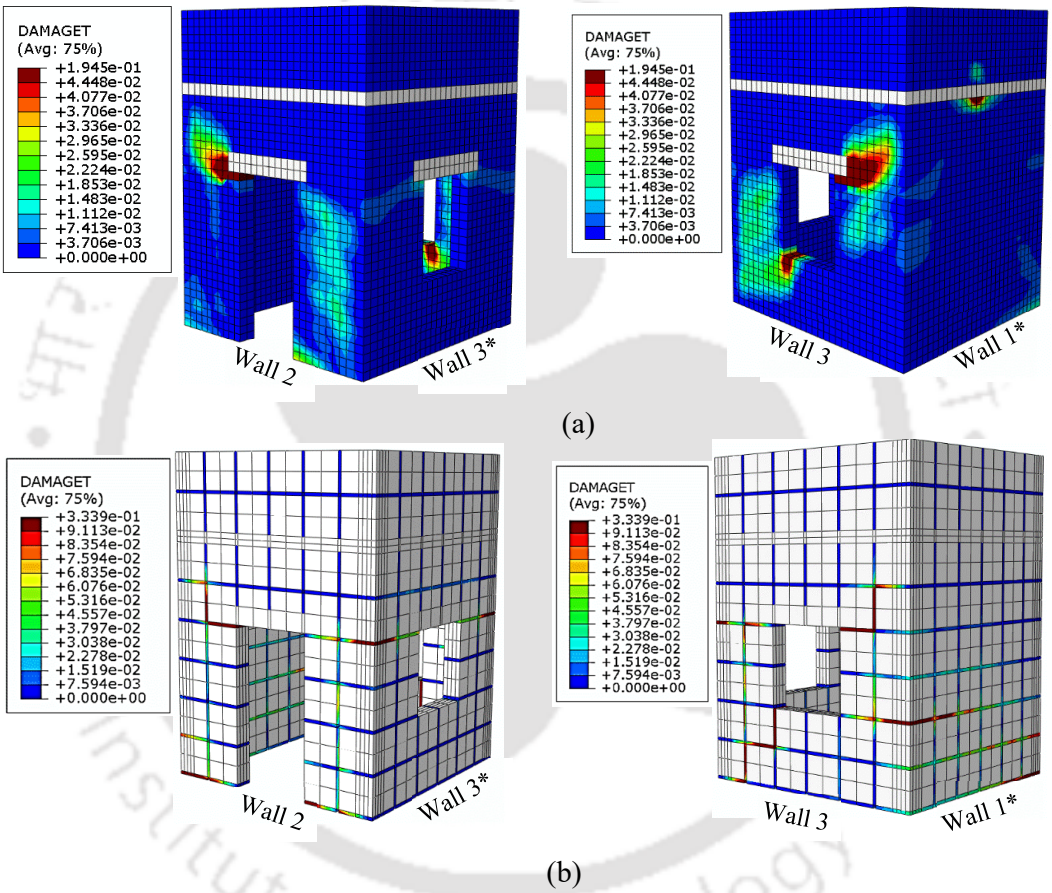

Figure 7.11. Damage pattern predicted by numerical simulation of full-scale URM building model: (a) using commonly used homogenized model, and (b) using proposed homogenized model.

On the other hand, the damage pattern obtained from the proposed discretization model matched well with that obtained experimentally (Figure 7.7b). The damage observed near the openings in the experimental study and that predicted by the proposed discretization model were found to be similar to each other. The connectivity of the cracks in different walls of the building model can also be seen clearly in the damage results predicted using the proposed approach; however, such connectivity in the cracks could not

be predicted using the commonly used discretization approach. Therefore, the proposed discretization model can be conveniently adopted to numerically analyze masonry buildings in order to predict the lateral capacity as well as damage pattern with acceptable accuracy. Although, adopting either of the discretization approach may result in slightly different damage observations as compared to the experimental observations, the predicted capacity curve was found to be very similar and in good agreement with the experimental results.

7.2.2.5. Parametric Numerical Study of URM Buildings

Adopting the proposed discretization model, numerous numerical simulations were carried out by varying the various parameters of the building like, the wall thickness, the aspect ratio (*l*/*h*) of the walls, and the tensile strength of the masonry. Realistic values of these parameters were considered in the parametric study to understand the influence of these important parameters on the lateral strength of the building. Four different wall thicknesses were considered in the study: half brick wall, full brick wall, one and a half brick wall and double brick wall. Five aspect ratios of the walls were considered for each of the wall thickness: 1.0, 1.1, 1.2, 1.3, and 1.4. These 20 models were were the numerically analysed by varying the tensile strength value from 0.04 to 0.2 MPa in an interval of 0.02 MPa. Thus, total 140 models were numerically simulated in the parametric study. The lateral strength of the buildings obtained from the numerical simulations was normalised with respect to the weight of the building, and termed as α_L. 3D plot of the variation in the normalized strength (α_L) with respect to the tensile strength and aspect ratio of various wall thicknesses are plotted and shown in Figure 7.8.

The lateral load values obtained by numerical simulation considering different combinations of the parameters were used to carry out unconstrained multiple linear regression analysis. An empirical equation was developed using the regression analysis as shown in Eq. (7.1).

$$\alpha_L = 0.23 f_t^{0.965} A_r^{0.83} t^{0.587} \tag{7.1}$$

Where α_L is the ratio of lateral load to the self-weight of the building, f_t is the tensile strength of masonry in MPa, A_r is the aspect ratio of the building (*l*/*h*), and *t* is the thickness

of the wall in the building in mm. The α_L values predicted using Eq. (7.1) were quite close to that obtianed from numerical simulation with maximum error less than 20%.

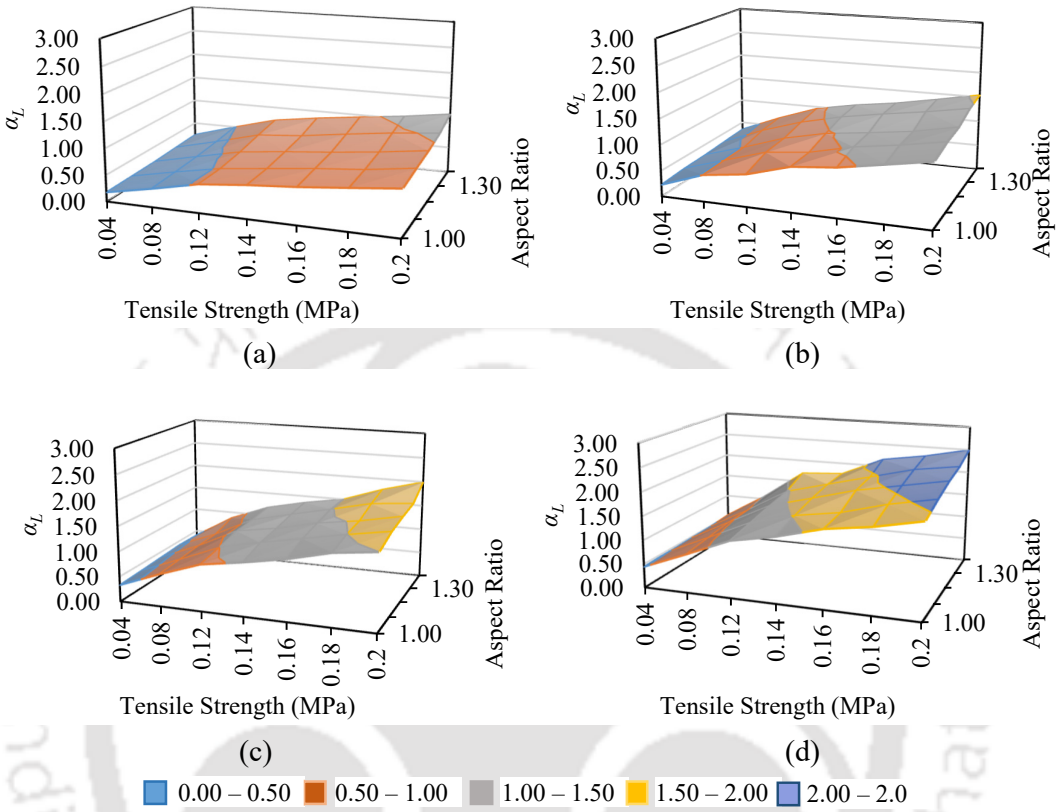

Figure 7.12 3D plot of variation of α_L with respect to tensile strength of masonry and aspect ratio for: (a) half brick wall, (b) full brick wall, (c) one and a half brick wall, and (d) double brick wall.

7.3. NUMERICAL SIMULATION OF STRENGTHENED URM BUILDING

The numerical simulation of the strengthened URM building (Model 2 – as discussed in Chapter 5) was also carried out. For strengthening purpose, horizontal steel bands were used at lintel as well as sill level on both the wall faces (externally as well as internally) throughout the length of the building, and additionally, vertical steel bands were provided adjacent to the openings on both the wall faces. Here it is worth noting that an efficient strengthening is achieved when the steel bands remain in the elastic range, therefore, an elastic material model is adequate for the steel bands, which were modeled using beam elements. They were rigidly connected node by node to the masonry material (no interface elements were used). The perfect connectivity of steel element with the masonry elements resulted in a very high lateral strength of the building, which was not observed when the

building was tested under quasi-static loading. Due to these challenges, the equivalent nodal connectivity of the beam elements was tried and numerically tested. Four Simulation types were considered for the strengthened models with reduced nodal connectivity as shown in Figure 7.9. The same simulation type was used for all the walls of the building.

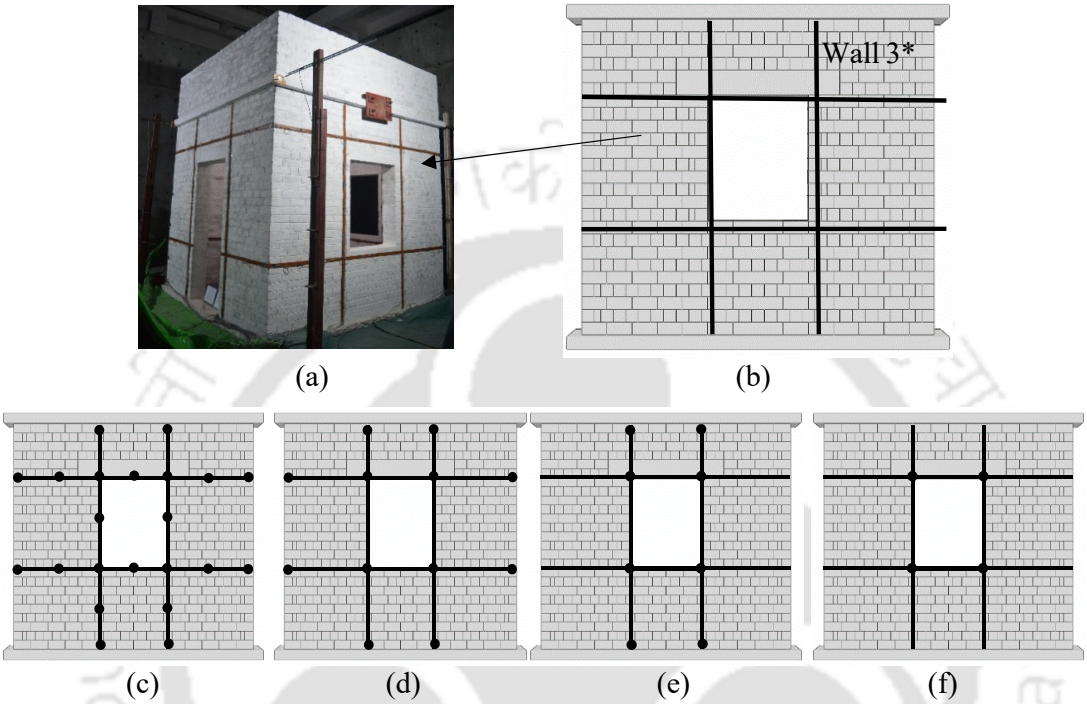

Figure 7.13. Reduced nodal connectivity between steel bands and masonry elements: (a) strengthened URM building, (b) simulation of Wall 3*, (c) simulation type 1, (d) simulation type 2, (e) simulation type 3, and (f) simulation type 4.

In real building, the steel flats were mounted on the surface of the walls on both inside and outside face. However, due to modeling difficulties, initially the FE model consisted of steel flats mounted only on the outer face of masonry with twice the area of the steel flats. With this assumption, the numerical analyses were carried out considering the four types of simulation techniques. It was observed that the lateral strength obtained from simulation type 4 matched quite well with the experimentally obtained strength (see Figure 7.10).

The strengthened URM model considering the nodal connectivity of type 4 was further analyzed to study the influence of cross-sectional area of steel flats over the lateral strength of the URM building. The numerical simulation was performed on the strengthened URM building model by varying the cross-sectional area of the steel flats based on the sizes of the steel flats available in the market. Most commonly available sizes

of steel flats have cross-sectional area lying between 150 mm^2 to 480 mm^2, and the same were used in the numerical analyses of the strengthened URM building.

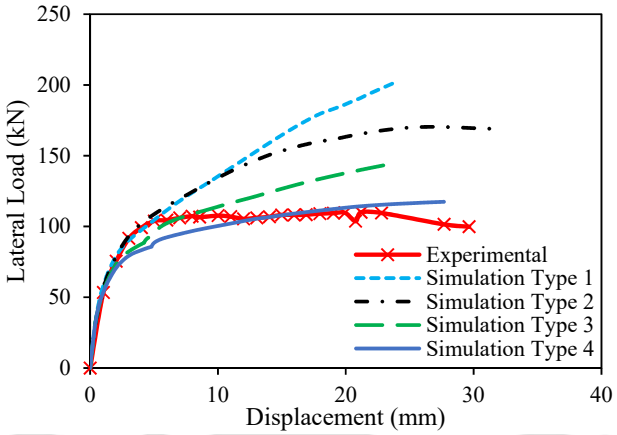

Figure 7.14. Capacity curve comparison of various reduced nodal connectivity schemes.

The simulation results displayed a small increase in the lateral strength of the building with an increase in the cross-sectional area of the steel flats. However, the increase became less significant at higher cross-sectional areas of the steel flats. This is due to the fact that the low tensile strength masonry resulted in masonry damage much earlier than the yielding of the steel flats. Therefore, analyses result in almost constant lateral strength when steel flats with large cross-sectional area were used for strengthening. Similar observation was also made experimentally (Chapter 5) when the masonry suffered significant damages prior to the failure of a steel band. Numerical results showed that overall only 10% increase in the lateral load carrying capacity of the building was observed when the cross-sectional area was increased 3 times from 150 mm^2 to 480 mm^2 (Figure 7.11).

Using the data obtained from the numerical simulation, an empirical equation was developed by curve fitting to relate the lateral strength of the strengthened building with the cross-sectional area of the steel flats used for strengthening (Eq. 7.2).

$$\alpha_L = 0.425A^{0.0554} \tag{7.2}$$

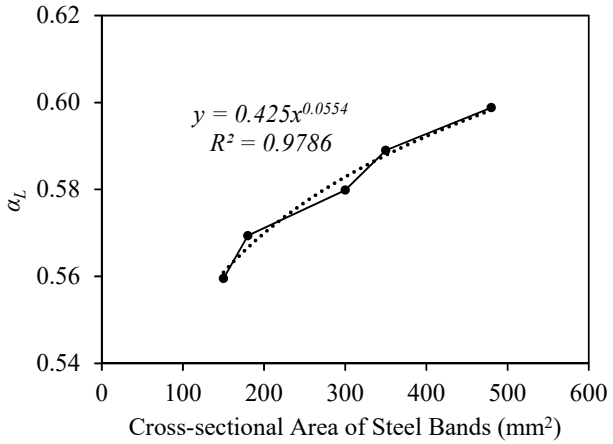

Figure 7.15. Capacity curves obtained for different cross-sectional areas of steel band.

7.4. SUMMARY

The present work is an attempt towards developing an effective numerical simulation modeling method for unreinforced masonry buildings using results of an exhaustive experimental study involving testing of full-scale shear URM walls and a full-scale URM building. Numerical simulation of all the tested specimens was carried out by adopting two different discretization schemes. In the first approach, masonry was considered to behave as a simple homogenous isotropic material exhibiting separate damage in tension and compression. This approach was used quite often because the predictions of the lateral load carrying capacity were accurate. In the present study too, this simulation technique was found to satisfactorily predict the lateral load carrying capacity of all the specimens. However, there were some reservations on accuracy of this commonly used discretization model in predicting the damaged pattern of masonry buildings. The numerically observed damage pattern was found to be significantly different from the experimental observations in most of the specimens.

Therefore, in the present study a new homogenized discretization model was proposed that relies on discretization of the individual walls and the whole building by means of elastic eight noded elements and homogenized interfaces. This proposed homogenized simulation model was found to predict the global behavior (the nonlinear capacity curves) for all the specimens with high accuracy. Moreover, the proposed model was also able to predict the damage patterns in various specimens satisfactorily, though there were some differences when compared with the experimentally observed damage patterns due to possible presence of weaker course of masonry in the test specimens. The proposed homogenized simulation technique was used for further numerical simulation by

varying various building paramaters, like aspect ratio, wall thickness and tensile strength of masonry. Regression analysis of the numerical results was carried out to develop an emperical equation to estimate the lateral strength of the building as a function of aspect ratio, wall thickness and tensile strength. Further numerical simulations were carrried out over a URM building strengthened with horizontal and vertical surface-mounted steel flats by varying the cross-sectional area of the steel flats. An insignificant increase of only 10% in lateral strength of the building was observed when the cross-sectional area of the steel bands was increased by about 3 times. Therefore, it is not recommended to provide higher cross-sectional areas of the steel bands.

Chapter 8
SUMMARY AND CONCLUSION

Contents

8.1. Overview 155
8.2. Summary 156
8.3. Conclusions 161
8.4. Recommendation for Future Work 163

8.1. OVERVIEW

Past earthquakes worldwide (in China, India, Indonesia, Italy, Iran, Nepal, New Zealand, etc.) have shown unreinforced masonry (URM) buildings to be one of the most affected structures among the building stocks. Seismic assessment of these buildings has been carried out in the past based on common features like architectural aspects, building configuration, structural details, load resisting systems, floor and roofing system, foundation and site conditions, etc., and it has been reported that these buildings can be classified to have medium to high seismic vulnerability. One of the primary reasons for such high seismic vulnerability of such buildings is the low tensile strength of masonry. Despite this, people still prefer to construct URM buildings in many parts of the world because of easier construction process and locally available construction materials that make these buildings quite inexpensive compared to some other building typologies.

Although construction of URM buildings is quite popular in many developing countries like India, the design codes concerning the masonry structures have not been revised for a very long time due to limited resources and unavailability of significant data. The experimental studies for estimation of lateral load carrying capacity of full-scale URM walls and buildings are feasible only for limited cases due to the requirement of large

laboratory setup and associated costs. In addition, the suitability of using the updated codes of various developed nations in other countries is required to be studied due to large variation in material properties and construction practices. It is not prudent to use the existing analytical and numerical assessment methods for assessment of URM walls and buildings without proper validation. It is important to develop simple methods for seismic assessment of buildings constructed with significantly weaker masonry in order to quickly assess the seismic vulnerability of such building stock in a region for seismic risk reduction. Along with the development of suitable assessment method, a study on development of a cost-effective strengthening schemes for URM building is equally essential. Earthquake resistant design of these buildings, their seismic assessment, and development of strengthening schemes require effective numerical simulation techniques that can predict their lateral load response and failure modes with sufficient accuracy. In order to achieve the above-mentioned objectives, a detailed experimental, numerical, and analytical study has been carried out in the present work on URM walls and buildings. Some of the important results and conclusions of the present study are discussed in this chapter. Some recommendations for future results are also provided.

8.2. SUMMARY

The present study can be broadly summarized into five main parts, which have been discussed elaborately in the previous chapters of the thesis: (i) preliminary numerical investigation of URM buildings; (ii) material characterization and experimental evaluation of URM walls; (iii) experimental evaluation of a strengthening scheme for URM buildings; (iv) numerical and analytical study for estimation of lateral strength of URM buildings; and (v) development of homogenized discretization method for numerical simulation of URM buildings.

8.2.1. Preliminary Numerical Investigation of URM buildings

The primary objective of this part of the study was to ascertain the suitability of various existing numerical approaches for lateral load analysis of URM buildings by validating the results with a past experimental study. Further the validated numerical models were used to study the effectiveness of a strengthening scheme in improving the lateral load behavior of URM buildings. Nonlinear pushover analyses were carried out on simulated models of a single storey, single room URM building using three FE commercial codes, namely, Strand7, Abaqus, and SAP2000. The nonlinear analyses using Strand7 were carried out by

simplifying the failure of the masonry material using isotropic Mohr-Coulomb failure criterion. The numerical simulation using Abaqus was carried out considering the material softening behavior with the adoption of Concrete Damage Plasticity (CDP) model. And, the same was performed using SAP2000 by adopting the "Equivalent Frame" approach where the frames and beams were assigned with elasto-plastic bending/shear concentrated hinges with limited deformation capacity and rigid links in the overlapping regions. Though the results obtained using the three numerical approaches matched quite well with the experimental results, especially the lateral strength and the damage region, there were certain limitations associated with all the approaches. For instance, the equivalent frame method could not predict the damaged area and progressive failure pattern. On the other hand, the numerical approaches of Strand7 and Abaqus showed good similarity with the damage observed experimentally. But the damage predicted by the numerical approaches were in the form of contours, whereas the damage in reality were in the form of cracks mostly between the mortar interface of the masonry units.

Further numerical study was carried out by strengthening the same numerical model by means of three different strengthening schemes using continuous steel bands mounted on wall surfaces. A sensitivity analysis was also carried out to study the influence of the thickness, width, and cross-sectional area of the steel flats on the effectiveness of the strengthening scheme. It was observed that the surface-mounted steel bands can be very effectively used as a suitable and cost-effective strengthening scheme for URM buildings. Steel flats with an increased thickness generally resulted in a slightly higher capacity than those with increased width (keeping cross-sectional area of the bands same). Higher values of the cross-sectional area of the bands did not contribute much to an increase in the lateral strength of the URM building. As expected, number of openings and their placement was found to have a large influence on the lateral strength of the building. Therefore, a critical combination of the walls with different openings was considered in a URM building for further experimental study.

8.2.2. Material Characterization and Experimental Evaluation of URM Walls

In this part of the study, the mechanical properties of the masonry used to construct the URM walls and buildings were determined. At least seven sets of specimens consisting of brick units, mortar cubes, masonry triplets, masonry prisms, and Z masonry specimens were used to conduct different tests. The average compressive strength of brick units and

mortars was about 21.2 MPa and 6.6 MPa, respectively. The triplet and tensile bond test resulted an average value of 0.17 MPa and 0.076 MPa, respectively. The average prism compressive strength and its modulus of elasticity obtained were 3.4 MPa and 1732 MPa, respectively.

The seismic vulnerability of a URM building can be determined by first evaluating the lateral load-carrying capacity of the individual walls constituting the building. This was achieved in the present study by conducting pseudo-static in-plane cyclic tests on three full-scale URM walls with different opening configurations (door, window). The URM wall with a central door exhibited the least lateral strength of about 19 kN. The URM wall with a central window resulted in nearly similar lateral strength in comparison to a solid wall (28 kN), but with significantly lower energy dissipation capacity. The tests also helped in understanding the various failure modes of the wall specimens. The sliding shear failure seemed to be the major governing failure criteria in the case of Wall 1 (solid wall) and Wall 3 (wall with central window) since the failure occurred at the base of the walls by formation of longitudinal cracks. Whereas, flexural failure was the governing failure criteria in the case of Wall 2 (wall with central door). The test results were further used for fine-tuning the numerical models already developed in the preceding chapter, and also in the development of the analytical methods for prediction of the lateral strength.

8.2.3. Experimental Evaluation of a Strengthening Scheme for URM Buildings

Numerous past studies have revealed that steel members can be economically and conveniently used in evolving strengthening strategies to improve the seismic performance of the URM buildings. The primary objective of this part of the study was to experimentally evaluate a novel strengthening scheme for URM buildings. The scheme used surface-mounted steel bands over the URM walls of the buildings at different levels. Three full-scale URM buildings were considered for pseudo-static, slow cyclic, lateral load testing. Among the three buildings, one was unstrengthened; while the other two buildings were strengthened using surface-mounted steel bands. One of the two strengthened URM building (Model 1) was strengthened using surface-mounted steel bands (40 mm × 5 mm steel flat) at lintel level on both faces of all the walls along the whole length of the building. The other URM building (Model 2) was strengthened using the horizontal steel bands mounted on the surface of the walls at lintel as well as sill level in all the walls on both the faces throughout the length of the building, and additionally, vertical steel bands were

provided adjacent to the openings. Size of the steel bands were kept same in the entire experimental study: 40 mm × 5 mm. Door and window openings were also considered in the walls of the building, in order to understand if there is an advantage of providing the steel bands in reducing the commonly observed damage around the openings.

It was observed that providing a single steel band at the lintel level on both faces of all the walls of the URM building (Model 1) did not result in any significant increase in its lateral load-carrying capacity. However, a remarkable improvement was observed in the deformation capacity of the strengthened specimen. On the other hand, the test results of Model 2 showed that the lateral load-carrying capacity increased by about 38%. The hysteresis response, lateral deformability, and ductility of Model 2 was also significantly better than the other specimens. It was observed that the combined in-plane capacity of the individual URM walls tested previously constitute about 55% of the lateral strength of the URM building. Therefore, it was evident that the remaining 45% of the lateral load carrying capacity of the building was constituted by the box action effect and out-of-plane strength of the orthogonal walls.

8.2.4. Numerical and Analytical Study for Estimation of Lateral Strength of URM Buildings

Based on the numerical simulation strategies developed in the previous part of the present study, numerical assessment of the experimentally tested URM walls and buildings was carried out in this part of the study using Strand7 and Abaqus. The results of the experimental study were also utilized in an analytical study considering several structural parameters. The numerical and analytical studies were essentially carried out to develop simple models for quick estimation of the lateral strength of the strengthened buildings. Both Strand7 and Abaqus provided strength estimation with reasonable accuracy for all the three URM walls and the buildings. However, due to the assumption of isotropic behavior of masonry, the damage and failure pattern obtained numerically differed with some of the experimental observations. Clearly, a need was felt of developing a suitable numerical simulation strategy for URM buildings. It should be simple enough to simulate entire URM buildings quickly, and capable enough of predicting the progressive damage pattern and failure modes in such buildings.

The analytical methods recommended in various codes and literature were used to estimate the lateral strength of URM walls along the in-plane as well as the out-of-plane

(OOP) directions. Among all the methods for in-plane strength estimation, the method recommended in the Indian code (BIS,1987a) was found to give very low strength when compared with the experimental results. Whereas, the lateral strength estimated using the Australian code (AS-3700, 2018) was very high for all the walls. The methods recommended by Magenes and Calvi (1997) and ASCE 41-13 (2014) estimated the in-plane strength of the solid wall with higher accuracy. However, the estimation error was quite high for walls with openings. The OOP strength of the walls estimated using IS 1905 (BIS,1897a) and AS-3700 (2018) was found to be about three times higher than that estimated by Griffith and Vaculik (2007). Therefore, the inconsistency of the available analytical methods in estimation of the lateral strength of URM walls was highlighted in the present study. It was also demonstrated that some of the analytical methods recommended in codes and literature for determining lateral strength of individual URM walls along the in-plane and out-of-plane directions can be methodically combined to obtain the lateral strength of URM building with acceptable accuracy. The method worked equally well even when door and window openings were present in the walls of the building.

8.2.5. Development of Homogenized Discretization Method for Numerical Simulation of URM Building

In the final part of the present study, a novel homogenized discretization model was developed for reducing the limitations associated with the existing numerical simulation techniques. The proposed model consisted of multiple sets of the elementary units, subdivided along its thickness in several layers. Each unit consisted of a set of discretized elastic cells, which were interfaced by a set of smaller units bearing the plastic damage properties. The proposed method was validated by comparing the results with that obtained in the experimental and numerical study on full-scale URM walls and building specimens. The results in the form of global pushover curves and crack pattern evolution obtained using the *Proposed Discretization Model* (PDM) were compared with the experimental results. The pushover analyses of the building model simulated using the proposed discretization model as well as the commonly used discretization model delivered capacity curves, which were in good agreement with the experimentally obtained capacity curves. However, the damage predicted using the two approaches were significantly different. The damage contour of the commonly used discretization model was widely spread and did not match well with the experimentally obtained damaged pattern. On the other hand, the

damage pattern obtained from the proposed discretization model matched well with that obtained experimentally.

Adopting the proposed discretization model, numerous numerical simulations were then carried out by varying some important structural parameters of the building like the wall thickness, the aspect ratio (*l/h*) of the walls, and the tensile strength of the masonry. In addition, the numerical simulation of the strengthened specimen carried out by varying the cross-sectional area of the steel flats showed only 10% increase in the lateral strength of the building when the cross-sectional area of the steel bands was increased by about 3 times. The lateral load values obtained from numerical simulation considering the different combinations of the parameters were used to carry out unconstrained multiple linear regression analysis for development of an empirical equation to estimate the lateral strength of the URM buildings.

8.3. CONCLUSIONS

The following major conclusions can be drawn from the present exhaustive study comprising of experimental, numerical, and analytical work:

- The pseudo-static, in-plane cyclic tests of full-scale URM walls as well as full-scale URM buildings once again proved that the presence of openings in walls played a significant role in the lateral load behavior of such buildings.
- The tests revealed that the shear and tensile failure of masonry were the primary reasons for the failure of the URM walls and buildings.
- The test results showed that the combined in-plane strength of the individual walls constitute about 55% of the overall lateral strength of the URM building. Clearly, the combined box action effect due to presence of rigid diaphragm and the out-of-plane strength of the orthogonal walls constitute the remaining 45% of the building strength.
- Surface-mounted steel bands can be effectively used for seismic strengthening of URM buildings. The best performance was shown by the strengthening scheme (Model 2) in which steel bands were mounted on both faces of all the walls of the building horizontally at lintel and sill level, and vertically around the openings.
- The high strain values recorded by the strain gauges installed on the steel bands signify that the steel bands contribute significantly to the lateral load resistance of the building by tying the walls together, and delay the formation of cracks and failure in the walls of the building.

- In case of Model 2, the lateral strength of the URM building was found to increase by about 38% and lateral deformability by about 50%. Similarly, tremendous enhancement of about 4.5 times was observed in the energy dissipation capacity of the strengthened building.
- Strengthening of the URM buildings using surface-mounted steel bands also reduced the torsional behavior of the building significantly. The out-of-plane displacement recorded at the top of the specimens reduced to about 50% after strengthening.
- Three commonly used numerical approaches (using Abaqus, Strand7, and SAP2000) can be conveniently used for predicting the lateral strength of URM buildings.
- Numerical results showed only a marginal increase in the lateral load carrying capacity of the building when the cross-sectional area of the steel bands was increased 3 times from 150 mm^2 to 480 mm^2. Therefore, it is not necessary to use thicker or wider steel bands for increasing the lateral strength of URM buildings. Using nominal steel bands of size 40 mm × 5 mm was proved to be quite effective in improving the lateral load behavior of URM buildings.
- The equivalent frame approach of simulating URM buildings using SAP2000 failed to predict the damage area and the progressive failure pattern. Though the numerical simulations using Strand7 and Abaqus predicted the damage area with better accuracy, the damage was predicted in the form of contours covering large areas on the walls, far from the experimental observations.
- The numerical simulations carried out using the proposed homogenized discretization method were found to be quite accurate in not only predicting the lateral strength and pushover curves of the URM building, but also in tracing the crack pattern evolution in the walls of the URM building.
- The analytical methods recommended in codes and literature for determining lateral strengths of individual URM walls along the in-plane and out-of-plane direction can be methodically combined to obtain the lateral strength of URM building with acceptable accuracy.
- An empirical model was developed for estimation of the lateral strength of the strengthened URM buildings by carrying out regression analyses of the results obtained in a parametric numerical study. The developed empirical equation can be conveniently used for assessing the possible increase in the lateral strength of the URM buildings due to the suggested strengthening scheme.

- The developed strengthening scheme using external and internal surface-mounted steel bands requires locally available equipment, materials, and manpower; therefore, it is extremely cost-effective. It is easily implementable without taking much time and without disturbing the movement of people inside or outside the building. The increase in mass or lateral stiffness of the building due to strengthening is negligible; hence, the strengthened building does not attract additional lateral loads during earthquakes. The steel bands are easily replaceable in case of such a demand in future. These advantages make the proposed strengthening scheme very efficient and sustainable, and likely to be easily adoptable by the people living in seismically vulnerable URM buildings.

8.4. RECOMMENDATION FOR FUTURE WORK

The results of the experimental, numerical, and analytical studies carried out in the present research work are based on a limited data. Therefore, care should be taken to validate the developed strengthening schemes, numerical models, and analytical techniques before using in a different scenario. Some recommendations for future work are listed below:

- Experiments can be conducted on different configurations of URM walls and buildings to gain more confidence on the results and to develop generalized design equations for the strengthening scheme.
- Influence of some important parameters, for example, masonry properties, wall aspect ratio, level of axial compression, boundary conditions, etc., on the results presented in the thesis can be evaluated by carrying out additional tests as well as numerical simulations.
- Effectiveness of the developed strengthening scheme, numerical models, and analytical techniques is required to be assessed for bigger buildings having multiple bays and floors. This can be done by a systematic experimental as well as numerical studies.

REFERENCES

ABAQUS (2010). "ABAQUS: theory manual." *version 6.10, 2010*.

Acito, M., Bocciarelli, M., Chesi, C., and Milani, G. (2014). "Collapse of the clock tower in Finale Emilia after the May 2012 Emilia Romagna earthquake sequence: Numerical insight." *Engineering Structures*, 72, 70–91.

Acito, M., Chesi, C., Milani, G., and Torri, S. (2016). "Collapse analysis of the Clock and Fortified towers of Finale Emilia, Italy, after the 2012 Emilia Romagna seismic sequence: Lesson learned and reconstruction hypotheses." *Construction and Building Materials*, Elsevier Ltd, 115, 193–213.

Aldemir, A., Binici, B., Canbay, E., and Yakut, A. (2015). "Lateral load testing of an existing two story masonry building up to near collapse." *Bulletin of Earthquake Engineering*, Springer Netherlands.

Allen, C., Masia, M. J., Page, A. W., Griffith, M. C., and Derakhshan, H. (2015). "Cyclic in-plane shear testing of unreinforced masonry walls with openings." *Proceedings of the Tenth Pacific Conference on Earthquake Engineering Building an Earthquake-Resilient Pacific*, 1401–1408.

Ansary, A. (2003). "Housing Report Unreinforced Brick Masonry Buildings with GI Sheet." *World Housing Encyclopedia*, EERI(IAEE).

AS-3700, (AustralianStandards). (2018). *Australian standards for masonry structures*. Standards Australia International, Sydney, NSW 2001, Australia.

ASCE/SEI 41-13. (2014). *Seismic Evaluation and Retrofit of Existing Buildings*. Structural Engineering Institute, American Society of Civil Engineers, United States of America.

ASTM. (2012). "Standard test method for compressive strength of masonry prisms." *ASTM C1314-12*, ASTM International, USA.

ASTM. (2013a). "Standard test methods for sampling and testing brick and structural clay tile." *ASTM C67-13*, ASTM International, USA.

ASTM. (2013b). "Standard test method for compressive strength of hydraulic cement mortars using 2-in or 50-mm cube specimens." *ASTM C109/C109M-13*, ASTM International, USA.

Barbieri, G., Biolzi, L., Bocciarelli, M., Fregonese, L., and Frigeri, A. (2013). "Assessing the seismic vulnerability of a historical building." *Engineering Structures*, 57, 523–535.

Bayraktar, A., Sahin, A., Özcan, M., and Yildirim, F. (2010). "Numerical damage assessment of Haghia Sophia bell tower by nonlinear FE modeling." *Applied Mathematical Modelling*, 34, 92–121.

Benedetti, D., Carydis, P., and Pezzoli, P. (1998). "Shake Table Tests on 24 Simple Masonry Buildings." *Earthquake Engineering and Structural Dynamics*, 27, 67–90.

Bertolesi, E., Milani, G., and Casolo, S. (2018). "Homogenization towards a mechanistic Rigid Body and Spring Model (HRBSM) for the non-linear dynamic analysis of 3D masonry structures." *Meccanica*, 53(7), 1819–1855.

Bertolesi, E., Milani, G., and Lourenço, P. B. (2016). "Implementation and validation of a total displacement non-linear homogenization approach for in-plane loaded masonry." *Computers and Structures*, 176, 13–33.

Borri, A., Castori, G., and Grazini, A. (2009). "Retrofitting of Masonry Building with Reinforced Masonry Ring-beam." *Construction and Building Materials*, 23(5), 1982–1901.

Branco, M., and Guerreiro, L. M. (2011). "Seismic Rehabilitation of Historical Masonry Building." *Engineering Structures*, 33(5), 1626–1634.

Brandonisio, G., Lucibello, G., Mele, A., and De Luca, A. (2013). "Damage and performance evaluation of masonry churches in the 2009 L'Aquila earthquake." *Engineering Failure Analysis*, 34, 693–714.

Brencich, A., Gambarotta, L., and Lagomarsino, S. (1998). "A macroelement approach to the three-dimensional seismic analysis of masonry buildings." *11th Europe an Conferen ce on Ear thqua ke Engineering*, 90(JANUARY), 1–10.

BS EN. (2002). "Methods of test for masonry - Part 3: Determination of initial shear strength." *BS EN 1052-3*, (European standard), European Committee for standardization.

Bureau of Indian Standards (BIS). (1993a). "Earthquake resistant desigh and construction of buildings — Code of practice." *IS 4326*, New Delhi, India.

Bureau of Indian Standards (BIS). (1993b). "Improving Earthquake Resistance of Low Strength Masonry Buildings-Guidelines." *IS 13828*, New Delhi, India.

Bureau of Indian Standards (BIS). (1995). "Indian standard code of practice for preparation and use of masonry mortars." *IS 2250*, New Delhi, India.

Bureau of Indian Standards (BIS). (2000). "Code of Practice for Plain and Reinforced Concrete." *IS 456*, (New Delhi, India).

Bureau of Indian Standards (BIS). (1992). "Indian standard methods of test of burn clay building bricks—Part 1: Determination of compressive strength." *IS 3495*, New Delhi, India.

Bureau of Indian Standards (BIS). (1987a). "Code of Practice for Structural use of Unreinforced Masonry." *IS 1905*, New Delhi, India.

Bureau of Indian Standards (BIS). (1987b). "Code of Practice for Design Loads(Other than Earthquake) for Buildings and Structures." *IS 875 (Part 1)*, (New Delhi, India).

Bureau of Indian Standards (BIS). (2009). "Repair and Seismic Strengthening of Buildings-Guidelines." *IS 13935*, New Delhi, India.

Bureau of Indian Standards (BIS). (2016). "Crtiteria for Earthquake Resistant Design of Structures." *IS 1893*, Part 1, New Delhi, India.

Calderini, C., Cattari, S., and Lagomarsino, S. (2009). "In-plane strength of unreinforced masonry piers." *Earthquake Engineering & Structural Dynamics*, 38, 243–267.

Cardoso, R., Lopes, M., and Bento, R. (2005). "Seismic evaluation of old masonry buildings. Part I: Method description and application to a case-study." *Engineering Structures*, 27(14), 2024–2035.

Casolo S, Milani G. (2010). "A simplified homogenization-discrete element model for the non-linear static analysis of masonry walls out-of-plane loaded." *Engineering Structures*, 32(8), 2352-2366.

Cecchi A, Milani G. (2008) "A kinematic FE limit analysis model for thick English bond masonry walls." *International Journal of Solids and Structures*, 45(5), 1302-1331.

Choudhury, T., Milani, G., and Kaushik, H. B. (2015). "Comprehensive numerical approaches for the design and safety assessment of masonry buildings retrofitted with steel bands in developing countries: The case of India." *Construction and Building Materials*, Elsevier Ltd, 85, 227–246.

Clementi, F., Gazzani, V., Poiani, M., Mezzapelle, P. A., and Lenci, S. (2018). "Seismic Assessment of a Monumental Building through Nonlinear Analyses of a 3D Solid Model." *Journal of Earthquake Engineering*, 22(suo1), 35–61.

Costley, A. C., and Abrams, D. P. (1996). "Dynamic Response of Unreinforced Masonry Buildings with Flexible Diaphragms." *Technical Report NCEER-96-0001*, University of Illinois at Urbana-Champaign, Illinois, USA.

Cundari, G., and Milani, G. (2013). "Homogenized and Heterogeneous Limit Analysis

Model for Pushover Analysis of Ancient Masonry Walls with Irregular Texture." *International Journal of Architectural Heritage*, 7, 303–338.

D'Altri, A. M., de Miranda, S., Castellazzi, G., and Sarhosis, V. (2018). "A 3D detailed micro-model for the in-plane and out-of-plane numerical analysis of masonry panels." *Computers and Structures*, Elsevier Ltd, 206, 18–30.

Derakhshan, H., Lucas, W., Visintin, P., and Griffith, M. C. (2018). "Out-of-plane Strength of Existing Two-way Spanning Solid and Cavity Unreinforced Masonry Walls." *Structures*, 13(October 2017), 88–101.

Dolatshahi, K. M., Nikoukalam, M. T., and Beyer, K. (2018). "Numerical study on factors that influence the in-plane drift capacity of unreinforced masonry walls." *Earthquake Engineering & Structural Dynamics*, 47(6), 1440–1459.

Drysdale, R. G., Hamid, A. A., and Baker, L. R. (1999). *Masonry structures: behavior and design*. The Masonry Society (TMS), Boulder, Colorado, USA.

El-Borgi, S., Smaoui, H., Casciati, F., Jerbi, K., and Kanoun, F. (2005). "Seismic evaluation and innovative retrofit of a historical building in Tunisia." *Structural Control and Health Monitoring*, 12(2), 179–195.

Elgawady, M. A., Lestuzzi, P., and Badoux, M. A. (2004). "Review of conventional seismic retrofitting techniques for URM." *13th International brick and block masonry conference*, Amsterdam, July 4-7.

EN 1996-1-1, B. (2005). *Euro code 6: Design of masonry structures-Part 1-1: General rules for reinforced and unreinforced masonry structures*. European Committee for Standardization.

EN 1998-3. (2005). *Euro code 8: Design of Structures for Earthqauke Resistance- Part 3: Assesment and Retrofitting of buildings*. European Committee for Standardization, B-1050 Brussels.

FEMA 547. (2006). *Techniques for the Seismic Rehabilitation of Existing Buildings*. *Fema 547*, (Federal Emergency Management Agency, ed.), U.S Department of Homeland Security.

Gattesco, N., Macorini, L., and Dudine, A. (2015). "Experimental Response of Brick-Masonry Spandrels under In-Plane Cyclic Loading." *Journal of Structural Engineering*, 142(2), 1–14.

Giovanni, R., Amadio, C., and Macorini, L. (2016). "A macro-model with nonlinear springs for seismic analysis of URM buildings." *Earthquake Engineering & Structural Dynamics*, 45, 2261–2281.

Graziotti, F., Tomassetti, U., Penna, A., and Magenes, G. (2016). "Out-of-plane shaking

table tests on URM single leaf and cavity walls." *Engineering Structures*, 125, 455–470.

Graziotti, F., Tomassetti, U., Sharma, S., Grottoli, L., and Magenes, G. (2019). "Experimental response of URM single leaf and cavity walls in out-of-plane two-way bending generated by seismic excitation." *Construction and Building Materials*, 195, 650–670.

Griffith, M. C., Lam, N. T. K., Wilson, J. L., and Doherty, K. (2004). "Experimental Investigation of Unreinforced Brick Masonry Walls in Flexure." *Journal of Structural Engineering*, 130(3), 423–432.

Griffith, M., and Vaculik, J. (2007). "Out-of-plane flexural strength of unreinforced clay brick masonry walls." *TMS Journal*, 25(1).

Hamid, A. A., Dakhakhni, W. W., Hakam, Z. H. R., and Elgaaly, M. (2005). "The behavior of composite unreinforced masonry–fiber-reinforced polymer wall assemblages un-der in-plane loading." *Journal of Composites for Construction*, 9(1), 73–83.

Hare, J. (2013). "Rebuilding the Garden City (Impacts to the Canterbury Built Environment)." *Christchurch Earthquakes Workshop*, Earthquake.

Hendry, A., Sinha, B., and Davies, S. (1997). *Design of masonry Structures*. E & FN Spon., Taylor and Francis, CRC Press.

Ip, K., Dizhur, D., Sorrentino, L., Masia, M. J., and Griffith, M.C. Ingham, J. M. (2018). "Critical Review of Numerical Modelling Techniques for Seismic Response of Complex URM Buildings." *10th Australasian Masonry Conference, 11 - 14 February, Sydney, Australia*, 35.

Jain, S. K., Murty, C. V. R., Dayal, U., Arlekar, J. N., and Chaubey, S. K. (2002). *Learning from Earthquakes :: A field report on structural and geotechnical damages sustained during the 26 January 2001 M7.9 Bhuj Earthquake in Western India*. Earthquake Engineering Research Institute, USA.

Javed, M., Magenes, G., Alam, B., Khan, A. N., Ali, Q., and Syed, A. M. (2015). "Experimental Seismic Performance Evaluation of Unreinforced Brick Masonry Shear Walls." *Earthquake Spectra*, 31(1), 215–246.

Joshi, V., and Kaushik, H. B. (2017). "Historic earthquake resilient structures in Nepal and other Himalayan regions and their seismic res-toration." *Earthquake Spectra*, 33(S1), S299–S319.

Kadam, S. B., Singh, Y., and Li, B. (2014). "Strengthening of unreinforced masonry using welded wire mesh and micro-concrete – behavior un-der in-plane action." *Construction and Building Materials*, 54, 247–257.

Kadam, S. B., Singh, Y., and Li, B. (2015). "Out-of-plane behaviour of unreinforced masonry strengthened using ferrocement overlay." *Materials and Structures*, 48, 3187–3203.

Kadam, S. B., Singh, Y., and Li, B. (2018). "Shock Table Test on Masonry Buildings Strengthened using Welded Wire Mesh and Micro Concrete." *10th Australasian Masonry Conference, 11 - 14 February, Sydney, Australia*.

Kallioras, S., Guerrini, G., Tomassetti, U., Marchesi, B., Penna, A., Graziotti, F., and Magenes, G. (2018). "Experimental seismic performance of a full-scale unreinforced clay-masonry building with flexible timber diaphragms." *Engineering Structures*, Elsevier, 161, 231–249.

Kappos, A. J., Penelis, G. G., and Drakopoulos, C. G. (2002). "Evaluation of simplified models for lateral load analysis of unreinforced masonry buildings." *Journal of Structural Engineering*, 128(July), 890.

Kaushik, H. B., and Dasgupta, K. (2014). "Assessment of Seismic Vulnerability of Structures in Sikkim , India , Based on Damage Observation during Two Recent Earthquakes." *Journal of Performance of Constructed Facilities*, 27(6), 697–720.

Kaushik, H. B., Dasgupta, K., Sahoo, D. R., and Kharel, G. (2006). "Performance of structures during the Sikkim earthquake of 14 February 2006." *Current Science*, 91(4), 449–455.

Kaushik, H. B., and Jain, S. K. (2007). "Impact of great December 26, 2004 Sumatra earthquake and tsunami on structures in Port Blair." *Journal of Performance of Constructed Facilities*, 21(2), 128–142.

Kaushik, H. B., Rai, D. C., and Jain, S. K. (2007). "Stress-Strain Characteristics of Clay Brick Masonry under Uniaxial Compression." *Journal of Materials in Civil Engineering*, 19(9), 728–739.

Khan, A. A., and Khalid, M. (2002). "Housing Report Unreinforced Brick Masonry Walls In Mud Mortar With Flat Timber Roof." *World Housing Encyclopedia*, EERI(IAEE).

Konthesingha, K. M. C., Masia, M. J., Petersen, R. B., and Page, A. W. (2015). "Experimental Evaluation of Static Cyclic In-Plane Shear Behavior of Unreinforced Masonry Walls Strengthened with NSM FRP Strips." *Journal of Composites for Construction*, 13(3).

Kumar, A. (2002). "Housing Report Unreinforced Brick Masonry Walls In Mud Mortar With Flat Timber Roof." *World Housing Encyclopedia*, EERI(IAEE).

Lagomarsino, S., Abbas, N., Calderini, C., Cattari, S., Rossi, M., Ginanni Corradini, R., Marghella, G., Mattolin, F., and Piovanello, V. (2011). "Classification of cultural

heritage assets and seismic damage variables for the identification of performance levels." *WIT Transactions on the Built Environment*, 118, 697–708.

Lawrence, S., and Marshall, R. (2000). "Virtual Work Design Method for Masonry Panels under Lateral Load." *12th International Brick/Block Masonry Conference*, 1063–1073.

Lawrence, S., and Page, A. W. (2013). *Manual 4: Design of clay masonry for wind and earthquake*, ThinkBrick Technical Manuals. Artarmon, NSW 1570 Australia.

Lizundia, B., Shrestha, S. N., Bevington, J., Davidson, R., Jaiswal, K., Jimee, G. K., Kaushik, H. B., Kumar, H., Kupec, J., Mitrani-Reiser, J., Poland, C., Shrestha, S., Welton-Mitchell, C., Tremayne, H., and Ortiz, M. (2016). *M7.8 Gorkha, Nepal earthquake on April 25, 2015, and its aftershocks*. EERI Earthquake Reconnaissance Team Report, Earthquake Engineering Research Institute, Oakland, California.

López-Patiño, G; Adam, J, M; Gimeno P, V; Milani, G (2017), Causes of damage to industrial brick masonry chimneys. *Engineering Failure Analysis,* (74), 188-201

Lubliner, J., Oliver, J., Oller, S., and Oñate, E. (1989). "A plastic-damage model for concrete." *International Journal of Solids and Structures*, 25(3), 299–326.

Lucchesi, M., Padovani, C., Pasquinelli, G., and Zani, N. (1997). "On the Collapse of Masonry Arches." *Meccanica*, 32(4), 327–346.

Maccarini, H., Vasconcelos, G., Rodrigues, H., Ortega, J., and Lourenço, P. B. (2018). "Out-of-plane behavior of stone masonry walls: Experimental and numerical analysis." *Construction and Building Materials*, Elsevier Ltd, 179, 430–452.

Magenes, G. (2000). "A Method for Pushover Analysis in Seismic assessment of Masonry Buildings." *Proceedings of the 12th World Conference on Earthquake Engineering*, Auckland, New Zealand.

Magenes, G., and Calvi, G. M. (1997). "In-plane seismic response of brick masonry walls." *Earthquake Engineering & Structural Dynamics*, 26(11), 1091–1112.

Magenes, G., and Della Fontana, A. (1998). "Simplified Non-linear Seismic Analysis of Masonry Buildings." *Proceedings No. 8 of the British Masonry Society*, (December), 190–195.

Magenes, G., Kingsley, G. R., and Calvi, G. M. (1996). "Testing of Masonry Structures for Seismic Assesment." *Earthquake Spectra*, Italy, 12(1), 145–162.

Mallarddo, V., Malvezzi, R., Milani, E., and Milani, G. (2008). "Seismic vulnerability of historical masonry buildings: a case study in Ferrara." *Engineering Structures*, 30(8), 2223–2241.

Mann, W., and Müller, H. (1980). "Failure of shear-stressed masonry—an enlarged theory,

tests and application to shear-walls." *Proceedings of the International Symposium on Load bearing Brickwork*, London, 1–13.

Marshall, O. S. J., Sweeney, S. C., and Trovillion, J. C. (2000). *Performance testing of fiber-reinforced polymer composite overlays for seismic rehabilitation of unreinforced masonry walls*. ERDC/CERL TR-00-18, Construction Engineering Research Laboratory (CERL), Engineer Research and Development Center, US Army Corps of Engineers, Champaign, IL.

Miglietta, P. C., Bentz, E. C., and Grasselli, G. (2017). "Finite/discrete element modelling of reversed cyclic tests on unreinforced masonry structures." *Engineering Structures*, Elsevier Ltd, 138, 159–169.

Milani G. (2011). "Simple homogenization model for the non-linear analysis of in-plane loaded masonry walls." *Computer Structures*, 89 (17-18),1586-1601.

Milani G. (2011). "Simple lower bound limit analysis homogenization model for in- and out-of-plane loaded masonry walls." *Construction and Building Materials*, ,25(12), 4426-4443.

Milani, G., and Bertolesi, E. (2017). "Quasi-analytical homogenization approach for the non-linear analysis of in-plane loaded masonry panels." *Construction and Building Materials*, 146, 723–743.

Milani, G., Beyer, K., and Dazio, A. (2009). "Upper bound analysis limit analysis of meso –mechanical spandrel models for the pushover analysis of 2D masonry frames." *Engineering Structures*, 7, 303–338.

Milani, G., Lourenço, P. B., and Tralli, A. (2006). "Homogenised limit analysis of masonry walls, Part I: Failure surfaces." *Computers and Structures*, 84(3–4), 166–180.

Milani, G., Lourenço, P., and Tralli, A. (2007). "3D homogenized limit analysis of masonry buildings under horizontal loads." *Engineering Structures*, 29(11), 3134–3148.

Mojsilović, N. (2011). "Strength of masonry subjected to in-plane loading: A contribution." *International Journal of Solids and Structures*, 48(6), 865–873.

Moon, F. L., Yi, T., Leon, R. T., and Kahn, L. F. (2006). "Recommendations for seismic evaluation and retrofit of low-rise URM structures." *Journal of Structural Engineering*, 132(5), 663–672.

Munjiza, A. (2005). *The Combined Finite-Discrete Element Method*. John Wiley & Sons, Ltd.

Murty, C. V. R. (2002). "IITK-BMTPC Earthquake Tip 12." *NICEE*, IIT Kanpur, India.

Murty, C. V. R., Rai, D. C., Jain, S. K., Kaushik, H. B., Mondal, G., and Dash, S. R. (2006).

"Performance of structures in the Andaman and Nicobar islands (India) during the December 2004 Great Sumatra earthquake and Indian Ocean tsunami." *Earthquake Spectra*, 22(SUPPL. 3), 321–354.

National Disaster Management Division. (2006). *Guidelines on Repair, Restoration and Retrofitting of Masonry Buildings in Earthquake Affected Areas of Jammu & Kashmir*. Ministry of Home affairs, Government of India.

Noor-E-Khuda, S., and Dhanasekar, M. (2018). "Masonry Walls under Combined In-Plane and Out-of-Plane Loadings." *Journal of Structural Engineering (United States)*, 144(2), 1–10.

NTC. (2008). *Nuove norme tecniche per le costruzioni*. Ministero delle Infrastrutture (GU n.29 04/02/2008), Rome, Italy.

NZSEE, SESOC, NZGS, MBIE, and EQC. (2017). *New Zealand Seismic Assesment Guideline*. Ministry of Business, Innovation and Employment, the Earthquake Commission, the New Zealand Society for Earthquake Engineering, the Structural Engineering Society and the New Zealand Geotechnical Society, www.EQ-Assess.org.nz, New Zealand.

Page, A. (1981a). "The Biaxial Compressive Strength of Brick Masonry." *Proceedings of the Institution of Civil Engineers*, 71(3), 893–906.

Pantò, B., Cannizzaro, F., Caddemi, S., and Caliò, I. (2016). "3D macro-element modelling approach for seismic assessment of historical masonry churches." *Advances in Engineering Software*, 97, 40–59.

Parisi, F., and Augenti, N. (2013). "Seismic capacity of irregular unreinforced masonry walls with openings." *Earthquake Engineering & Structural Dynamics*, 42, 101–121.

Pasticier, L., Amadio, C., and Fragiacomo, M. (2008). "Non-linear seismic analysis and vulnerability evaluation of a masonry building by means of the SAP2000 V.10 code." *Earthquake Engineering and Structural Dynamics*, 37, 467–485.

Pelà, L., and Benedetti, A. (2009). "Seismic assessment of masonry arch bridges." *Engineering Structures*, 31, 1777–1788.

Penner, O., and Elwood, K. J. (2016). "Out-of-plane dynamic stability of unreinforced masonry walls in one-way bending: parametric study and assessment guidelines." *Earthquake Spectra*, 32(3), 1699–1723.

Petry, S., and Beyer, K. (2015). "Cyclic Test Data of Six Unreinforced Masonry Walls with Different Boundary Conditions." *Earthquake Spectra*, 31(4), 2459–2484.

Pluijim, R., and Van Der. (1993). "Shear Behaviour of bed joints." *6th North American Masonry Conference*, A. A. Hamid and H. G. Harris, eds., Technomic Publ. Co.,

Philadelphia, Pennsylvania, US, 125–136.

Priestley, M. J. N. (1985). "Seismic behavior of unreinforced masonry walls." *Bulletin of the New Zealand Society for Earthquake Engineering,* 18(2), 191–205.

Quagliarini, E., Maracchini, G., and Clementi, F. (2017). "Uses and limits of the Equivalent Frame Model on existing unreinforced masonry buildings for assessing their seismic risk: A review." *Journal of Building Engineering*, 10, 166–182.

Rahman, A., and Ueda, T. (2016). "In-Plane Shear Performance of Masonry Walls after Strengthening by Two Different FRPs." *Journal of Composites for Construction*, 20(5).

Rai, D. C., and Murty, C. V. R. (2005). *Preliminary report on the 2005 North Kashmir Earthquake of October 8,2005*. NICEE, IIT Kanpur, India.

Rao, K. V. ., Reddy, B. V. V, and Jagadish, K. S. (1996). "Flexural bond strength of masonry using various blocks and mortars." *Materials and Structures*, 29(2), 119–124.

Razzaghi, M. S., and Ashtiany, M. . (2012). "A Preliminary Reconnaissance Report on August 11th 2012, Varzaghan-Ahar Twin Earthquakes in NW of Iran." *EERI, USA*, Iran, www.eeri.org.

Roca, P., Molins, C., and Marí, A. R. (2005). "Strength Capacity of Masonry Wall Structures by the Equivalent Frame Method." *Journal of Structural Engineering*, 131(10), 1601–1610.

Russel, A. P., and Ingham, J. M. (2010). "The influence of flanges on the in-plane seismic performance of URM walls in New Zealand buildings." *Proceedings of 2010 NZSEE Conference*, New Zealand.

Salonikios, T., Karakostas, C., Lekidis, V., & Anthoine, A. (2003). Comparative inelastic pushover analysis of masonry frames. *Engineering Structures*, 25(12), 1515–1523.

SAP2000 (2011). *SAP2000 v15 Analysis Reference Manual*. Computers and Structures Inc. (CSI), Berkeley, USA.

Sarangapani, G., Reddy, B. V. V, and Jagadish, K. S. (2002). "Structural Chracteristics of Bricks Mortars and Masonry." *Journal of Structural Engineering*, 29(2), 101–107.

Sathiparan, N., Mayorca, P., and Meguro, K. (2012). "Shake Table Tests on One-Quarter Scale Models of Masonry Houses Retrofitted with PP-Band Mesh." *Earthquake Spectra*, 28(1), 277–299.

Scacco J, Ghiassi B, Milani G, Lourenço PB. (2020). "A fast modeling approach for numerical analysis of unreinforced and FRCM reinforced masonry walls under out-of-plane loading." *Composites Part B: Engineering*, 180.

Shahzada, K., Khan, A. N., Elnashai, A. S., Ashraf, M., Javed, M., Naseer, A., and Alam, B. (2012). "Experimental seismic performance evaluation of unreinforced brick masonry buildings." *Earthquake Spectra*, 28(3), 1269–1290.

Shariq, M., Abbas, H., Irtaza, H., and Qamaruddin, M. (2008). "Influence of openings on seismic performance of masonry building walls." *Building and Environment*, 43(7), 1232–1240.

Shrestha, K. C., Araki, Y., Nagae, T., Omori, T., and Sutou, Y. (2011). "Applicability of Cu-Al-Mn shape memory alloy bars to retrofitting of historical masonry constructions." *Earthquake and Structures*, 2(3), 233–256.

Silva LC, Lourenço PB, Milani G. (2017). "Nonlinear discrete homogenized model for out-of-plane loaded masonry walls." Journal of Structural Engineering, 143 (9).

Singh, Y., Lang, D. H., Prasad, J., and Deoliya, R. (2013). "An Analytical Study on the Seismic Vulnerability of Masonry Buildings in India." *Journal of Earthquake Engineering*, 17(3), 399–422.

Sinha, B. (1978). "An ultimate load analysis of laterally loaded brickwork panels." *International Journal of Masonry Construction*, 1(2), 57–61.

Sinha, R., and Brzev, S. N. (2002). "Housing Report Unreinforced Brick Masonry Building With Reinforced Concrete Roof Slab." *World Housing Encyclopedia*, EERI(IAEE).

Strand7. (2013). "Strand 7.2 user's manual." *www.strand7.com*.

Tabbakhha, M., and Deodatis, G. (2016). "Effect of Uncertainty of Tensile Strength of Mortar Joints on the Behavior of Masonry Walls under Lateral Loads." *Journal of Structural Engineering*, 143(2).

Tassios, T. P. (2010). "Seismic Engineering of Monuments." *Bulletin of Earthquake Engineering*, 8(6), 1231–1265.

Tomaževič, M. (1999). *Earthquake resistant design of masonry buildings, Series on Innovation in Structures and Con-struction: Volume 1*. Imperial College Press, London, UK.

Tomaževič, M. (2011). *Earthquake - Resistant Design of Masonry Buildings*. Imperial College Press, London, UK.

Tomaževič, M., Lutman, M., and Weiss, P. (1996). "Seismic Upgrading of Old Brick Masonry Urban Houses: Tying of wall with steel Ties." *Earthquake Spectra*, 12(3), 559–622.

Turnšek, V., and Čačovič, F. (1970). "Some experimental results on the strength of brick masonry walls." *Proceedings of the 2nd International Brick Masonry Conference*,

Stoke-on-Trent, 149–156.

Vaculik, J., and Griffith, M. C. (2018). "Out-of-plane shaketable testing of unreinforced masonry walls in two-way bending." *Bulletin of Earthquake Engineering*, 16(7), 2839–2876.

Valente, M., and Milani, G. (2016). "Non-linear dynamic and static analyses on eight historical masonry towers in the North-East of Italy." *Engineering Structures*, 114, 241–270.

Valente, M., and Milani, G., (2016), Seismic assessment of historical masonry towers using simplified approaches and standard FEM. *Construction and Building Materials*, 108, 74-104.

Varum, H., Dumaru, R., Furtado, A., Barbosa, A. R., and Gautam, D. (2018). "Seismic performance of buildings in Nepal after the Gorkha earthquake." *Impacts and insights of the Gorkha earthquake*, Elsevier, 47–63.

Vincente, R., Rodrigues, H., Varum, H., and Mandes da Silva, A. R. (2011). "Evaluation of Strengthening Techniques of Traditional Masonry Buildings: Case Study of a Four-Building aggregate." *Journal of Performance of Constructed Facilities*, 25(3), 202–216.

Vintzileou, E. (2008). "Effect of Timber Ties on the Behavior of Historical Masonry." *Journal of Structural Engineering*, 134(6), 961–972.

Walsh, K., Dizhur, D., Giongo, I., Derakhshan, H., and Ingham, J. (2018). "Predicted Versus Experimental Out-of-plane Force-displacement Behaviour of Unreinforced Masonry Walls." *Structures*, Elsevier, 15(May), 292–306.

Walsh, K. Q., Dizhur, D. Y., Giongo, I., Derakhshan, H., and Ingham, J. M. (2017). "Effect of Boundary Conditions And Other Factors On URM Wall Out-Of-Plane Behaviour : Design Demands , Predicted Capacity and In-Situ Proof Test results." *SESOC Journal*, 30(1), 57–81.

Wilding, B. V., and Beyer, K. (2016). "Force-displacement response of in-plane loaded unreinforced brick masonry walls: the Critical Diagonal Crack model." *Bulletin of Earthquake Engineering*, Springer Netherlands, 15(5), 2201–2244.

Wilding, B. V., and Beyer, K. (2018a). "The effective stiffness of modern unreinforced masonry walls." *Earthquake Engineering & Structural Dynamics*, 47(8), 1683–1705.

Wilding, B. V., and Beyer, K. (2018b). "Analytical and empirical models for predicting the drift capacity of modern unreinforced masonry walls." *Earthquake Engineering and Structural Dynamics*, 47(10), 2012–2031.

Willis, C. R., Griffith, M. C., and Lawrence, S. J. (2006). "Moment Capacities of

Unreinforced Masonry Sections in Bending." *Australian Journal of Structural Engineering*, 6(April), 133–146.

Yi, T., Moon, F. L., Leon, R. T., and Kahn, L. F. (2006a). "Lateral load tests on a two-story unreinforced masonry building." *Journal of Structural Engineering*, 132(5), 643–652.

Yi, T., Moon, F. L., Leon, R. T., and Kahn, L. F. (2006b). "Analyses of a Two-Story Unreinforced Masonry Building." *Journal of Structural Engineering*, 132(5), 653–662.

Yi, T., Moon, F. L., Leon, R. T., and Kahn, L. F. (2008). "Flange Effects on the Nonlinear Behaviour of URM Piers." *The Masonry Society Journal*, 26(2), 31–42.

LIST OF PUBLICATION

REFEREED INTERNATIONAL JOURNALS

- Choudhury, T., Milani, G., and Kaushik, H. B. (2015). Comprehensive numerical approaches for the design and safety assessment of masonry buildings retrofitted with steel bands in developing countries: The case of India. *Construction and Building Materials*, *85*, 227–246.
- Choudhury, Thainswemong; Kaushik, Hemant B., (2019), "Influence of Individual Wall Strengths on Lateral Strength of URM Buildings Constructed using Low-Strength Masonry," *Journal of Earthquake Engineering (Available online)*
- Choudhury, T., Milani, G. and Kaushik, H. B. (2020). Experimental and Numerical Analyses of Unreinforced Masonry Wall Components and Building, *Construction and Building Materials*, 257.
- Choudhury, T., Kaushik, H. B. (2020). Experimental Evaluation of Full-Scale URM Buildings Strengthened using Surface-Mounted Steel Bands. *Journal of Structural engineering* (Accepted in September, 2020 and in press)

INTERNATIONAL CONFERENCES

- Choudhury, T., and Kaushik, H. B. (2019). Experimental Evaluation of an Unreinforced Masonry Building Strengthened with Steel Bands. *13th North American Masonry Conference*, Salt Lake City, Utah, USA, 16-19 June 2019.
- Choudhury, T., and Kaushik, H. B. (2018). Assessment of In-plane Capacity of Unreinforced Masonry Walls. *16th Symposium on Earthquake Engineering*, IIT Roorkee, 20-22 December, 2018.
- Choudhury, T., and Kaushik, H. B. (2018). Steel Bands: A sustainable strengthening technique to strengthen unreinforced masonry buildings. *2nd International Conference on Civil Engineering for Sustainable Development – Opportunities and Challenges (CESDOC 2018)*, Assam Engineering College, Guwahati, Assam, 18-19 December, 2018.
- Choudhury, T., and Kaushik, H. B. (2018). Numerical and experimental study on unreinforced masonry buildings with various opening configurations strengthened with steel bands. *10th Australasian Masonry Conference*, Sydney, Australia, 11-14 February 2018.